

# **Regional prediction of rainfall change - an energy budget approach**

by

Thomas Benjamin Richardson

Submitted in accordance with the requirements for the degree of Doctor of  
Philosophy

The University of Leeds  
School of Earth and Environment  
April 2017

## **Declaration of Authorship**

The candidate confirms that the work submitted is his own, except where work which has formed part of jointly-authored publications has been included. The contribution of the candidate and the other authors to this work has been explicitly indicated below. The candidate confirms that appropriate credit has been given within the thesis where reference has been made to work of others.

Half of the research included in the thesis has been peer reviewed and published. The remaining research has been prepared for submission to suitable journals. This thesis is published using the University of Leeds alternative thesis format so that the research within can be readily identified and accessed. The thesis consists of an introductory chapter, four first-author articles, a discussion chapter and appendices.

The publication Richardson et al., 2016, An assessment of precipitation adjustment and feedback computation methods, *Journal of Geophysical Research: Atmospheres*, 121(19), doi: 10.1002/2016JD025625, jointly authored with B. H. Samset, T. Andrews, G. Myhre and P. M. Forster, is included as Chapter 2 of this thesis. The text was solely written by the candidate, with comments from co-authors. The candidate performed data analysis and produced all figures. T. Andrews and P. M. Forster contributed to interpretation of results. The candidate performed the majority of HadGEM2 simulations. T. Andrews and B. H. Samset performed additional simulations.

The publication Richardson et al., 2016, Understanding the rapid precipitation response to CO<sub>2</sub> and aerosol forcing on a regional scale, *Journal of Climate*, 29(2), doi: <http://dx.doi.org/10.1175/JCLI-D-15-0174.1>, jointly authored with P. M. Forster, T. Andrews and D. J. Parker, is included as Chapter 3 of this thesis. The text was solely written by the candidate with advice from co-authors. The candidate performed data analysis and produced all figures. All co-authors contributed to interpretation of results.

The publication Richardson et al., 2017, Drivers of precipitation change: an energetic understanding, prepared for submission to the *Journal of Climate*, jointly authored with P. M. Forster, T. Andrews, O. Boucher, G. Faluvegi, D. Fläschner, Ø. Hodnebrog, M. Kasoar, V. Kharin, A. Kirkevåg, J.-F. Lamarque, G. Myhre, D. Olivié, B. H.

Samset, D. Shawki, D. Shindell, T. Takemura and A. Voulgarakis, is included as Chapter 4. The text was solely written by the candidate with comments from co-authors. The candidate performed data analysis and produced all figures. The candidate performed the majority of HadGEM2 simulations. All co-authors contributed to additional simulations. T. Andrews and P. M. Forster contributed to interpretation of results.

The publication Richardson et al., 2017, Importance of carbon dioxide physiological forcing on projected Amazonian precipitation change, prepared for submission to Geophysical Research Letters, jointly authored with P. M. Forster, T. Andrews, O. Boucher, G. Faluvegi, D. Fläschner, Ø. Hodnebrog, M. Kasoar, V. Kharin, A. Kirkevåg, J.-F. Lamarque, G. Myhre, D. Olivié, B. H. Samset, D. Shawki, D. Shindell, T. Takemura and A. Voulgarakis, is included as Chapter 5. The candidate performed data analysis and produced all figures. The candidate performed the majority of HadGEM2 simulations. All co-authors contributed to additional simulations. T. Andrews and P. M. Forster contributed to interpretation of results.

This copy has been supplied on the understanding that it is copyright material and that no quotation from the thesis may be published without proper acknowledgement.

© 2017 The University of Leeds and Thomas Benjamin Richardson

## **Acknowledgements**

First and foremost I would like to thank my supervisors Piers Forster, Tim Andrews and Doug Parker for their encouragement, guidance and considerable enthusiasm throughout this project. I would like to thank the Met Office climate sensitivity and feedbacks group, and Rob Chadwick for many interesting discussions. I am also very thankful to Richard Rigby for assisting on various computing issues with incredible speed.

I am extremely grateful to all participants of the Precipitation Driver and Response Model Intercomparison Project (PDRMIP) for providing model data which was integral to much of this work. In particular, I would like to thank Gunnar Myhre, Bjørn Samset and Øivind Hodnebrog for making me welcome at CICERO, and for many useful discussions. I would also like to thank all the modelling groups who supplied data to the Coupled Model Intercomparison Project phase 5 (CMIP5), which has made much of this work possible. Many anonymous reviewers have also provided constructive comments on the manuscripts submitted for publication, I would like to thank them for their time and input. This project would not have been possible without the financial support of the National Environment Research Council and CASE award with the Met Office.

I would like to thank all my friends here in Leeds who have made the journey such a top experience. I would like to thank all the rest of my friends and family for their encouragement.

Finally, I would like to express special thanks to my wife Harriett for her incredible support throughout.

## Abstract

Changes in the hydrological cycle are one of the most important aspects of climate change prediction. Globally, precipitation change is well understood in terms of the atmospheric energy budget, whereby the latent heat released is balanced by net atmospheric cooling. As a result, forcing agents affect precipitation directly through forcing-dependent adjustments, as well as through temperature-driven feedbacks. However, the physical processes driving regional precipitation changes are less understood, particularly over land, and regional projections exhibit significant uncertainties.

The global energetic perspective can be extended to regional scales through incorporating horizontal transport of dry static energy. Therefore, the aim of this thesis was to utilize analysis of the local atmospheric energy budget to improve understanding of how forcing agents affect regional precipitation patterns through both forcing-dependent adjustments and temperature-driven feedbacks. The precipitation response to a range of atmospheric forcing agents was analysed using the Met Office Hadley Centre climate model, HadGEM2, as well as output from a large number of the latest generation of global climate models.

Land-mean precipitation was shown to have a weak sensitivity to global temperature change. Therefore, adjustment processes have a strong influence on land-mean precipitation trends. During the historical period temperature-driven intensification of land-mean precipitation has been entirely masked by negative adjustments in response to anthropogenic sulphate and volcanic forcing. However, as projected sulphate concentrations decline, temperature-driven changes will soon dominate.

The rapid land surface response to forcing was found to play a key role in driving regional precipitation adjustment patterns. Adjustment processes were found to be particularly important for precipitation in the eastern Amazon. Projected drying of the eastern Amazon was shown to be dominated by the physiological effects of CO<sub>2</sub> on plant stomata, through reducing evapotranspiration.

These results highlight the importance of short-timescale adjustment processes in understanding historical and future precipitation changes over land.

# Table of Contents

<b>Declaration of Authorship.....</b>	<b>i</b>
<b>Acknowledgements.....</b>	<b>iii</b>
<b>Abstract.....</b>	<b>iv</b>
<b>Table of Contents.....</b>	<b>v</b>
<b>List of Figures.....</b>	<b>viii</b>
<b>List of Tables.....</b>	<b>xiv</b>
<b>Abbreviations.....</b>	<b>xv</b>
<b>Chapter 1: Introduction.....</b>	<b>1</b>
1.1 Motivation.....	1
1.2 Observed and Projected Precipitation Change.....	4
1.3 Constraints on Precipitation.....	5
1.3.1 Atmospheric Moisture Budget.....	5
1.3.2 Atmospheric Energy Budget.....	6
1.4 Radiative forcing of Climate.....	8
1.4.1 Concept.....	8
1.4.2 Forcing Agents.....	10
1.5 Adjustment and Feedback Framework.....	11
1.5.1 Concept and Utility.....	11
1.5.2 Computation Methods.....	13
1.6 Regional Precipitation Change Mechanisms.....	14
1.6.1 Response to Warming.....	14
1.6.2 Response to Forcing.....	15
1.7 Thesis Aims and Structure.....	17

<b>Chapter 2: An Assessment of Precipitation Adjustment and Feedback Computation Techniques.....</b>	<b>29</b>
<b>Chapter 3: Understanding the Rapid Precipitation Response to CO<sub>2</sub> and Aerosol Forcing on a Regional Scale.....</b>	<b>42</b>
<b>Chapter 4: Drivers of Precipitation Change: An Energetic Understanding.....</b>	<b>55</b>
4.1 Abstract.....	56
4.2 Introduction.....	57
4.3 Methods.....	58
4.3.1 Data.....	58
4.3.2 Rapid Adjustment and Hydrological Sensitivity.....	59
4.3.3 Atmospheric Energy Budget.....	60
4.3.4 Simple Precipitation Model.....	60
4.4 Results and Discussion.....	62
4.4.1 Precipitation and Energy Budget Response.....	62
4.4.2 Simple Precipitation Model.....	69
5. Conclusions.....	73
Acknowledgements.....	76
References.....	77
<b>Chapter 5: Importance of carbon dioxide physiological forcing on projected Amazonian precipitation change.....</b>	<b>82</b>
5.1 Abstract.....	83
5.2 Introduction.....	84
5.3 Methods.....	85
5.4 Results and Discussion.....	88
5.4.1 Precipitation Response to Forcing.....	88
5.4.2 Energy and Moisture Budget Changes.....	91

5.4.3 CO <sub>2</sub> Physiological Effect.....	93
5.4.4 Projections of Precipitation Change.....	95
5.5 Conclusions.....	97
Acknowledgements.....	99
References.....	100
<b>Chapter 6: Conclusions and Recommendations.....</b>	<b>105</b>
6.1 Summary and Conclusions.....	105
6.2 Limitations and Recommendations for Future Research.....	109
References.....	111
<b>Appendices.....</b>	<b>113</b>
Appendix 1: Supporting Information for Chapter 2.....	114
Appendix 2: Supporting Information for Chapter 3.....	125
Appendix 3: Supporting Information for Chapter 4.....	134
Appendix 4: Supporting Information for Chapter 5.....	146



# List of Figures

<b>Figure 1.1:</b> Multi-model mean change in annual precipitation for 2081-2100 relative to 1986-2005.....	4
<b>Figure 1.2:</b> The Earth’s annual global energy budget for the period March 2000 to May 2004.....	6
<b>Figure 1.3:</b> Change in global mean precipitation against surface air temperature for HadSM3 abrupt doubling of CO <sub>2</sub> and 2% in insolation.....	13
<b>Figure 2.1:</b> Global mean rapid adjustment and hydrological sensitivity terms against integration length for fSST and regression methods.....	33
<b>Figure 2.2:</b> Standard error of global mean rapid adjustment and hydrological sensitivity values against integration length for fSST and regression methods.....	35
<b>Figure 2.3:</b> PDRMIP multi-model global mean rapid adjustment and hydrological sensitivity values diagnosed using fSST, regression and YR1 methods.....	36
<b>Figure 2.4:</b> Global mean surface temperature change in response to five forcing scenarios for fSST simulations, first year of coupled simulations and final 50 years of coupled simulations.....	36
<b>Figure 2.5:</b> HadGEM2 zonally averaged precipitation adjustment and hydrological sensitivity in response to 2xCO <sub>2</sub> calculated using fSST and regression methods.....	37
<b>Figure 2.6:</b> CESM1-CAM4 regional precipitation adjustment and hydrological sensitivity in response to doubling CO <sub>2</sub> calculated using fSST, regression and YR1 methods .....	38
<b>Figure 2.7:</b> HadGEM2 precipitation adjustment in response to quadrupling CO <sub>2</sub> calculated using fSST simulations with different SST climatology’s.....	39

<b>Figure 3.1:</b> Multi-model mean atmospheric energy budget response for sstClim4xCO <sub>2</sub> , sstClimSulfate, and sstClimAerosol.....	45
<b>Figure 3.2:</b> Multi-model mean regional precipitation and surface temperature change for sstClim4xCO <sub>2</sub> , sstClimSulfate and sstClimAerosol.....	46
<b>Figure 3.3:</b> Mean precipitation change over the globe, land, sea, midlatitude land, midlatitude sea, tropical land and tropical sea for sstClim4xCO <sub>2</sub> , sstClimSulfate and sstClimAerosol .....	47
<b>Figure 3.4:</b> sstClim4xCO <sub>2</sub> response of local atmospheric energy budget for HadGEM2 .....	49
<b>Figure 3.5:</b> Components of the change in dry static energy flux divergence for HadGEM2 sstClim4xCO <sub>2</sub> .....	50
<b>Figure 3.6:</b> HadGEM2 sstClim4xCO <sub>2</sub> changes in atmospheric cloud, surface and TOA radiative fluxes.....	51
<b>Figure 3.7:</b> HadGEM2 vertical profile of tropospheric adjustments in response to quadrupling CO <sub>2</sub> .....	52
<b>Figure 4.1:</b> Multi-model global mean precipitation adjustment and hydrological sensitivity in response to the PDRMIP forcing scenarios. Contributions from atmospheric energy budget terms are shown.....	63
<b>Figure 4.2:</b> Multi-model mean land and sea mean precipitation adjustment and hydrological sensitivity in response to the PDRMIP forcing scenarios. Contributions from the atmospheric energy budget are shown.....	65
<b>Figure 4.3:</b> Multi-model mean global, land and sea mean precipitation adjustments per unit top of the atmosphere forcing for the PDRMIP forcing scenarios.....	68

<b>Figure 4.4:</b> Historical and future land-mean and sea-mean precipitation change relative to pre-industrial for RCP4.5 and RCP8.5, calculated using CMIP5 multi-model mean and the simple PDRMIP model. The simple model is also compared with observed land-mean precipitation for the historical period.....	70
<b>Figure 4.5:</b> Driver contributions to historical and future land-mean and sea-mean precipitation change relative to pre-industrial for RCP4.5 and RCP8.5 in the simple PDRMIP model.....	73
<b>Figure 5.1:</b> Multi-model mean precipitation response to PDRMIP abrupt forcing scenarios over the Amazon region.....	90
<b>Figure 5.2:</b> PDRMIP multi-model mean ECA region mean precipitation, energy budget and moisture budget responses to 2xCO <sub>2</sub> and 10xBC, split into adjustment and feedback terms.....	91
<b>Figure 5.3:</b> CMIP5 multi-model mean precipitation response to quadrupling CO <sub>2</sub> in amip and sstClim simulations and the difference between the two for the Amazon region .....	94
<b>Figure 5.4:</b> Projected precipitation change for the period 2081-2100 relative to pre-industrial following RCP4.5 and RCP8.4, calculated using CMIP5 multi-model mean and a simple model based on the PDRMIP response to CO <sub>2</sub> .....	96
<b>Figure A1.S1:</b> CESM1-CAM4 zonally averaged precipitation adjustment and hydrological sensitivity in response to 2xCO <sub>2</sub> calculated using fSST and regression methods .....	116
<b>Figure A1.S2:</b> CESM1-CAM4 zonally averaged precipitation adjustment and hydrological sensitivity in response to 5xSul calculated using fSST and regression methods .....	117

<b>Figure A1.S3:</b> HadGEM2 zonally averaged precipitation adjustment and hydrological sensitivity in response to 5xSul calculated using fSST and regression methods.....	118
<b>Figure A1.S4:</b> HadGEM2 regional precipitation adjustment and hydrological sensitivity in response to 2xCO <sub>2</sub> calculated using the fSST, regression and YR1 methods .....	119
<b>Figure A1.S5:</b> HadGEM2 regional precipitation adjustment and hydrological sensitivity in response to 5xSul calculated using the fSST, regression and YR1 methods .....	120
<b>Figure A1.S6:</b> CESM1-CAM4 regional precipitation adjustment and hydrological sensitivity in response to 5xSul calculated using the fSST, regression and YR1 methods .....	121
<b>Figure A1.S7:</b> PDRMIP multi-model global mean atmospheric energy budget and precipitation feedback response to 10xBC calculated using the fSST and regression methods .....	122
<b>Figure A1.S8:</b> HadGEM2 atmospheric energy budget response to quadrupling CO <sub>2</sub> calculated using fSST simulations with different SST climatology's.....	123
<b>Figure A2.S1:</b> sstClim4xCO <sub>2</sub> precipitation response across CMIP5 models.....	128
<b>Figure A2.S2:</b> sstClimSulphate precipitation response across CMIP5 models.....	129
<b>Figure A2.S3:</b> sstClimAerosol precipitation response across CMIP5 modles.....	130
<b>Figure A2.S4:</b> CMIP5 multi-model mean sstClim4xCO <sub>2</sub> surface energy budget anaomaly over land and sea.....	131

<b>Figure A2.S5:</b> Precipitation and surface temperature change for sstClimSulphate simulation. Model are split into those which include only the direct aerosol effect, those which include the direct and first indirect effect, and those which include the direct and first and second indirect effects.....	132
<b>Figure A2.S6:</b> Precipitation and surface temperature change for sstClimAerosol simulation. Model are split into those which include only the direct aerosol effect, those which include the direct and first indirect effect, and those which include the direct and first and second indirect effects.....	133
<b>Figure A3.S1:</b> Global mean precipitation adjustment and hydrological sensitivity responses to the five PDRMIP forcing scenarios for individual models. Contributions from atmospheric energy budget terms are shown.....	138
<b>Figure A3.S2:</b> Land and sea mean precipitation adjustment and hydrological sensitivity responses to the five PDRMIP forcing scenarios for individual models. Contributions from atmospheric energy budget terms are shown.....	139
<b>Figure A3.S3:</b> Multi-model global mean forcing and feedbacks for surface fluxes in response to the five PDRMIP forcing scenarios.....	140
<b>Figure A3.S4:</b> Multi-model land mean forcing and feedbacks for surface fluxes in response to the five PDRMIP forcing scenarios.....	141
<b>Figure A3.S5:</b> Multi-model sea mean forcing and feedbacks for surface fluxes in response to the five PDRMIP forcing scenarios.....	142
<b>Figure A3.S6:</b> Multi-model global mean forcing and feedbacks for the top of the atmosphere fluxes in response to the five PDRMIP forcing scenarios.....	143
<b>Figure A3.S7:</b> Multi-model mean forcing and feedbacks for the top of the atmosphere fluxes over land and sea in response to the five PDRMIP forcing scenarios.....	144

<b>Figure A3.S8:</b> Global mean top of the atmosphere radiative forcing from 1850 to 2100 for each of the forcing agents included in the simple PDRMIP model.....	145
<b>Figure A4.S1:</b> Multi-model mean precipitation adjustment in response to the five PDRMIP forcing scenarios over the Amazon region.....	149
<b>Figure A4.S2:</b> Multi-model mean precipitation feedback response to the five PDRMIP forcing scenarios over the Amazon region.....	150
<b>Figure A4.S3:</b> Multi-model mean precipitation adjustment and hydrological sensitivity in response to the five PDRMIP forcing scenarios for the ECA region...	151
<b>Figure A4.S4:</b> CMIP5 multi-model mean atmospheric energy budget and moisture budget responses to quadrupling CO <sub>2</sub> in amip and sstClim simulations.....	152
<b>Figure A4.S5:</b> Contribution to projected precipitation change relative to pre-industrial from CO <sub>2</sub> adjustment and temperature-driven feedback for the period 2081-2100, following RCP4.5 and RCP8.5, calculated using a simple model.....	153
<b>Figure A4.S6:</b> CMIP5 multi-model mean precipitation response over the Amazon region to quadrupling CO <sub>2</sub> in sstClim and amip simulations and the difference between the two.....	154

## List of Tables

<b>Table 2.1:</b> Hydrological sensitivity calculated using regression technique for HadGEM2 and CESM1-CAM4.....	34
<b>Table 3.1:</b> List of models analysed for each simulation.....	53
<b>Table A1.S1:</b> Rapid precipitation adjustment results calculated using the first month of coupled abrupt forcing simulations for HadGEM2 and CESM1-CAM4.....	124
<b>Table A2.S1:</b> Models categorized based on their representation of aerosol indirect effects .....	127
<b>Table A3.S1:</b> PDRMIP model details.....	135
<b>Table A3.S2:</b> List of CMIP5 models used for historical and future analysis.....	136
<b>Table A3.S3:</b> PDRMIP multi-model mean and median <i>R</i> factors and hydrological sensitivities in response to the five PDRMIP forcing scenarios for the global, land and sea mean.....	137
<b>Table A4.S1:</b> List of CMIP5 model output used for analysis.....	147
<b>Table A4.S2:</b> List of vegetation scheme references for models which performed sstClim simulations.....	148

# Abbreviations

**AeroCom** Aerosol Comparison between Observations and Models project

**BC** Black Carbon

**CCN** Cloud Condensation Nuclei

**CMIP5** Coupled Model Intercomparison Project Phase 5

**CRE** Cloud Radiative Effect

**CRU TS** Climate Research Unit Time-Series

**ECA** Eastern and Central Amazon Region

**ERF** Effective Radiative Forcing

**FB** Feedback

**FSST** Fixed Sea Surface Temperature

**GHG** Greenhouse Gas

**GPCC** Global Precipitation Climatology Centre

**HadCRUT4** Temperature record compiled by Met Office Hadley Centre and Climate Research Unit

**HadGEM2** Met Office Hadley Centre Global Environment Model Version 2

**HS** Hydrological Sensitivity

**IN** Ice Nuclei

**IPCC** Inter-governmental Panel on Climate Change

**ITCZ** Inter-Tropical Convergence Zone

**LW** Longwave

**LWC** Net Atmospheric Longwave cooling

**NERC** Natural Environment Research Council

**PDRMIP** Precipitation Driver and Response Model Intercomparison Project

**RA** Rapid Adjustment

**RCP** Representative Concentration Pathway

**SE** Standard Error

**SH** Sensible Heat Flux

**SST** Sea Surface Temperature

**SW** Shortwave

**SWA** Net Atmospheric Shortwave Absorption

**TOA** Top of the atmosphere

**WaGW** Warmer Get Wetter

**WeGW** Wet Get Wetter

**YR1** Year One



# Chapter 1: Introduction

## 1.1 Motivation

Over the past century the Earth's climate has warmed, most of which can be attributed to anthropogenic greenhouse gas emissions from the burning of fossil fuels (Stocker et al., 2014). This warming is expected to continue in the future, as greenhouse gas emissions continue to rise. One of the most important aspects of climate change prediction is understanding how regional precipitation may be affected by anthropogenic and natural drivers. Precipitation plays a key role in human society due to its importance for freshwater availability and food production (Hoekstra and Mekonnen, 2011). Significant changes in precipitation could have severe humanitarian and financial implications (Piao et al., 2010; Wake, 2013). However, unlike temperature, precipitation projections still exhibit considerable uncertainty, and physical understanding remains incomplete (Stephens et al., 2010; Knutti and Sedláček, 2012; Stevens and Bony, 2013; Greve et al., 2014; Shepherd, 2014).

As the climate warms global mean precipitation is expected to increase (Allan et al., 2014), but changes will likely exhibit substantial spatial variation. Observations have shown both wetting and drying trends over land areas over the past century (Greve et al., 2014). During the 21<sup>st</sup> century, as the climate continues to warm, precipitation changes are expected to become more evident (Stocker et al., 2014). Current global climate models exhibit some robust changes in regional precipitation patterns for the industrial era and future climate, including enhanced precipitation at high latitudes and drying in many subtropical arid regions (Knutti and Sedláček, 2012). However, projections remain uncertain in many regions, particularly in the tropics where there is considerable diversity among models. Despite the uncertain spatial pattern, models consistently predict large precipitation changes in the tropics (Chadwick et al., 2015).

Precipitation is constrained by both atmospheric moisture availability and the atmospheric energy budget, due to the latent heat released (Mitchell et al., 1987; Allen and Ingram, 2002). Globally, the latent heating of the atmosphere is balanced by the net atmospheric radiative cooling and sensible heat flux from the surface (Mitchell et

al., 1987; O’Gorman et al., 2011). The energy budget tightly controls global precipitation, and explains the low apparent hydrological sensitivity (precipitation change per unit Kelvin of global surface temperature change) of 1-3%  $\text{K}^{-1}$  predicted by climate models (Pendergrass and Hartmann, 2014), despite a larger increase in moisture availability following Clausius-Clapeyron scaling ( $\sim 7\% \text{K}^{-1}$ ).

As a result of the energetic constraint on precipitation, climate drivers can produce near-instantaneous changes in precipitation, independent of global temperature change (Mitchell et al., 1987; Lambert and Faull, 2007; Bala et al., 2009; Andrews et al., 2010b). This is due to their near-instantaneous effect on the atmospheric energy budget, due to direct radiative effects and rapid adjustments of the troposphere and land surface. These short-timescale changes in response to forcing agents are known as rapid precipitation adjustments. Separating the response of global mean precipitation into a forcing-dependent adjustment and temperature-driven feedback helps explain the different apparent hydrological sensitivities for different climate drivers (Andrews et al., 2010b; Kvalevåg et al., 2013; Fläschner et al., 2016). The adjustment and feedback framework is therefore vital in understanding projected global precipitation changes.

The global energetic perspective on precipitation change can be extended to regional scales by taking into account horizontal transport of dry static energy (Muller and O’Gorman, 2011). The local dry static energy budget provides a simple framework for analysing the regional precipitation response to forcing, directly relating radiative effects to precipitation change. However, on regional scales most previous work has made use of the atmospheric moisture budget to understand precipitation changes (e.g. Held and Soden, 2006; Seager et al., 2010; Huang, 2013), and few have made the adjustment and feedback separation.

Regional precipitation changes in response to warming have generally been understood in terms of thermodynamic changes associated with increasing specific humidity, and dynamic changes associated with circulation (Held and Soden, 2006; Seager et al., 2010; Bony et al., 2013). Using this approach some key mechanisms for driving precipitation changes have been identified. The wet-get-wetter and dry-get-drier mechanism (WeGW) acts to increase precipitation in regions of convergence, and decrease precipitation in regions of divergence, due to increasing tropospheric

water vapour with increasing temperature (Chou et al., 2009). Deviations from the WeGW pattern occur due to the warmer-get-wetter mechanism (WaGW), whereby areas of convergence shift following regions with greater surface temperature increase (Xie et al., 2010; Chadwick et al., 2013; Huang, 2013). However, these mechanisms do not hold well over land, where precipitation changes have the most impact. Observations indicate only a very small fraction of land areas follow the WeGW trend (Greve et al., 2014).

To improve our understanding of regional precipitation changes over land it is important we understand the influence of forcing-dependent precipitation adjustments. Increasing CO<sub>2</sub> levels have been shown to drive a significant precipitation adjustment which exhibits substantial spatial variability (Bony et al., 2013; Samset et al., 2016; Tian et al., 2016). Bony *et al.* (2013) showed that around half the 30-year mean change in tropical overturning circulation due to quadrupling CO<sub>2</sub> occurs within the first five days, driving much of the tropical precipitation pattern. Recently, Samset *et al.* (2016) showed that precipitation adjustments dominate the long-term precipitation response for various land regions, including South America and Africa, across a range of drivers.

The principal aim of this research is to improve understanding of how forcing agents affect regional precipitation patterns through both rapid adjustments and temperature-driven feedbacks, using analysis of the local atmospheric energy budget. There is considerable potential for improving understanding of regional precipitation change processes by extending the global energetic perspective to regional scales. Through analysis of the local atmospheric energy budget, the radiative effects of forcing agents can be directly related to regional precipitation and circulation change, enabling us to identify the key drivers, and mechanisms by which they affect change. This understanding is vital for improving our ability to predict and mitigate regional precipitation changes, particularly over land where changes will be most felt by society.

## 1.2 Observed and projected precipitation change

It is virtually certain that global mean precipitation will increase with surface temperature (Allan et al., 2014). Climate models predict the rate of change to be in the region of 1-3%  $K^{-1}$  (Held and Soden, 2006; Lambert and Webb, 2008; Andrews et al., 2010b; Fläschner et al., 2016). Some observational studies find evidence supporting this increasing trend. However, the magnitude is highly variable, and due to large internal climate variability, results are very dependent on the time period analysed (Arkin et al., 2010; Allan et al., 2014).

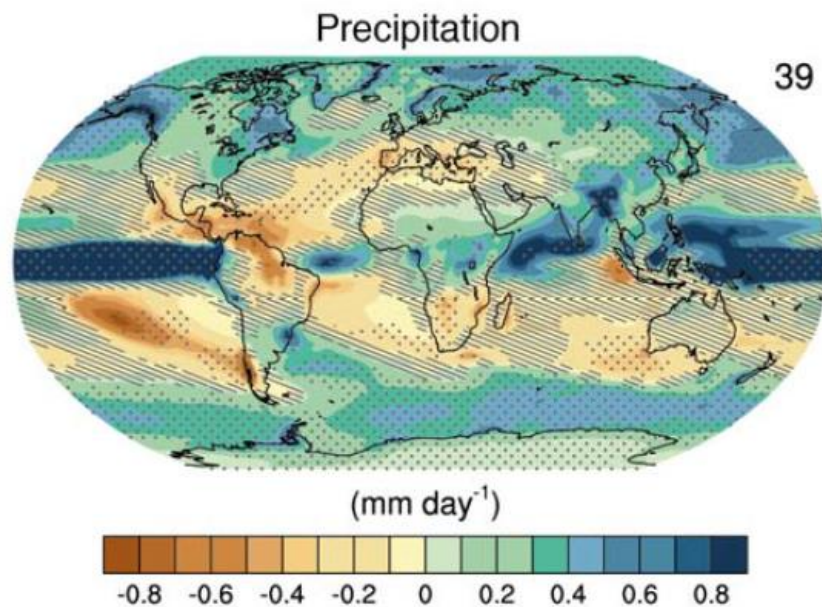


**Figure 1.1:** CMIP5 multi-model mean change in annual precipitation for 2081-2100 relative to 1986-2005 under the Representative Concentration Pathway 8.5 (RCP8.5) scenario. Stippling represents areas with robust changes and hatching indicates areas where the multi-model mean is less than one standard deviation of internal variability. (Taken from Stocker et al. 2014).

On regional scales, it is expected there will be substantial spatial variation in precipitation change, as seen in Figure 1.1. The mid-to-high latitudes are projected to experience increased precipitation, whereas many subtropical and semi-arid regions are likely to experience reductions. Significant increases in precipitation are projected along the equatorial Pacific, Maritime Continent, North Indian Ocean and Southern Asia. The largest changes are projected to occur in the tropics. There remain many regions where model agreement is low, particularly over tropical land regions.

Observations indicate a likely increasing trend in northern hemisphere mid-latitude land mean precipitation since 1901 (Hartmann et al., 2013). Spatially, over land both wetting and drying trends have been observed (Greve et al., 2014).

## 1.3 Constraints on Precipitation

### 1.3.1 Atmospheric moisture budget

Atmospheric moisture provides an important constraint on regional precipitation (Allen and Ingram, 2002; Held and Soden, 2006). Neglecting variations in surface pressure the local atmospheric moisture budget can be written as shown in Equation 1.1:

$$P = E - \int \bar{\mathbf{u}} \cdot \nabla \bar{q} - \int \bar{q} \nabla \cdot \bar{\mathbf{u}} - \int \nabla \cdot (\overline{\mathbf{u}'q'}), \quad (1.1)$$

where,  $P$  is precipitation,  $E$  is evaporation,  $\mathbf{u}$  is the horizontal wind vector,  $\nabla$  is the horizontal gradient,  $q$  is specific humidity, overbars denote monthly means, primes indicate departures from the monthly mean, and  $\int$  denotes mass-weighted vertical integration over the column:

$$\int = \int \frac{dp}{g}, \quad (1.2)$$

Where,  $p$  is pressure and  $g$  is acceleration due to gravity. Many studies have made use of the atmospheric moisture budget to understand regional precipitation changes (e.g. Held and Soden, 2006; Chou et al., 2009; Seager et al., 2010; Huang, 2013). The changes are often decomposed into dynamic and thermodynamic components (Emori, 2005; Seager et al., 2010). The dynamic component is due to changes in atmospheric motion, and the thermodynamic component due to changes in atmospheric moisture content. The changes in atmospheric circulation have in turn been analysed using the moist static energy budget (Chou and Neelin, 2004). The dynamic component is responsible for a large portion of the uncertainty in projected regional precipitation changes, due to uncertain circulation changes (Shepherd, 2014).

### 1.3.2 Atmospheric energy budget

The Earth's weather and climate are determined by the energy flows driven by incoming solar radiation. A schematic of the Earth's global-annual energy budget is shown in Figure 1.2. Precipitation provides a link between the hydrological cycle and Earth's energy balance through latent heating of the atmosphere. Globally the latent heat released through precipitation is balanced by the net atmospheric longwave cooling, shortwave absorption and sensible heat flux from the surface. Analysis of the tropospheric energy budget (Mitchell et al., 1987; Allen and Ingram, 2002; Andrews et al., 2010b) or surface energy budget (Andrews et al., 2009; Wild and Liepert, 2010) can therefore be used to place constraints on precipitation.

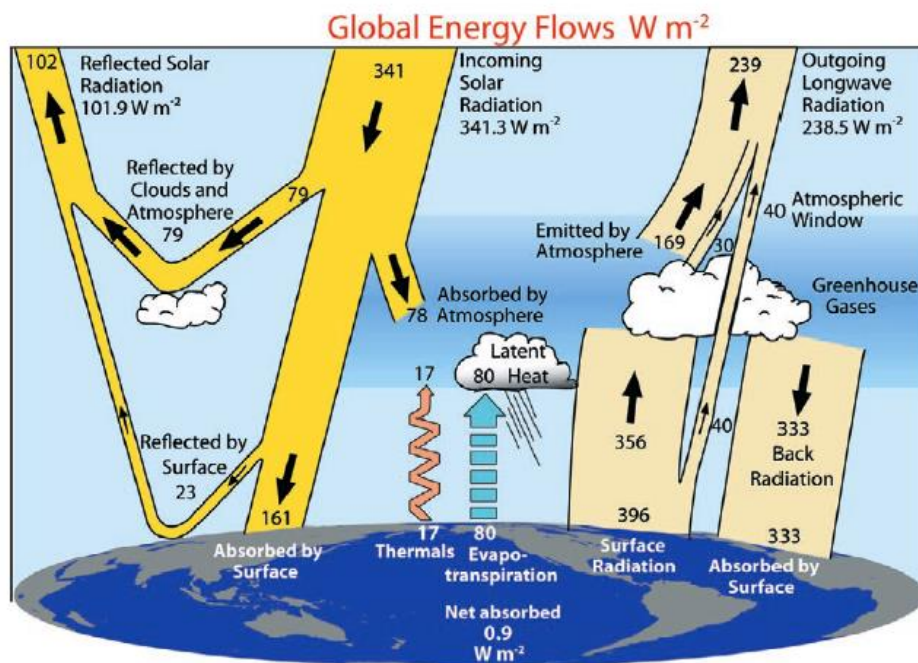


**Figure 1.2:** The Earth's annual global energy budget for the period March 2000 to May 2004 ( $W m^{-2}$ ). (Taken from Trenberth et al. 2009)

In the context of climate change this means for a given perturbation in the climate system, precipitation must respond accordingly to maintain energy balance. Conservation of energy presents a more severe constraint on global precipitation change than the availability of atmospheric moisture (Mitchell et al., 1987; Allen and Ingram, 2002). This accounts for the low hydrological sensitivity observed in current climate models ( $1-3\% K^{-1}$ ).

Muller and O’Gorman (2011) demonstrated that the energy budget framework for analysing precipitation change can be extended to regional scales through incorporating horizontal transport of dry static energy. A perturbation between two climates may be expressed in terms of the local atmospheric energy budget using Equation 1.3:

$$L_c \delta P = \delta Q + \delta H = \delta LWC - \delta SWA - \delta SH + \delta H, \quad (1.3)$$

where  $L_c$  is the latent heat of condensation,  $P$  is precipitation,  $Q$  is the net diabatic cooling of the atmosphere (excluding latent heat),  $H$  is the column-integrated dry static energy flux divergence associated with circulation,  $LWC$  is net atmospheric longwave cooling,  $SWA$  is net atmospheric shortwave absorption,  $SH$  is the sensible heat flux from the surface, and  $\delta$  represents a perturbation between climates. Equation 1.3 assumes that changes in atmospheric energy storage are negligible. This has previously been shown to be true for one model (Muller and O’Gorman, 2011). Equation 1.3 can be usefully employed to analyse transient changes due to the small heat capacity of the atmosphere (O’Gorman et al., 2011), which means the energy budget responds on very short timescales (within days) (Cao et al., 2012). The dry static energy flux divergence term  $H$ , can be calculated using Equation 1.4:

$$H = \int \bar{\mathbf{u}} \cdot \nabla \bar{s} + \int \bar{s} \nabla \cdot \bar{\mathbf{u}} + \int \nabla \cdot (\overline{\mathbf{u}'s'}), \quad (1.4)$$

where,  $H$  is dry static energy flux divergence,  $\mathbf{u}$  is the horizontal wind vector,  $\nabla$  is the horizontal gradient,  $s$  is dry static energy, overbars denote monthly means, primes indicate departures from the monthly mean, and  $\int$  denotes mass-weighted vertical integration over the column (Eq. 1.2). For the analysis in this thesis the transient component (third term in Eq. 1.4) is calculated as a residual. This assumes that the atmospheric energy budget closes for the climate models used. This has previously been shown to be true for one model (Muller and O’Gorman, 2011), but may vary in some models. All models used for energy budget analysis were verified to be energy conserving globally for the atmospheric energy budget. In the tropics,  $H$  can be well approximated from the first two terms in equation 1.4, based on monthly means. This is because eddy dry static energy fluxes are negligible in the tropics because of the weak local temperature gradients (Trenberth and Stepaniak, 2003). Outside of the tropics, changes in eddy dry static energy fluxes may contribute to changes in  $H$  due

to changes in the pole-to-equator temperature gradient or storm track winds (Muller and O’Gorman, 2011).

The change in dry static energy flux divergence by mean motions due to a perturbation in climate can be calculated as shown in Equation 1.5. For this formulation, the second term in Equation 1.4 was rewritten in terms of vertical velocity (obtainable by using the continuity equation and neglecting surface pressure variations).

$$\delta H = \int \delta(\bar{\mathbf{u}}) \cdot \nabla \bar{s} + \int \bar{\mathbf{u}} \cdot \delta(\nabla \bar{s}) + \int \delta(\bar{\omega}) \frac{\partial \bar{s}}{\partial p} + \int \bar{\omega} \delta \left( \frac{\partial \bar{s}}{\partial p} \right), \quad (1.5)$$

where,  $H$  is dry static energy flux divergence,  $\mathbf{u}$  is the horizontal wind vector,  $\nabla$  is the horizontal gradient,  $s$  is dry static energy,  $\omega$  is vertical velocity,  $p$  is pressure, overbars denote monthly means,  $\int$  denotes mass-weighted vertical integration over the column (Eq. 1.2), and  $\delta$  denotes a perturbation between climates.

By decomposing the change in dry static energy flux divergence into the separate terms in Equation 1.5, the contribution to precipitation change from changes in different atmospheric parameters can be identified. In a similar manner to moisture budget analyses, the change in dry static energy flux divergence can be separated into a dynamic and thermodynamic component. The dynamic term includes change associated with changes in atmospheric motion (terms 1 and 3 in Eq. 1.5), and the thermodynamic term includes change associated with changes in dry static energy gradients (terms 2 and 4 in Eq. 1.5). In the tropics, where horizontal gradients in dry static energy are generally small, the first two terms in Equation 1.5 can be neglected.

Analysis of the local atmospheric energy budget enables precipitation change to be directly related to the radiative effects of forcing agents, through their impact on net atmospheric cooling as well as atmospheric circulation.

## 1.4 Radiative Forcing of Climate

### 1.4.1 Concept

The ubiquitous framework for analysing climate change involves an external forcing that induces a change in the global top of the atmosphere (TOA) energy balance, an opposing climate response to regain equilibrium, and feedbacks which amplify or



dampen the overall climate response (Myhre et al., 2013; Sherwood et al., 2015). Radiative forcing is a key concept in understanding the climate response to anthropogenic and natural drivers of change. There are various ways in which radiative forcing can be defined, which are important to distinguish between.

Radiative forcing was first defined as the instantaneous change in the Earth's radiative balance due to an external driver. It was soon established that allowing stratospheric temperatures to adjust to a new radiative equilibrium before calculating the radiative forcing provided a more useful result. The stratospherically adjusted method became the standard approach for computing radiative forcing (RF) (Ramaswamy et al., 2001). However, more recently it has been established that short timescale adjustments, which are largely independent of surface temperature change, can also occur in the troposphere (Andrews and Forster, 2008; Andrews et al., 2011; Boucher et al., 2013). The rapid adjustments can either enhance or reduce the initial radiative perturbation through changes in tropospheric properties such as clouds. Including these effects into the radiative forcing calculation provides a better indication of the overall climate response (Chung and Soden, 2015; Sherwood et al., 2015). The case where rapid adjustments in the stratosphere and troposphere are incorporated into the forcing calculation is termed the effective radiative forcing (ERF).

Various methods can be used to diagnose ERF in climate models (Forster et al., 2016). ERF can be calculated by regressing global mean surface temperature change against the TOA radiative flux change in abrupt forcing simulations (Gregory, 2004). Alternatively, ERF can be isolated by fixing sea surface temperatures to inhibit surface temperature dependent feedbacks (Hansen et al., 2005). This definition includes the effects of changes in land surface temperature in the ERF calculation. It has also been suggested to fix both land and sea surface temperatures to provide a more useful predictive measure of ERF (Shine et al., 2003). However, fixing land temperatures is more difficult to implement in models that include physical and biological processes at the land surface and requires prescription of additional parameters. Therefore, in some models it can be difficult to obtain results which are a good predictor of the climate response when also fixing land temperature (Hansen et al., 2005).

### 1.4.2 Forcing Agents

There are a large number of anthropogenic and natural forcing agents which can alter the global energy balance and thus affect the climate. Greenhouse gases (GHGs) drive warming primarily through enhanced atmospheric absorption of longwave radiation. GHGs reduce the outgoing longwave radiation at the TOA, and increase by a smaller amount the downwelling longwave radiation at the surface. This reduces the net radiative cooling of the atmosphere, and the climate system as a whole. In response, surface temperature increase to restore balance in the Earth's energy budget. Carbon dioxide is the largest contributor to present day ERF since the preindustrial period due to significant anthropogenic emissions increasing atmospheric concentrations (Myhre et al., 2013).

Carbon dioxide is a well-mixed greenhouse gas (WMGHG), meaning it is homogeneously distributed due to its long atmospheric lifetime. Other WMGHGs that are important for the climate include methane, nitrous oxide and halocarbons (Myhre et al., 2013). Greenhouse gases with shorter atmospheric lifetimes, such as ozone, produce more heterogeneous forcing patterns (Myhre et al., 2013).

Atmospheric aerosols can affect the Earth's energy budget both through their radiative properties (aerosol-radiation interactions) and due to their role as cloud condensation nuclei (CCN) and ice nuclei (IN) (aerosol-cloud interactions) (Boucher et al., 2013). Different aerosol species can drive very different radiative forcing responses depending on their radiative and microphysical properties. Two of the most important aerosol species for observed climate change since the preindustrial period are sulphate and black carbon, which are the focus of various analyses in this thesis. Sulphate is mainly a scattering aerosol across the solar spectrum, and therefore reduces the net downwelling shortwave radiation both at the TOA and surface (Ramanathan et al., 2001). Sulphate also acts as CCN and IN (Twomey, 1974), and therefore affects the atmospheric energy budget through aerosol-cloud interactions. Increased sulphate concentrations can increase the albedo of clouds through increasing the number of small cloud droplets (Twomey, 1977). Smaller cloud droplets may also reduce precipitation efficiency and increase the lifetime of clouds (Rosenfeld et al., 2008).

Black carbon is a strong absorber of shortwave radiation, so an increased abundance reduces downwelling shortwave radiation at the surface and increases net

downwelling shortwave radiation at the TOA (Bond et al., 2013). As a result, black carbon strongly heats the atmosphere, but has a weaker effect on surface temperature (Stjern et al., Submitted). Black carbon can also affect cloud properties through a variety of processes. Changes in the vertical temperature structure of the troposphere can affect cloud distribution (semi-direct effect), changes in the number concentration of CCN and IN can affect cloud albedo and lifetime and by changing phase partitioning and precipitation in mixed-phase clouds (Bond et al., 2013). However the effects of black carbon on clouds remain highly uncertain (Boucher et al., 2013).

The total global mean ERF due to anthropogenic drivers between 1750 and 2011 is estimated to be 2.3 (1.1 to 3.3)  $\text{W m}^{-2}$ , with a positive contribution from WMGHGs of 2.83 (2.26 to 3.40)  $\text{W m}^{-2}$ , and negative contributions of -0.45 (-0.95 to +0.05)  $\text{W m}^{-2}$  from aerosol-radiation interactions, and -0.45 (-1.2 to 0.0)  $\text{W m}^{-2}$  from aerosol-cloud interactions (Myhre et al., 2013).

Natural forcing agents can also drive changes in the atmospheric energy budget, such as volcanic forcing and solar irradiance. Volcanic eruptions can significantly reduce the net downwelling shortwave radiation at the TOA and surface due to injection of  $\text{SO}_2$  into the stratosphere (Forster et al., 2007). Similarly changes in solar irradiance alter the incoming shortwave radiation at the TOA.

## **1.5 Adjustment and feedback framework**

### **1.5.1 Concept and utility**

Precipitation is directly affected by individual forcing agents (Lambert and Faull, 2007; Andrews et al., 2010b; Kvalevåg et al., 2013), as well as global warming (Held and Soden, 2006; Previdi, 2010). On a global scale this is well understood through energetic arguments. The response of global mean precipitation to forcing can be separated into a forcing-dependent adjustment, and a temperature-driven feedback (Bala et al., 2009; Andrews et al., 2010b; Kvalevåg et al., 2013; MacIntosh et al., 2016; Samset et al., 2016). The adjustment is due to changes in the atmospheric energy budget driven by the direct radiative effects of the forcing agent, as well as rapid adjustments of the troposphere and land surface (Gregory and Webb, 2008; Wyant et al., 2012; Sherwood et al., 2015), which are independent of global mean surface

temperature change. The feedback response is due to radiative feedbacks driven by changes in global mean surface temperature (Previdi, 2010).

The adjustment and feedback framework explains the different apparent hydrological sensitivities in response to different forcing agents (Andrews et al., 2010b; Kvalevåg et al., 2013; Fläschner et al., 2016). The apparent hydrological sensitivity here refers to the precipitation change per unit global mean surface temperature change, without separating out any non-linear effects independent of temperature change. The variation in apparent hydrological sensitivities is almost entirely a result of the forcing-dependent adjustments. For example, carbon dioxide produces a smaller increase in global mean precipitation than solar forcing for a given surface warming (Andrews et al., 2010b; Samset et al., 2016). This is because carbon dioxide significantly enhances atmospheric LW absorption, which is balanced by a reduction in latent heating, and consequently a negative precipitation adjustment. In contrast, solar forcing has little effect on atmospheric absorption, and therefore only drives precipitation change through the temperature-driven feedback. After the initial adjustment, the feedback response per unit Kelvin (hydrological sensitivity) is very consistent between the forcing agents, as shown in Figure 1.3.

The adjustment and feedback framework is vital in understanding projected global precipitation changes. A simple energetically constrained adjustment and feedback model can be used to accurately emulate historical and 21st century global mean precipitation changes predicted by current climate models (Thorpe and Andrews, 2014).

There is much less understanding of precipitation adjustments on a regional scale. Most previous work on regional precipitation change has not separated out adjustment and feedback responses. However, recent studies have shown that precipitation adjustments can play a significant role in the regional precipitation response to forcing (Bony et al., 2013; Samset et al., 2016). The adjustment component may contribute significantly to the long-term precipitation response in many regions (Samset et al., 2016). Understanding the mechanisms that drive the spatial pattern of precipitation adjustments is important for improving understanding of regional precipitation change.

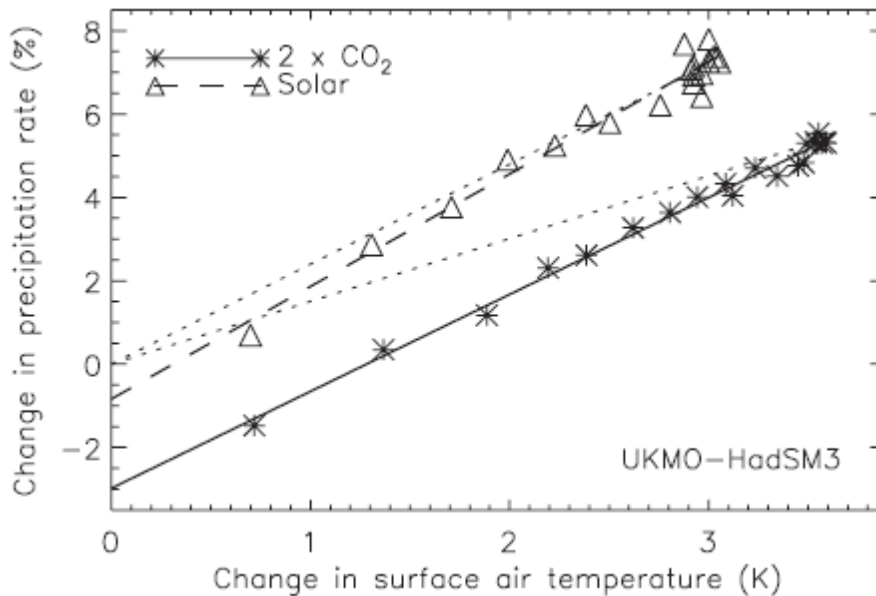


**Figure 1.3:** The change in global mean precipitation against global mean change in surface air temperature for HadSM3 abrupt doubling of CO<sub>2</sub> and 2% increase in insolation. (Taken from Andrews et al. 2009)

### 1.5.2 Computation Methods

There is no definitive method for making the decomposition into precipitation adjustment and feedback components. There are a range of methods which can be used to calculate the terms, similar to the ERF computation methods outlined in section 1.4.1. These include using fixed sea surface temperature (SST) experiments (Bala et al., 2009; Andrews et al., 2010b; Samset et al., 2016; Tian et al., 2016), linear regression of precipitation change against surface temperature change (Lambert and Faull, 2007; Andrews et al., 2009), or separating based on timescale (Cao et al., 2012; Bony et al., 2013). However, these different methods result in subtly different adjustment and feedback definitions. Chapter 2 investigates how different methodological choices affect results and uncertainties, and how they relate to physical understanding.

Fixing both land and sea surface temperatures in model simulations could also be used to isolate the rapid adjustment, as Shine et al. (2003) showed for calculating ERF. However, as noted in section 1.4.1, fixing land surface temperatures is difficult to implement in a consistent manner in models which include physical and biological

processes at the land surface (Hansen et al., 2005). In addition, given that the atmosphere and land surface respond on a similar timescale, which is distinct from the slower ocean response, it may not be physically useful to separate them. Fixing both land and sea temperatures to isolate the adjustment component is therefore not investigated in this thesis.

## 1.6 Regional Precipitation Change Mechanisms

### 1.6.1 Response to Warming

Various mechanisms have been identified by which warming drives regional precipitation change. At large scales over the oceans, precipitation change exhibits a ‘wet-get-wetter’ and ‘dry-get-drier’ spatial pattern (Mitchell et al., 1987; Held and Soden, 2006; Chou et al., 2009; Seager et al., 2010). This arises due to the higher atmospheric water vapour content with warming. The saturation vapour pressure can be related to temperature using the Clausius-Clapeyron relation as shown in equation 1.6.

$$\frac{de_s}{dT} = \frac{L_v}{RT^2} \equiv \alpha(T), \quad (1.6)$$

where,  $e_s$  is the saturation vapour pressure,  $T$  is temperature,  $L_v$  is the latent heat of vaporization and  $R$  is the gas constant. For typical temperatures in the lower troposphere,  $\alpha \approx 0.07 \text{ K}^{-1}$ . Therefore the saturation vapour pressure increases by approximately 7% per Kelvin of temperature increase. As a result, the existing atmospheric circulation transports more moisture from dry regions to wet regions, creating a wet-get-wetter and dry-get-drier pattern of change. The wet-get-wetter mechanism is incorporated in the thermodynamic component of equation 1.5.

The WeGW mechanism is partially counteracted, particularly in dry regions, by an expected slowdown of atmospheric circulation due to changes in dry static stability with warming (Chou et al., 2009; Chadwick et al., 2013). Globally, precipitation can be approximated in terms of convective mass flux from the boundary layer to the free troposphere using equation 1.7.

$$P \approx Mq_b, \quad (1.7)$$

where,  $P$  is precipitation,  $M$  is mass flux from the boundary layer to the free troposphere, and  $q_b$  is a typical boundary layer water vapour mixing ratio. Given that lower tropospheric specific humidity is expected to increase by approximately  $7\% \text{ K}^{-1}$ , yet global mean precipitation is expected to increase at a rate of  $1\text{-}3\% \text{ K}^{-1}$  due to the energetic constraints discussed in section 1.3.2, this implies a weakening of circulation,  $M$ .

The ‘warmer-get-wetter’ (WaGW) mechanism drives significant local deviations from the WeGW pattern (Xie et al., 2010; Huang, 2013; Chadwick et al., 2014). Sea surface temperatures in the tropics tend to warm more in regions where winds are weak, and consequently have a smaller damping effect on warming. In addition, the larger increase in land temperatures compared to the oceans can also influence atmospheric circulation and precipitation (Joshi et al., 2007). However, understanding of regional precipitation change over land remains low (Boucher et al., 2013), and soil moisture-precipitation feedbacks remain uncertain in global climate models (Hohenegger et al., 2009).

### 1.6.2 Response to Forcing

Forcing agents can drive regional precipitation adjustments independent of global mean surface temperature change as discussed in section 1.4.  $\text{CO}_2$  has been shown to have a strong direct effect on tropical circulation (Bony et al., 2013; Merlis, 2015). Bony et al. (2013) suggest that the reduced net atmospheric cooling weakens tropical overturning circulation. Rapid warming of the land surface in response to  $\text{CO}_2$  is also thought to produce shifts in tropical circulation patterns due to the land-sea thermal contrast (Chadwick et al., 2014; Tian et al., 2016). Samset et al. (2016) showed that a range climate forcings, including greenhouse gases and aerosols, can drive significant precipitation adjustments in various regions (Samset et al., 2016). However, the regional adjustment processes are not well understood.

$\text{CO}_2$  causes rapid adjustments in precipitation not only due to radiative effects, but also due to effects on plant stomata (Cao et al., 2009; Andrews et al., 2010a). Higher  $\text{CO}_2$  concentrations mean plant stomata do not open as wide, resulting in reduced evapotranspiration flux to the atmosphere, known as the  $\text{CO}_2$  physiological effect (Field et al., 1995; Sellers et al., 1996; Betts et al., 1997). This effect tends to reduce precipitation over forested regions, particularly in the tropics (Andrews et al., 2010a).

Aerosols can have complex interactions with key tropical dynamical systems affecting local precipitation. The spatially heterogeneous nature of aerosols means that local precipitation change is highly sensitive to the location of the forcing (Shindell et al., 2012). Various studies have linked aerosols with historical drying in the Sahel (Ackerley et al., 2011; Kawase et al., 2011). Reduced precipitation over southern Africa has been attributed to drying of the atmosphere due to local black carbon and organic carbon emissions (Hodnebrog et al., 2016). Aerosols can affect the position of the inter-tropical convergence zone due to the hemispheric asymmetry of the forcing, thus shifting tropical precipitation patterns (Ridley et al., 2015).

Aerosols are thought to have complex interactions with tropical monsoon systems, with a large number of studies investigating the Asian monsoon systems (Ramanathan et al., 2005; Meehl et al., 2008; Bollasina et al., 2011, 2014; Guo et al., 2015). Negative surface forcing due to aerosols is thought to reduce the meridional SST gradient and reduce surface evaporation over land (Ramanathan et al., 2005; Bollasina et al., 2011; Ganguly et al., 2012; Guo et al., 2015). This weakens the South Asian summer monsoon circulation and reduces the associated precipitation.

Black carbon is thought to be a key aerosol species in affecting the South Asian monsoon, but there are significant uncertainties (Meehl et al., 2008; Ramanathan and Carmichael, 2008; Bond et al., 2013). Atmospheric heating from absorbing aerosols (e.g. black carbon and dust) may induce a water cycle feedback via the Elevated Heat Pump (EHP) effect (Lau et al., 2006). According to the EHP hypothesis, during the early monsoon period aerosol driven atmospheric heating over the Indo-Gangetic Plain and central India enhances rising motion and increases advection of moisture to northern India and the Himalayan foothills. This may drive enhanced precipitation in the early monsoon season, but reduced precipitation later in the season (Lau and Kim, 2006; Meehl et al., 2008; Bollasina et al., 2013). Aerosol impacts on the East Asian monsoon are even more complex due to the influence of various natural and anthropogenic aerosol sources and greater scale of the monsoon system (Rosenfeld et al., 2014).

In addition to their radiative effects aerosols can also affect precipitation through their role as cloud condensation nuclei (CCN) and ice nuclei (IN) (Ramanathan et al., 2001; Rosenfeld et al., 2008, 2014; Tao Wei-Kao, 2012; Boucher et al., 2013). In regions of



low aerosol loading increased aerosol concentration leads to an increase in droplet concentration and decrease in droplet size, but the magnitude of this effect remains uncertain (Boucher et al., 2013). How the changes in droplet characteristics affect precipitation is complex and depends on various parameters.

In warm-rain formation smaller rain droplets are expected to suppress light precipitation due to lower fall speeds, smaller collision efficiencies and narrowing of the cloud droplet size spectrum (Albrecht, 1989; Boucher et al., 2013). Conversely, delaying the onset of precipitation and the formation of ice particles may invigorate or intensify convective storms due to changes in the vertical distribution and total amount of latent heating (Koren et al., 2005; Rosenfeld et al., 2008, 2014; Tao Wei-Kao, 2012; Alizadeh-Choobari and Gharaylou, 2017). There is some evidence for effects on convective precipitation intensity from both modelling and observations (Koren et al., 2005, 2014; Rosenfeld et al., 2014; Alizadeh-Choobari and Gharaylou, 2017), but the magnitude and sign of the effects remain highly uncertain. Aerosol-cloud interactions are highly complex and the effects on precipitation remain highly uncertain (Boucher et al., 2013).

### **1.7 Thesis aims and structure**

This thesis aims to use analysis of the local atmospheric energy budget to improve understanding of how forcing agents affect regional precipitation patterns through both rapid adjustments and temperature-driven feedbacks. The precipitation response to a range of drivers will be assessed through targeted climate simulations using the Met Office Hadley Centre Global Environment Model version 2 (HadGEM2) (Martin et al., 2011), as well as output from the Coupled Model Intercomparison Project Phase 5 (CMIP5) (Taylor et al., 2011), and the Precipitation Driver and Response Model Intercomparison Project (PDRMIP) (Myhre et al., 2016). A summary of the specific aims and content for each chapter is given below.

Chapter 2 assesses different computation methods for separating precipitation adjustment and feedback components in response to forcing. There is currently no definitive method for making the decomposition, with different studies using a variety of techniques. Current methods employed include fixing sea surface temperatures,

using linear regression of precipitation change against surface temperature change, or separating based on timescale. This chapter quantifies the effects of different methodological choices on the adjustment and feedback results and uncertainties, and how they relate to physical understanding on both global and regional scales. The analysis focuses on the responses of two global climate models (HadGEM2 and CESM1-CAM4) to five different forcing scenarios.

Chapter 3 investigates the mechanisms which drive the spatial pattern of the precipitation adjustment in response to CO<sub>2</sub> and aerosol forcing in CMIP5 models. The precipitation and energy budget responses to CO<sub>2</sub>, sulphate and all anthropogenic aerosol are analysed using fixed sea surface temperature simulations for 16 global climate models. This chapter determines the key processes driving spatial changes in the tropics and mid-latitudes, and how they differ between forcings. Regions where the spatial pattern of change is robust between models are established.

Chapter 4 analyses the global, land and sea mean precipitation and energy budget responses to five forcing agents (CO<sub>2</sub>, CH<sub>4</sub>, SO<sub>4</sub>, black carbon and solar), across the Precipitation Driver and Response Model Intercomparison Project (PDRMIP) model ensemble. This chapter establishes how global mean precipitation adjustment and feedback responses are partitioned between land and sea, and uses analysis of the atmospheric energy budget to understand the processes driving change, and isolate sources of uncertainty. The PDRMIP results are used to assess the extent to which historical and projected precipitation changes over land and sea can be emulated using a simple model based on the adjustment and feedback framework. The simple model is compared with CMIP5 ensemble mean output and observational datasets. The simple model is used to try and isolate the contribution of different drivers to historical and future precipitation change over land and sea.

Chapter 5 investigates the influence of different atmospheric drivers on Amazonian precipitation, and in particular the physiological forcing of CO<sub>2</sub>. The Amazon rainforest is a key component of the climate system but precipitation projections are uncertain and poorly understood. This chapter assesses the sensitivity of Amazonian rainfall change to five forcing agents across the PDRMIP models. Analysis of the atmospheric energy and moisture budgets is used to understand the mechanisms driving change. The effects of CO<sub>2</sub> physiological forcing are isolated using CMIP5

## Chapter 1: Introduction

---

simulations. This chapter aims to quantify the contribution of CO<sub>2</sub> physiological forcing to projected Amazonian precipitation change.

Chapter 6 provides a summary and discussion of the findings outlined in chapters 2-5, as well as recommendations for future research. Appendices include the supplementary materials for chapters 2-5.

## References – Chapter 1

- Ackerley, D., Booth, B.B.B., Knight, S.H.E., Highwood, E.J., Frame, D.J., Allen, M.R., Rowell, D.P., 2011. Sensitivity of Twentieth-Century Sahel Rainfall to Sulfate Aerosol and CO<sub>2</sub> Forcing. *J. Clim.* 24, 4999–5014. doi:10.1175/JCLI-D-11-00019.1
- Albrecht, B.A., 1989. Aerosols, Cloud Microphysics, and Fractional Cloudiness. *Science* (80-. ). 245, 1227–1230. doi:10.1126/science.245.4923.1227
- Alizadeh-Choobari, O., Gharaylou, M., 2017. Aerosol impacts on radiative and microphysical properties of clouds and precipitation formation. *Atmos. Res.* 185, 53–64. doi:10.1016/j.atmosres.2016.10.021
- Allan, R.P., Liu, C., Zahn, M., Lavers, D. a., Koukouvagias, E., Bodas-Salcedo, A., 2014. Physically Consistent Responses of the Global Atmospheric Hydrological Cycle in Models and Observations. *Surv. Geophys.* 35, 533–552. doi:10.1007/s10712-012-9213-z
- Allen, M.R., Ingram, W.J., 2002. Constraints on future changes in climate and the hydrologic cycle. *Nature* 419, 224–232. doi:10.1038/nature01092
- Andrews, T., Doutriaux-Boucher, M., Boucher, O., Forster, P.M., 2010a. A regional and global analysis of carbon dioxide physiological forcing and its impact on climate. *Clim. Dyn.* 36, 783–792. doi:10.1007/s00382-010-0742-1
- Andrews, T., Forster, P.M., 2008. CO<sub>2</sub> forcing induces semi-direct effects with consequences for climate feedback interpretations. *Geophys. Res. Lett.* 35, L04802. doi:10.1029/2007GL032273
- Andrews, T., Forster, P.M., Boucher, O., Bellouin, N., Jones, A., 2010b. Precipitation, radiative forcing and global temperature change. *Geophys. Res. Lett.* 37, doi:10.1029/2010GL043991
- Andrews, T., Forster, P.M., Gregory, J.M., 2009. A Surface Energy Perspective on Climate Change. *J. Clim.* 22, 2557–2570. doi:10.1175/2008JCLI2759.1
- Andrews, T., Gregory, J.M., Forster, P.M., Webb, M.J., 2011. Cloud Adjustment and its Role in CO<sub>2</sub> Radiative Forcing and Climate Sensitivity: A Review. *Surv. Geophys.* 33, 619–635. doi:10.1007/s10712-011-9152-0
- Arkin, P. a, Smith, T.M., Sapiano, M.R.P., Janowiak, J., 2010. The observed sensitivity of the global hydrological cycle to changes in surface temperature. *Environ. Res. Lett.* 5, 35201. doi:10.1088/1748-9326/5/3/035201
- Bala, G., Caldeira, K., Nemani, R., 2009. Fast versus slow response in climate change: implications for the global hydrological cycle. *Clim. Dyn.* 35, 423–434. doi:10.1007/s00382-009-0583-y
- Betts, A. R., Cox, P. M., Lee, S.E., 1997. Contrasting Physiological and Structural Vegetation Feedbacks in Climate Change Simulations. *Nature* 387, 796–799.

doi:10.1038/42924

- Bollasina, M.A., Ming, Y., Ramaswamy, V., 2013. Earlier onset of the Indian monsoon in the late twentieth century : The role of anthropogenic aerosols 40, 3715–3720. doi:10.1002/grl.50719
- Bollasina, M.A., Ming, Y., Ramaswamy, V., Schwarzkopf, M.D., Naik, V., 2014. Contribution of local and remote anthropogenic aerosols to the twentieth century weakening of the South Asian Monsoon. *Geophys. Res. Lett.* 41, 680–687. doi:10.1002/2013GL058183
- Bollasina, M. a, Ming, Y., Ramaswamy, V., 2011. Anthropogenic aerosols and the weakening of the South Asian summer monsoon. *Science* 334, 502–5. doi:10.1126/science.1204994
- Bond, T.C., Doherty, S.J., Fahey, D.W., Forster, P.M., Berntsen, T., Deangelo, B.J., Flanner, M.G., Ghan, S., K?rcher, B., Koch, D., Kinne, S., Kondo, Y., Quinn, P.K., Sarofim, M.C., Schultz, M.G., Schulz, M., Venkataraman, C., Zhang, H., Zhang, S., Bellouin, N., Guttikunda, S.K., Hopke, P.K., Jacobson, M.Z., Kaiser, J.W., Klimont, Z., Lohmann, U., Schwarz, J.P., Shindell, D., Storelvmo, T., Warren, S.G., Zender, C.S., 2013. Bounding the role of black carbon in the climate system: A scientific assessment. *J. Geophys. Res. Atmos.* 118, 5380–5552. doi:10.1002/jgrd.50171
- Bony, S., Bellon, G., Klocke, D., Sherwood, S., Fermepin, S., Denvil, S., 2013. Robust direct effect of carbon dioxide on tropical circulation and regional precipitation. *Nat. Geosci.* 6, 447–451. doi:10.1038/ngeo1799
- Boucher, O., Randall, D., Artaxo, P., Bretherton, C., Feingold, G., Forster, P., Kerminen, V.-M.V.-M., Kondo, Y., Liao, H., Lohmann, U., Rasch, P., Satheesh, S.K., Sherwood, S., Stevens, B., Zhang, X.Y., Zhan, X.Y., 2013. Clouds and Aerosols. *Clim. Chang.* 2013 Phys. Sci. Basis. Contrib. Work. Gr. I to Fifth Assess. Rep. Intergov. Panel Clim. Chang. doi:10.1017/CBO9781107415324.016
- Cao, L., Bala, G., Caldeira, K., 2012. Climate response to changes in atmospheric carbon dioxide and solar irradiance on the time scale of days to weeks. *Environ. Res. Lett.* 7, 34015. doi:10.1088/1748-9326/7/3/034015
- Cao, L., Bala, G., Caldeira, K., Nemani, R., Ban-Weiss, G., 2009. Climate response to physiological forcing of carbon dioxide simulated by the coupled Community Atmosphere Model (CAM3.1) and Community Land Model (CLM3.0). *Geophys. Res. Lett.* 36, 1–5. doi:10.1029/2009GL037724
- Chadwick, R., Boutle, I., Martin, G., 2013. Spatial Patterns of Precipitation Change in CMIP5: Why the Rich Do Not Get Richer in the Tropics. *J. Clim.* 26, 3803–3822. doi:10.1175/JCLI-D-12-00543.1
- Chadwick, R., Good, P., Andrews, T., Martin, G., 2014. Surface warming patterns drive tropical rainfall pattern responses to CO<sub>2</sub> forcing on all timescales. *Geophys. Res. Lett.* 41, 610–615. doi:10.1002/2013GL058504

- Chadwick, R., Good, P., Martin, G., Rowell, D.P., 2015. Large rainfall changes consistently projected over substantial areas of tropical land. *Nat. Clim. Chang.* 1–6. doi:10.1038/nclimate2805
- Chou, C., Neelin, J., 2004. Mechanisms of global warming impacts on regional tropical precipitation. *J. Clim.* 2688–2701.
- Chou, C., Neelin, J.D., Chen, C.-A., Tu, J.-Y., 2009. Evaluating the “Rich-Get-Richer” Mechanism in Tropical Precipitation Change under Global Warming. *J. Clim.* 22, 1982–2005. doi:10.1175/2008JCLI2471.1
- Chung, E.-S., Soden, B.J., 2015. An assessment of methods for computing radiative forcing in climate models. *Environ. Res. Lett.* 10, 74004. doi:10.1088/1748-9326/10/7/074004
- Emori, S., 2005. Dynamic and thermodynamic changes in mean and extreme precipitation under changed climate. *Geophys. Res. Lett.* 32, L17706. doi:10.1029/2005GL023272
- Field, C.B., Jackson, R.B., Mooney, H.A., 1995. Stomatal responses to increased CO<sub>2</sub>: implications from the plant to the global scale. *Plant, Cell Environ.* 18, 1214–1225. doi:10.1111/j.1365-3040.1995.tb00630.x
- Fläschner, D., Mauritsen, T., Stevens, B., 2016. Understanding the intermodel spread in global-mean hydrological sensitivity. *J. Clim.* 29, 801–817. doi:10.1175/JCLI-D-15-0351.1
- Forster, P., Ramaswamy, V., Artaxo, P., Berntsen, T., Betts, R., Fahey, D.W., Haywood, J., Lean, J., Lowe, D.C., Myhre, G., Nganga, J., Prinn, R., Raga, G., Schulz, M., Van Dorland, R., 2007. Changes in Atmospheric Constituents and in Radiative Forcing. *Clim. Chang. 2007 Phys. Sci. Basis. Contrib. Work. Gr. I to Fourth Assess. Rep. Intergov. Panel Clim. Chang.* doi:10.1103/PhysRevB.77.220407
- Forster, P.M., Richardson, T.B., Maycock, A.C., Smith, C.J., Samset, B.H., Myhre, G., Andrews, T., Pincus, R., Schulz, M., 2016. Recommendations for diagnosing effective radiative forcing from climate models for CMIP6. *J. Geophys. Res. Atmos.* 121, 12,460–12,475. doi:10.1002/2016JD025320
- Ganguly, D., Rasch, P.J., Wang, H., Yoon, J., 2012. Fast and slow responses of the South Asian monsoon system to anthropogenic aerosols. *Geophys. Res. Lett.* 39, n/a-n/a. doi:10.1029/2012GL053043
- Gregory, J., Webb, M., 2008. Tropospheric adjustment induces a cloud component in CO<sub>2</sub> forcing. *J. Clim.* 2, 1–20.
- Gregory, J.M., 2004. A new method for diagnosing radiative forcing and climate sensitivity. *Geophys. Res. Lett.* 31, L03205. doi:10.1029/2003GL018747
- Greve, P., Orlowsky, B., Mueller, B., Sheffield, J., Reichstein, M., Seneviratne, S.I., 2014. Global assessment of trends in wetting and drying over land. *Nat. Geosci.* 7, 716–721. doi:10.1038/ngeo2247

- Guo, L., Turner, A.G., Highwood, E.J., 2015. Impacts of 20th century aerosol emissions on the South Asian monsoon in the CMIP5 models. *Atmos. Chem. Phys.* 15, 6367–6378. doi:10.5194/acp-15-6367-2015f
- Hansen, J., Sato, M., Ruedy, R., Nazarenko, L., Lacis, a., Schmidt, G. a., Russell, G., Aleinov, I., Bauer, M., Bauer, S., Bell, N., Cairns, B., Canuto, V., Chandler, M., Cheng, Y., Del Genio, a., Faluvegi, G., Fleming, E., Friend, a., Hall, T., Jackman, C., Kelley, M., Kiang, N., Koch, D., Lean, J., Lerner, J., Lo, K., Menon, S., Miller, R., Minnis, P., Novakov, T., Oinas, V., Perlwitz, J., Perlwitz, J., Rind, D., Romanou, a., Shindell, D., Stone, P., Sun, S., Tausnev, N., Thresher, D., Wielicki, B., Wong, T., Yao, M., Zhang, S., 2005. Efficacy of climate forcings. *J. Geophys. Res. D Atmos.* 110, 1–45. doi:10.1029/2005JD005776
- Hartmann, D.J., Klein Tank, A.M.G., Rusticucci, M., Alexander, L. V, Brönnimann, S., Charabi, Y.A.-R., Dentener, F.J., Dlugokencky, E.J., Easterling, D.R., Kaplan, A., Soden, B.J., Thorne, P.W., Wild, M., Zhai, P., 2013. Observations: Atmosphere and Surface. *Clim. Chang. 2013 Phys. Sci. Basis. Contrib. Work. Gr. I to Fifth Assess. Rep. Intergov. Panel Clim. Chang.* 159–254. doi:10.1017/CBO9781107415324.008
- Held, I., Soden, B., 2006. Robust responses of the hydrological cycle to global warming. *J. Clim.* 5686–5699.
- Hodnebrog, Ø., Myhre, G., Forster, P.M., Sillmann, J., Samset, B.H., 2016. Local biomass burning is a dominant cause of the observed precipitation reduction in southern Africa. *Nat. Commun.* 7, 11236. doi:10.1038/ncomms11236
- Hoekstra, A.Y., Mekonnen, M.M., 2011. The water footprint of humanity. *Proc. Natl. Acad. Sci.* 109, 3232–3237. doi:10.1016/B978-0-12-799968-5.00007-5
- Hohenegger, C., Brockhaus, P., Bretherton, C.S., Schär, C., 2009. The Soil Moisture–Precipitation Feedback in Simulations with Explicit and Parameterized Convection. *J. Clim.* 22, 5003–5020. doi:10.1175/2009JCLI2604.1
- Huang, P., 2013. Regional response of annual-mean tropical rainfall to global warming. *Atmos. Sci. Lett.* 5, n/a-n/a. doi:10.1002/asl2.475
- Joshi, M.M., Gregory, J.M., Webb, M.J., Sexton, D.M.H., Johns, T.C., 2007. Mechanisms for the land/sea warming contrast exhibited by simulations of climate change. *Clim. Dyn.* 30, 455–465. doi:10.1007/s00382-007-0306-1
- Kawase, H., Takemura, T., Nozawa, T., 2011. Impact of carbonaceous aerosols on precipitation in tropical Africa during the austral summer in the twentieth century. *J. Geophys. Res.* 116, D18116. doi:10.1029/2011JD015933
- Knutti, R., Sedláček, J., 2012. Robustness and uncertainties in the new CMIP5 climate model projections. *Nat. Clim. Chang.* 3, 369–373. doi:10.1038/nclimate1716
- Koren, I., Dagan, G., Altaratz, O., 2014. From aerosol-limited to invigoration of

- warm convective clouds. *Science* (80-. ). 344, 1143–1146.  
doi:10.1126/science.1252595
- Koren, I., Kaufman, Y.J., Rosenfeld, D., Remer, L.A., Rudich, Y., 2005. Aerosol invigoration and restructuring of Atlantic convective clouds. *Geophys. Res. Lett.* 32, 1–4. doi:10.1029/2005GL023187
- Kvalevåg, M.M., Samset, B.H., Myhre, G., 2013. Hydrological sensitivity to greenhouse gases and aerosols in a global climate model. *Geophys. Res. Lett.* 40, 1432–1438. doi:10.1002/grl.50318
- Lambert, F.H., Faull, N.E., 2007. Tropospheric adjustment: The response of two general circulation models to a change in insolation. *Geophys. Res. Lett.* 34, L03701. doi:10.1029/2006GL028124
- Lambert, F.H., Webb, M.J., 2008. Dependency of global mean precipitation on surface temperature. *Geophys. Res. Lett.* 35, L16706.  
doi:10.1029/2008GL034838
- Lau, K., Kim, K., 2006. Observational relationships between aerosol and Asian monsoon rainfall , and circulation 33, 1–5. doi:10.1029/2006GL027546
- Lau, K.M., Kim, M.K., Kim, K.M., 2006. Asian summer monsoon anomalies induced by aerosol direct forcing: The role of the Tibetan Plateau. *Clim. Dyn.* 26, 855–864. doi:10.1007/s00382-006-0114-z
- MacIntosh, C.R., Allan, R.P., Baker, L.H., Bellouin, N., Collins, W., Mousavi, Z., Shine, K.P., 2016. Contrasting fast precipitation responses to tropospheric and stratospheric ozone forcing. *Geophys. Res. Lett.* 43, 1263–1271.  
doi:10.1002/2015GL067231
- Martin, G.M., Bellouin, N., Collins, W.J., Culverwell, I.D., Halloran, P.R., Hardiman, S.C., Hinton, T.J., Jones, C.D., McDonald, R.E., McLaren, a. J., O'Connor, F.M., Roberts, M.J., Rodriguez, J.M., Woodward, S., Best, M.J., Brooks, M.E., Brown, a. R., Butchart, N., Dearden, C., Derbyshire, S.H., Dharssi, I., Doutriaux-Boucher, M., Edwards, J.M., Falloon, P.D., Gedney, N., Gray, L.J., Hewitt, H.T., Hobson, M., Huddleston, M.R., Hughes, J., Ineson, S., Ingram, W.J., James, P.M., Johns, T.C., Johnson, C.E., Jones, a., Jones, C.P., Joshi, M.M., Keen, a. B., Liddicoat, S., Lock, a. P., Maidens, a. V., Manners, J.C., Milton, S.F., Rae, J.G.L., Ridley, J.K., Sellar, a., Senior, C. a., Totterdell, I.J., Verhoef, a., Vidale, P.L., Wiltshire, a., 2011. The HadGEM2 family of Met Office Unified Model climate configurations. *Geosci. Model Dev.* 4, 723–757. doi:10.5194/gmd-4-723-2011
- Meehl, G. A., Arblaster, J.M., Collins, W.D., 2008. Effects of Black Carbon Aerosols on the Indian Monsoon. *J. Clim.* 21, 2869–2882.  
doi:10.1175/2007JCLI1777.1
- Merlis, T.M., 2015. Direct weakening of tropical circulations from masked CO<sub>2</sub> radiative forcing. *Proc. Natl. Acad. Sci.* 112, 13167–13171.  
doi:10.1073/pnas.1508268112



- Mitchell, J., Wilson, C., Cunnington, W., 1987. On CO<sub>2</sub> climate sensitivity and model dependence of results. *Q. J. R. Meteorol. Soc.* 113, 293–322. doi:10.1256/smsqj.47516
- Muller, C.J., O’Gorman, P. a., 2011. An energetic perspective on the regional response of precipitation to climate change. *Nat. Clim. Chang.* 1, 266–271. doi:10.1038/nclimate1169
- Myhre, G., Forster, P.M., Samset, B.H., Hodnebrog, Ø., Sillmann, J., Aalbergstjø, S.G., Andrews, T., Boucher, O., Faluvegi, G., Fläschner, D., Iversen, T., Kasoar, M., Kharin, V., Kirkevåg, A., Lamarque, J.-F., Olivié, D., Richardson, T.B., Shindell, D., Shine, K.P., Stjern, C.W., Takemura, T., Voulgarakis, A., Zwiers, F., 2016. PDRMIP: A Precipitation Driver and Response Model Intercomparison Project, Protocol and preliminary results. *Bull. Am. Meteorol. Soc. BAMS-D-16-0019.1*. doi:10.1175/BAMS-D-16-0019.1
- Myhre, G., Shindell, D., Bréon, F.-M., Collins, W., Fuglestedt, J., Huang, J., Koch, D., Lamarque, J.-F., Lee, D., Mendoza, B., Nakajima, T., Robock, A., Stephens, G., Takemura, T., Zhang, H., 2013. Anthropogenic and Natural Radiative Forcing, in: *Intergovernmental Panel on Climate Change (Ed.), Climate Change 2013 - The Physical Science Basis*. Cambridge University Press, Cambridge, pp. 659–740. doi:10.1017/CBO9781107415324.018
- O’Gorman, P.A., Allan, R.P., Byrne, M.P., Previdi, M., 2011. Energetic Constraints on Precipitation Under Climate Change. *Surv. Geophys.* 33, 585–608. doi:10.1007/s10712-011-9159-6
- Pendergrass, A.G., Hartmann, D.L., 2014. The Atmospheric Energy Constraint on Global-Mean Precipitation Change. *J. Clim.* 27, 757–768. doi:10.1175/JCLI-D-13-00163.1
- Piao, S., Ciais, P., Huang, Y., Shen, Z., Peng, S., Li, J., Zhou, L., Liu, H., Ma, Y., Ding, Y., Friedlingstein, P., Liu, C., Tan, K., Yu, Y., Zhang, T., Fang, J., 2010. The impacts of climate change on water resources and agriculture in China. *Nature* 467, 43–51. doi:10.1038/nature09364
- Previdi, M., 2010. Radiative feedbacks on global precipitation. *Environ. Res. Lett.* 5, 25211. doi:10.1088/1748-9326/5/2/025211
- Ramanathan, V., Carmichael, G., 2008. Global and regional climate changes due to black carbon. *Nat. Geosci.* 1, 221–227. doi:10.1038/ngeo156
- Ramanathan, V., Chung, C., Kim, D., Bettge, T., Buja, L., Kiehl, J.T., Washington, W.M., Fu, Q., Sikka, D.R., Wild, M., 2005. Atmospheric brown clouds: impacts on South Asian climate and hydrological cycle. *Proc. Natl. Acad. Sci. U. S. A.* 102, 5326–33. doi:10.1073/pnas.0500656102
- Ramanathan, V., Crutzen, P.J., Kiehl, J.T., Rosenfeld, D., 2001. Aerosols, climate, and the hydrological cycle. *Science* 294, 2119–24. doi:10.1126/science.1064034
- Ramaswamy, V., Boucher, O., Haigh, J., Hauglustaine, D., Haywood, J., Myhre, G.,

- Nakajima, T., Shi, G., Solomon, S., Betts, R.E., Charlson, R., Chuang, C.C., Daniel, J.S., Del Genio, A.D., Feichter, J., Fuglestedt, J., Forster, P.M., Ghan, S.J., Jones, A., Kiehl, J.T., Koch, D., Land, C., Lean, J., Lohmann, U., Minschwaner, K., Penner, J.E., Roberts, D.L., Rodhe, H., Roelofs, G.-J., Rotstayn, L.D., Schneider, T.L., Schumann, U., Schwartz, S.E., Schwartzkopf, M.D., Shine, K.P., Smith, S.J., Stevenson, D.S., Stordal, F., Tegen, I., van Dorland, R., Zhang, Y., Srinivasan, J., Joos, F., 2001. Radiative Forcing of Climate Change, *Climate Change 2001: The Scientific Basis*.
- Ridley, H.E., Asmerom, Y., Baldini, J.U.L., Breitenbach, S.F.M., Aquino, V. V., Prüfer, K.M., Culleton, B.J., Polyak, V., Lechleitner, F.A., Kennett, D.J., Zhang, M., Marwan, N., Macpherson, C.G., Baldini, L.M., Xiao, T., Peterkin, J.L., Awe, J., Haug, G.H., 2015. Aerosol forcing of the position of the intertropical convergence zone since AD 1550. *Nat. Geosci.* 8, 195–200. doi:10.1038/ngeo2353
- Rosenfeld, D., Andreae, M.O., Asmi, A., Chin, M., Leeuw, G., Donovan, D.P., Kahn, R., Kinne, S., Kivekäs, N., Kulmala, M., Lau, W., Schmidt, K.S., Suni, T., Wagner, T., Wild, M., Quaas, J., 2014. Global observations of aerosol-cloud-precipitation- climate interactions. *Rev. Geophys* 52, 750–808. doi:10.1002/2013RG000441.Received
- Rosenfeld, D., Lohmann, U., Raga, G.B., O’Dowd, C.D., Kulmala, M., Fuzzi, S., Reissell, A., Andreae, M.O., 2008. Flood or drought: how do aerosols affect precipitation? *Science* 321, 1309–13. doi:10.1126/science.1160606
- Samset, B.H., Myhre, G., Forster, P.M., Hodnebrog, Ø., Andrews, T., Faluvegi, G., Fläschner, D., Kasoar, M., Kharin, V., Kirkevåg, A., Lamarque, J.-F., Olivie, D., Richardson, T.B., Shindell, D., Shine, K.P., Takemura, T., Voulgarakis, A., 2016. Fast and slow precipitation responses to individual climate forcings: A PDRMIP multi-model study. *Geophys. Res. Lett.* doi:10.1002/2016GL068064
- Seager, R., Naik, N., Vecchi, G.A., 2010. Thermodynamic and dynamic mechanisms for large-scale changes in the hydrological cycle in response to global warming. *J. Clim.* 23, 4651–4668. doi:10.1175/2010JCLI3655.1
- Sellers, P.J., Bounoua, L., Collatz, G.J., Randall, D.A., Dazlich, D.A., Los, S.O., Berry, J.A., Fung, I., Tucker, C.J., Field, C.B., Jensen, T.G., 1996. Comparison of Radiative and Physiological Effects of Doubled Atmospheric CO<sub>2</sub> on Climate. *Science* (80- ). 271, 1402–1406. doi:10.1126/science.271.5254.1402
- Shepherd, T.G., 2014. Atmospheric circulation as a source of uncertainty in climate change projections. *Nat. Geosci.* 7, 703–708. doi:10.1038/ngeo2253
- Sherwood, S.C., Bony, S., Boucher, O., Bretherton, C., Forster, P.M., Gregory, J.M., Stevens, B., 2015. Adjustments in the forcing-feedback framework for understanding climate change. *Bull. Am. Meteorol. Soc.* 96, 217–228. doi:10.1175/BAMS-D-13-00167.1
- Shindell, D.T., Voulgarakis, A., Faluvegi, G., Milly, G., 2012. Precipitation response to regional radiative forcing. *Atmos. Chem. Phys.* 12, 6969–6982.

doi:10.5194/acp-12-6969-2012

Shine, K.P., Cook, J., Highwood, E.J., Joshi, M.M., 2003. An alternative to radiative forcing for estimating the relative importance of climate change mechanisms. *Geophys. Res. Lett.* 30, n/a-n/a. doi:10.1029/2003GL018141

Stephens, G.L., L'Ecuyer, T., Forbes, R., Gettleman, A., Golaz, J.-C., Bodas-Salcedo, A., Suzuki, K., Gabriel, P., Haynes, J., 2010. Dreary state of precipitation in global models. *J. Geophys. Res.* 115, D24211. doi:10.1029/2010JD014532

Stevens, B., Bony, S., 2013. What are Climate Models Missing? *Science* (80-. ). 340, 1053–1054.

Stjern, C.W., Samset, B.H., Myhre, G., Forster, P.M., Hodnebrog, Ø., Sillmann, J., Andrews, T., Boucher, O., Faluvegi, G., Iversen, T., Kasoar, M., Kharin, V., Kirkevåg, A., Lamarque, J.-F., Olivié, D., Richardson, T.B., Shindell, D., Shine, K.P., Smith, C., Takemura, T., Voulgarakis, A., Zwiers, F., Submitted. Rapid adjustments cause weak surface temperature response to increased black carbon concentrations.

Stocker, T.F., Plattner, G.-K., Tignor, M.M.B., Allen, S.K., Boschung, J., Nauels, A., Xia, Y., Bex, V., Midgley, P.M., 2014. *Climate Change 2013 - The Physical Science Basis*. Cambridge University Press, Cambridge. doi:10.1017/CBO9781107415324

Tao Wei-Kao, 2012. Impact of Aerosols on Convective clouds and Precipitation. *Rev. Geophys.* doi:10.1029/2011RG000369.1.INTRODUCTION

Taylor, K.E., Stouffer, R.J., Meehl, G. A., 2011. A Summary of the CMIP5 Experiment Design 4, 1–33.

Thorpe, L., Andrews, T., 2014. The physical drivers of historical and 21st century global precipitation changes. *Environ. Res. Lett.* 9, 64024. doi:10.1088/1748-9326/9/6/064024

Tian, D., Dong, W., Gong, D., Guo, Y., Yang, S., 2016. Fast responses of climate system to carbon dioxide, aerosols and sulfate aerosols without the mediation of SST in the CMIP5. *Int. J. Climatol.* doi:10.1002/joc.4763

Trenberth, K.E., Fasullo, J.T., Kiehl, J., 2009. Earth's Global Energy Budget. *Bull. Am. Meteorol. Soc.* 90, 311–323. doi:10.1175/2008BAMS2634.1

Trenberth, K.E., Stepaniak, D.P., 2003. Covariability of components of poleward atmospheric energy transports on seasonal and interannual timescales. *J. Clim.* 16, 3691–3705. doi:10.1175/1520-0442(2003)016<3691:COCOPA>2.0.CO;2

Twomey, S., 1977. The Influence of Pollution on the Shortwave Albedo of Clouds. *J. Atmos. Sci.* doi:10.1175/1520-0469(1977)034<1149:TIOPOT>2.0.CO;2

Twomey, S., 1974. Pollution and the Planetary Albedo. *Atmos. Environ.* 41, 120–125. doi:10.1016/j.atmosenv.2007.10.062

- Wake, B., 2013. Flooding costs. *Nat. Clim. Chang.* 3, 778–778. doi:10.1038/nclimate1997
- Wild, M., Liepert, B., 2010. The Earth radiation balance as driver of the global hydrological cycle. *Environ. Res. Lett.* 25203. doi:10.1088/1748-9326/5/2/025003
- Wyant, M.C., Bretherton, C.S., Blossey, P.N., Khairoutdinov, M., 2012. Fast cloud adjustment to increasing CO<sub>2</sub> in a superparameterized climate model. *J. Adv. Model. Earth Syst.* 4, M05001. doi:10.1029/2011MS000092
- Xie, S.-P., Deser, C., Vecchi, G. A., Ma, J., Teng, H., Wittenberg, A.T., 2010. Global Warming Pattern Formation: Sea Surface Temperature and Rainfall. *J. Clim.* 23, 966–986. doi:10.1175/2009JCLI3329.1

## **Chapter 2: An Assessment of Precipitation Adjustment and Feedback Computation Methods**

Published in the Journal of Geophysical Research:  
Atmospheres (2016)



## RESEARCH ARTICLE

10.1002/2016JD025625

## Key Points:

- Important physical and quantitative differences in precipitation adjustment and feedback results arise due to computation method
- Fixed SST method provides a consistent and clear mechanistic decomposition
- Fixed SST method is less dependent on methodological choices and exhibits less variability

## Supporting Information:

- Supporting Information S1

## Correspondence to:

T. B. Richardson,  
eetbr@leeds.ac.uk

## Citation:

Richardson, T. B., B. H. Samset, T. Andrews, G. Myhre, and P. M. Forster (2016), An assessment of precipitation adjustment and feedback computation methods, *J. Geophys. Res. Atmos.*, *121*, 11,608–11,619, doi:10.1002/2016JD025625.

Received 11 JUL 2016

Accepted 26 SEP 2016

Accepted article online 28 SEP 2016

Published online 14 OCT 2016

©2016. The Authors.

This is an open access article under the terms of the Creative Commons Attribution License, which permits use, distribution and reproduction in any medium, provided the original work is properly cited.

## An assessment of precipitation adjustment and feedback computation methods

T. B. Richardson<sup>1</sup>, B. H. Samset<sup>2</sup>, T. Andrews<sup>3</sup>, G. Myhre<sup>2</sup>, and P. M. Forster<sup>1</sup>

<sup>1</sup>School of Earth and Environment, University of Leeds, Leeds, UK, <sup>2</sup>Center for International Climate and Environmental Research, Oslo, Norway, <sup>3</sup>Met Office Hadley Centre, Exeter, UK

**Abstract** The precipitation adjustment and feedback framework is a useful tool for understanding global and regional precipitation changes. However, there is no definitive method for making the decomposition. In this study we highlight important differences which arise in results due to methodological choices. The responses to five different forcing agents (CO<sub>2</sub>, CH<sub>4</sub>, SO<sub>4</sub>, black carbon, and solar insolation) are analyzed using global climate model simulations. Three decomposition methods are compared: using fixed sea surface temperature experiments (fSST), regressing transient climate change after an abrupt forcing (regression), and separating based on timescale using the first year of coupled simulations (YR1). The YR1 method is found to incorporate significant SST-driven feedbacks into the adjustment and is therefore not suitable for making the decomposition. Globally, the regression and fSST methods produce generally consistent results; however, the regression values are dependent on the number of years analyzed and have considerably larger uncertainties. Regionally, there are substantial differences between methods. The pattern of change calculated using regression reverses sign in many regions as the number of years analyzed increases. This makes it difficult to establish what effects are included in the decomposition. The fSST method provides a more clear-cut separation in terms of what physical drivers are included in each component. The fSST results are less affected by methodological choices and exhibit much less variability. We find that the precipitation adjustment is weakly affected by the choice of SST climatology.

### 1. Introduction

Global mean precipitation is tightly constrained by the tropospheric energy budget, whereby the latent heat released from precipitation balances tropospheric cooling [Mitchell, 1983; Allen and Ingram, 2002; O’Gorman et al., 2011; Pendergrass and Hartmann, 2014]. As a result, the change in global mean precipitation in response to forcing can be decomposed into a rapid adjustment and feedback response. The adjustment is due to direct changes in atmospheric cooling in response to the forcing and any associated rapid adjustments in the climate system which affect the atmospheric energy budget, such as rapid changes in atmospheric temperature, water vapor, and clouds [Lambert and Faull, 2007; Bala et al., 2009; Andrews et al., 2010]. The feedback response is driven by surface temperature-dependent radiative feedbacks [Previdi, 2010]. The decomposition is highly useful for understanding the different hydrological responses to different forcing agents [Andrews et al., 2010; Cao et al., 2011; Kravitz et al., 2013; Kvalevåg et al., 2013; Fläschner et al., 2016; Samset et al., 2016]. The simple energetically constrained adjustment and feedback model can be used to accurately emulate historical and 21st century global mean precipitation changes predicted by general circulation models [Thorpe and Andrews, 2014]. A recent study [Cao et al., 2015] found that the linear combination of adjustment and feedback can be used to emulate precipitation change predicted by climate models under different CO<sub>2</sub> and solar forcing scenarios.

One problem with the adjustment and feedback framework is that there is no definitive method for making the decomposition. There are a range of methods which can be used to calculate the precipitation adjustment and feedback components. These include using fixed sea surface temperature (SST) experiments [Bala et al., 2009; Andrews et al., 2010; Richardson et al., 2016; Samset et al., 2016; Tian et al., 2016], linear regression of precipitation change against surface temperature change [Lambert and Faull, 2007; Andrews et al., 2009], or separating based on timescale [Cao et al., 2012; Bony et al., 2013]. However, these different methods result in subtly different adjustment and feedback definitions. It is not well understood how the results and uncertainties vary between methods. It is important to understand the effects of different methodological choices on the adjustment and feedback framework and how they relate to physical understanding.

On regional scales the decomposition becomes more complicated as local precipitation is strongly influenced by circulation changes [Bony *et al.*, 2013; Chadwick *et al.*, 2013; Huang, 2013; Richardson *et al.*, 2016]. As a result any surface temperature change which may be included in the rapid adjustment calculation can strongly affect the spatial pattern of precipitation change [Chadwick *et al.*, 2014; Richardson *et al.*, 2016]. This makes the regional decomposition nontrivial, and careful consideration is required for methodology. In this study we compare methods for calculating adjustment and feedback precipitation responses to five different forcing scenarios, on global and regional scales using two global climate models.

## 2. Methods

### 2.1. Adjustment and Feedback Calculation

Three different methodologies are analyzed for decomposing the precipitation adjustment and feedback terms in response to forcing: using fixed sea surface temperature experiments (fSST), separating based on timescale (YR1), and linear regression during transient climate change (regression). The decomposition is used to aid physical understanding, and there is no true value with which to compare. In this study we compare how the different methods affect the physical interpretation of results and assess their usefulness based on error characteristics and consistency.

#### 2.1.1. fSST Method

The adjustment component can be estimated using fixed sea surface temperature experiments (fSST) [Bala *et al.*, 2009; Andrews *et al.*, 2010]. In these simulations the fixed SST inhibits oceanic temperature-dependent feedbacks, thus isolating the adjustment component. Land surface temperatures can change, which will influence the precipitation adjustment. The feedback response ( $\Delta P_{fb}$ ) is calculated by subtracting the fixed SST precipitation change ( $\Delta P_{ra}$ ) from the total response in fully coupled simulations ( $\Delta P_{tot}$ ). The hydrological sensitivity (precipitation feedback per unit kelvin) is calculated by dividing the feedback response by global mean surface temperature change, as shown in equation (1). It should be noted that this differs from the apparent hydrological sensitivity [Fläschner *et al.*, 2016; Samset *et al.*, 2016] which is the total precipitation response per unit kelvin.

$$HS = \frac{\Delta P_{fb}}{\Delta T_{tot} - \Delta T_{ra}} = \frac{\Delta P_{tot} - \Delta P_{ra}}{\Delta T_{tot} - \Delta T_{ra}} \quad (1)$$

where HS is the hydrological sensitivity,  $\Delta P_{fb}$  is the precipitation feedback response,  $\Delta P_{tot}$  is the total precipitation response,  $\Delta P_{ra}$  is the precipitation adjustment,  $\Delta T_{tot}$  is the total surface temperature response, and  $\Delta T_{ra}$  is any surface temperature change included in the adjustment calculation. Fully coupled climate models can take millennia to reach true equilibrium after large step forcings [Caldeira and Myhrvold, 2013]; however, this is not necessary for calculating the precipitation feedback per unit temperature change (hydrological sensitivity). For slab ocean model simulations, as used for CESM1-CAM4, a shorter time period is required to reach a new equilibrium (several decades). Here the total precipitation/temperature response is taken as the mean change 50 years after introducing a forcing, by which time significant temperature change has occurred. In our uncertainty analysis the meaning period is adjusted in length along with the fSST integration length.

#### 2.1.2. Regression Method

The adjustment and hydrological sensitivity can also be estimated through linear regression during transient climate change [Gregory and Webb, 2008; Andrews *et al.*, 2009], hereafter denoted as the “regression” method. By regressing precipitation change against global mean surface temperature change after an abrupt forcing, the adjustment is given by the intercept and the hydrological sensitivity obtained from the slope. This methodology implies that no global mean surface temperature effects are included in the adjustment component. However, it has been noted that rapid SST change can produce a spatial pattern with zero global mean but which still affects the atmospheric energy budget [Andrews *et al.*, 2015]. This method has typically only been used for global mean analysis; however, we will also assess the suitability of regression for local precipitation. The local precipitation at each grid point is regressed against the global mean temperature change to calculate the regional adjustment and hydrological sensitivity.

#### 2.1.3. YR1 Method

The precipitation response to forcing can also be separated based on timescale [Cao *et al.*, 2012; Bony *et al.*, 2013], defining the adjustment as any changes which occur within a designated time period after a forcing is applied. Following Bony *et al.* [2013], we take the first year precipitation response as the adjustment, hereafter

denoted as the “YR1” method. Using this method, any change in precipitation which occurs within 1 year of an abrupt forcing is included. Consequently, some changes in precipitation driven by surface temperature change are included in the adjustment component, as both land and sea surface temperatures are free to change. The feedback response can be calculated by subtracting the first year response ( $\Delta P_{ra}$ ) from the total response ( $\Delta P_{tot}$ ). The total response is calculated using the mean change in precipitation for years 51–70 in the abrupt forcing coupled simulations. The hydrological sensitivity is then calculated by dividing the feedback response by surface temperature change, as shown in equation (1).

### 2.2. Simulations

We analyze simulations from the Precipitation Driver Response Model Intercomparison Project (PDRMIP) [Samset et al., 2016]. The uncertainty analysis focuses on output from HadGEM2 [Martin et al., 2011] and CESM1-CAM4 [Neale et al., 2010; Gent et al., 2011] for which extended runs were performed. Data from nine PDRMIP models (CanESM2, GISS-E2-R, HadGEM2, HadGEM3, MPI-ESM, CESM1-CAM4, CESM1-CAM5, NorESM1, and MIROC-SPRINTARS) are used for an overall comparison of the three methods (Figure 3). For details on PDRMIP protocols, see Samset et al. [2016]. Five different abrupt forcing scenarios were implemented: a doubling of CO<sub>2</sub> concentration (2xCO<sub>2</sub>), tripling of CH<sub>4</sub> concentration (3xCH<sub>4</sub>), 2% increase in solar insolation (SOL), 5 times SO<sub>4</sub> concentration or emissions (5xSO<sub>4</sub>), and 10 times black carbon concentration or emissions (10xBC).

HadGEM2 and CESM1 implemented the scenarios with some differences, so responses would not be expected to be quantitatively similar. HadGEM2 used a preindustrial baseline for all simulations, whereas CESM1 used a present-day baseline. For the aerosol experiments HadGEM2 scaled emissions, whereas CESM1 scaled concentrations based on AeroCom Phase II [see, e.g., Samset et al., 2013]. In addition, HadGEM2 employed a fully coupled ocean model, whereas CESM1 used a slab-ocean model. All simulations were performed both with sea surface temperatures held fixed (fSST) and coupled to an ocean. The fSST simulations were run for 30 years and the coupled runs for 100 years. Five 20 year coupled 2xCO<sub>2</sub> ensemble runs were also performed in CESM1.

An additional set of simulations were performed using HadGEM2 to investigate the effect of SST climatology on the precipitation adjustment. Two fixed SST simulations with CO<sub>2</sub> levels quadrupled were run for 20 years, one with preindustrial SST climatology (sstClim4xCO<sub>2</sub>) and one with a uniform increase of 4 K from preindustrial SST climatology (sstClim4K4xCO<sub>2</sub>). Corresponding baseline simulations were run for the two SST climatologies, denoted sstClim and sstClim4K, respectively. The precipitation adjustment was calculated as the difference between the forced run and corresponding control run averaged across the full 20 years.

### 2.3. Error Calculations

The standard error for the precipitation adjustment and hydrological sensitivity is computed to compare methods. For fSST simulations equation (2) is used to calculate the standard error (SE), where “ $\sigma$ ” is the standard deviation of the annual mean anomaly and “ $n$ ” is the length (in years) of the run:

$$SE = \frac{\sigma}{\sqrt{n}} \tag{2}$$

Because the coupled runs have not reached true equilibrium, there is still a temperature-dependent trend in the precipitation response. Therefore, the standard deviation ( $\sigma$ ) is computed based solely on the control run. The annual mean standard deviation of the control run is multiplied by the square root of 2 to account for the fact that the precipitation response is the difference between two means.

The standard error for the regression adjustment ( $SE_{ra}$ ) is taken as the standard error of the intercept using equation (3) and the standard error of the hydrological sensitivity ( $SE_{hs}$ ) taken as the standard error of the slope using equation (4):

$$SE_{ra} = \sqrt{\frac{\sum x_i^2 \sum (y_i - \bar{y}_i)^2}{n(n-2) \sum (x_i - \bar{x}_i)^2}} \tag{3}$$

$$SE_{hs} = \sqrt{\frac{\sum (y_i - \bar{y}_i)^2}{(n-2) \sum (x_i - \bar{x}_i)^2}} \tag{4}$$



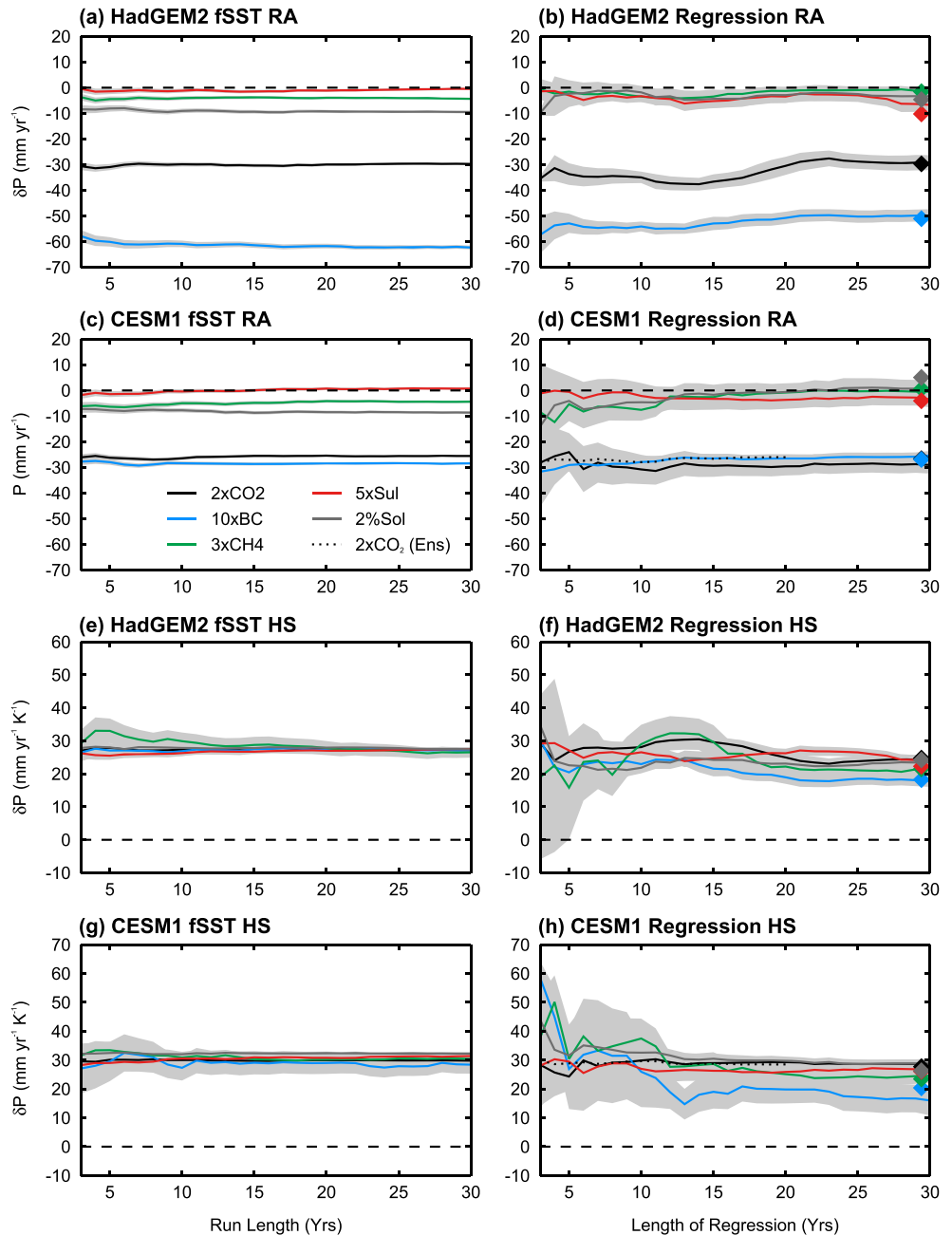


**Figure 1.** Global mean rapid adjustment (RA) and hydrological sensitivity (HS) terms against integration length for (a, c, e, and g) fsST and (b, d, f, and h) regression methods. Results are shown for the five forcing scenarios (colored lines) implemented in HadGEM2 and CESM1. Also shown in the CESM1 regression plots are RA and HS values obtained from regression of five 2xCO<sub>2</sub> ensemble members (dotted line). The grey shading denotes the standard error. Diamonds indicate regression values after 100 years.

where  $x_i$  is temperature change each year,  $y_i$  is precipitation change each year,  $n$  is the number of years regressing over, and overbars denote the average value of that quantity.

### 3. Results and Discussion

#### 3.1. Global Mean Method Comparison

The choice of integration length and regression length impacts on both the adjustment and hydrological sensitivity results and their error characteristics. Figure 1 shows how the precipitation adjustment and

**Table 1.** Hydrological Sensitivity Calculated Using Regression Technique Over Years 1–10 and 11–100 of Abrupt Forcing Simulations for HadGEM2 and CESM1-CAM4<sup>a</sup>

	HadGEM2		CESM1-CAM4	
	Years 1–10	Years 11–100	Years 1–10	Years 11–100
2xCO <sub>2</sub>	28.1 ± 1.5	22.9 ± 1.5	29.9 ± 2.7	22.7 ± 2.9
3xCH <sub>4</sub>	29.0 ± 5.9	21.4 ± 1.9	37.5 ± 6.9	18.4 ± 4.2
5xSul	26.5 ± 1.6	19.5 ± 1.5	27.0 ± 4.4	19.9 ± 4.5
10xBC	23.0 ± 1.9	20.1 ± 2.6	26.0 ± 12.3	20.0 ± 4.0
SOL	21.8 ± 1.7	24.5 ± 2.1	32.6 ± 2.6	19.2 ± 3.9

<sup>a</sup>Uncertainty values are the standard error of the regression slope.

drive smaller temperature changes (see Figure 4), thus resulting in larger errors per unit kelvin. There is also more natural variability associated with the hydrological sensitivity calculation, arising from the coupled ocean. The variation in the fSST hydrological sensitivity is small for all forcing scenarios when using over 15 years for the calculation.

Regression length has a much larger impact on the adjustment and hydrological sensitivity (Figures 1b, 1d, 1f, and 1h). Particularly with a regression length less than 15 years, the adjustment and hydrological sensitivity vary considerably dependent on the number of years analyzed. Using a five-member ensemble for regression reduces the variability (Figures 1d and 1h dotted line). The hydrological sensitivity generally reduces as regression length increases (Figures 1f and 1h), particularly for CESM1. It has previously been shown that top of the atmosphere energy budget feedbacks are not constant in many models following abrupt forcings [Andrews *et al.*, 2012]. The changing hydrological sensitivity with regression length implies that net atmospheric energy budget feedbacks are also not constant throughout the abrupt forcing simulations. Table 1 shows the hydrological sensitivity calculated separately using the first 10 years and the following 90 years of the simulations. For both models the hydrological sensitivity is generally larger when computed using the first 10 years. This slight nonlinearity means that methodological choices will affect results. As a consequence, it should be noted that using a longer regression to improve statistics (as shown in Figure 2) may not be beneficial for capturing the initial adjustment component.

Increasing the integration length and regression length reduces the adjustment and hydrological sensitivity uncertainties (Figure 2). Across most forcing agents a standard error of less than  $1 \text{ mm yr}^{-1}$  for the fSST adjustment can be obtained with a minimum integration length of 8 years. The only exception is 10xBC for HadGEM2 which exhibits a slightly larger variability than the other scenarios. Using the regression method, it is not possible to constrain the adjustment response to within  $1 \text{ mm yr}^{-1}$ , even after 100 years, for any forcing scenario. Using five 20 year ensemble members, regression still fails to constrain the adjustment to within  $1 \text{ mm yr}^{-1}$  (Figure 2d). The fSST adjustment error is not strongly affected by forcing scenario, whereas the regression adjustment error is generally larger for stronger forcings. The YR1 adjustment uncertainty is large due to the short time period ( $4.6 \text{ mm yr}^{-1}$  and  $4.7 \text{ mm yr}^{-1}$  for HadGEM2 and CESM1, respectively). Multiple ensemble members could be used to reduce this uncertainty.

For the hydrological sensitivity regression errors are again larger than the fSST errors; however, the difference is smaller. Errors in the hydrological sensitivity for both methods are strongly influenced by the magnitude of surface temperature change. Forcing scenarios which produce more surface temperature change in the coupled runs (see Figure 4) have smaller errors in the hydrological sensitivity. The use of a five-member ensemble for regression reduces the hydrological sensitivity uncertainty, and a standard error of less than  $1 \text{ mm yr}^{-1}$  can be achieved using 10 years (Figure 2h).

Figure 3 shows the PDRMIP multimodel mean precipitation adjustment and hydrological sensitivity calculated using the fSST, regression, and YR1 methods diagnosed using an integration/regression length of 15 years. Across the forcing scenarios the fSST and regression precipitation adjustments (Figures 3a and 3b) are generally in close agreement. The YR1 adjustments show more disagreement, particularly in response to 2xCO<sub>2</sub> and 5xSul. This is due to the influence of temperature-dependent feedbacks occurring in the first year of coupled simulations. In particular, significant surface temperature change occurs in the first year of the 2xCO<sub>2</sub>, 5xSO<sub>4</sub>, and SOL simulations (Figure 4), which have the largest radiative forcings of the five

hydrological sensitivity vary with changing integration/regression length. For all forcing scenarios the fSST precipitation adjustment is very consistent irrespective of the number of years analyzed (Figures 1a and 1c). Integration length has a larger effect on the fSST hydrological sensitivity (Figures 1e and 1g) in response to 3xCH<sub>4</sub> and 10xBC. This is likely because these forcing scenarios

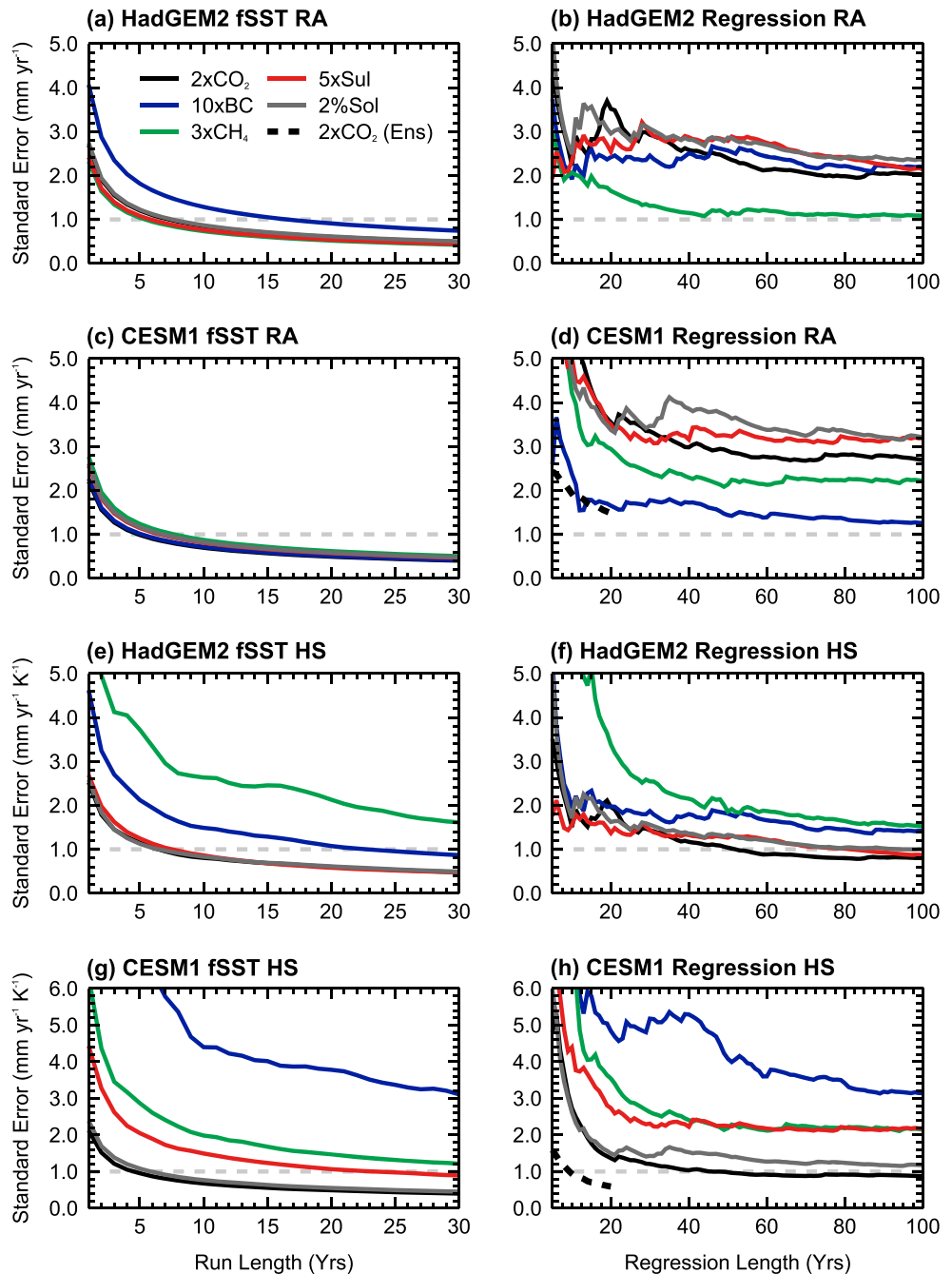


**Figure 2.** Standard error of global mean rapid adjustment (RA) and hydrological sensitivity (HS) values against integration length for (a, c, e, and g) fSST and (b, d, f, and h) regression methods. Results are shown for the five different forcing scenarios (colored lines) implemented for HadGEM2 and CESM1. The dotted line in CESM1 regression plots shows the RA and HS standard error computed using five 2xCO<sub>2</sub> ensemble members.

scenarios. Some surface temperature change also occurs in the fSST experiments, but it is much smaller in magnitude. In addition, accounting for the fSST surface temperature change generally does not bring the adjustment value into better agreement with the alternate methods, also discussed in *Samset et al.* [2016]. Similar findings have been shown in previous studies for top of the atmosphere effective radiative forcing calculated using fSST methods [*Hansen et al., 2005; Sherwood et al., 2015*]. Using a shorter time period, such as 1 month, to calculate the adjustment reduces the incorporation of temperature-dependent effects.

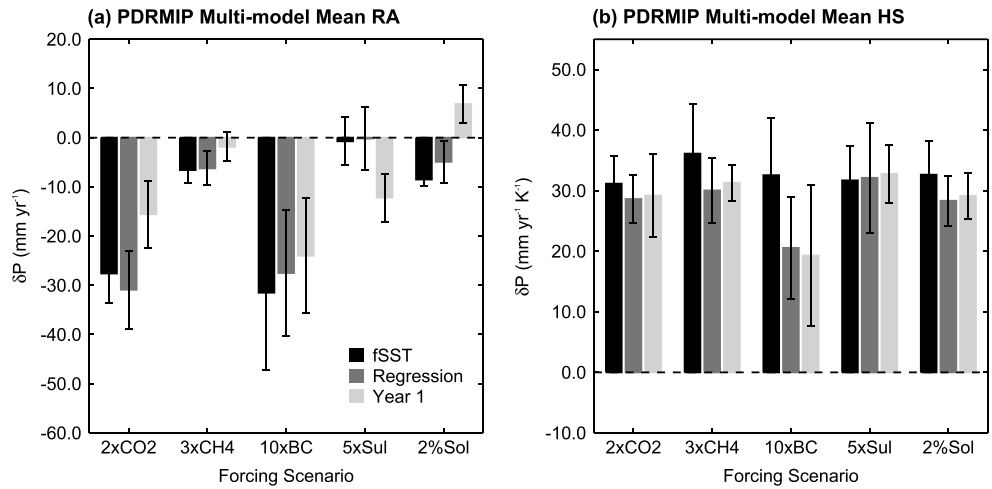


**Figure 3.** PDRMIP multimodel global mean rapid adjustment (RA) and hydrological sensitivity (HS) values across forcing scenarios diagnosed using fSST, regression, and YR1 methods. A run and regression length of 15 years is utilized. Error bars denote the standard deviation of the model spread.

However, the uncertainty becomes very large due to monthly natural variability, and the results differ greatly from the other methods (see supporting information Table S1).

The hydrological sensitivity (Figures 3c and 3d) is mostly consistent between the three methodologies across forcing scenarios, but there are some noteworthy differences. The fSST method gives a systematically larger sensitivity, but the methods generally agree within their uncertainties. There is a notable difference between the 10xBC hydrological sensitivity calculated using fSST and the other methods. The fSST hydrological sensitivity is very consistent with other forcing scenarios, whereas the regression and YR1 values for 10xBC are somewhat lower. The precipitation response to black carbon does not scale as well with surface temperature change in the first few years after introducing a forcing, as seen from the varying hydrological sensitivity with regression length

in Figures 1f and 1h. This could lead to discrepancies between decomposition methods. *Rugenstein et al. [2016]* found that shortwave cloud radiative effects in response to forcing do not scale well with surface temperature and are, in fact, driven by ocean-atmosphere adjustments with a characteristic timescale of a few years. Black carbon strongly affects atmospheric shortwave cooling, and it can be seen that the difference between methods arises mainly from the top of the atmosphere shortwave feedback (see supporting information Figure S7). It should be noted that ocean-driven effects on adjustments will not be included in the fSST adjustment results. For the regression method it is unclear how potential ocean adjustments would be partitioned as they occur over multiple years and do not scale with global surface temperature change.

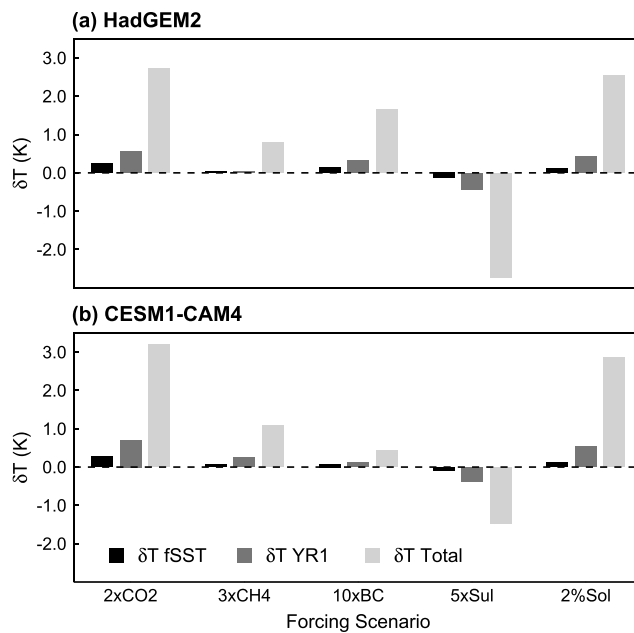


**Figure 4.** Global mean surface temperature change ( $\delta T$ ) in response to the five forcing scenarios for the fSST simulations (averaged over full 30 years), first year of coupled simulations (YR1), and final 50 years of coupled simulations (Total). Results are shown for (a) HadGEM2 and (b) CESM1-CAM4.

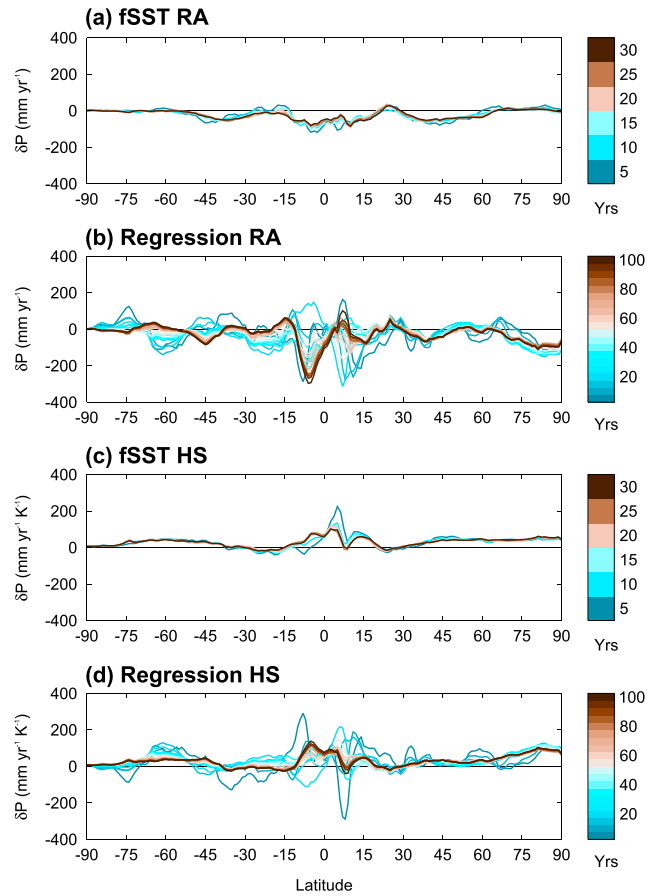


**Figure 5.** HadGEM2 zonally averaged precipitation adjustment (RA) and hydrological sensitivity (HS) in response to 2xCO<sub>2</sub> calculated using (a, c) fSST and (b, d) regression methods. Each shaded line shows the response calculated using an integration/regression length increasing incrementally by 5 years.

### 3.2. Regional Method Comparison

Figure 5 shows how integration/regression length affects the zonal mean precipitation adjustment and hydrological sensitivity in response to doubling CO<sub>2</sub> for HadGEM2. It can be seen that the fSST zonal mean adjustment and hydrological sensitivity are fairly independent of integration length, with only small variations within the tropics. In contrast, the adjustment and sensitivity calculated using regression are highly dependent on the number of years analyzed. Particularly for the adjustment component, in many regions the response is completely reversed as the regression length increases. This is likely because local shifts in precipitation patterns may not scale well with global mean temperature change and therefore lead to erroneous regression results. This makes the choice of regression length very difficult, as increasing the number of years will improve statistics, but may not give a good representation of the initial adjustment. Similar results are seen for CESM1 and the other forcing scenarios (see supporting information Figures S1–S3).

A comparison of the 2xCO<sub>2</sub> regional adjustment and hydrological sensitivity calculated using the three methodologies for CESM1-CAM4 is shown in Figure 6 (for 5xSul and HadGEM2 responses, see supporting information Figures S4–S6). An integration/regression length of 20 years is used for the calculations. The spatial pattern of the adjustment and hydrological sensitivity exhibit significant differences between methods, particularly for the adjustment component. In many regions the methods disagree substantially on the magnitude and sign of precipitation changes. Even the zonally averaged responses exhibit large differences, particularly in the tropics. The regression and YR1 responses have large uncertainties; over most of the globe the signal is smaller than the standard error (stippling denotes where signal is greater than the standard error), particularly for the adjustment component. In contrast, in most regions where large changes occur using the fSST method, the signal is larger than the standard error.

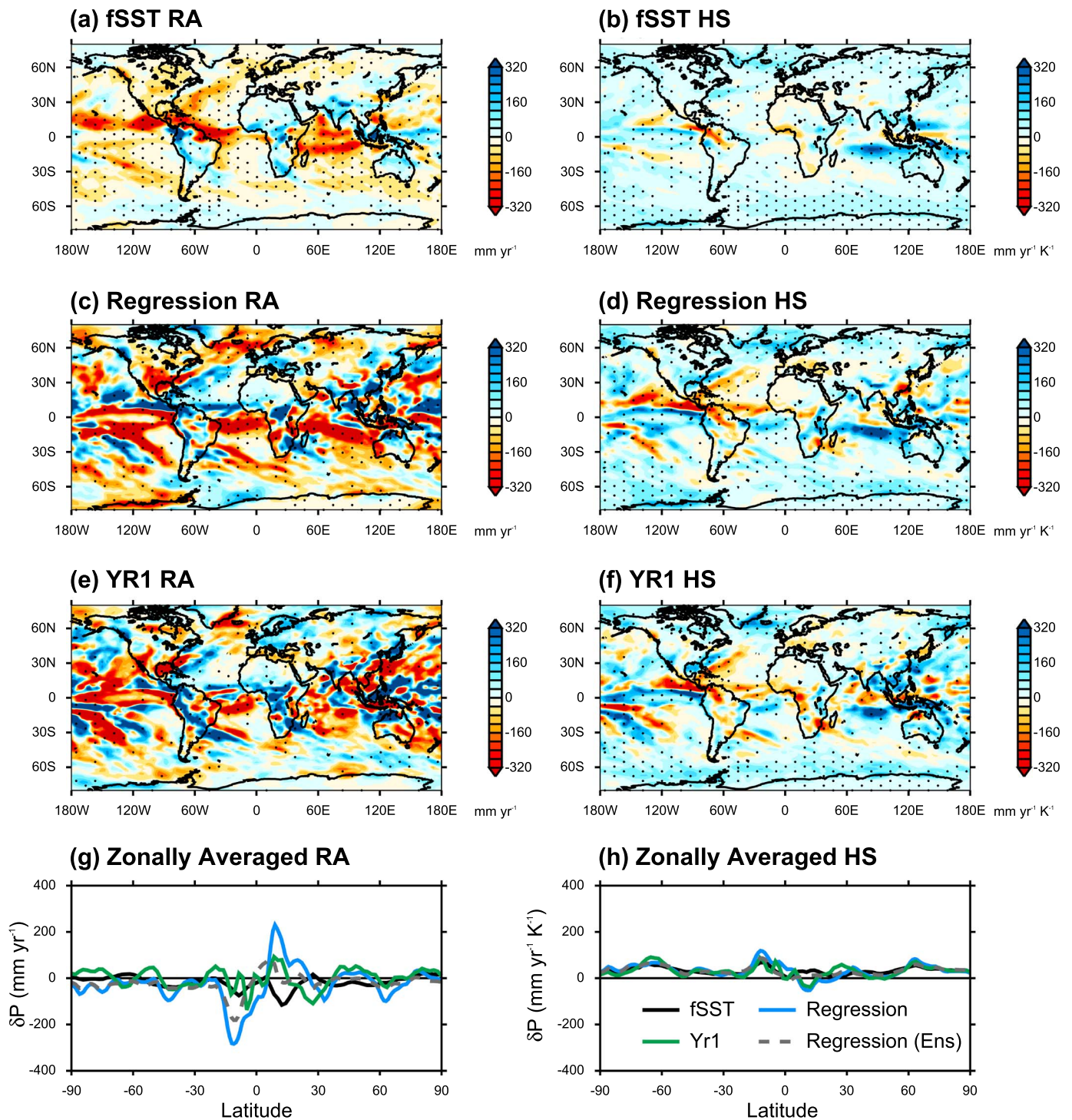


**Figure 6.** CESM1-CAM4 regional (a, c, e, and g) precipitation adjustment (RA) and (b, d, f, and h) hydrological sensitivity (HS) response to doubling CO<sub>2</sub> calculated using fSST (Figures 6a and 6b), regression (Figures 6c and 6d), and YR1 (Figures 6e and 6f) methods. Figures 6g and 6h show the zonally averaged response for all three methods. Stippling shows where the signal is greater than the standard error. An integration/regression length of 20 years is used to compute the responses.

The hydrological sensitivity shows slightly more agreement between methods, especially in the midlatitudes. This is likely because precipitation change is mainly thermodynamically driven in the midlatitudes [Emori, 2005; Seager et al., 2010] and follows global mean temperature change well. In the tropics, however, where dynamic changes play a key role [Chou et al., 2009; Bony et al., 2013], large differences arise. Given that these

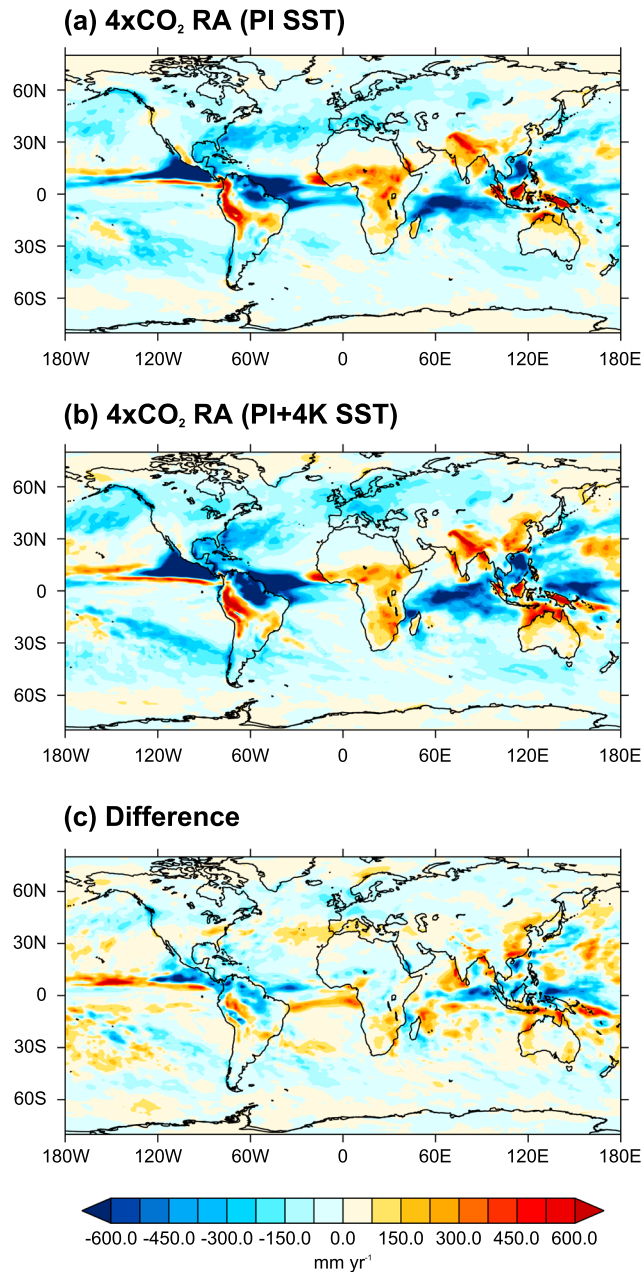


**Figure 7.** HadGEM2 precipitation adjustment in response to quadrupling CO<sub>2</sub> calculated using fixed SST simulations with (a) preindustrial SST climatology, (b) preindustrial plus 4 K SST climatology, and (c) the difference between the two.

### 3.3. SST Climatology

Another methodological choice which must be considered is the base state climatology. To investigate the effect of different sea surface temperature (SST) climatologies, we analyze the precipitation response to quadrupling CO<sub>2</sub> with preindustrial SST climatology, and preindustrial plus 4 K SST climatology, using HadGEM2 as outlined in section 2.2. Globally, there is a small difference in precipitation adjustments, with a reduction of  $-65.0 \pm 0.5 \text{ mm yr}^{-1}$  and  $-73.3 \pm 0.6 \text{ mm yr}^{-1}$  for sstClim4xCO<sub>2</sub> and sstClim4K4xCO<sub>2</sub>, respectively. The difference arises mainly due to the change in longwave cooling of the troposphere (see supporting information Figure S8). In the warmer climate the upwelling longwave radiation at the surface and top of the atmosphere are increased, and the atmospheric temperature and humidity profiles altered. As a result, an

dynamic changes do not necessarily scale well with global mean temperature change, regional regression may not yield useful information within the adjustment and feedback framework. It can be seen in Figure 6 that the pattern of adjustment and hydrological sensitivity using regression tend to be similar but opposite in sign in the tropics. This could be indicative of a statistical artifact arising due to the regression methodology, rather than a physically meaningful result.

The fSST method provides a more clear-cut decomposition in terms of which drivers are included in the precipitation adjustment and feedback components regionally. Within the fSST simulations, only the direct impact of the forcing agent on the troposphere and the effects of land surface temperature change are included. This enables a better mechanistic understanding of what processes drive precipitation change. The YR1 method incorporates significant global surface temperature change over both land and sea into the adjustment and therefore is not a useful tool in separating drivers of precipitation change. The huge variation in regression results as the number of years analyzed changes makes it difficult to understand what effects are being included. In addition, it has previously been noted that rapid SST adjustment in response to CO<sub>2</sub> can produce a spatial pattern of surface temperature change, but with zero global mean [Andrews *et al.*, 2015]. These local SST changes may impact the local precipitation adjustment.

equivalent increase in CO<sub>2</sub> concentration produces a larger reduction in longwave cooling from the atmosphere. Although there is a significant difference in the absolute precipitation response, the percentage change in precipitation is in close agreement, with changes of  $-5.77 \pm 0.04\%$  and  $-5.82 \pm 0.05\%$ .

Figure 7 shows the regional precipitation adjustment for the two experiments and difference between the two. The spatial pattern of the precipitation response is largely unaffected by the different SST climatologies. There are locally some larger differences in precipitation change within the tropics, due to small shifts in the pattern of change resulting from the different SST climatologies. If the spatial pattern of SST climatology was significantly altered, this may have a larger effect on the regional adjustment.

#### 4. Conclusions

The adjustment and feedback framework is a useful tool for understanding global and regional precipitation changes. However, it has been highlighted here that important differences arise in results based upon the decomposition method employed, which are important to understand and consider. Globally, the precipitation adjustment and hydrological sensitivity calculated using fSST and regression methods are generally in good agreement. However, the regression values can vary considerably when using a short regression length (less than  $\sim 20$  years). In addition, the fSST method gives a systematically larger and more consistent hydrological sensitivity. The YR1 method exhibits significant differences to the other methods, particularly in response to doubling CO<sub>2</sub>. This is due to the substantial surface temperature change which occurs within the first year of coupled simulations. The YR1 method is therefore not a very useful tool for making the adjustment and feedback decomposition. Using a shorter timescale, such as 1 month, considerably increases the uncertainty.

The uncertainties associated with the regression method are much larger than for fSST. To an extent this can be improved through the use of ensembles; however, the regression errors for the adjustment in response to 2xCO<sub>2</sub> are still larger with a five-member ensemble. Increasing integration and regression length improves the error characteristics for both fSST and regression methods. Using a fSST integration length of at least 8 years reduces the standard error for the global mean precipitation adjustment to under  $1 \text{ mm yr}^{-1}$ . The errors are larger for the hydrological sensitivity, and a longer integration is recommended.

Regionally, significant differences arise between methods. Using regression, the adjustment and hydrological sensitivity are highly dependent on regression length, with the pattern of change completely reversing in many regions as the number of years increases. This makes it difficult to understand what effects are being represented in the regression decomposition. In contrast, the fSST method gives a consistent spatial pattern of adjustment and hydrological sensitivity irrespective of integration length. The YR1 response includes a high level of noise and is influenced by rapid SST changes within the first year. There is better agreement between methods for the hydrological sensitivity in the midlatitudes, where the precipitation response is thermodynamically driven, scaling well with global mean temperature change.

The choice of SST climatology has a weak effect on the absolute precipitation adjustment. An increase in SST of 4 K increases the magnitude of the global mean precipitation adjustment from  $-65.0 \pm 0.5 \text{ mm yr}^{-1}$  to  $-73.3 \pm 0.6 \text{ mm yr}^{-1}$ . However, the percentage change in precipitation from the control state is in close agreement despite the different SST climatologies. The spatial pattern of precipitation adjustment is largely unaffected by a warmer SST climatology. Locally, in the tropics there are some differences in precipitation change due to small shifts in the pattern of change.

Based on these results, we find that the fSST method provides a more clearly defined separation. The adjustment term includes the direct impact of a forcing agent on the troposphere and the effects of land surface temperature change. The feedback term includes any effects mediated by SST change. The fSST method is less affected by methodological choices and exhibits much less variability. An integration length of at least 15 years is recommended to reduce uncertainties, particularly for regional analysis.

#### References

- Allen, M. R., and W. J. Ingram (2002), Constraints on future changes in climate and the hydrologic cycle, *Nature*, *419*, 224–232, doi:10.1038/nature01092.
- Andrews, T., P. M. Forster, and J. M. Gregory (2009), A surface energy perspective on climate change, *J. Clim.*, *22*(10), 2557–2570, doi:10.1175/2008JCLI2759.1.

#### Acknowledgments

The PDRMIP model output is all publicly available; for data access, visit <http://www.cicero.uio.no/en/PDRMIP/PDRMIP-data-access>. T.R. was supported by a NERC CASE award in collaboration with the Met Office NE/K007483/1. HadGEM2 simulations were performed using the MONSooN system, a collaborative facility supplied under the Joint Weather and Climate Research Programme, which is a strategic partnership between the Met Office and the Natural Environment Research Council. P.M.F. was supported by a Royal Society Wolfson Merit Award and NERC grant NE/K006038/1. T.A. was supported by the Joint UK BEIS/Defra Met Office Hadley Centre Climate Programme (GA01101). B.H.S. and G.M. were funded by the Research Council of Norway, through the grant NAPEX (229778). Supercomputer facilities were provided by NOTUR.



- Andrews, T., P. M. Forster, O. Boucher, N. Bellouin, and A. Jones (2010), Precipitation, radiative forcing and global temperature change, *Geophys. Res. Lett.*, *37*, L14701, doi:10.1029/2010GL043991.
- Andrews, T., J. M. Gregory, M. J. Webb, and K. E. Taylor (2012), Forcing, feedbacks and climate sensitivity in CMIP5 coupled atmosphere-ocean climate models, *Geophys. Res. Lett.*, *39*, L09712, doi:10.1029/2012GL051607.
- Andrews, T., J. M. Gregory, and M. J. Webb (2015), The dependence of radiative forcing and feedback on evolving patterns of surface temperature change in climate models, *J. Clim.*, *28*(4), 1630–1648, doi:10.1175/JCLI-D-14-00545.1.
- Bala, G., K. Caldeira, and R. Nemani (2009), Fast versus slow response in climate change: Implications for the global hydrological cycle, *Clim. Dyn.*, *35*(2–3), 423–434, doi:10.1007/s00382-009-0583-y.
- Bony, S., G. Bellon, D. Kloocke, S. Sherwood, S. Fermepin, and S. Denvil (2013), Robust direct effect of carbon dioxide on tropical circulation and regional precipitation, *Nat. Geosci.*, *6*(6), 447–451, doi:10.1038/ngeo1799.
- Caldeira, K., and N. P. Myhrvold (2013), Projections of the pace of warming following an abrupt increase in atmospheric carbon dioxide concentration, *Environ. Res. Lett.*, *8*(3), 34,039, doi:10.1088/1748-9326/8/3/034039.
- Cao, L., G. Bala, and K. Caldeira (2011), Why is there a short-term increase in global precipitation in response to diminished CO<sub>2</sub> forcing?, *Geophys. Res. Lett.*, *38*, L06703, doi:10.1029/2011GL046713.
- Cao, L., G. Bala, and K. Caldeira (2012), Climate response to changes in atmospheric carbon dioxide and solar irradiance on the time scale of days to weeks, *Environ. Res. Lett.*, *7*(3), 34,015, doi:10.1088/1748-9326/7/3/034015.
- Cao, L., G. Bala, M. Zheng, and K. Caldeira (2015), Fast and slow climate responses to CO<sub>2</sub> and solar forcing: A linear multivariate regression model characterizing transient climate change, *J. Geophys. Res. Atmos.*, *120*, 12,037–12,053, doi:10.1002/2014JD022994. Received.
- Chadwick, R., I. Boutle, and G. Martin (2013), Spatial patterns of precipitation change in CMIP5: Why the rich do not get richer in the tropics, *J. Clim.*, *26*(11), 3803–3822, doi:10.1175/JCLI-D-12-00543.1.
- Chadwick, R., P. Good, T. Andrews, and G. Martin (2014), Surface warming patterns drive tropical rainfall pattern responses to CO<sub>2</sub> forcing on all timescales, *Geophys. Res. Lett.*, *41*, 610–615, doi:10.1002/2013GL058504.
- Chou, C., J. D. Neelin, C.-A. Chen, and J.-Y. Tu (2009), Evaluating the “rich-get-richer” mechanism in tropical precipitation change under global warming, *J. Clim.*, *22*(8), 1982–2005, doi:10.1175/2008JCLI2471.1.
- Emori, S. (2005), Dynamic and thermodynamic changes in mean and extreme precipitation under changed climate, *Geophys. Res. Lett.*, *32*, L17706, doi:10.1029/2005GL023272.
- Fläschner, D., T. Mauritsen, and B. Stevens (2016), Understanding the intermodel spread in global-mean hydrological sensitivity, *J. Clim.*, *29*(2), 801–817, doi:10.1175/JCLI-D-15-0351.1.
- Gent, P. R., et al. (2011), The community climate system model version 4, *J. Clim.*, *24*(19), 4973–4991, doi:10.1175/2011JCLI4083.1.
- Gregory, J., and M. Webb (2008), Tropospheric adjustment induces a cloud component in CO<sub>2</sub> forcing, *J. Clim.*, *21*, 1–20.
- Hansen, J., et al. (2005), Efficacy of climate forcings, *J. Geophys. Res. D Atmos.*, *110*(18), 1–45, doi:10.1029/2005JD005776.
- Huang, P. (2013), Regional response of annual-mean tropical rainfall to global warming, *Atmos. Sci. Lett.*, *15*, 103, doi:10.1002/asl2.475.
- Kravitz, B., et al. (2013), An energetic perspective on hydrological cycle changes in the Geoenvironment Model Intercomparison Project, *J. Geophys. Res. Atmos.*, *118*, 13,087–13,102, doi:10.1002/2013JD020502.
- Kvalevåg, M. M., B. H. Samset, and G. Myhre (2013), Hydrological sensitivity to greenhouse gases and aerosols in a global climate model, *Geophys. Res. Lett.*, *40*, 1432–1438, doi:10.1002/grl.50318.
- Lambert, F. H., and N. E. Faull (2007), Tropospheric adjustment: The response of two general circulation models to a change in insolation, *Geophys. Res. Lett.*, *34*, L03701, doi:10.1029/2006GL028124.
- Martin, G. M., et al. (2011), The HadGEM2 family of Met Office Unified Model climate configurations, *Geosci. Model Dev.*, *4*(3), 723–757, doi:10.5194/gmd-4-723-2011.
- Mitchell, B. (1983), The seasonal response of a general circulation model to changes in CO<sub>2</sub>, and sea temperatures By, *Q. J. R. Meteorol. Soc.*, *109*(459), 113–152.
- Neale, R. B., et al. (2010), Description of the NCAR community atmosphere model (CAM 5.0) *NCAR Tech. Note NCAR/TN-486+ STR*, (April).
- O’Gorman, P. A., R. P. Allan, M. P. Byrne, and M. Previdi (2011), Energetic constraints on precipitation under climate change, *Surv. Geophys.*, *33*(3–4), 585–608, doi:10.1007/s10712-011-9159-6.
- Pendergrass, A. G., and D. L. Hartmann (2014), The atmospheric energy constraint on global-mean precipitation change, *J. Clim.*, *27*(2), 757–768, doi:10.1175/JCLI-D-13-00163.1.
- Previdi, M. (2010), Radiative feedbacks on global precipitation, *Environ. Res. Lett.*, *5*(2), 25,211, doi:10.1088/1748-9326/5/2/025211.
- Richardson, T. B., P. M. Forster, T. Andrews, and D. J. Parker (2016), Understanding the rapid precipitation response to CO<sub>2</sub> and aerosol forcing on a regional scale\*, *J. Clim.*, *29*(2), 583–594, doi:10.1175/JCLI-D-15-0174.1.
- Rugenstein, M. A. A., J. M. Gregory, N. Schaller, J. Sedlacek, and R. Knutti (2016), Oceanic adjustments to radiative forcing, *J. Clim.*, *29*, 5643–5659, doi:10.1175/JCLI-D-16-0312.1.
- Samset, B. H., et al. (2013), Black carbon vertical profiles strongly affect its radiative forcing uncertainty, *Atmos. Chem. Phys.*, *13*(5), 2423–2434, doi:10.5194/acp-13-2423-2013.
- Samset, B. H., et al. (2016), Fast and slow precipitation responses to individual climate forcings: A PDRMIP multi-model study, *Geophys. Res. Lett.*, *43*, 2782–2791, doi:10.1002/2016GL068064.
- Seager, R., N. Naik, and G. A. Vecchi (2010), Thermodynamic and dynamic mechanisms for large-scale changes in the hydrological cycle in response to global warming\*, *J. Clim.*, *23*(17), 4651–4668, doi:10.1175/2010JCLI3655.1.
- Sherwood, S. C., S. Bony, O. Boucher, C. Bretherton, P. M. Forster, J. M. Gregory, and B. Stevens (2015), Adjustments in the forcing-feedback framework for understanding climate change, *Bull. Am. Meteorol. Soc.*, *96*(2), 217–228, doi:10.1175/BAMS-D-13-00167.1.
- Thorpe, L., and T. Andrews (2014), The physical drivers of historical and 21st century global precipitation changes, *Environ. Res. Lett.*, *9*(6), 64,024, doi:10.1088/1748-9326/9/6/064024.
- Tian, D., W. Dong, D. Gong, Y. Guo, and S. Yang (2016), Fast responses of climate system to carbon dioxide, aerosols and sulfate aerosols without the mediation of SST in the CMIP5, *Int. J. Climatol.*, doi:10.1002/joc.4763.

## **Chapter 3: Understanding the Rapid Precipitation Response to CO<sub>2</sub> and Aerosol forcing on a Regional Scale**

Published in the Journal of Climate (2016)

## Understanding the Rapid Precipitation Response to CO<sub>2</sub> and Aerosol Forcing on a Regional Scale\*

THOMAS B. RICHARDSON AND PIERS M. FORSTER

*School of Earth and Environment, University of Leeds, Leeds, United Kingdom*

TIMOTHY ANDREWS

*Met Office Hadley Centre, Exeter, United Kingdom*

DOUG J. PARKER

*School of Earth and Environment, University of Leeds, Leeds, United Kingdom*

(Manuscript received 4 March 2015, in final form 14 October 2015)

### ABSTRACT


Precipitation exhibits a significant rapid adjustment in response to forcing, which is important for understanding long-term climate change. In this study, fixed sea surface temperature (SST) simulations are used to analyze the spatial pattern of the rapid precipitation response. Three different forcing scenarios are investigated using data obtained from phase 5 of CMIP (CMIP5): an abrupt quadrupling of CO<sub>2</sub>, an abrupt increase in sulfate, and an abrupt increase in all anthropogenic aerosol levels from preindustrial to present day. Analysis of the local energy budget is used to understand the mechanisms that drive the observed changes.

It is found that the spatial pattern of the rapid precipitation response to forcing is primarily driven by rapid land surface temperature change, rather than the change in tropospheric diabatic cooling. As a result, the pattern of response due to increased CO<sub>2</sub> opposes that due to sulfate and all anthropogenic aerosols, because of the opposing surface forcing. The rapid regional precipitation response to increased CO<sub>2</sub> is robust among models, implying that the uncertainty in long-term changes is mainly associated with the response to SST-mediated feedbacks. Increased CO<sub>2</sub> causes rapid warming of the land surface, which destabilizes the troposphere, enhancing convection and precipitation over land in the tropics. Precipitation is reduced over most tropical oceans because of a weakening of overturning circulation and a general shift of convection to over land. Over most land regions in the midlatitudes, circulation changes are small. Reduced tropospheric cooling therefore leads to drying over many midlatitude land regions.

### 1. Introduction

Regional precipitation change is one of the most uncertain aspects of climate change prediction (Stephens et al. 2010; Liepert and Previdi 2012; Stevens and Bony

2013) and can have major societal implications (Wake 2013). On a global scale, the precipitation response to a forcing can be understood through atmospheric energy budget arguments (Mitchell et al. 1987; Allen and Ingram 2002; O’Gorman et al. 2012). Tropospheric radiative cooling tightly constrains global precipitation (Pendergrass and Hartmann 2014), leading to a slow sea surface temperature (SST)-dependent response due to radiative feedbacks (Previdi 2010) and a forcing-dependent rapid adjustment (or fast response) due to the near-instantaneous change in atmospheric cooling (Lambert and Faull 2007; Bala et al. 2010; Andrews et al. 2010; Kvalevåg et al. 2013; Kravitz et al. 2013). The rapid

 Denotes Open Access content.

\* Supplemental information related to this paper is available at the Journals Online website: <http://dx.doi.org/10.1175/JCLI-D-15-0174.s1>.

*Corresponding author address:* Thomas B. Richardson, School of Earth and Environment, University of Leeds, Leeds LS2 9JT, United Kingdom.  
E-mail: eetbr@leeds.ac.uk



This article is licensed under a [Creative Commons Attribution 4.0 license](https://creativecommons.org/licenses/by/4.0/).

adjustment is vital for understanding the different hydrological sensitivities between forcing agents (Andrews and Forster 2010; Andrews et al. 2010; Cao et al. 2011).

On a regional scale, precipitation changes are more difficult to predict because of complex variations in circulation patterns (Bony et al. 2013). Many studies on regional precipitation have utilized the water vapor budget (Emori 2005; Bony et al. 2013; Huang et al. 2013) to analyze change. There has been very little previous work on understanding the regional drivers of precipitation as a response to forcing. However, local precipitation change can be understood in a similar fashion to global change, through incorporating horizontal dry static energy transport into the atmospheric energy budget (Muller and O’Gorman 2011). The local energy budget provides a simple framework for analyzing the regional precipitation response to forcing.

It has been shown that increasing CO<sub>2</sub> levels produces a significant rapid reduction in precipitation (Mitchell et al. 1987; Andrews et al. 2010), which exhibits substantial spatial variation (Bony et al. 2013; Chadwick et al. 2014). Bony et al. (2013) showed that around half the 30-yr mean change in tropical overturning circulation due to quadrupling CO<sub>2</sub> occurs within the first five days, driving much of the tropical precipitation pattern. The rapid adjustment makes an important contribution to long-term precipitation change, and therefore it is important to understand the mechanisms involved.

The rapid tropical precipitation response is likely affected by land surface temperature adjustments influencing atmospheric stability (Cao et al. 2012; Chadwick et al. 2014) and reduced tropospheric radiative cooling affecting general circulation (Bony et al. 2013). However, it is not well established which of these mechanisms is the principal driver of the spatial pattern. In addition, it is not known what mechanisms drive the precipitation pattern outside of the tropics. In this study, we utilize the local energy budget framework to help understand the spatial pattern of rapid precipitation adjustments. We use idealized experiments from phase 5 of the Coupled Model Intercomparison Project (CMIP5) to investigate the mechanisms driving the regional rapid precipitation response to CO<sub>2</sub> and aerosol forcing.

## 2. Methods

### a. Data and experiments

There are three methods available to isolate the rapid precipitation adjustment: fixed sea surface temperature experiments, regression, or using the first year of fully coupled simulations. However, regression is noisy on a

regional scale, and using the first year of coupled simulations incorporates a significant amount of SST change (Sherwood et al. 2014). Therefore, we chose to isolate the rapid adjustment using 30-yr fixed SST experiments, in which only the land surface and atmosphere are allowed to adjust. In these simulations, SSTs and sea ice are prescribed using data from preindustrial control runs, thus suppressing any feedbacks mediated by SST change. Vegetation maps for land are also prescribed, but the vegetation may respond (e.g., through stomatal opening or leaf area index) (Taylor et al. 2009).

Data were obtained from models participating in CMIP5 (see Table A1). We analyze the precipitation response to three different forcing scenarios: an abrupt quadrupling of CO<sub>2</sub> levels (sstClim4xCO<sub>2</sub>), an abrupt increase of sulfate levels from preindustrial to present day (sstClimSulfate), and an abrupt increase of all anthropogenic aerosol from preindustrial to present day (sstClimAerosol). The models analyzed in this study represent the effects of aerosols in varying detail, as shown in Table S1 in the supplementary information (Allen et al. 2015). Changes in climate variables were calculated by subtracting the 30-yr mean of control runs from the 30-yr mean of forced runs. Multimodel mean errors are taken as the 5%–95% uncertainty range assuming a normal distribution.

### b. Global and local atmospheric energy budget

We utilize both the global and local atmospheric energy budgets to help understand the precipitation response to forcing. Globally the latent heat released by precipitation is balanced by the longwave (LW) and shortwave (SW) cooling of the troposphere and the surface sensible heat flux (SH) (O’Gorman et al. 2012). Following Muller and O’Gorman (2011), we decompose regional precipitation  $P$  by incorporating dry static energy flux divergence  $H$  into the global budget, as shown in Eq. (1):

$$L_c \delta P = \delta Q + \delta H = \delta LW + \delta SW - \delta SH + \delta H, \quad (1)$$

where  $L_c$  is the latent heat of condensation,  $Q$  is the diabatic cooling of the troposphere (excluding latent heat), and  $\delta$  denotes the perturbation between climates. Change in  $H$  is given by the sum of mean  $H_m$  and eddy  $H_{\text{trans}}$  components. The total change in  $H$  and  $H_{\text{trans}}$  are calculated as residuals. The change in  $H_m$  is calculated as the sum of components due to advection across horizontal  $H_{\text{hor}}$ , and vertical  $H_{\text{vert}}$  gradients of mean dry static energy, as shown in Eq. (2):

$$\delta H_m = \delta H_{\text{hor}} + \delta H_{\text{vert}} = \delta \int \bar{\mathbf{u}} \cdot \nabla \bar{s} + \delta \int \bar{\omega} \frac{\partial \bar{s}}{\partial p}, \quad (2)$$

where  $\mathbf{u}$  is the horizontal velocity,  $s$  is dry static energy,  $\omega$  is the vertical velocity, and  $p$  is pressure. Integral signs

represent mass-weighted integration over the column, and overbars denote climate means. The horizontal-advective term is further decomposed into components associated with changes in horizontal winds  $H_u$ , and changes in horizontal gradients of dry static energy  $H_s$ , as shown in Eq. (3):

$$\delta H_{\text{hor}} = \delta H_u + \delta H_s = \int \delta[\bar{\mathbf{u}}] \cdot \nabla \bar{s} + \int \bar{\mathbf{u}} \cdot \delta[\nabla \bar{s}]. \quad (3)$$

The vertical component is decomposed into a thermodynamic term  $H_{\text{therm}}$ , associated with changes in the vertical gradient of dry static energy, and a dynamic term  $H_{\text{dyn}}$  associated with changes in mean vertical velocity [Eq. (4)]:

$$\delta H_{\text{vert}} = \delta H_{\text{dyn}} + \delta H_{\text{therm}} = \int \delta[\bar{\omega}] \frac{\partial \bar{s}}{\partial p} + \int \bar{\omega} \delta \left[ \frac{\partial \bar{s}}{\partial p} \right]. \quad (4)$$

All energy budget terms are converted into precipitation units ( $\text{mm yr}^{-1}$ ).

### 3. Results and discussion

#### a. Global mean adjustment

Figure 1 shows the multimodel mean globally averaged precipitation and atmospheric energy budget response for the three forcing scenarios. The dominant effect of quadrupling  $\text{CO}_2$  (Fig. 1a) is a strong reduction in LW cooling at the top of the atmosphere (TOA), and a smaller magnitude increase in downwelling LW radiation at the surface, producing a net increase in atmospheric absorption. Overall, the diabatic cooling of the troposphere is reduced by  $-51.28 \pm 14.7 \text{ mm yr}^{-1}$ , and is balanced by a global mean reduction in precipitation of  $-50.02 \pm 14.4 \text{ mm yr}^{-1}$ . This is consistent with previous studies showing rapid reductions in global mean precipitation following increased  $\text{CO}_2$  (Andrews et al. 2010; Cao et al. 2012; Kvalevåg et al. 2013). The reduction is significant in comparison to the feedback response, which is currently estimated at around  $20\text{--}30 \text{ mm yr}^{-1} \text{ K}^{-1}$  ( $2\%\text{--}3\% \text{ K}^{-1}$ ) (Andrews et al. 2010).

For increased sulfate levels, the dominant effect is a decrease in the net downwelling SW radiation at both the TOA and surface, resulting in a negligible change in global mean tropospheric cooling and precipitation (Fig. 1b). This is consistent with previous global mean studies (Andrews et al. 2010; Kvalevåg et al. 2013). Increasing all anthropogenic aerosol levels also mainly affects the SW radiative fluxes (Fig. 1c). In addition to the sulfate effects, black carbon causes increased SW absorption in the troposphere. Because of the black carbon, global mean tropospheric cooling is reduced

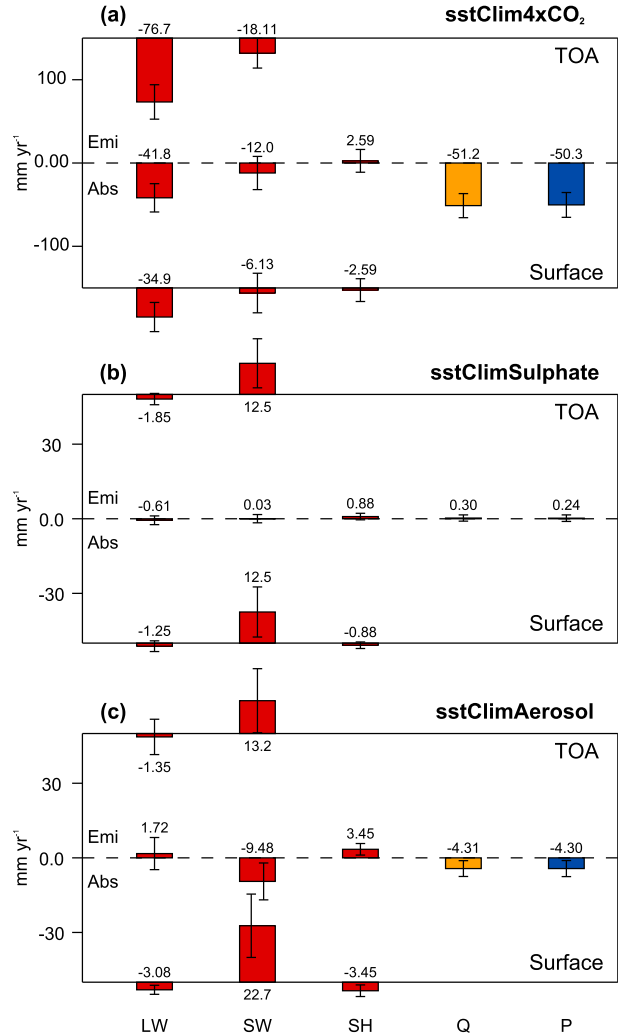


FIG. 1. Multimodel mean energy budget response at the TOA (upper line) and surface (lower line), and the net result for the troposphere (middle dashed line) for (a) sstClim4xCO<sub>2</sub>, (b) sstClimSulphate, and (c) sstClimAerosol. The columns depict change in longwave radiation, shortwave radiation, sensible heat flux, tropospheric diabatic cooling, and precipitation (all converted to  $\text{mm yr}^{-1}$ ). All values are positive upward at the TOA and surface. For the troposphere, positive values represent increased net emission (Emi) of energy, and negative values represent net absorption (Abs) of energy. Error bars represent the 5%–95% uncertainty assuming a normal distribution.

by  $-4.31 \pm 3.2 \text{ mm yr}^{-1}$  and precipitation by  $-4.30 \pm 3.2 \text{ mm yr}^{-1}$ . The changes in tropospheric cooling due to the different forcing agents tightly constrain the global mean rapid precipitation adjustment across the models, in agreement with previous work (Andrews et al. 2010; Kvalevåg et al. 2013).

#### b. Regional adjustment

The precipitation response to quadrupling  $\text{CO}_2$  exhibits a robust spatial pattern across models, with

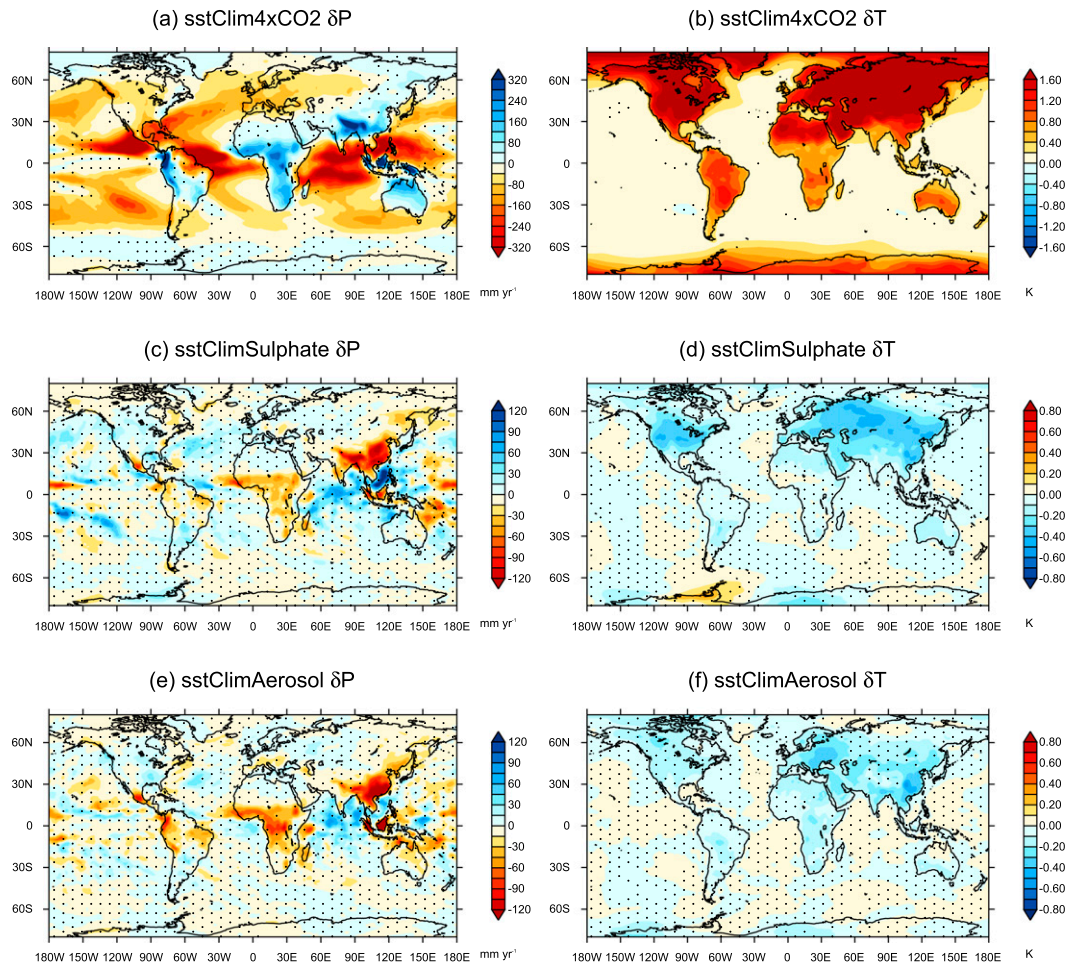


FIG. 2. Multimodel mean precipitation  $P$  ( $\text{mm yr}^{-1}$ ) change for (a) sstClim4xCO<sub>2</sub>, (c) sstClimSulfate, and (e) sstClimAerosol simulations. Multimodel mean near-surface air temperature  $T$  (K) change for (b) sstClim4xCO<sub>2</sub>, (d) sstClimSulfate, and (f) sstClimAerosol. Stippling indicates where less than 80% of the models agree on sign. The color scale is reversed for (left) precipitation and (right) temperature such that blue represents increased precipitation and reduced temperature. Also note the changes in magnitude of color scales between experiments.

disagreement in sign mainly confined to regions of negligible change (Fig. 2a). The most prominent features are observed in the tropics, with significant reductions in regions of climatological large-scale ascent over the Indian Ocean, equatorial Atlantic, and western and eastern Pacific. Conversely, significant increases are observed over southern Asia, the Maritime Continent, Australia, Africa, and western South America. Figure 3a shows the mean precipitation response in the midlatitudes and tropics over land and sea for all models. It can be seen that, excluding one outlier, all the models agree on the sign of the change for each region, further demonstrating the robustness of the precipitation response. The robust spatial pattern implies uncertainty in long-term predictions is mainly associated with the response to SST-driven feedbacks (Ma and Xie 2013).

There is a significant shift of precipitation from over oceans to over land (Fig. 3a), with a mean increase of  $15.3 \pm 32.4 \text{ mm yr}^{-1}$  over land and a decrease of  $-81.4 \pm 19.7 \text{ mm yr}^{-1}$  over oceans (Table 1). This land-sea contrast indicates the importance of the rapid land surface adjustment to increasing CO<sub>2</sub>. The increased downwelling LW radiation due to increased CO<sub>2</sub> levels causes rapid warming of the land surface (Fig. 2b). Over land, there is an increase in mean near-surface air temperature of  $1.22 \pm 0.4 \text{ K}$ , which tends to destabilize the troposphere, enhancing convection and precipitation. The contrast in precipitation change is most prominent in the tropics (Fig. 3a), where precipitation increases by  $54.6 \pm 60.2 \text{ mm yr}^{-1}$  over land, and decreases by  $-111.6 \pm 30.1 \text{ mm yr}^{-1}$  over the sea. A similar land-sea contrast in precipitation is observed in the first month of fully coupled simulations with increased CO<sub>2</sub> (Cao

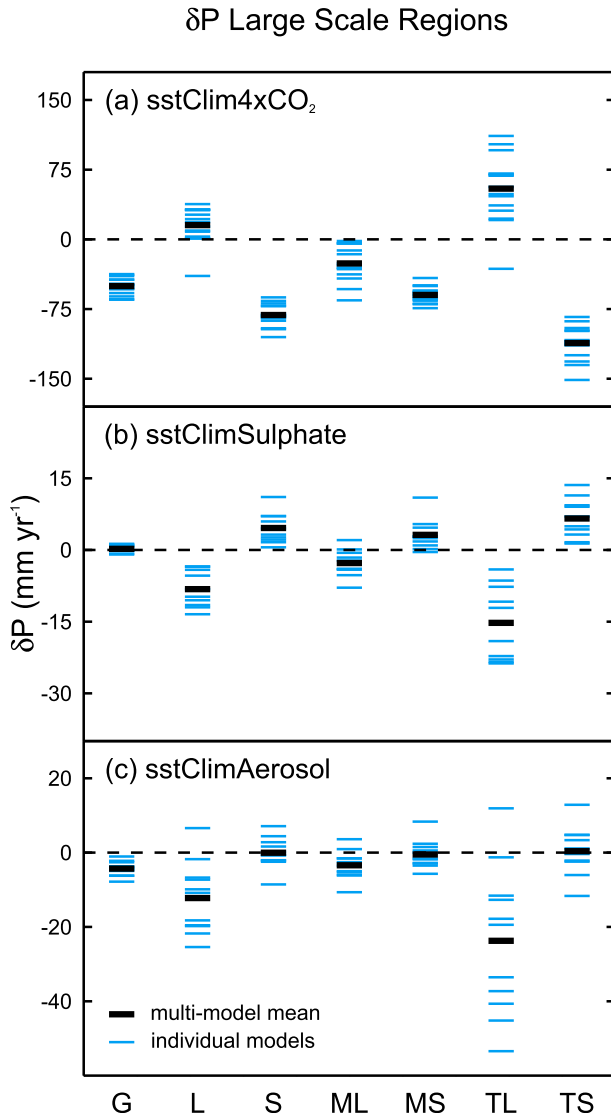


FIG. 3. Mean precipitation change ( $\text{mm yr}^{-1}$ ) over the globe (G), land (L), sea (S), midlatitude land (ML), midlatitude sea (MS), tropical land (TL), and tropical sea (TS) for (a) *sstClim4xCO<sub>2</sub>*, (b) *sstClimSulphate*, and (c) *sstClimAerosol*. Black lines indicate multi-model mean values, and blue lines indicate individual model values.

et al. 2012). The enhanced land–sea temperature contrast strengthens the African and Asian summer monsoons. However, there are large regions over land, predominantly in the midlatitudes, for which precipitation decreases. Notably, precipitation also decreases in the northeastern of South America.

The *sstClimSulphate* and *sstClimAerosol* multimodel mean precipitation adjustments exhibit very similar spatial patterns to one another (Figs. 2c,e). Significant reductions in precipitation occur over Africa, southern Asia, and the Maritime Continent. There is a shift of precipitation from land to sea for both simulations (see Table 1), most

prominent in the tropics (Figs. 3b,c). The precipitation pattern shown in both the sulfate and aerosol simulations is clearly opposed to that observed in the  $\text{CO}_2$  experiment. Given the lack of opposing tropospheric forcing (see Fig. 1), this indicates that the surface forcing is the principal driver of the precipitation pattern through influencing land surface temperatures. The reduced downwelling SW radiation at the surface in both the aerosol experiments causes cooling of the land (Figs. 2d,f) and therefore tends to increase atmospheric stability over land regions. The small difference between the *sstClimSulphate* and *sstClimAerosol* global mean tropospheric forcing and precipitation (Fig. 1) has little effect on the spatial pattern, as the regional changes induced by the land surface adjustment are significantly larger in magnitude. The feedback responses of precipitation to increased greenhouse gases and reduced aerosols have also been shown to project onto similar spatial patterns to one another because of similar SST pattern change (Xie et al. 2013).

The largest reduction in precipitation for the *sstClimSulphate* and *sstClimAerosol* simulations occurs over southern Asia. This is consistent with Ganguly et al. (2012), who found that the rapid adjustment to increased aerosol of one model exhibited significant reductions in precipitation over Southeast Asia. Reducing the land–sea surface temperature contrast weakens the South Asian summer monsoon. The reduction in precipitation over Africa and southern Asia is fairly consistent between models (Figs. 2c,e). However, over most of the globe there is significantly more variability between models in the *sstClimSulphate* and *sstClimAerosol* simulations, most likely because the forcing at the TOA and surface is significantly less than for the  $\text{CO}_2$  experiment. The resulting change in precipitation is therefore small relative to natural internal variability.

Aerosols can also affect precipitation through their role as cloud condensation and ice nuclei. The spatial pattern of precipitation change for the aerosol experiments is very similar between models that include aerosol effects on precipitation efficiency (second indirect effect) and those that do not (Figs. S5 and S6 in the supplementary information). This indicates that the radiative effects primarily drive the spatial pattern of precipitation change. The second indirect effect may enhance the spatial pattern through further reducing precipitation over tropical land regions. For the *sstClimAerosol* simulation, the cloud albedo effect contributes significantly to the changes in land surface temperature and precipitation pattern (Fig S6).

#### c. $4 \times \text{CO}_2$ local energy budget

To understand the mechanisms driving the regional rapid precipitation adjustment to increased  $\text{CO}_2$  in more

TABLE 1. Multimodel mean precipitation  $P$ , tropospheric diabatic cooling  $Q$ , and land surface temperature  $T$  response. Errors represent the 5%–95% uncertainties assuming a normal distribution.

Experiment	Global mean $\delta P$ (mm yr <sup>-1</sup> )	Global mean $\delta Q$ (mm yr <sup>-1</sup> )	Land mean $\delta P$ (mm yr <sup>-1</sup> )	Sea mean $\delta P$ (mm yr <sup>-1</sup> )	Land mean $\delta T$ (K)
sstClim4xCO <sub>2</sub>	-50.3 ± 14.9	-51.2 ± 14.5	15.3 ± 32.4	-81.4 ± 19.7	1.22 ± 0.4
sstClimSulfate	0.24 ± 1.3	0.30 ± 1.3	-8.19 ± 6.3	4.59 ± 5.3	-0.13 ± 0.1
sstClimAerosol	-4.30 ± 3.2	-4.31 ± 3.2	-12.2 ± 15.9	-0.03 ± 6.8	-0.11 ± 0.1

detail, we analyze the local energy budget response of one model, HadGEM2-A. The rapid precipitation response and tropospheric energy budget components are shown in Fig. 4. The dry static energy flux divergence components are shown in Fig. 5. The spatial pattern of the precipitation response (Fig. 4a) is very consistent with the multimodel mean response (Fig. 2a).

The change in dry static energy flux divergence  $H$  (Fig. 4b) accounts for most of the large regional variations observed within the tropics and exhibits a clear land–sea contrast. The contribution from transient eddies (Fig. 5b) is small relative to that by mean motions (Fig. 5a), particularly in the tropics. The thermodynamic component (Fig. 5d) is negligible over much of the globe because of the fixed SSTs. The dynamic component, associated with changes in mean vertical velocity (Fig. 5c), dominates the adjustment in  $H$  in the tropics. Bony et al. (2013) similarly found that the first year tropical precipitation response in fully coupled simulations is dominated by changes in circulation patterns. Over most land areas  $\delta H_{\text{dyn}}$  is positive, with notable exceptions over northeastern South America and northern Asia. This indicates enhanced convection over land regions, due to increased land surface temperatures, destabilizing the troposphere. Over the ocean, in regions of large-scale ascent there are large reductions in  $H_{\text{dyn}}$ . In contrast, in descent regions,  $H_{\text{dyn}}$  generally increases. This implies an overall weakening of overturning circulation, coupled with a shift of convection to over land. This is consistent with the rapid circulation response observed in fully coupled simulations (Bony et al. 2013).

Outside of the tropics, the horizontal-advective components  $H_u$  and  $H_s$  (Figs. 5e,f) become more significant because of the large meridional dry static energy gradients. The spatial patterns of changes in  $H_u$  and  $H_s$  are generally opposed; however, the magnitude of changes in  $H_u$  is significantly larger. The net effect is that changes in horizontal advection of dry static energy counteract the dynamic component (Fig. 5c). As a result, changes in horizontal energy transport are reduced in the mid-to-high latitudes. Therefore, this reduces the magnitude of precipitation changes required for energy balance.

Over much of the globe, the tropospheric cooling is reduced (Fig. 4c), contributing to a decrease in precipitation and dominating the global mean. The reduction is mainly due to increased absorption of LW radiation by CO<sub>2</sub> (Fig. 4e), as well as increased SH flux from the surface over many land areas (Fig. 4d). The change in SW cooling is negligible over most of the globe (Fig. 4f).

The change in cloud fraction, atmospheric cloud radiative effect (CRE), and radiative fluxes at the TOA and surface are shown in Fig. 6. The CRE is defined as the difference between net radiative fluxes out of the troposphere in all-sky and clear-sky conditions. The change in CRE includes “cloud masking” effects (Soden et al. 2004). CRE changes (Fig. 6a) strongly influence the spatial pattern of the LW tropospheric cooling (Fig. 4e) (Lambert et al. 2014). In the tropics,  $\delta \text{CRE}$  (Fig. 6a) and  $\delta H_{\text{dyn}}$  (Fig. 5c) are strongly negatively correlated ( $r = -0.85$ ). In regions where  $\delta H_{\text{dyn}}$  is positive, indicating enhanced convection, there is decreased radiative cooling because of clouds. Conversely, in regions with negative  $\delta H_{\text{dyn}}$ , there is increased radiative cooling because of clouds. This effect slightly dampens the large regional variations driven by circulation changes in the tropics.

Over most land in the midlatitudes (North and South America, Europe, and western/central Asia), where  $\delta H$  is small, the change in tropospheric cooling dominates the precipitation response (Fig. 4c). A significant increase in surface sensible heat flux, due to increased surface temperature, contributes strongly to the reduced tropospheric cooling in these regions (Fig. 4d). There is little change in TOA LW cooling (Fig. 6e), whereas net downwelling LW radiation at the surface decreases (Fig. 6c). The net reduction in tropospheric cooling leads to reduced precipitation. The surface warming does not trigger enhanced moist convection, as seen over most tropical land regions. Cloud cover decreases significantly (Fig. 6b), which increases downwelling SW radiation at the surface and TOA (Figs. 6d,f). This enhances the land surface warming, causing further increases in upwelling LW and SH fluxes. The tropospheric cooling in the northeast of South America behaves similarly to the midlatitudes, though the dynamical mechanisms likely differ. This, coupled with a reduction in dry static energy



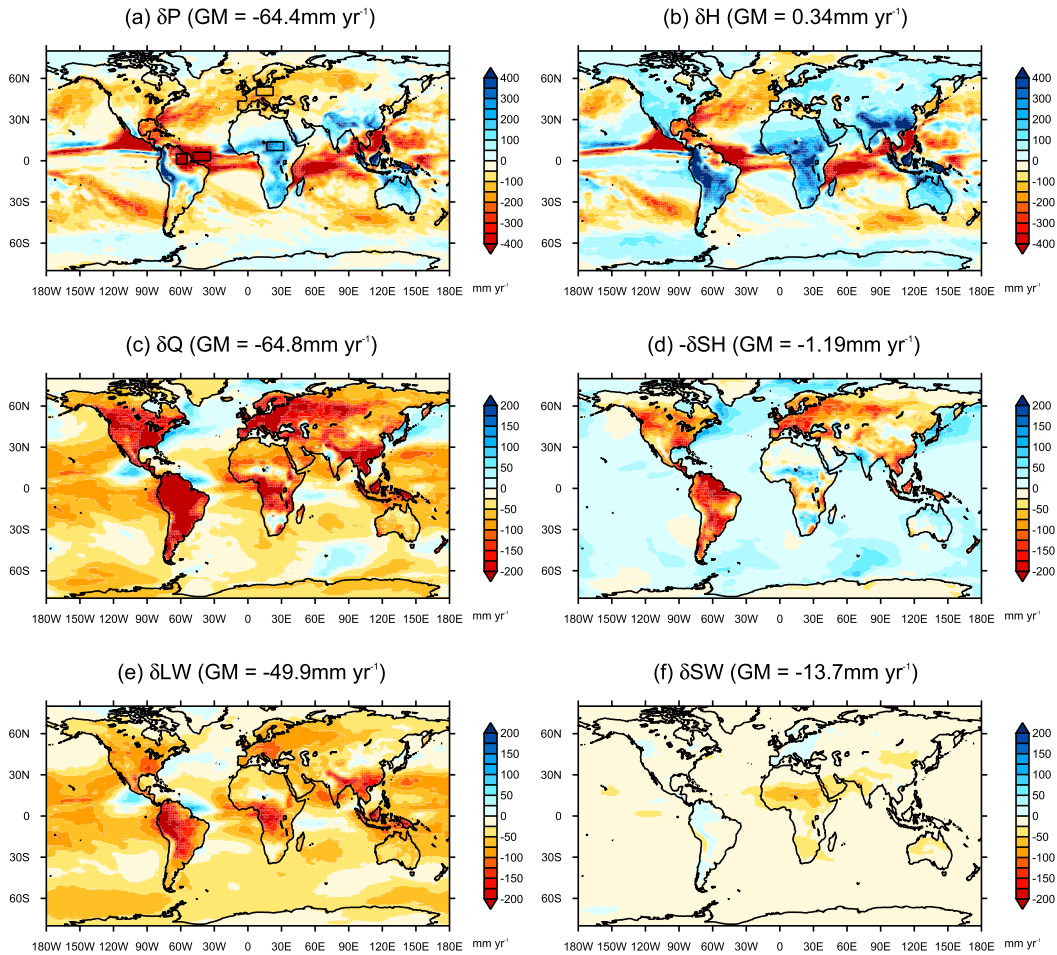


FIG. 4. Local energy budget changes for HadGEM2-A sstClim4xCO<sub>2</sub> simulation: (a) precipitation, (b) dry static energy flux divergence, (c) tropospheric diabatic cooling, (d) negative surface sensible heat flux, (e) LW cooling, and (f) SW cooling. All values are converted into precipitation units ( $\text{mm yr}^{-1}$ ), and blue represents positive contributions to precipitation in all panels. Global mean (GM) values are given for each panel. The boxes in (a) show the regions Europe, Africa, South America, and the Atlantic Ocean (for which the vertical profiles are analyzed in Fig. 7). Note that the color scale magnitude is larger for (a) and (b).

flux divergence, causes the reduction in precipitation observed there (discussed further in section 3d).

#### d. $4 \times \text{CO}_2$ tropospheric vertical profile

To help understand the tropospheric response in different regions to quadrupling CO<sub>2</sub>, we analyze the change in vertical profiles of temperature  $T$ , equivalent potential temperature  $\theta_e$ , relative humidity RH, and specific humidity  $q$  for HadGEM2-A, as shown in Fig. 7. The global mean response (Fig. 7a) is dominated by the response of the oceans (Fig. 7c). Tropospheric temperature change grows with height above the surface, with a maximum increase at 850 hPa and a corresponding reduction in relative humidity. This warming and drying around the upper part of the boundary layer inhibits vertical motion, stabilizing the atmosphere and reducing

precipitation. In contrast, over land the largest temperature increase is at the surface, specific humidity increases throughout most of the troposphere, and there is a weaker reduction in lower-tropospheric relative humidity than over the ocean (Fig. 7b). This pattern destabilizes the troposphere, enhancing convection and precipitation. Dong et al. (2009) observed similar differences in the rapid tropospheric response over land and sea to increased CO<sub>2</sub>.

The tropospheric response varies greatly between different regions, as seen in Figs. 7d–g (geographical locations of the regions are shown in Fig. 4a). Over central Africa, where precipitation increases significantly, the tropospheric temperature increases near the surface (Fig. 7d). This is accompanied by an increase in specific humidity at around 500–800 hPa. As a result,

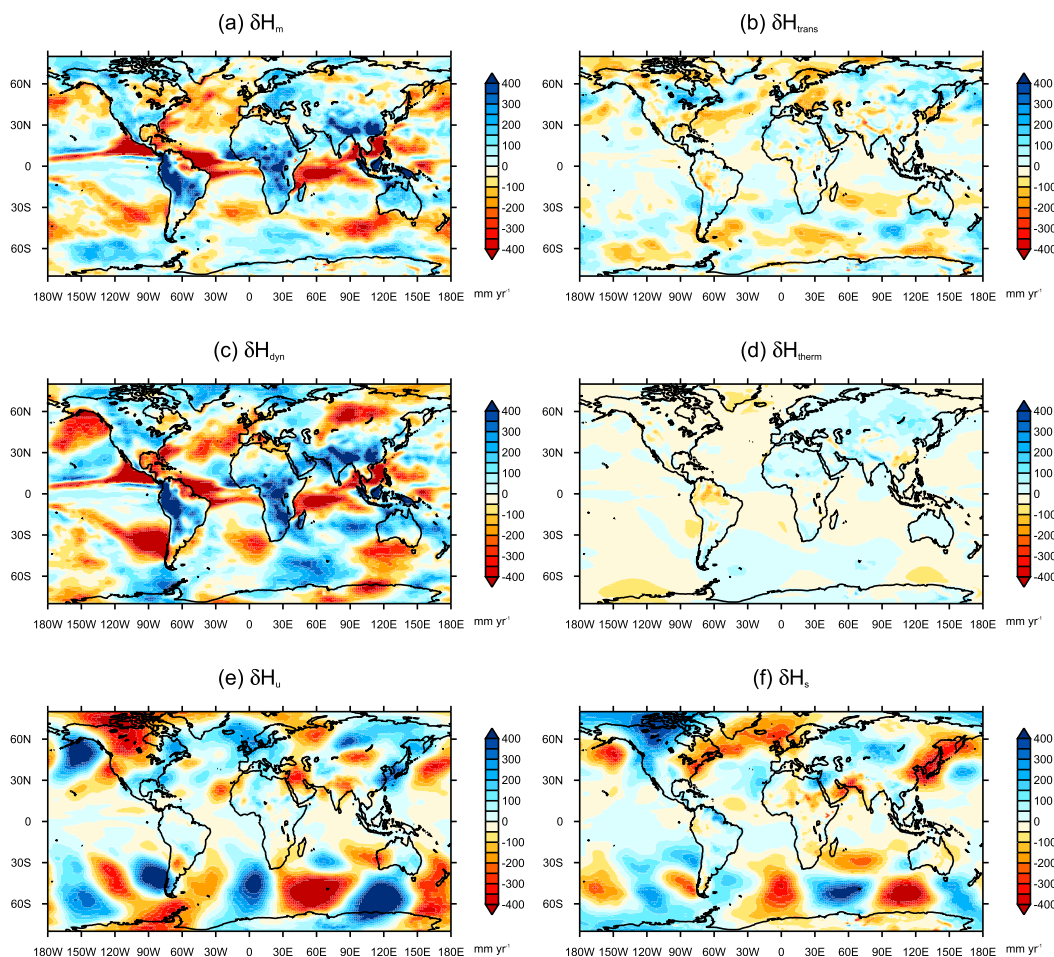


FIG. 5. (a) Mean  $H_m$  and (b) eddy  $H_{trans}$  components of the change in dry static energy flux divergence for HadGEM2-A sstClim4xCO<sub>2</sub> simulation. (c)–(f) The mean term decomposed into (c) dynamic  $H_{dyn}$ , (d) thermodynamic  $H_{therm}$ , (e) horizontal wind  $H_u$ , and (f) horizontal gradient  $H_s$  components, as outlined in Eqs. (2)–(4). All values are converted to precipitation units ( $\text{mm yr}^{-1}$ ), with blue representing a positive contribution to precipitation.

the equivalent potential temperature is significantly increased in the lower half of the troposphere, while temperature remains almost unchanged in the upper troposphere. This combination increases the deep convective instability and drives increased convection and precipitation. Over Europe, where precipitation decreases, the temperature increases throughout most of the troposphere, with a peak at around 900 hPa (Fig. 7e). Unlike over Africa, the specific humidity does not increase anywhere in the troposphere and decreases below 600 hPa. As a result, the relative humidity reduces significantly, causing a reduction in precipitation. This indicates that a lack of available moisture prevents enhanced moist convection, as seen over tropical land regions.

Figure 7f shows the tropospheric adjustment in a region of significantly reduced precipitation over the

tropical Atlantic. It can be seen that there is an increase in temperature between 850 and 500 hPa, which inhibits vertical motion. There is also a reduction in specific and relative humidity above 800 hPa. As a result, precipitation decreases considerably in this region. Figure 7g shows the tropospheric adjustment over northeastern South America, which responds differently to most tropical land regions, with a significant reduction in precipitation. The temperature increases near the surface, which would tend to destabilize the troposphere. However, there is a large reduction in moisture levels near the surface, causing a peak in equivalent potential temperature at around 850 hPa, and almost no change in the surface values. This pattern implies a lifted cloud base, which, combined with the warming just above the boundary layer, inhibits moist convection and reduces

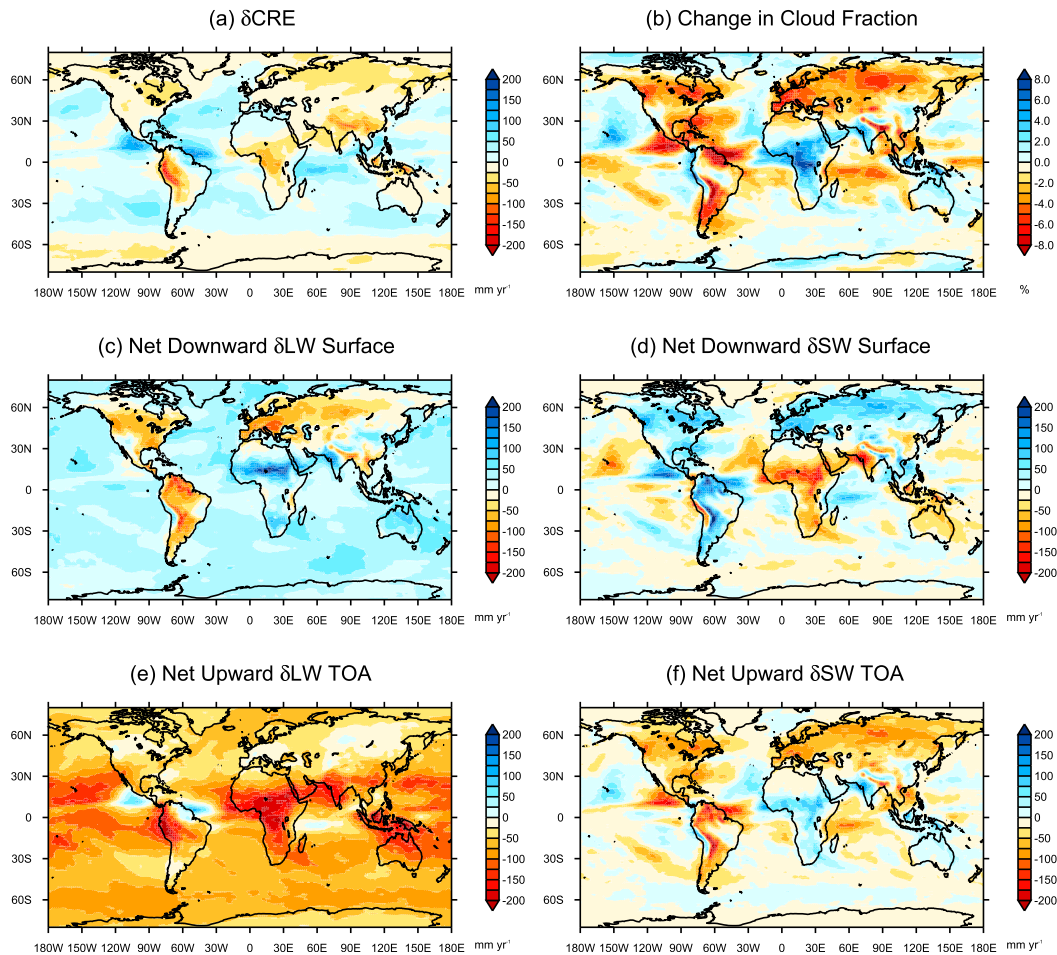


FIG. 6. HadGEM2-A sstClim4xCO<sub>2</sub> changes in (a) atmospheric CRE (mm yr<sup>-1</sup>), (b) total cloud fraction (%), (c) net downward LW radiation at the surface (mm yr<sup>-1</sup>), (d) net downward SW radiation at the surface (mm yr<sup>-1</sup>), (e) net upward LW radiation at the TOA (mm yr<sup>-1</sup>), and (f) net upward SW radiation at the TOA (mm yr<sup>-1</sup>). All radiative changes are converted to precipitation units (mm yr<sup>-1</sup>).

precipitation. Various studies have found that the physiological forcing of CO<sub>2</sub> significantly reduces evapotranspiration over the Amazonian basin (Andrews et al. 2011; Pu and Dickinson 2014). This occurs because, under increased CO<sub>2</sub> concentration, plant stomata do not open as wide. This likely contributes to the large reduction in humidity over South America.

#### 4. Conclusions

The rapid climate response to forcing can have important implications for long-term climate change (Andrews et al. 2010; Bony et al. 2013). In this study, we find that the spatial pattern of rapid precipitation adjustment due to forcing is primarily driven by the rapid land surface response, rather than the change in tropospheric diabatic cooling. As a result, the spatial pattern

due to quadrupling CO<sub>2</sub> opposes that due to increased sulfate or all anthropogenic aerosols. Increasing CO<sub>2</sub> levels causes warming of the land surface because of enhanced downwelling LW radiation. This destabilizes the atmosphere by warming the lower troposphere, producing an overall shift of convection and precipitation to over land. The opposite happens in response to aerosols: increased sulfate levels cool the land surface because of reduced downwelling SW radiation. This stabilizes the troposphere and reduces precipitation over land. The same effect occurs for an increase in all anthropogenic aerosol levels.

Current climate models exhibit a robust pattern of rapid precipitation change due to quadrupling CO<sub>2</sub>. This implies that the uncertainty in long-term predictions is mainly associated with the response to SST-mediated feedbacks. The most significant regional changes occur in the tropics, mainly because of circulation adjustments

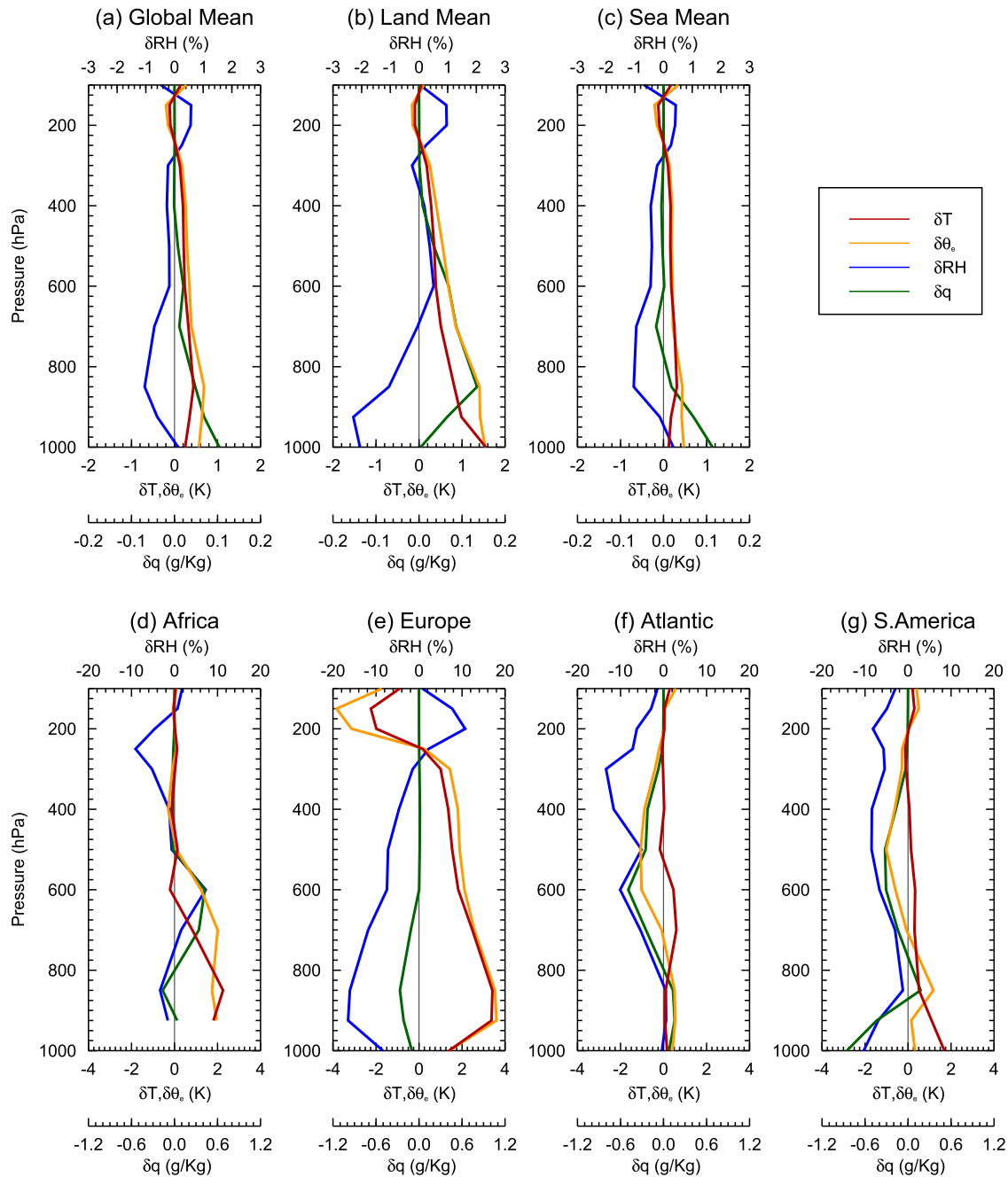


FIG. 7. HadGEM2-A vertical profile adjustment in temperature  $T$  (K), equivalent potential temperature  $\theta_e$  (K), relative humidity RH (%), and specific humidity  $q$  ( $\text{g Kg}^{-1}$ ) for (a) the global mean, (b) land mean, (c) sea mean, (d) a region of increased precipitation over Africa, (e) a region of decreased precipitation over Europe, (f) a region of decreased precipitation over the tropical Atlantic, and (g) a region of decreased precipitation over northeastern South America. The specific locations of the regions are shown in Fig. 4a.

associated with changes in vertical motions. Increased land surface temperature drives enhanced moist convection over central Africa, southern Asia, the Maritime Continent, and western South America. Over the tropical oceans, there are significant reductions in precipitation due to a weakening of overturning circulation

and a general shift of convection to over land. Increased tropospheric temperature, due to LW absorption by  $\text{CO}_2$ , above unchanged SST strongly inhibits vertical motion.

Over midlatitude land regions, the change in tropospheric cooling generally dominates the precipitation

TABLE A1. List of models analyzed for each simulation. An X indicates that the model was available, and a dash indicates that a model was not available. (Expansions of acronyms are available at <http://www.ametsoc.org/PubsAcronymList>.)

Model	sstClim4xCO <sub>2</sub>	sstClimSulfate	sstClimAerosol
BCC_CSM1.1	X	X	X
CanESM2	X	X	X
CCSM4	X	—	—
CESM1(CAM5)	X	—	—
CSIRO Mk3.6.0	X	X	X
FGOALS-s2	X	X	X
GFDL CM3	—	X	X
HadGEM2-A	X	X	X
INM-CM4.0	X	—	—
IPSL-CM5A-LR	X	X	X
MIROC5	X	X	X
MPI-ESM-LR	X	X	X
MPI-ESM-MR	X	—	—
MPI-ESM-P	X	—	—
MRI-CGCM3	X	X	X
NorESM1-M	X	—	X

response to CO<sub>2</sub>. Horizontal advection of dry static energy counteracts energy imbalances due to changes in vertical motions. This, combined with lower moisture levels, prevents enhanced moist convection. Reduced tropospheric cooling therefore leads to drying over many midlatitude land regions.

In the future it would be useful to investigate the rapid precipitation response to black carbon using a larger forcing, as the rapid adjustment can be larger than the feedback response (Andrews et al. 2010; Ming et al. 2010), and the forcing can vary depending on the height at which it is situated (Ban-Weiss et al. 2012). In addition, given the short time scale of rapid precipitation adjustments, higher-resolution convection-permitting models could be utilized for analysis. Convection-permitting models can improve simulations of convective circulations (Sato et al. 2009; Oouchi et al. 2009) and could improve our understanding of long-term climate change.

*Acknowledgments.* TBR was supported by an NERC Ph.D. Case Award with the Met Office, PMF was supported by a Royal Society Wolfson Merit Award and EPSRC Grant EP/I014721/1, and TA was supported by the Joint UK DECC/Defra Met Office Hadley Centre Climate Programme (GA01101). TBR would like to thank Øivind Hodnebrog for useful discussions on figure presentation. We acknowledge the World Climate Research Programme's Working Group on Coupled Modelling, which is responsible for CMIP, and we thank the climate modeling groups (listed in Table A1) for producing and making available their model output. For CMIP the U.S. Department of Energy's Program for Climate Model

Diagnosis and Intercomparison provides coordinating support and led development of software infrastructure in partnership with the Global Organization for Earth System Science Portals.

## APPENDIX

### List of Models

The list of models participating in CMIP5 from which the data were obtained is presented in Table A1.

### REFERENCES

- Allen, M. R., and W. J. Ingram, 2002: Constraints on future changes in climate and the hydrologic cycle. *Nature*, **419**, 224–232, doi:10.1038/nature01092.
- Allen, R. J., A. T. Evan, and B. B. Booth, 2015: Interhemispheric aerosol radiative forcing and tropical precipitation shifts during the late twentieth century. *J. Climate*, **28**, 8129–8246, doi:10.1175/JCLI-D-15-0148.1.
- Andrews, T., and P. M. Forster, 2010: The transient response of global-mean precipitation to increasing carbon dioxide levels. *Environ. Res. Lett.*, **5**, 025212, doi:10.1088/1748-9326/5/2/025212.
- , —, O. Boucher, N. Bellouin, and A. Jones, 2010: Precipitation, radiative forcing and global temperature change. *Geophys. Res. Lett.*, **37**, L14701, doi:10.1029/2010GL043991.
- , M. Doutriaux-Boucher, O. Boucher, and P. M. Forster, 2011: A regional and global analysis of carbon dioxide physiological forcing and its impact on climate. *Climate Dyn.*, **36**, 783–792, doi:10.1007/s00382-010-0742-1.
- Bala, G., K. Caldeira, and R. Nemani, 2010: Fast versus slow response in climate change: Implications for the global hydrological cycle. *Climate Dyn.*, **35**, 423–434, doi:10.1007/s00382-009-0583-y.
- Ban-Weiss, G. A., L. Cao, G. Bala, and K. Caldeira, 2012: Dependence of climate forcing and response on the altitude of black carbon aerosols. *Climate Dyn.*, **38**, 897–911, doi:10.1007/s00382-011-1052-y.
- Bony, S., G. Bellon, D. Klocke, S. Sherwood, S. Fermepin, and S. Denvil, 2013: Robust direct effect of carbon dioxide on tropical circulation and regional precipitation. *Nat. Geosci.*, **6**, 447–451, doi:10.1038/ngeo1799.
- Cao, L., G. Bala, and K. Caldeira, 2011: Why is there a short-term increase in global precipitation in response to diminished CO<sub>2</sub> forcing? *Geophys. Res. Lett.*, **38**, L06703, doi:10.1029/2011GL046713.
- , —, and —, 2012: Climate response to changes in atmospheric carbon dioxide and solar irradiance on the time scale of days to weeks. *Environ. Res. Lett.*, **7**, 034015, doi:10.1088/1748-9326/7/3/034015.
- Chadwick, R., P. Good, T. Andrews, and G. Martin, 2014: Surface warming patterns drive tropical rainfall pattern responses to CO<sub>2</sub> forcing on all timescales. *Geophys. Res. Lett.*, **41**, 610–615, doi:10.1002/2013GL058504.
- Dong, B., J. M. Gregory, and R. T. Sutton, 2009: Understanding land–sea warming contrast in response to increasing greenhouse gases. Part I: Transient adjustment. *J. Climate*, **22**, 3079–3097, doi:10.1175/2009JCLI2652.1.

- Emori, S., 2005: Dynamic and thermodynamic changes in mean and extreme precipitation under changed climate. *Geophys. Res. Lett.*, **32**, L17706, doi:10.1029/2005GL023272.
- Ganguly, D., P. J. Rasch, H. Wang, and J. Yoon, 2012: Fast and slow responses of the South Asian monsoon system to anthropogenic aerosols. *Geophys. Res. Lett.*, **39**, L18804, doi:10.1029/2012GL053043.
- Huang, P., S. Xie, K. Hu, G. Huang, and R. Huang, 2013: Patterns of the seasonal response of tropical rainfall to global warming. *Nat. Geosci.*, **6**, 357–361, doi:10.1038/ngeo1792.
- Kravitz, B., and Coauthors, 2013: An energetic perspective on hydrological cycle changes in the Geoengineering Model Intercomparison Project. *J. Geophys. Res.*, **118**, 13 087–13 102, doi:10.1002/2013JD020502.
- Kvalevåg, M. M., B. H. Samset, and G. Myhre, 2013: Hydrological sensitivity to greenhouse gases and aerosols in a global climate model. *Geophys. Res. Lett.*, **40**, 1432–1438, doi:10.1002/grl.50318.
- Lambert, F. H., and N. E. Faull, 2007: Tropospheric adjustment: The response of two general circulation models to a change in insolation. *Geophys. Res. Lett.*, **34**, L03701, doi:10.1029/2006GL028124.
- , M. J. Webb, M. Yoshimori, and T. Yokohata, 2014: The cloud radiative effect on the atmospheric energy budget and global mean precipitation. *Climate Dyn.*, **44**, 2301–2325, doi:10.1007/s00382-014-2174-9.
- Liepert, B. G., and M. Previdi, 2012: Inter-model variability and biases of the global water cycle in CMIP3 coupled climate models. *Environ. Res. Lett.*, **7**, 014006, doi:10.1088/1748-9326/7/1/014006.
- Ma, J., and S.-P. Xie, 2013: Regional patterns of sea surface temperature change: A source of uncertainty in future projections of precipitation and atmospheric circulation. *J. Climate*, **26**, 2482–2501, doi:10.1175/JCLI-D-12-00283.1.
- Ming, Y., V. Ramaswamy, and G. Persad, 2010: Two opposing effects of absorbing aerosols on global-mean precipitation. *Geophys. Res. Lett.*, **37**, L13701, doi:10.1029/2010GL042895.
- Mitchell, J., C. Wilson, and W. Cunnington, 1987: On CO<sub>2</sub> climate sensitivity and model dependence of results. *Quart. J. Roy. Meteor. Soc.*, **113**, 293–322, doi:10.1256/smsqj.47516.
- Muller, C. J., and P. A. O’Gorman, 2011: An energetic perspective on the regional response of precipitation to climate change. *Nat. Climate Change*, **1**, 266–271, doi:10.1038/nclimate1169.
- O’Gorman, P. A., R. P. Allan, M. P. Byrne, and M. Previdi, 2012: Energetic constraints on precipitation under climate change. *Surv. Geophys.*, **33**, 585–608, doi:10.1007/s10712-011-9159-6.
- Oouchi, K., A. T. Noda, M. Satoh, B. Wang, S.-P. Xie, H. G. Takahashi, and T. Yasunari, 2009: Asian summer monsoon simulated by a global cloud-system-resolving model: Diurnal to intra-seasonal variability. *Geophys. Res. Lett.*, **36**, L11815, doi:10.1029/2009GL038271.
- Pendergrass, A. G., and D. L. Hartmann, 2014: The atmospheric energy constraint on global-mean precipitation change. *J. Climate*, **27**, 757–768, doi:10.1175/JCLI-D-13-00163.1.
- Previdi, M., 2010: Radiative feedbacks on global precipitation. *Environ. Res. Lett.*, **5**, 025211, doi:10.1088/1748-9326/5/2/025211.
- Pu, B., and R. E. Dickinson, 2014: Hydrological changes in the climate system from leaf responses to increasing CO<sub>2</sub>. *Climate Dyn.*, **42**, 1905–1923, doi:10.1007/s00382-013-1781-1.
- Sato, T., H. Miura, M. Satoh, Y. N. Takayabu, and Y. Wang, 2009: Diurnal cycle of precipitation in the tropics simulated in a global cloud-resolving model. *J. Climate*, **22**, 4809–4826, doi:10.1175/2009JCLI2890.1.
- Sherwood, S. C., S. Bony, O. Boucher, C. Bretherton, P. M. Forster, J. M. Gregory, and B. Stevens, 2014: Adjustments in the forcing-feedback framework for understanding climate change. *Bull. Amer. Meteor. Soc.*, **96**, 217–228, doi:10.1175/BAMS-D-13-00167.1.
- Soden, B. J., A. J. Broccoli, and R. S. Hemler, 2004: On the use of cloud forcing to estimate cloud feedback. *J. Climate*, **17**, 3661–3665, doi:10.1175/1520-0442(2004)017<3661:OTUOCF>2.0.CO;2.
- Stephens, G. L., and Coauthors, 2010: Dreary state of precipitation in global models. *J. Geophys. Res.*, **115**, D24211, doi:10.1029/2010JD014532.
- Stevens, B., and S. Bony, 2013: What are climate models missing? *Science*, **31**, 1053–1054, doi:10.1126/science.1237554.
- Taylor, K. E., R. J. Stouffer, and G. A. Meehl, 2009: A summary of the CMIP5 experiment design. WCRP Tech. Rep., 33 pp. [Available online at [http://cmip-pcmdi.llnl.gov/cmip5/docs/Taylor\\_CMIP5\\_design.pdf](http://cmip-pcmdi.llnl.gov/cmip5/docs/Taylor_CMIP5_design.pdf).]
- Wake, B., 2013: Flooding costs. *Nat. Climate Change*, **3**, 778–778, doi:10.1038/nclimate1997.
- Xie, S.-P., B. Lu, and B. Xiang, 2013: Similar spatial patterns of climate responses to aerosol and greenhouse gas changes. *Nat. Geosci.*, **6**, 828–832, doi:10.1038/ngeo1931.

## **Chapter 4: Drivers of Precipitation Change: An Energetic Understanding**

T. B. Richardson<sup>1</sup>, P. M. Forster<sup>1</sup>, T. Andrews<sup>2</sup>, O. Boucher<sup>3</sup>, G. Faluvegi<sup>4</sup>, D. Fläschner<sup>5</sup>, Ø. Hodnebrog<sup>6</sup>, M. Kasoar<sup>7</sup>, V. Kharin<sup>8</sup>, A. Kirkevåg<sup>9</sup>, J.-F. Lamarque<sup>10</sup>, G. Myhre<sup>6</sup>, D. Olivie<sup>9</sup>, B. H. Samset<sup>6</sup>, D. Shawki<sup>7</sup>, D. Shindell<sup>11</sup>, T. Takemura<sup>12</sup>, A. Voulgarakis<sup>7</sup>

Prepared for submission to the Journal of Climate

1. University of Leeds, United Kingdom
2. Met Office Hadley Centre, United Kingdom
3. Institut Pierre-Simon Laplace, Université Pierre et Marie Curie / CNRS, 4 place Jussieu, Paris, France
4. NASA Goddard Institute for Space Studies and Center for Climate Systems Research, Columbia University, New York, USA
5. Max-Planck-Institut für Meteorologie, Hamburg, Germany
6. CICERO Center for International Climate and Environmental Research – Oslo, Norway
7. Imperial College London, London, United Kingdom
8. Canadian Centre for Climate Modelling and Analysis, Gatineau, Canada
9. Norwegian Meteorological Institute, Oslo, Norway
10. NCAR/UCAR, Boulder, USA
11. Duke University, Durham, USA
12. Kyushu University, Fukuoka, Japan

## 4.1 Abstract

Different drivers of climate change cause different hydrological responses due to impacts on the atmospheric energy budget. In this study precipitation and energy budget responses to five forcing agents are analysed using ten global climate models participating in the Precipitation Driver Response Model Intercomparison Project (PDRMIP). The responses are split into a forcing-dependent adjustment, due to near-instantaneous changes in the atmospheric energy budget, and a temperature-driven hydrological sensitivity. Globally, CO<sub>2</sub> and black carbon produce the largest negative adjustments in precipitation per unit top of the atmosphere (TOA) radiative forcing, due to enhanced atmospheric absorption. Over land, sulphate and solar forcing drive the strongest precipitation adjustments due to circulation changes, but CO<sub>2</sub> and black carbon exhibit more model spread. Globally, the hydrological sensitivity is consistent across forcings, driven mainly by increased longwave cooling. The land-mean hydrological sensitivity is considerably weaker due to limited moisture availability. The PDRMIP results are used to construct a simple model for land-mean and sea-mean precipitation change based on surface temperature change and TOA forcing. The model matches well with CMIP5 ensemble mean historical and future projections, and is used to understand the contributions of different drivers. During the 20<sup>th</sup> century, temperature-driven intensification of land-mean precipitation has been entirely masked by reductions due to anthropogenic sulphate and volcanic forcing, consistent with the small observed trend. However, as projected sulphate forcing decreases, and warming continues, increased land-mean precipitation may soon become clearly observable. Sea-mean precipitation is projected to increase more rapidly, due to the higher sensitivity to temperature.



## 4.2 Introduction

Understanding changes in the hydrological cycle is of great importance due to the potential impact on society (Wake, 2013). Precipitation is directly affected by individual forcing agents (Lambert and Faull, 2007; Andrews et al., 2010b; Kvalevåg et al., 2013) as well as global warming (Held and Soden, 2006; Previdi, 2010). This is because precipitation is tightly constrained by the atmospheric energy budget, such that globally the latent and sensible heat fluxes are balanced by net atmospheric radiative cooling (Mitchell et al., 1987; Allen and Ingram, 2002; O’Gorman et al., 2011; Pendergrass and Hartmann, 2014). As a result, the precipitation response to forcing can be split into a rapid adjustment, due to the near-instantaneous impact on the atmospheric energy budget, and a feedback response, driven by surface temperature change (Bala et al., 2009; Andrews et al., 2010b; Kvalevåg et al., 2013; Sherwood et al., 2015; MacIntosh et al., 2016; Samset et al., 2016). The precipitation adjustment includes the direct radiative effects of the forcing agent, as well as any rapid adjustments of the troposphere and land surface.

The adjustment framework has significantly improved understanding of global precipitation changes, and has been used to accurately emulate historical and 21<sup>st</sup> century changes predicted by global climate models (Thorpe and Andrews, 2014). However, uncertainties and inter-model differences in the precipitation response to forcing remain, particularly (but not only) for the effects of black carbon (Fläschner et al., 2016; Samset et al., 2016). Uncertainty in shortwave absorption feedbacks, due to atmospheric moistening, is thought to drive significant model spread in the temperature-mediated precipitation response to forcing (DeAngelis et al., 2015). Improving understanding of the uncertainties and mechanisms involved is vital for improving prediction of future precipitation changes.

On local scales precipitation is strongly affected by circulation changes (Seager et al., 2010; Bony et al., 2013; Chadwick et al., 2013; Richardson et al., 2016a). Rapid circulation changes have been linked to changes in atmospheric absorption (Bony et al., 2013) as well as the rapid land surface response (Richardson et al., 2016a). Due to the importance of the short-timescale land surface response, forcings which have little effect on atmospheric absorption can still drive rapid spatial shifts in precipitation due to the surface forcing (Dong et al., 2014). Precipitation adjustments and feedbacks

have been shown to differ significantly over land and sea for many climate drivers (Samset et al., 2016). It is important to understand the differing processes involved, particularly over land where changes will be most felt by society. The different regional responses can be analysed energetically by taking into account horizontal energy transport as well as atmospheric cooling (Muller and O’Gorman, 2011).

In this study we present the global, land and sea mean precipitation and atmospheric energy budget responses to five different climate drivers (CO<sub>2</sub>, CH<sub>4</sub>, black carbon, sulphate and insolation) across ten global climate models participating in the Precipitation Driver Response Model Inter-comparison Project (PDRMIP) (Myhre et al., 2016a). The responses are split into a forcing-dependent adjustment and a temperature-driven feedback. We analyse the atmospheric energy budget to understand the processes driving precipitation changes and isolate sources of uncertainty and inter-model spread. We use the PDRMIP results to construct a simple model for land-mean and sea-mean precipitation change based on global mean surface temperature change and top of the atmosphere (TOA) forcing. The simple model is used to emulate historical and future precipitation changes, and compared with CMIP5 output and observational records.

## **4.3 Methods**

### **4.3.1 Data**

We analyse data from ten global climate models (see Table S1) participating in PDRMIP (Myhre et al., 2016a; Samset et al., 2016). References and more details can be found in Table 3 in Myhre et al. (2016). Five abrupt climate forcing scenarios were implemented: doubling CO<sub>2</sub> concentration (2xCO<sub>2</sub>), tripling methane concentration (3xCH<sub>4</sub>), five times sulphate concentration or SO<sub>2</sub> emissions (5xSO<sub>4</sub>), ten times black carbon concentration or emissions (10xBC), and a two percent increase in solar insolation (2%SOL). Perturbations are relative to either present-day or pre-industrial values depending on the model (see Table S1).

For models which are able to prescribe aerosol concentration fields, a common set of baseline and perturbed fields were used. The baseline concentrations were constructed from the multi-model mean of phase 2 of the Aerosol Comparisons between

Observations and Models (AeroCom) initiative (see Myhre et al., 2013a, 2016). For the perturbation runs the baseline aerosol fields were scaled by the appropriate scaling factor. For models in which it was not possible to impose the given baseline concentrations, the models native baseline emissions were scaled by the prescribed factors (see Table S1). Full details of the PDRMIP experiment design and implementation of aerosol perturbations are outlined in Myhre et al. (2016b). Simulations were performed with fixed sea surface temperatures (fSST) for 15 years, and with a slab ocean or fully coupled ocean (coupled) for 100 years.

Precipitation and near-surface air temperature time-series data were also obtained for 26 models (Table S2) participating in the Coupled Model Intercomparison Project Phase 5 (CMIP5) for the historical period (1850-2005), and two Representative Concentration Pathway (RCP) scenarios out to 2100: RCP4.5 and RCP8.5 (Meinshausen et al., 2011). Two precipitation observational datasets are used: the Global Precipitation Climatology Centre (GPCC) full data reanalysis version 7.0 at 0.5° resolution (1901-2013) (Becker et al., 2013), and the Climate Research Unit time-series (CRU TS) version 3.23 at 0.5° resolution (1901-2014) (Harris et al., 2014). The HadCRUT4 observational time-series dataset is used to provide global mean near-surface air temperature from 1901-2015 (Morice et al., 2012).

### 4.3.2 Rapid Adjustment and Hydrological Sensitivity

The precipitation response in the PDRMIP experiments is split into a rapid adjustment component, which scales with atmospheric forcing, and a feedback component, which scales with global mean surface temperature change. Following Richardson et al. (2016b), the precipitation adjustment ( $P_{adj}$ ) is given by the fSST response to forcing (mean difference between perturbed and control simulations for years 2-15). The precipitation feedback response per unit Kelvin of global mean surface temperature change (Hydrological Sensitivity) is calculated using Eq. (1):

$$HS = \frac{P_{tot} - P_{adj}}{T_{tot} - T_{adj}}, \quad (1)$$

where,  $HS$  is the hydrological sensitivity,  $P_{tot}$  is the total coupled precipitation response,  $P_{adj}$  is the precipitation adjustment,  $T_{tot}$  is the total coupled global mean surface temperature response, and  $T_{adj}$  is the fSST global mean surface temperature response (due to land surface adjustment). The total coupled response is taken as the

mean difference between perturbed and control simulations for years 51-100 after the abrupt forcing is imposed. It should be noted that our definition of the hydrological sensitivity differs from the apparent hydrological sensitivity commonly referred to in papers (Held and Soden, 2006; Pendergrass and Hartmann, 2014; Fläschner et al., 2016; Samset et al., 2016), which incorporates the adjustment component.

### 4.3.3 Atmospheric Energy Budget

Globally the latent heat released by precipitation is balanced by the net atmospheric cooling. We therefore decompose the global precipitation adjustment and feedback response into contributions from atmospheric longwave cooling (LWC), shortwave absorption (SWA), and sensible heating (SH). On local scales horizontal energy transport must also be taken into account. Following Muller and O’Gorman (2011) we introduce a dry static energy flux divergence term, as shown in Eq. (2):

$$L_c \Delta P = \Delta Q + \Delta H = \Delta LWC - \Delta SWA - \Delta SH + \Delta H, \quad (2)$$

where  $\Delta$  denotes the perturbation between the two climate states,  $L_c$  is the latent heat of condensation,  $P$  is precipitation,  $Q$  is the net atmospheric cooling,  $H$  is dry static energy flux divergence,  $LWC$  is atmospheric longwave cooling,  $SWA$  is atmospheric shortwave absorption, and  $SH$  is the sensible heat flux from the surface. Equation 2 is used to analyse the precipitation response to forcing over land and sea separately.  $H$  is calculated as a residual. Energy budget terms are split into adjustment and feedback components using the same method outlined for precipitation in Section 4.3.2.

### 4.3.4 Simple Precipitation Model

Using the PDRMIP output we construct a simple model for land mean and sea mean precipitation change based upon the adjustment and feedback framework. Precipitation change is estimated using a linear combination of forcing dependent adjustments, and a temperature dependent feedback as shown in Eq. (3) and (4):

$$\Delta P_L(t) = \sum_i R_{L_i} F_i(t) + HS_L \times \Delta T(t), \quad (3)$$

$$\Delta P_S(t) = \sum_i R_{S_i} F_i(t) + HS_S \times \Delta T(t), \quad (4)$$

where  $\Delta P_L(t)$  (or  $\Delta P_S(t)$ ) is the change in land (or sea) mean precipitation at time  $t$ ,  $F_i(t)$  is the global mean top of the atmosphere forcing for a given climate driver  $i$  at time  $t$ , and  $\Delta T(t)$  is the global mean surface temperature change at time  $t$ .  $R_{L_i}$  is the

land (or sea for  $R_{S_i}$ ) mean precipitation adjustment per unit top of the atmosphere forcing for a given climate driver  $i$ . The  $R$  factors are calculated from the PDRMIP simulations and shown in Table S3. To reduce the impact of outlying models the multi-model median values from the PDRMIP results are used for the simple model.  $HS_L$  (or  $HS_S$ ) is the land (or sea) mean hydrological sensitivity. For each model, the hydrological sensitivity is taken as the mean of the 2xCO<sub>2</sub>, 5xSO<sub>4</sub>, and 2%SOL experiments (10xBC and 3xCH<sub>4</sub> are not included as they generally produce much less surface temperature change, which introduces large uncertainties when computing the hydrological sensitivity). The median  $HS$  of the PDRMIP models is used for the simple model.

The simple model is used to estimate historical and future precipitation change following RCP4.5 and RCP8.5.  $F_i$  time-series data is taken from Meinshausen et al. (2011), as shown in Figure S8.  $\Delta T$  time-series data is taken as the CMIP5 ensemble mean. The black carbon forcing time-series includes only the direct radiative effects. Sulphate direct radiative forcing is grouped with cloud albedo (indirect) forcing. Other aerosol species will contribute to the cloud albedo changes, but sulphate is consistently found to dominate aerosol indirect effects on clouds (Takemura, 2012; Shindell et al., 2013). Some of the CMIP5 models only include sulphate effects on cloud albedo (see Table 12.1 in (Collins et al., 2013)).

As well as the five PDRMIP climate drivers, forcings due to volcanoes and greenhouse gases (GHGs) other than CO<sub>2</sub> and CH<sub>4</sub> are included in the simple model. Volcanic forcing is assumed to have the same  $R$  factor as 2%SOL, as the predominant effect is a reduction in incoming solar irradiance (Myhre et al., 2013b). GHGs apart from CH<sub>4</sub> are assumed to have the same  $R$  factor as CO<sub>2</sub>, as they affect the atmospheric energy budget through the same mechanism of LW absorption. Given that CO<sub>2</sub> dominates GHG forcing we do not expect this assumption to significantly affect the results. It should be noted that various forcings such as Ozone, land-use change and biomass burning are not included.

The simple model is also compared against precipitation observations over land, using the HadCRUT4 dataset instead of CMIP5 data for the  $\Delta T$  time-series.

## 4.4 Results and Discussion

### 4.4.1 Precipitation and Energy Budget Response

We first decompose the multi-model global, land and sea mean precipitation response to the five PDRMIP drivers into a rapid adjustment and hydrological sensitivity (Fig. 1 and 2). The global hydrological sensitivity (Fig. 1b) is very consistent between drivers ranging from 31.2 to 34.9 mm yr<sup>-1</sup> K<sup>-1</sup> (2.9-3.2% K<sup>-1</sup>). This lies at the higher end of results from previous studies (Andrews et al., 2010b; Kvalevåg et al., 2013; Fläschner et al., 2016). Differencing fSST and coupled simulations to calculate the hydrological sensitivity, as used in the present study, tends to produce higher values than regression techniques (Richardson et al., 2016b). The adjustment term (Fig. 1a) varies significantly between drivers, with 2xCO<sub>2</sub> and 10xBC producing large reductions in precipitation consistent with previous single-model studies (Andrews et al., 2010b; Kvalevåg et al., 2013).

The global precipitation changes can be explained through the impact of each forcing agent on the atmospheric energy budget (also shown in Fig. 1). Doubling CO<sub>2</sub> produces a large negative adjustment in global mean precipitation due to the initial reduction in atmospheric LW cooling. This is robust across the PDRMIP models (see Fig. S1a), however the model spread in the energy budget response is larger than for 2%SOL, 3xCH<sub>4</sub> and 5xSO<sub>4</sub>. The greater spread can largely be explained by the stronger forcing, the global adjustment per unit TOA forcing exhibits a similar spread to other scenarios (Fig. 3). The change in SH flux contributes more strongly to the spread in the CO<sub>2</sub> precipitation adjustment than for other forcings (except black carbon). The cross-model correlation between  $P_{\text{adj}}$  and SH flux ( $r = -0.77$ ) is considerably larger than for LW cooling ( $r = 0.32$ ) or SW absorption ( $r = -0.14$ ). This is mainly attributable to the land surface response discussed below. Tripling methane produces a smaller reduction in net atmospheric cooling (Fig. 1a), however the forcing is somewhat smaller for this scenario (Fig. S6). The CH<sub>4</sub> precipitation adjustment per unit TOA forcing is more comparable to the CO<sub>2</sub> response (Fig. 3).

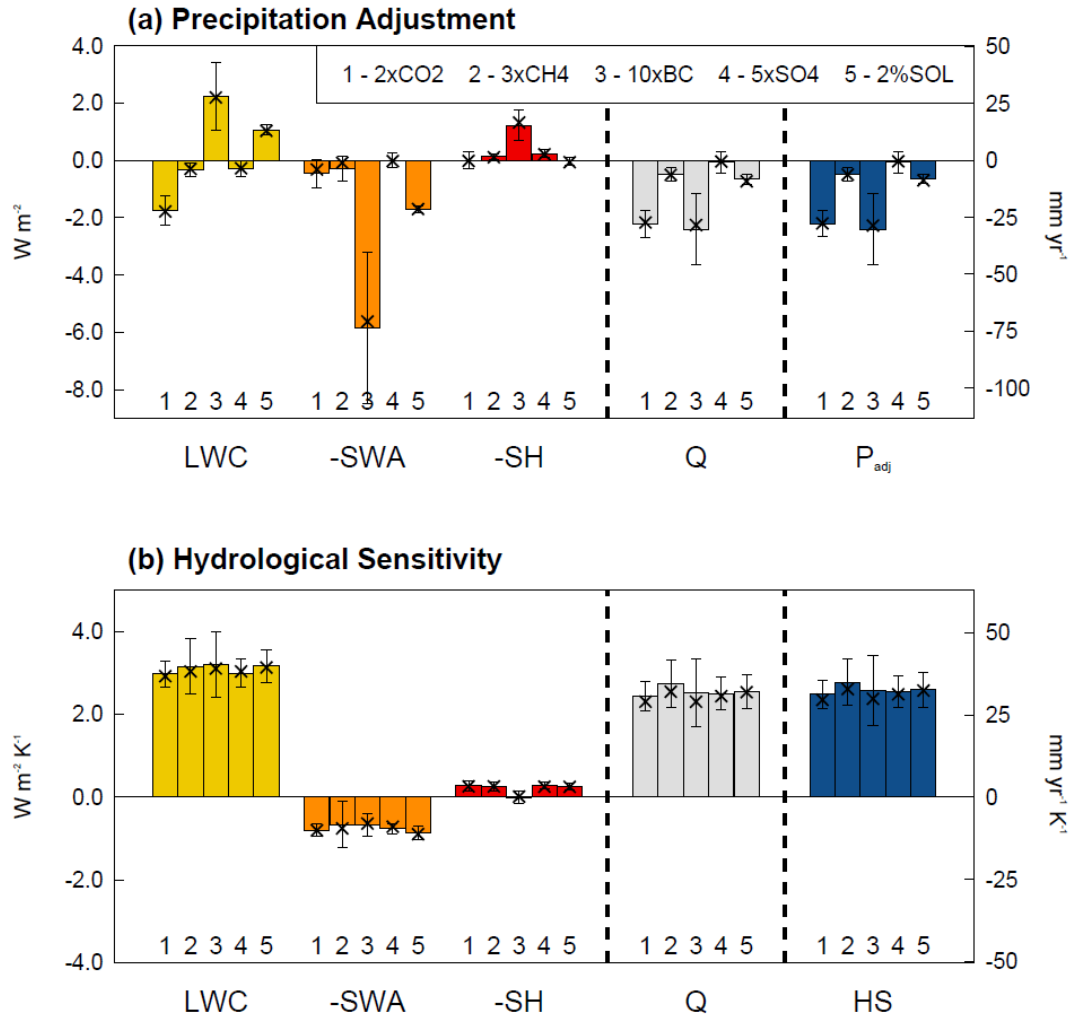


**Figure 1:** Multi-model global mean (a) precipitation adjustment ( $P_{adj}$ , blue) and (b) hydrological sensitivity ( $HS$ , blue) in response to the five PDRMIP forcing scenarios.  $P_{adj}$  and  $HS$  are decomposed into the contributions from the atmospheric energy budget: net longwave cooling ( $LWC$ , yellow), net shortwave absorption ( $SWA$ , orange), sensible heat flux from the surface ( $SH$ , red) and the net atmospheric cooling ( $Q$ , light grey). The sign of change in each component is given such that a positive value contributes positively to precipitation change. Results are shown in both energetic units (left axis) [(a)  $W m^{-2}$ , (b)  $W m^{-2} K^{-1}$ ], and precipitation units (right axis) [(a)  $mm yr^{-1}$  and (b)  $mm yr^{-1} K^{-1}$ ]. Error bars denote the standard deviation of model spread, and crosses show the median value.

10xBC produces a large negative precipitation adjustment due to a substantial increase in atmospheric shortwave absorption (Fig. 1a). Warming of the atmosphere causes increased LW cooling and a reduction in surface SH flux, which partially counteracts the increased shortwave absorption. Per unit TOA forcing black carbon causes an adjustment in precipitation over 3.5 times larger than any other driver (Fig. 3), due to

its strong impact on SW radiation. Therefore, given the large uncertainty associated with industrial era radiative forcing from black carbon (Bond et al., 2013; Samset et al., 2014; Boucher et al., 2016), and the complex relationship between BC forcing and surface temperature change (Chung et al., 2012; Bond et al., 2013; Myhre and Samset, 2015), the influence on global precipitation is considerably more uncertain than for the other drivers. The black carbon adjustment exhibits considerable model spread (Fig. S1a), with the increase in SW absorption ranging from 2.9 to 10.3  $\text{Wm}^{-2}$ . The large spread mainly arises from the emissions-based models (Fig. S1a), which will be affected by the individual model setup and how the emissions perturbation translates into concentration and atmospheric forcing. However, the model spread in the precipitation adjustment per unit TOA forcing is also considerably larger than for other drivers (Fig. 3). Therefore, there is a large uncertainty in the precipitation response to a uniform black carbon forcing.

Sulphate has very little impact on the net atmospheric cooling, and therefore produces a negligible precipitation adjustment (Fig. 1a). Increased solar irradiance causes a small negative adjustment due to increased atmospheric SW absorption (Fig. 1a), compensated partially by an increase in LW cooling.

The hydrological sensitivity for all forcing scenarios is driven mainly by an increase in LW cooling as the climate warms (Fig. 1b). There is a small negative feedback due to increased SW absorption attributable to Clausius-Clapyron driven increases in water vapour. Surface sensible heat flux is affected very little by changing surface temperature. This is generally consistent across forcing scenarios and models. Inter-model spread in the hydrological sensitivity mainly arises from the LW cooling feedback (Fig. S1b). For 2xCO<sub>2</sub> the cross-model correlation coefficient between the hydrological sensitivity and LW cooling ( $r = 0.82$ ) is considerably larger than for SW absorption ( $r = -0.19$ ), or SH flux ( $r = -0.44$ ). This is in contrast to previous studies which attribute a significant portion of the inter-model spread to shortwave absorption (Takahashi, 2009; DeAngelis et al., 2015). This may be linked to uncertain cloud feedbacks which have little effect on atmospheric shortwave absorption (Lambert et al., 2014), but contribute strongly to inter-model spread in net atmospheric cooling (O’Gorman et al., 2011).



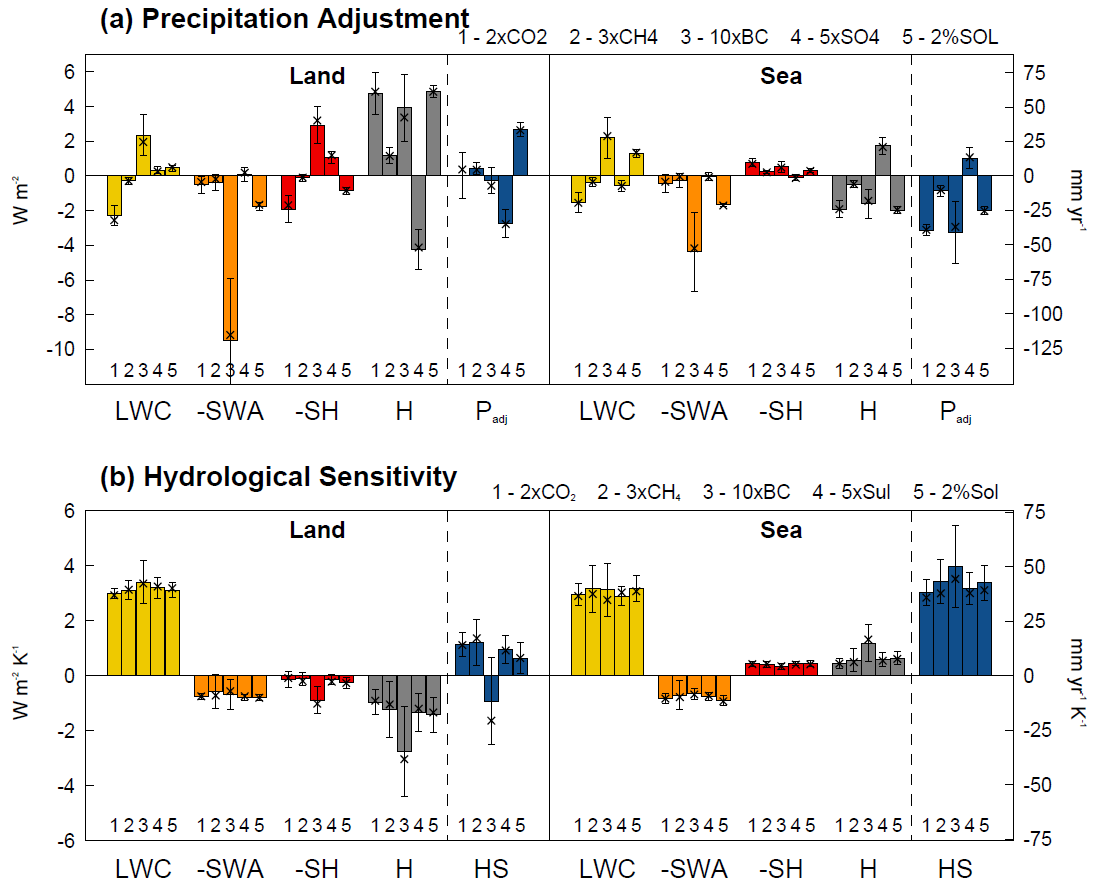


**Figure 2:** Multi-model land and sea mean (a) precipitation adjustment ( $P_{adj}$ , blue) and (b) hydrological sensitivity ( $HS$ , blue) in response to the PDRMIP forcing scenarios.  $P_{adj}$  and  $HS$  are decomposed into the contributions from the local atmospheric energy budget: net longwave cooling ( $LWC$ , yellow), net shortwave absorption ( $SWA$ , orange), sensible heat flux from the surface ( $SH$ , red) and the dry static energy flux divergence ( $H$ , dark grey). The hydrological sensitivity over land and sea is normalized by global mean temperature change. The sign of change in each component is given such that a positive value contributes positively to precipitation change. Results are shown in both energetic units (left axis) [(a)  $W m^{-2}$ , (b)  $W m^{-2} K^{-1}$ ], and precipitation units (right axis) [(a)  $mm yr^{-1}$  and (b)  $mm yr^{-1} K^{-1}$ ]. Error bars denote the standard deviation of model spread, and crosses show the median value.

In Figure 2, we split the precipitation and energy budget responses to forcing into land and sea means. It can be seen that the adjustment and feedback components are very different over land and sea. In response to CO<sub>2</sub> the land mean precipitation adjustment is negligible, whereas over the sea there is a reduction of  $-39.3 mm yr^{-1}$  (Fig. 2a). As seen for the global mean, over both land and sea doubling CO<sub>2</sub> causes a large reduction in atmospheric LW cooling. However, over land this is counteracted by changes in horizontal energy transport associated with induced circulation changes. This is due

to warming of the land surface in response to forcing, which occurs on very short timescales. Higher CO<sub>2</sub> concentrations cause increased downwelling LW radiation at the surface (Fig. S3a). To restore balance, over land there is an increase in upwelling LW radiation and surface sensible heat flux (Fig. S4a). This warms the lower troposphere, thus increasing instability and driving enhanced convection and precipitation. This does not occur over the oceans where the sea surface temperature is fixed in our experiments (Fig. S5a). Therefore, over the oceans the increased atmospheric LW absorption, combined with a shift of convection to over land, results in a large negative precipitation adjustment. A similar response is seen for 3xCH<sub>4</sub>, but with a somewhat smaller magnitude.

The precipitation adjustment over land in response to CO<sub>2</sub> exhibits the largest model spread of any forcing scenario (Fig. S2a). For all drivers, the horizontal heat transport associated with circulation changes contributes significantly to the land adjustment model spread. For 2xCO<sub>2</sub>, land SH flux also contributes significantly to the spread in land  $P_{\text{adj}}$ , with a higher cross-model correlation ( $r = -0.60$ ) than for any other scenario. This is likely due to the physiological effects of CO<sub>2</sub>, which affect stomatal closure leading to reduced evapotranspiration (Andrews et al., 2010a; Cao et al., 2010; Pu and Dickinson, 2014). This can be seen from the reduced latent heat (LH) flux from the surface over land (Fig. S4a), which also exhibits more variability in response to CO<sub>2</sub> than any other driver. Given the dependency of the CO<sub>2</sub> land precipitation adjustment on physiological effects, the importance of reducing uncertainty associated with vegetation schemes is evident. The global mean  $P_{\text{adj}}$  model spread is even more dependent on land surface fluxes, with a cross-model correlation coefficient between land SH flux and global  $P_{\text{adj}}$  of  $-0.79$ , as has also been seen in CMIP5 simulations (DeAngelis et al., 2016).

Changes in SO<sub>4</sub> and solar insolation drive the largest precipitation adjustments over land, despite having little effect on the global mean (Fig. 2a). Per unit TOA forcing sulphate produces the strongest land precipitation adjustment out of the five drivers (Fig. 3). Increased SO<sub>4</sub> strongly reduces downwelling SW radiation at the surface (Fig. S3a). As a result, the land surface cools, resulting in a decrease in upwelling LW radiation, and sensible and latent heat fluxes over land (Fig. S4a). This stabilizes the troposphere, inhibiting convection and precipitation over land. Unlike CO<sub>2</sub>, there is very little effect on atmospheric radiative cooling, therefore the shift in precipitation

from land to sea dominates. Increased insolation drives the opposite effect, with precipitation shifting from sea to land, due to the enhanced downwelling *SW* radiation at the surface. A small increase in atmospheric shortwave absorption results in a smaller magnitude land precipitation adjustment per unit TOA forcing than for sulphate.

Despite being shown to produce a large negative global mean precipitation adjustment (Andrews et al., 2010b; Samset et al., 2016), black carbon has very little effect on land mean precipitation (Fig. 2a). The reduction in precipitation is focused over the ocean. Atmospheric *SW* absorption increases significantly more over land than over sea ( $-9.5$  and  $-4.4 \text{ Wm}^{-2}$ , respectively), presumably due to the higher concentrations of BC over land (see Stjern et al. (Submitted)). However, the increase in *SW* absorption over land is largely offset by a decrease in *SH* flux and an increase in *LW* cooling and dry static energy flux divergence. The increased *LW* cooling will largely be due to warming of the atmosphere. *SW* dimming at the surface combined with atmospheric warming will reduce surface *SH* flux. The increase in dry static energy flux divergence indicates that circulation adjustments occur which act to enhance precipitation over land. Black carbon is thought to affect large-scale monsoonal circulation patterns (Ramanathan and Carmichael, 2008), particularly in India and South Asia (Ramanathan et al., 2005; Lau et al., 2006; Meehl et al., 2008; Kim et al., 2016). Increased *SW* absorption increases the atmospheric meridional heating gradient, therefore enhancing the south Asian monsoonal circulation (Lau et al., 2006; Meehl et al., 2008; Kim et al., 2016), which is consistent with the increased dry static energy flux divergence over land. For the adjustment there is no counteracting effect on circulation from changes in SST gradients. Over the oceans, the increased *SW* absorption dominates the adjustment, resulting in a large decrease in precipitation.

As seen in the global 10xBC response, the emissions driven models introduce a large amount of model spread over both land and sea (see triangles in Fig. S2a). In particular, there is a very large model spread in the *SW* absorption over land ranging from  $5.0$  to  $15.0 \text{ Wm}^{-2}$ . Both the land and ocean precipitation adjustments per unit TOA forcing also exhibit larger uncertainties than for any other driver (Fig. 3). This demonstrates there is also considerable uncertainty in the response which is not due to different perturbations in concentration.

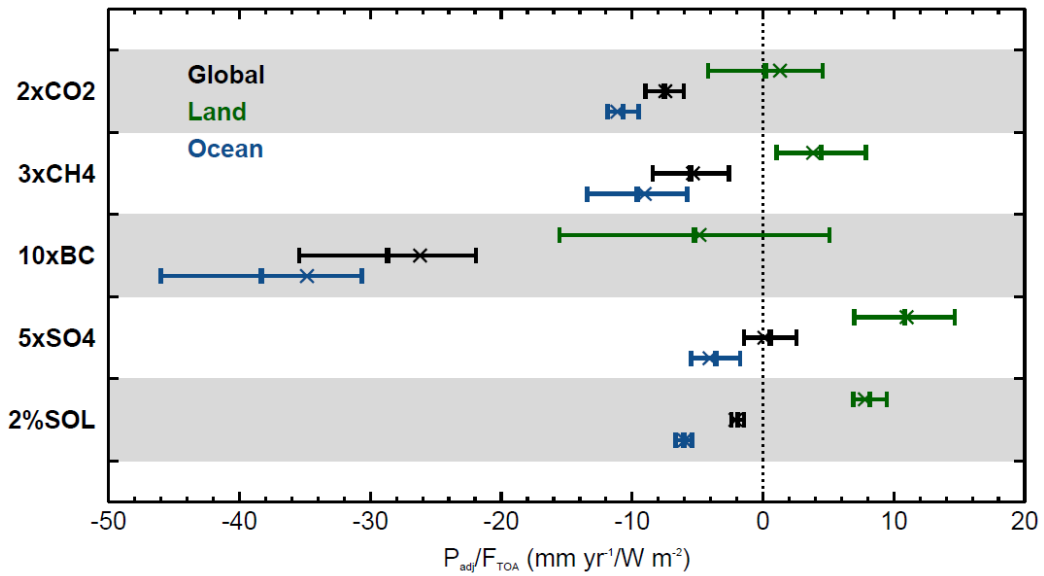


**Figure 3:** Multi-model mean precipitation adjustment ( $P_{adj}$ ) per unit global mean top of the atmosphere forcing ( $F_{TOA}$ ) for the PDRMIP forcing scenarios. Results are shown for global (black), land (green) and ocean (blue) mean precipitation adjustments. The error bars denote the standard deviation of model spread, and the crosses show the median value.

Excluding 10xBC (discussed below), the hydrological sensitivities over land and sea are fairly consistent between forcing scenarios, ranging from 8.0-15.1 mm yr<sup>-1</sup>K<sup>-1</sup> over land, and 38.1-43.1 mm yr<sup>-1</sup>K<sup>-1</sup> over sea (Fig. 2b). The hydrological sensitivity is considerably weaker over land than over sea for all scenarios. However, the radiative response is very similar, dominated by an increase in atmospheric LW cooling as temperature increases. There is also a small negative feedback due to enhanced SW absorption. Temperature has little effect on sensible heat flux over land, whereas over the sea there is a small negative feedback. The difference in hydrological sensitivity over land and sea mainly arises from the horizontal energy transport (Fig. 2b). As global mean surface temperature increases, dry static energy flux divergence increases over the ocean. This enhances the hydrological sensitivity over the ocean and reduces the hydrological sensitivity over land. This is likely driven by increased LH flux (evaporation) over the ocean as sea surface temperatures increase (Fig. S5b), providing moisture for convection and precipitation. Whereas over land, the increase in LH flux is limited by moisture availability (Fig. S4b). The enhanced heat transport from sea to land acts to suppress precipitation over land.

The feedback response for 10xBC is notably different to the other scenarios over both land and sea (Fig. 2b), and again exhibits the largest model spread (Fig. S2b). The very weak surface temperature response to black carbon (Stjern et al., Submitted) contributes to the high uncertainty of the feedbacks. Over land there is an increase in SH flux and a much larger decrease in dry static energy flux divergence. These effects result in a negative hydrological sensitivity over land. Conversely over the sea, the hydrological sensitivity for 10xBC is notably larger than for other drivers, caused by the larger dry static energy flux divergence.

#### **4.4.2 Simple Precipitation Model**

Based on the precipitation adjustment and feedback results from the PDRMIP simulations we construct a simple model to estimate land mean and sea mean precipitation change (for details on methods, see Section 4.3.4 and Eq. 3). Precipitation change at any given time is estimated using a linear combination of forcing-dependent adjustments (see Fig. 3), and a global mean temperature driven feedback. We use this simple model to emulate historical and future precipitation change over land and sea from 1850 to 2100 following RCP4.5 and RCP8.5 (Fig. 4).

The simple model matches well with the CMIP5 ensemble mean over both land and sea for both future pathways. Up to the end of the 20<sup>th</sup> century there is very little long term trend over the sea, before a projected rise during the 21<sup>st</sup> century for both scenarios (Fig. 4b, d). The rate of increase is higher and more sustained for RCP8.5. Over land there is a small reduction in precipitation during the second half of the 20<sup>th</sup> century, before a projected increase during the 21<sup>st</sup> century for both scenarios (Fig. 4a, c). The predicted rate of increase is higher over the oceans than over the land. Good agreement between the simple model and the CMIP5 historical and future trends indicates that modelled precipitation change over land and sea can be well described using the adjustment and feedback framework. This enables us to isolate the contributions of each climate driver to precipitation change over land and sea as discussed below.

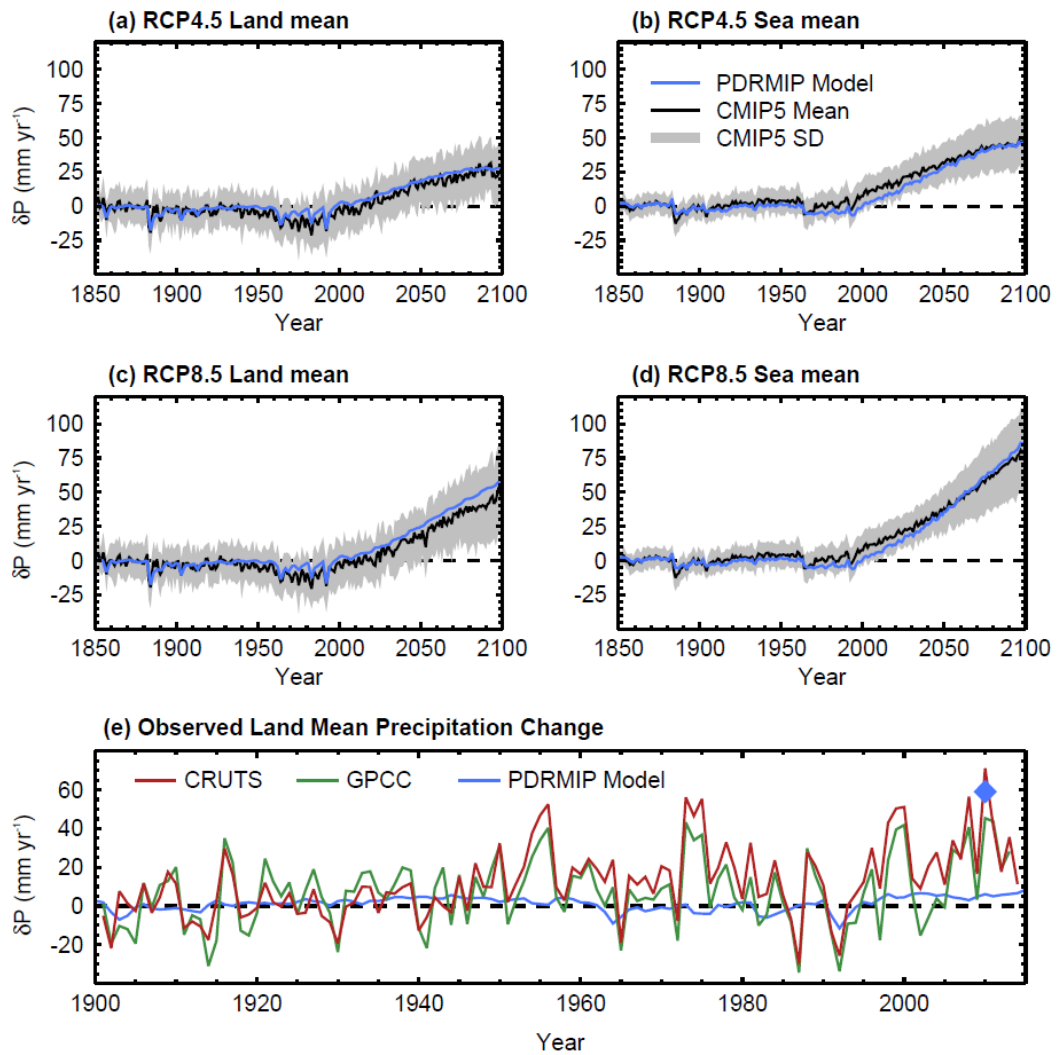


**Figure 4:** Historical and future (a, c) land-mean and (b, d) sea-mean precipitation change relative to pre-industrial for (a, b) RCP4.5 and (c, d) RCP8.5, calculated using the CMIP5 multi-model mean (black), and simple PDRMIP model (blue). Light grey shading denotes the standard deviation of CMIP5 model spread. In panel (e) the simple model (blue) is compared to observed land-mean precipitation change relative to the 1900-1930 climatology, calculated using the CRU TS v.3.23 data set (red), and the GPCC data set (green). The blue diamond denotes the predicted precipitation change by the year 2100 using the simple model following RCP8.5. For details of the simple model formulation see methods section 4.3.4.

The simple model is also used to estimate observed land mean precipitation change from 1900 to 2015 using observed temperature records (Fig. 4e). This is compared with CRU TS and GPCC land mean precipitation records. Despite an observed global mean warming trend of 0.07 K per decade from 1901 to 2010 (Morice et al., 2012), observations exhibit very little intensification of the hydrological cycle over land (Dai et al., 2009; Hartmann et al., 2013; Wu et al., 2013), as seen in Figure 4e. The simple model also exhibits an insignificant land precipitation trend during the 20<sup>th</sup> century when driven with observed temperatures. Anthropogenic aerosols are thought to have been important in reducing intensification of the global hydrological cycle over this period (Wu et al., 2013; Salzmänn, 2016). To understand why the modelled and observed trend is small, and to isolate which individual drivers are important over land and over sea, we can analyse the individual components of the simple model as discussed below.

Despite the model and observations being consistent in exhibiting no significant trend in land precipitation during the 20<sup>th</sup> century, it is clear from Figure 4e that the simple model does not capture much of the observed inter-annual variability. This indicates that the processes controlling inter-annual variability may be different from the adjustment and feedback processes driving the long-term trend represented in the simple model. Kramer and Soden (2016) found that on global scales the sensitivity of the hydrological cycle to surface warming differs fundamentally between internal variability and anthropogenically forced changes. Clear-sky radiative processes were found to dominate the global hydrological response to anthropogenic driven warming, while cloud processes dominate internal variability.

Figure 5 shows the separate contributions to precipitation change in the simple model from rapid adjustments for each forcing agent and the temperature driven feedback (see Section 4.3.4 and Figure S8 for details on forcings). Over land (Fig. 5a, c) during the 20<sup>th</sup> century the positive influence of rising global mean temperature (red) is entirely cancelled out by the negative sulphate and cloud albedo adjustment (dark blue). The combination of anthropogenic sulphate and volcanic forcing (light blue) drives a slight decrease in land mean precipitation between around 1950 and 1980. No other drivers strongly impact land mean precipitation through adjustments. Notably, CO<sub>2</sub> and black carbon have little direct impact on land mean precipitation, despite

significantly weakening the increase in global mean precipitation (Thorpe and Andrews, 2014).

During the 21<sup>st</sup> century as sulphate concentrations decline, rising global mean temperature increasingly dominates land mean precipitation change (Fig. 5a, c). As forcing-driven adjustments become less important during the 21<sup>st</sup> century, intensification of land precipitation should become more clearly observable. The inter-annual variability in the observations is large, with a de-trended standard deviation of 16.6 mm yr<sup>-1</sup> and 17.3 mm yr<sup>-1</sup> for CRU TS and GPCC, respectively. However, the simple model predicts that the increase in land mean precipitation from pre-industrial levels will exceed the observational standard deviation by 2039 and 2044, for RCP8.5 and RCP4.5, respectively. Therefore, anthropogenically driven intensification of land precipitation may become more evident in the near future.

The rate of increase in land precipitation is lower than over the sea, due to the weaker sensitivity of land precipitation to global temperature, associated with limited moisture availability. Therefore, land-only based observations are not suited for inferring the global hydrological sensitivity to validate models.

Sea mean precipitation change also exhibits very little trend over the 20<sup>th</sup> century, but it is different drivers which counteract the warming-driven intensification than seen for land. The influence of rising temperature is counteracted by the absorbing drivers, mainly CO<sub>2</sub> (grey) and black carbon (purple) (Fig. 5b, d). During the 21<sup>st</sup> century, rising global mean temperature increasingly dominates sea mean precipitation changes. However, the rate of increase in sea mean precipitation is limited by the negative CO<sub>2</sub> adjustment due to increasing concentrations.



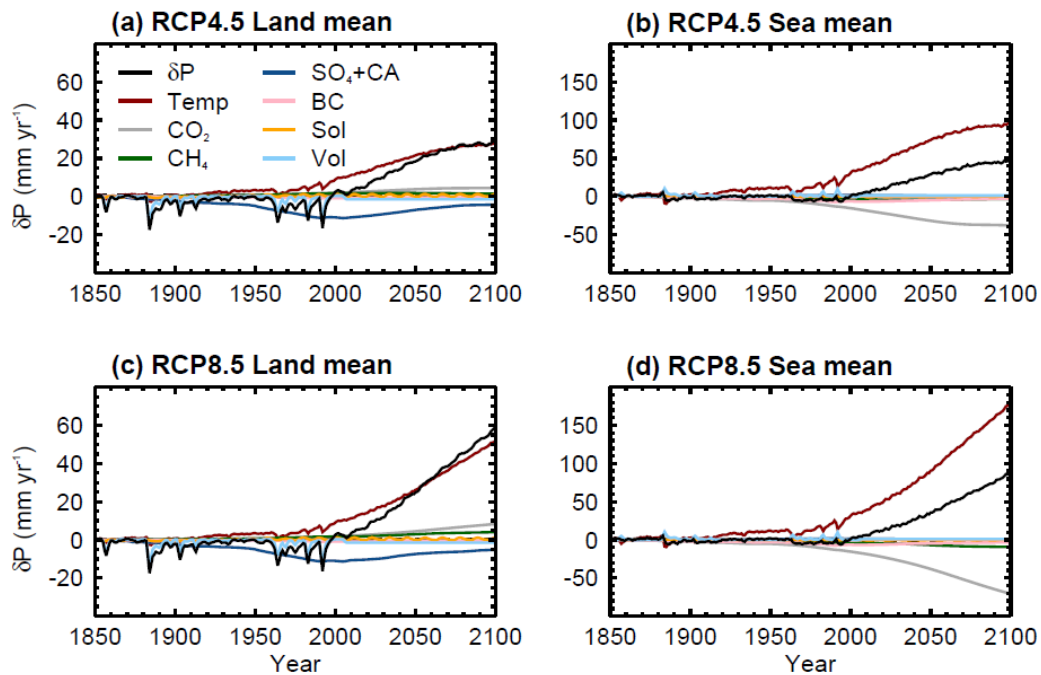


**Figure 5:** Driver contributions to historical and future (a, c) land and (b, d) sea mean precipitation change relative to pre-industrial, for (a, b) RCP4.5 and (c, d) RCP8.5 in the simple model. Coloured lines indicate the precipitation adjustment contribution from carbon dioxide ( $\text{CO}_2$ , grey), methane ( $\text{CH}_4$ , green), sulphate and cloud albedo ( $\text{SO}_4+\text{CA}$ , dark blue), black carbon (BC, pink), solar insolation (Sol, yellow) and volcanoes (Vol, light blue). Precipitation change driven by global mean surface temperature change is shown in red. Total precipitation change is shown in black. For details on methods see section 4.3.4.

## 4.5 Conclusions

We have presented the adjustment and feedback responses of precipitation and the atmospheric energy budget to five different forcings, across ten global climate models. The response of global, land and sea mean precipitation can be well understood through energetic arguments.  $\text{CO}_2$  and black carbon produce the strongest global mean precipitation adjustments due to enhanced atmospheric absorption reducing precipitation, but they also exhibit considerable model spread. For  $\text{CO}_2$ , this can be traced to a variable land precipitation adjustment driven by uncertainty in the response of land-atmosphere heat fluxes, likely resulting from physiological effects. For black carbon, emissions-based models introduce a large proportion of the spread, but there

is also considerable uncertainty in the precipitation response to black carbon for a given atmospheric forcing. The global hydrological sensitivity is primarily driven by an increase in LW cooling, which is highly consistent across forcings, but contributes most strongly to the inter-model spread. There is a small negative feedback, due to enhanced SW absorption, which exhibits very little model spread.

Over land and sea, the adjustment and feedback responses to forcing are very different. Over land, rapid precipitation change is most sensitive to non-absorbing or weakly-absorbing drivers (SO<sub>4</sub>, solar). This is due to the rapid land surface response affecting atmospheric stability, and driving large circulation changes. For drivers which strongly affect atmospheric absorption (CH<sub>4</sub>, CO<sub>2</sub>, black carbon), the circulation changes are largely balanced by the changes in net atmospheric cooling. Over the sea, it is the absorbing drivers which produce the largest adjustments. The hydrological sensitivity is significantly smaller over land than over sea for all forcings, despite very similar changes in radiative cooling. The difference is driven by enhanced horizontal energy transport from sea to land, which arises due to the larger increase in latent heat flux (evaporation) over the oceans fuelling enhanced divergence.

Based on the adjustment and feedback framework, precipitation change over land and sea can be estimated using a linear combination of forcing-dependent adjustments, and a temperature-driven feedback. This simple model can be used to disentangle the roles of the different forcing-driven adjustments and the temperature-driven feedback. The model, based on PDRMIP results, matches well with CMIP5 ensemble mean historical and future precipitation changes for RCP4.5 and RCP8.5. The simple model suggests that throughout the 20<sup>th</sup> century the influence of rising global temperatures on land precipitation has been counteracted mainly by adjustments in response to anthropogenic sulphate and volcanic forcing. As a result, the estimated long-term trends are very small in comparison to inter-annual variability seen in observations. However, as sulphate forcing declines and global temperatures continue to rise in the 21<sup>st</sup> century, a sustained positive trend in land precipitation is expected. This suggests that anthropogenically driven intensification of land mean precipitation may become clearly evident within the next few decades.

Over the ocean, the simple model suggests that adjustments in response to absorbing drivers (mainly CO<sub>2</sub> and black carbon) have largely negated the influence on

precipitation by rising temperatures during the 20<sup>th</sup> century. During the 21<sup>st</sup> century the temperature driven feedback increasingly dominates, leading to enhanced precipitation. Increasing CO<sub>2</sub> concentrations limit the rate at which precipitation increases due to the associated negative adjustment. The projected rate of increase is higher over the sea than over land due to the considerably higher sensitivity to temperature change.

## Acknowledgements

T.B.R. was supported by a NERC CASE award in collaboration with the Met Office NE/K007483/1. P.M.F. was supported by a Royal Society Wolfson Merit Award and NERC grant NE/K006038/1. T.A. was supported by the Newton Fund through the Met Office Climate Science for Service Partnership Brazil (CSSP Brazil). B.H.S., G.M., and Ø.H. were funded by the Research Council of Norway, through the grant NAPEX (229778). D.S. and G. F. thank NASA GISS for funding and acknowledge the NASA High-End Computing Program through the NASA Center for Climate Simulation at Goddard Space Flight Center for computational resources. O.B. acknowledges HPC resources from TGCC under the gencmip6 allocation provided by GENCI (Grand Equipement National de Calcul Intensif). T.T. is supported by the NEC SX-ACE supercomputer system of the National Institute for Environmental Studies, Japan, the Environmental Research and Technology Development Fund (S-12-3) of the Ministry of Environment, Japan and JSPS KAKENHI Grant Numbers JP15H01728 and JP15K12190. M.K., D.S. and A.V. were supported by the Natural Environment Research Council under grant NE/K500872/1, and from the Grantham Institute at Imperial College. Simulations with HadGEM2 and HadGEM3-GA4 were performed using the MONSooN system, a collaborative facility supplied under the Joint Weather and Climate Research Programme, which is a strategic partnership between the Met Office and the Natural Environment Research Council. D.O and A.K were supported by the Norwegian Research Council through the projects EVA (229771), EarthClim (207711/E10), NOTUR (nn2345k), and NorStore (ns2345k).

## References

- Allen, M.R., Ingram, W.J., 2002. Constraints on future changes in climate and the hydrologic cycle. *Nature* 419, 224–232. doi:10.1038/nature01092
- Andrews, T., Doutriaux-Boucher, M., Boucher, O., Forster, P.M., 2010a. A regional and global analysis of carbon dioxide physiological forcing and its impact on climate. *Clim. Dyn.* 36, 783–792. doi:10.1007/s00382-010-0742-1
- Andrews, T., Forster, P.M., Boucher, O., Bellouin, N., Jones, A., 2010b. Precipitation, radiative forcing and global temperature change. *Geophys. Res. Lett.* 37, doi:10.1029/2010GL043991
- Bala, G., Caldeira, K., Nemani, R., 2009. Fast versus slow response in climate change: implications for the global hydrological cycle. *Clim. Dyn.* 35, 423–434. doi:10.1007/s00382-009-0583-y
- Becker, A., Finger, P., Meyer-Christoffer, A., Rudolf, B., Schamm, K., Schneider, U., Ziese, M., 2013. A description of the global land-surface precipitation data products of the Global Precipitation Climatology Centre with sample applications including centennial (trend) analysis from 1901-present. *Earth Syst. Sci. Data* 5, 71–99. doi:10.5194/essd-5-71-2013
- Bond, T.C., Doherty, S.J., Fahey, D.W., Forster, P.M., Berntsen, T., Deangelo, B.J., Flanner, M.G., Ghan, S., Kircher, B., Koch, D., Kinne, S., Kondo, Y., Quinn, P.K., Sarofim, M.C., Schultz, M.G., Schulz, M., Venkataraman, C., Zhang, H., Zhang, S., Bellouin, N., Guttikunda, S.K., Hopke, P.K., Jacobson, M.Z., Kaiser, J.W., Klimont, Z., Lohmann, U., Schwarz, J.P., Shindell, D., Storelvmo, T., Warren, S.G., Zender, C.S., 2013. Bounding the role of black carbon in the climate system: A scientific assessment. *J. Geophys. Res. Atmos.* 118, 5380–5552. doi:10.1002/jgrd.50171
- Bony, S., Bellon, G., Klocke, D., Sherwood, S., Fermepin, S., Denvil, S., 2013. Robust direct effect of carbon dioxide on tropical circulation and regional precipitation. *Nat. Geosci.* 6, 447–451. doi:10.1038/ngeo1799
- Boucher, O., Balkanski, Y., Hodnebrog, Ø., Lund, C., Myhre, G., 2016. Jury is still out on the radiative forcing by black carbon. *Proc. Natl. Acad. Sci.* 113, 5092–5093. doi:10.1073/pnas.1607005113
- Cao, L., Bala, G., Caldeira, K., Nemani, R., Ban-Weiss, G., 2010. Importance of carbon dioxide physiological forcing to future climate change. *Proc. Natl. Acad. Sci.* 107, 9513–9518. doi:10.1073/pnas.0913000107
- Chadwick, R., Boutle, I., Martin, G., 2013. Spatial Patterns of Precipitation Change in CMIP5: Why the Rich Do Not Get Richer in the Tropics. *J. Clim.* 26, 3803–3822. doi:10.1175/JCLI-D-12-00543.1
- Chung, C.E., Ramanathan, V., Decremmer, D., 2012. Observationally constrained estimates of carbonaceous aerosol radiative forcing. *Proc. Natl. Acad. Sci. U. S. A.* 109, 11624–9. doi:10.1073/pnas.1203707109
- Collins, M., Knutti, R., Arblaster, J., Dufresne, J.-L., Fichefet, T., Friedlingstein, P., Gao, X., Gutowski, W.J., Johns, T., Krinner, G., Shongwe, M., Tebaldi, C.,

- Weaver, A.J., Wehner, M., 2013. Long-term Climate Change: Projections, Commitments and Irreversibility. *Clim. Chang. 2013 Phys. Sci. Basis. Contrib. Work. Gr. I to Fifth Assess. Rep. Intergov. Panel Clim. Chang.* 1029–1136. doi:10.1017/CBO9781107415324.024
- Dai, A., Qian, T., Trenberth, K.E., Milliman, J.D., 2009. Changes in continental freshwater discharge from 1948 to 2004. *J. Clim.* 22, 2773–2792. doi:10.1175/2008JCLI2592.1
- DeAngelis, A.M., Qu, X., Hall, A., 2016. Importance of vegetation processes for model spread in the fast precipitation response to CO<sub>2</sub> forcing. *Geophys. Res. Lett.* 1–10. doi:10.1002/2016GL071392
- DeAngelis, A.M., Qu, X., Zelinka, M.D., Hall, A., 2015. An observational radiative constraint on hydrologic cycle intensification. *Nature* 528, 249–53. doi:10.1038/nature15770
- Dong, B., Sutton, R.T., Highwood, E., Wilcox, L., 2014. The impacts of European and Asian anthropogenic sulfur dioxide emissions on Sahel rainfall. *J. Clim.* 27, 7000–7017. doi:10.1175/JCLI-D-13-00769.1
- Fläschner, D., Mauritsen, T., Stevens, B., 2016. Understanding the intermodel spread in global-mean hydrological sensitivity. *J. Clim.* 29, 801–817. doi:10.1175/JCLI-D-15-0351.1
- Harris, I., Jones, P.D., Osborn, T.J., Lister, D.H., 2014. Updated high-resolution grids of monthly climatic observations - the CRU TS3.10 Dataset. *Int. J. Climatol.* 34, 623–642. doi:10.1002/joc.3711
- Hartmann, D.J., Klein Tank, A.M.G., Rusticucci, M., Alexander, L. V, Brönnimann, S., Charabi, Y.A.-R., Dentener, F.J., Dlugokencky, E.J., Easterling, D.R., Kaplan, A., Soden, B.J., Thorne, P.W., Wild, M., Zhai, P., 2013. Observations: Atmosphere and Surface. *Clim. Chang. 2013 Phys. Sci. Basis. Contrib. Work. Gr. I to Fifth Assess. Rep. Intergov. Panel Clim. Chang.* 159–254. doi:10.1017/CBO9781107415324.008
- Held, I., Soden, B., 2006. Robust responses of the hydrological cycle to global warming. *J. Clim.* 5686–5699.
- Kim, M.K., Lau, W.K.M., Kim, K.M., Sang, J., Kim, Y.H., Lee, W.S., 2016. Amplification of ENSO effects on Indian summer monsoon by absorbing aerosols. *Clim. Dyn.* 46, 2657–2671. doi:10.1007/s00382-015-2722-y
- Kramer, R.J., Soden, B.J., 2016. The Sensitivity of the Hydrological Cycle to Internal Climate Variability versus Anthropogenic Climate Change. *J. Clim.* 29, 3661–3673. doi:10.1175/JCLI-D-15-0408.1
- Kvalevåg, M.M., Samset, B.H., Myhre, G., 2013. Hydrological sensitivity to greenhouse gases and aerosols in a global climate model. *Geophys. Res. Lett.* 40, 1432–1438. doi:10.1002/grl.50318
- Lambert, F.H., Faull, N.E., 2007. Tropospheric adjustment: The response of two general circulation models to a change in insolation. *Geophys. Res. Lett.* 34, L03701. doi:10.1029/2006GL028124
- Lambert, F.H., Webb, M.J., Yoshimori, M., Yokohata, T., 2014. The cloud radiative

- effect on the atmospheric energy budget and global mean precipitation. *Clim. Dyn.* 2301–2325. doi:10.1007/s00382-014-2174-9
- Lau, K.M., Kim, M.K., Kim, K.M., 2006. Asian summer monsoon anomalies induced by aerosol direct forcing: The role of the Tibetan Plateau. *Clim. Dyn.* 26, 855–864. doi:10.1007/s00382-006-0114-z
- MacIntosh, C.R., Allan, R.P., Baker, L.H., Bellouin, N., Collins, W., Mousavi, Z., Shine, K.P., 2016. Contrasting fast precipitation responses to tropospheric and stratospheric ozone forcing. *Geophys. Res. Lett.* 43, 1263–1271. doi:10.1002/2015GL067231
- Meehl, G. A., Arblaster, J.M., Collins, W.D., 2008. Effects of Black Carbon Aerosols on the Indian Monsoon. *J. Clim.* 21, 2869–2882. doi:10.1175/2007JCLI1777.1
- Meinshausen, M., Smith, S.J., Calvin, K., Daniel, J.S., Kainuma, M.L.T., Lamarque, J., Matsumoto, K., Montzka, S.A., Raper, S.C.B., Riahi, K., Thomson, A., Velders, G.J.M., van Vuuren, D.P.P., 2011. The RCP greenhouse gas concentrations and their extensions from 1765 to 2300. *Clim. Change* 109, 213–241. doi:10.1007/s10584-011-0156-z
- Mitchell, J., Wilson, C., Cunnington, W., 1987. On CO<sub>2</sub> climate sensitivity and model dependence of results. *Q. J. R. Meteorol. Soc.* 113, 293–322. doi:10.1256/smsqj.47516
- Morice, C.P., Kennedy, J.J., Rayner, N.A., Jones, P.D., 2012. Quantifying uncertainties in global and regional temperature change using an ensemble of observational estimates: The HadCRUT4 data set. *J. Geophys. Res. Atmos.* 117, 1–22. doi:10.1029/2011JD017187
- Muller, C.J., O’Gorman, P. A., 2011. An energetic perspective on the regional response of precipitation to climate change. *Nat. Clim. Chang.* 1, 266–271. doi:10.1038/nclimate1169
- Myhre, G., Forster, P.M., Samset, B.H., Hodnebrog, Ø., Sillmann, J., Aalbergstjø, S.G., Andrews, T., Boucher, O., Faluvegi, G., Fläschner, D., Iversen, T., Kasoar, M., Kharin, V., Kirkevåg, A., Lamarque, J.-F., Olivié, D., Richardson, T.B., Shindell, D., Shine, K.P., Stjern, C.W., Takemura, T., Voulgarakis, A., Zwiers, F., 2016a. PDRMIP: A Precipitation Driver and Response Model Intercomparison Project, Protocol and preliminary results. *Bull. Am. Meteorol. Soc.* BAMS-D-16-0019.1. doi:10.1175/BAMS-D-16-0019.1
- Myhre, G., Forster, P.M., Samset, B.H., Hodnebrog, Ø., Sillmann, J., Andrews, T., Boucher, O., Faluvegi, G., Fläschner, D., Iversen, T., Kasoar, M., Kharin, V., Kirkevåg, A., Lamarque, J.-F., Olivié, D., Richardson, T.B., Shindell, D.T., Shine, K.P., Takemura, T., Voulgarakis, A., Zwiers, F.W., 2016b. PDRMIP: A Precipitation Driver and Response Model Intercomparison Project. Submitted.
- Myhre, G., Samset, B.H., 2015. Standard climate models radiation codes underestimate black carbon radiative forcing. *Atmos. Chem. Phys.* 15, 2883–2888. doi:10.5194/acp-15-2883-2015
- Myhre, G., Samset, B.H., Schulz, M., Balkanski, Y., Bauer, S., Bernsten, T.K., Bian, H., Bellouin, N., Chin, M., Diehl, T., Easter, R.C., Feichter, J., Ghan, S.J.,

- Hauglustaine, D., Iversen, T., Kinne, S., Kirkevåg, A., Lamarque, J.F., Lin, G., Liu, X., Lund, M.T., Luo, G., Ma, X., Van Noije, T., Penner, J.E., Rasch, P.J., Ruiz, A., Seland, Skeie, R.B., Stier, P., Takemura, T., Tsigaridis, K., Wang, P., Wang, Z., Xu, L., Yu, H., Yu, F., Yoon, J.H., Zhang, K., Zhang, H., Zhou, C., 2013a. Radiative forcing of the direct aerosol effect from AeroCom Phase II simulations. *Atmos. Chem. Phys.* 13, 1853–1877. doi:10.5194/acp-13-1853-2013
- Myhre, G., Shindell, D., Bréon, F.-M., Collins, W., Fuglestedt, J., Huang, J., Koch, D., Lamarque, J.-F., Lee, D., Mendoza, B., Nakajima, T., Robock, A., Stephens, G., Takemura, T., Zhang, H., 2013b. Anthropogenic and Natural Radiative Forcing, in: Intergovernmental Panel on Climate Change (Ed.), *Climate Change 2013 - The Physical Science Basis*. Cambridge University Press, Cambridge, pp. 659–740. doi:10.1017/CBO9781107415324.018
- O’Gorman, P.A., Allan, R.P., Byrne, M.P., Previdi, M., 2011. Energetic Constraints on Precipitation Under Climate Change. *Surv. Geophys.* 33, 585–608. doi:10.1007/s10712-011-9159-6
- Pendergrass, A.G., Hartmann, D.L., 2014. The Atmospheric Energy Constraint on Global-Mean Precipitation Change. *J. Clim.* 27, 757–768. doi:10.1175/JCLI-D-13-00163.1
- Previdi, M., 2010. Radiative feedbacks on global precipitation. *Environ. Res. Lett.* 5, 25211. doi:10.1088/1748-9326/5/2/025211
- Pu, B., Dickinson, R.E., 2014. Hydrological changes in the climate system from leaf responses to increasing CO<sub>2</sub>. *Clim. Dyn.* 42, 1905–1923. doi:10.1007/s00382-013-1781-1
- Ramanathan, V., Carmichael, G., 2008. Global and regional climate changes due to black carbon. *Nat. Geosci.* 1, 221–227. doi:10.1038/ngeo156
- Ramanathan, V., Chung, C., Kim, D., Bettge, T., Buja, L., Kiehl, J.T., Washington, W.M., Fu, Q., Sikka, D.R., Wild, M., 2005. Atmospheric brown clouds: impacts on South Asian climate and hydrological cycle. *Proc. Natl. Acad. Sci. U. S. A.* 102, 5326–33. doi:10.1073/pnas.0500656102
- Richardson, T.B., Forster, P.M., Andrews, T., Parker, D.J., 2016a. Understanding the Rapid Precipitation Response to CO<sub>2</sub> and Aerosol Forcing on a Regional Scale. *J. Clim.* 29, 583–594. doi:10.1175/JCLI-D-15-0174.1
- Richardson, T.B., Samset, B.H., Andrews, T., Myhre, G., Forster, P.M., 2016b. An assessment of precipitation adjustment and feedback computation methods. *J. Geophys. Res. Atmos.* 121, 11,608–11,619. doi:10.1002/2016JD025625
- Salzmann, M., 2016. Global warming without global mean precipitation increase? *Sci. Adv.* 2. doi:10.1126/sciadv.1501572
- Samset, B.H., Myhre, G., Forster, P.M., Hodnebrog, Ø., Andrews, T., Faluvegi, G., Fläschner, D., Kasoar, M., Kharin, V., Kirkevåg, A., Lamarque, J.-F., Olivie, D., Richardson, T.B., Shindell, D., Shine, K.P., Takemura, T., Voulgarakis, A., 2016. Fast and slow precipitation responses to individual climate forcings: A PDRMIP multi-model study. *Geophys. Res. Lett.* doi:10.1002/2016GL068064



- Samset, B.H., Myhre, G., Schulz, M., 2014. Upward adjustment needed for aerosol radiative forcing uncertainty. *Nat. Clim. Chang.* 4, 230–232. doi:10.1038/nclimate2170
- Seager, R., Naik, N., Vecchi, G. a., 2010. Thermodynamic and Dynamic Mechanisms for Large-Scale Changes in the Hydrological Cycle in Response to Global Warming. *J. Clim.* 23, 4651–4668. doi:10.1175/2010JCLI3655.1
- Sherwood, S.C., Bony, S., Boucher, O., Bretherton, C., Forster, P.M., Gregory, J.M., Stevens, B., 2015. Adjustments in the forcing-feedback framework for understanding climate change. *Bull. Am. Meteorol. Soc.* 96, 217–228. doi:10.1175/BAMS-D-13-00167.1
- Shindell, D.T., Lamarque, J.F., Schulz, M., Flanner, M., Jiao, C., Chin, M., Young, P.J., Lee, Y.H., Rotstayn, L., Mahowald, N., Milly, G., Faluvegi, G., Balkanski, Y., Collins, W.J., Conley, A.J., Dalsoren, S., Easter, R., Ghan, S., Horowitz, L., Liu, X., Myhre, G., Nagashima, T., Naik, V., Rumbold, S.T., Skeie, R., Sudo, K., Szopa, S., Takemura, T., Voulgarakis, A., Yoon, J.H., Lo, F., 2013. Radiative forcing in the ACCMIP historical and future climate simulations. *Atmos. Chem. Phys.* 13, 2939–2974. doi:10.5194/acp-13-2939-2013
- Stjern, C.W., Samset, B.H., Myhre, G., Forster, P.M., Hodnebrog, Ø., Sillmann, J., Andrews, T., Boucher, O., Faluvegi, G., Iversen, T., Kasoar, M., Kharin, V., Kirkevåg, A., Lamarque, J.-F., Olivié, D., Richardson, T.B., Shindell, D., Shine, K.P., Smith, C., Takemura, T., Voulgarakis, A., Zwiers, F., Submitted. Rapid adjustments cause weak surface temperature response to increased black carbon concentrations.
- Takahashi, K., 2009. The global hydrological cycle and atmospheric shortwave absorption in climate models under CO<sub>2</sub> forcing. *J. Clim.* 22, 5667–5675. doi:10.1175/2009JCLI2674.1
- Takemura, T., 2012. Distributions and climate effects of atmospheric aerosols from the preindustrial era to 2100 along Representative Concentration Pathways (RCPs) simulated using the global aerosol model SPRINTARS. *Atmos. Chem. Phys.* 12, 11555–11572. doi:10.5194/acp-12-11555-2012
- Thorpe, L., Andrews, T., 2014. The physical drivers of historical and 21st century global precipitation changes. *Environ. Res. Lett.* 9, 64024. doi:10.1088/1748-9326/9/6/064024
- Wake, B., 2013. Flooding costs. *Nat. Clim. Chang.* 3, 778–778. doi:10.1038/nclimate1997
- Wu, P., Christidis, N., Stott, P., 2013. Anthropogenic impact on Earth's hydrological cycle. *Nat. Clim. Chang.* 3, 807–810. doi:10.1038/nclimate1932

## **Chapter 5: Importance of carbon dioxide physiological forcing on projected Amazonian precipitation change**

T. B. Richardson<sup>1</sup>, P. M. Forster<sup>1</sup>, T. Andrews<sup>2</sup>, O. Boucher<sup>3</sup>, G. Faluvegi<sup>4</sup>, D. Fläschner<sup>5</sup>, Ø. Hodnebrog<sup>6</sup>, M. Kasoar<sup>7</sup>, V. Kharin<sup>8</sup>, A. Kirkevåg<sup>9</sup>, J.-F. Lamarque<sup>10</sup>, G. Myhre<sup>6</sup>, D. Olivie<sup>9</sup>, B. H. Samset<sup>6</sup>, D. Shawki<sup>7</sup>, D. Shindell<sup>11</sup>, T. Takemura<sup>12</sup>, A. Voulgarakis<sup>7</sup>

Prepared for submission to Geophysical Research Letters

1. University of Leeds, United Kingdom
2. Met Office Hadley Centre, United Kingdom
3. Institut Pierre-Simon Laplace, Université Pierre et Marie Curie / CNRS, 4 place Jussieu, Paris, France
4. NASA Goddard Institute for Space Studies and Center for Climate Systems Research, Columbia University, New York, USA
5. Max-Planck-Institut für Meteorologie, Hamburg, Germany
6. CICERO Center for International Climate and Environmental Research – Oslo, Norway
7. Imperial College London, London, United Kingdom
8. Canadian Centre for Climate Modelling and Analysis, Gatineau, Canada
9. Norwegian Meteorological Institute, Oslo, Norway
10. NCAR/UCAR, Boulder, USA
11. Duke University, Durham, USA
12. Kyushu University, Fukuoka, Japan

## 5.1 Abstract

Future projections of east Amazonian precipitation indicate drying, but they are uncertain and poorly understood. In this study we analyse the precipitation response over the Amazon region to individual atmospheric forcings using a number of global climate models. Black carbon is found to drive reduced precipitation over the Amazon, due to temperature-driven circulation feedbacks, but the magnitude is uncertain. CO<sub>2</sub> drives reductions in precipitation concentrated in the east, mainly due to a robustly negative, but highly variable in magnitude, precipitation adjustment. We find that the physiological effect of CO<sub>2</sub> is the dominant driver of the adjustment due to reduced latent heating, and is mainly responsible for the large model spread. Using a simple model we show that CO<sub>2</sub> physiological effects may dominate future multi-model mean projections over the Amazon. However, in individual models temperature-driven circulation feedbacks can be large, but due to little agreement, they largely cancel out in the model-mean.

## 5.2 Introduction

The Amazon rainforest is a key component of the global climate system, accounting for 40% of global tropical forest area (Aragão et al., 2014). An estimated 120 billion tonnes of carbon are stored in the Amazon rainforest (Malhi et al., 2006), playing an important role in the global carbon cycle. Vegetation and the carbon balance in the Amazon are sensitive to changes in precipitation patterns (Phillips et al., 2009; Gatti et al., 2014; Hilker et al., 2014; Zhang et al., 2015). Reduced forest productivity over the Amazon could exacerbate atmospheric CO<sub>2</sub> levels, and consequently enhance global warming (Fung et al., 2005; Booth et al., 2012; Brienen et al., 2015). However, observed trends and future projections of Amazonian precipitation are highly uncertain (Fu et al., 2013; Joetzjer et al., 2013; Orłowsky and Seneviratne, 2013; Boisier et al., 2015; Duffy et al., 2015).

Observations suggest an increasing trend in drought conditions (Li et al., 2008), and a lengthening of the dry season over parts of the Amazon (Fu et al., 2013). In spite of this, total precipitation is thought to have increased in recent decades due to a stronger wet season (Gloor et al., 2013). Global climate model future projections generally indicate drying and lengthening of the dry season (Joetzjer et al., 2013; Boisier et al., 2015), but the spread is large. It is difficult to disentangle what drivers are responsible for the projected changes and associated uncertainties. A number of factors could influence precipitation over the Amazon, including a warming climate (Joetzjer et al., 2013; Duffy et al., 2015), land-use change (Spracklen and Garcia-Carreras, 2015; Alves et al., 2017) and rapid adjustments in response to atmospheric forcing agents (Andrews et al., 2010a; Samset et al., 2016). Rapid adjustments occur due to the near-instantaneous impact on the atmospheric energy budget (Mitchell et al., 1987; Lambert and Faull, 2007; Andrews et al., 2010b). Forcing agents, such as CO<sub>2</sub> and black carbon, have been shown to induce significant circulation and regional precipitation adjustments in the absence of global mean warming (Bony et al., 2013; Richardson et al., 2016a; Samset et al., 2016).

CO<sub>2</sub> causes rapid adjustments in precipitation not only due to radiative effects, but also due to effects on plant stomata (Cao et al., 2009; Andrews et al., 2010a). Higher CO<sub>2</sub> concentrations mean plant stomata do not open as wide, resulting in reduced evapotranspiration flux to the atmosphere, known as the CO<sub>2</sub> physiological effect

(Field et al., 1995; Betts et al., 1997). Given the high level of vegetation and recycling of water which occurs in the Amazon, the CO<sub>2</sub> physiological effect could strongly affect precipitation in this region. Previous studies have highlighted the Amazon as a region where physiological effects may be important (Andrews et al., 2010a; Pu and Dickinson, 2014; Abe et al., 2015; Chadwick et al., 2017). However, the precipitation and circulation response is uncertain and poorly understood.

In this study we analyse output from a number of global climate models participating in the Precipitation Driver and Response Model Intercomparison Project (PDRMIP), and the Coupled Model Intercomparison Project Phase 5 (CMIP5). We investigate the precipitation response in the Amazon region to five individual forcing scenarios (CO<sub>2</sub>, CH<sub>4</sub>, SO<sub>4</sub>, black carbon and solar insolation), separating the response into forcing-dependent adjustments and temperature-driven feedbacks. The precipitation response due to CO<sub>2</sub> physiological forcing is isolated using CMIP5 simulations. The potential impact of CO<sub>2</sub> on precipitation in the Amazon region by the end of the 21<sup>st</sup> century is estimated using a simple model, based on top of the atmosphere forcing and global surface temperature change.

### 5.3 Methods

We analyse output from ten global climate models (CanESM2, NorESM1, HadGEM2-ES, HadGEM3-GA4, GISS-E2-R, IPSL-CM5A, CESM1-CAM4, CESM1-CAM5, MPI-ESM and MIROC-SPRINTARS) participating in PDRMIP (see Myhre et al., (2016) for details). Five abrupt global forcing scenarios are investigated: doubling CO<sub>2</sub> concentration (2xCO<sub>2</sub>), tripling methane concentration (3xCH<sub>4</sub>), ten times black carbon concentration or emissions (10xBC), five times sulphate concentration or SO<sub>2</sub> emissions (5xSO<sub>4</sub>), and a two percent increase in solar insolation (2%SOL). Perturbations were relative to either present-day or preindustrial values. The simulations were performed with sea surface temperatures (SSTs) fixed for 15 years, and with a slab or fully coupled ocean (coupled) for 100 years. All changes were calculated as the difference between the perturbed run and corresponding control run.

We also use output from 21 CMIP5 global climate models for four sets of experiments (see Table S1). To isolate CO<sub>2</sub> physiological effects on precipitation we analyse two

sets of CMIP5 atmosphere-only simulations in which SSTs are prescribed, and atmospheric CO<sub>2</sub> quadrupled. The first set of simulations prescribe SSTs and sea ice based on the model-simulated preindustrial climatology (sstClim and sstClim4xCO<sub>2</sub>), and the second set prescribe SSTs and sea ice based on observations over the period 1979-2008 (amip and amip4xCO<sub>2</sub>). A key difference between the two setups is that the sstClim simulations include CO<sub>2</sub> physiological effects and the amip experiments do not (Taylor et al., 2011). There were some models which did not follow these protocols, but these have previously been identified and they are not included our analysis (DeAngelis et al., 2016a). The precipitation response for each set of experiments is calculated by differencing the perturbed run with the corresponding control run. We then isolate the physiological effects by differencing the sstClim and amip responses to CO<sub>2</sub>.

The models used for the sstClim simulations include a sensitivity of stomatal conductance to CO<sub>2</sub> concentration, whereby the stomatal conductance is parameterised as a function of CO<sub>2</sub> concentration. The stomatal conductance determines the evapotranspiration flux to the atmosphere, influencing the hydrological cycle. For details on individual model vegetation schemes see the references listed in Table S2. In contrast, in the amip simulations the vegetation schemes are not affected by the increase in CO<sub>2</sub> (Taylor et al., 2011).

In our analysis, we use the comparison of the sstClim and amip experiments to infer the physiological effects of CO<sub>2</sub> on precipitation. It should be noted, however, that the baseline SSTs are different which could influence results. Nevertheless, the changes in precipitation are shown to be driven locally through changes in land surface fluxes, rather than through changes in circulation or advection of moisture or energy (Figure 3). This suggests that the different SSTs do not strongly affect the hydrological responses. In addition, it should be noted that not all the same models are available for both the sstClim and amip experiments (see Table S1). A comparison of the sstClim and amip responses using a subset of five models that performed both simulations is shown in Figure S6. The results are very consistent with those presented in Figure 3 in the main text that includes all available models. This indicates that the use of different models for each experiment does not significantly affect the results.

To help understand the precipitation responses we analyse the atmospheric energy and moisture budgets. Due to the latent heat released, changes in global mean precipitation are tightly constrained by changes in net atmospheric cooling, and this can be extended to local scales by taking into account divergence in dry static energy flux as shown in Equation 1. Atmospheric moisture also provides an additional constraint on local precipitation as shown in Equation 1.

$$L\delta P = \delta LWC - \delta SWA - \delta SH + \delta H = \delta LH + L\delta M, \quad (1)$$

where  $L$  is the latent heat of condensation,  $P$  is local precipitation,  $LWC$  is the net atmospheric longwave radiative cooling,  $SWA$  is the net atmospheric shortwave absorption,  $SH$  is the sensible heat flux from the surface,  $H$  is the dry static energy flux divergence,  $LH$  is the latent heat flux from the surface,  $M$  is moisture convergence, and  $\delta$  represents a perturbation between climates. The  $\delta H$  and  $\delta M$  terms are calculated as residuals.

Previous work has shown that it is useful to separate the precipitation response to climate drivers into a forcing-dependent adjustment and a temperature-driven feedback. Following the methods outlined by Richardson et al. (2016b), we separate the precipitation response to the PDRMIP scenarios into an adjustment and feedback. The adjustment is taken as the fixed SST response, in which temperature driven feedbacks are inhibited. The feedback response is calculated by subtracting the fixed SST response from the total response in the ocean coupled simulations. The total response is taken as the mean change for the last 50 years of the coupled simulations. It should be noted that the models will not have yet reached equilibrium, so some further temperature-driven feedbacks would be expected.

Based on the PDRMIP 2xCO<sub>2</sub> simulations, we construct a simple model to estimate the potential contribution of CO<sub>2</sub> and increasing temperature to projected precipitation change at the end of the 21<sup>st</sup> century (2081-2100) over the Amazon region. Using similar methods to Richardson et al. (in prep) we calculate an  $R$  factor for CO<sub>2</sub>, which is the precipitation adjustment over the Amazon region per unit global mean top of the atmosphere (TOA) forcing, and a hydrological sensitivity ( $HS$ ), which is the precipitation feedback over the Amazon region per unit global mean temperature change. The  $R$  factor and hydrological sensitivity is taken as the PDRMIP multi-model mean. We then use equation 2 to estimate the contribution of CO<sub>2</sub> and temperature

change to precipitation change over the Amazon region for the end of the 21<sup>st</sup> century following two different Representative Concentration Pathways, RCP4.5 and RCP8.5.

$$\delta P = (R \times F_{CO_2}) + (\delta T \times HS), \quad (2)$$

where,  $\delta P$  is the change in precipitation,  $F_{CO_2}$  is the global mean TOA forcing, and  $\delta T$  is the global mean surface temperature change.  $F_{CO_2}$  values for 2081-2100 are taken from Meinshausen et al. (2011), and  $\delta T$  is taken as the CMIP5 multi-model mean. Equation 2 is used to estimate precipitation change for the region mean shown in Figure 1a, and also spatially for the Amazon region by calculating  $R$  and  $HS$  for each gridpoint.

## 5.4 Results and Discussion

### 5.4.1 Precipitation response to forcing

We first look at the precipitation response in the Amazon region to individual atmospheric forcings using the PDRMIP model ensemble. Figure 1 shows the PDRMIP multi-model mean precipitation response to abrupt increases in CO<sub>2</sub>, CH<sub>4</sub>, SO<sub>4</sub>, black carbon and solar insolation. In response to doubling CO<sub>2</sub>, precipitation is reduced over much of the Amazon, in particular the central and eastern regions (Fig 1a). Conversely, along the western edge of South America precipitation is enhanced. The models exhibit good agreement on reduced precipitation in the northeast. However, the magnitude of the change, and how far it extends west is variable.

The 10xBC response also shows considerable drying over the Amazon region (Fig 1d). Over much of northern South America 80% of models agree on reduced precipitation in response to enhanced black carbon. The forcing scenarios 3xCH<sub>4</sub>, 5xSO<sub>4</sub> and 2%Sol produce only small multi-model mean responses in the central and eastern Amazon region (Fig. 1b, 1c, 1e). Sulphate and solar forcing affect precipitation more in the west, with increased solar insolation enhancing precipitation, and increased sulphate causing drying. 3xCH<sub>4</sub> produces very little change in precipitation, but the tripling of methane concentrations induces a smaller forcing than the other scenarios.



Figure 1f shows the mean precipitation response for the region outlined in 1a, encompassing eastern and central Amazonia (ECA), for each of the PDRMIP forcing scenarios. The responses are also split into the contributions from forcing-dependent adjustments (grey), and temperature driven feedbacks (red). The ECA region mean responses to 3xCH<sub>4</sub>, 5xSO<sub>4</sub> and 2%SOL are very small, though the model spread is large. The negligible precipitation response to SO<sub>4</sub> and solar forcing arises due to opposing adjustment and feedback terms. Increased SO<sub>4</sub> produces a negative adjustment, mainly due to reduced dry static energy flux divergence. This can be explained by the reduced downwelling shortwave radiation at the surface, which reduces the land-sea temperature contrast, reducing convection and precipitation over the land (Chadwick et al., 2014; Richardson et al., 2016a). The opposite effect occurs for solar forcing. The feedback response then counteracts these changes; increasing precipitation as global temperatures cool in response to SO<sub>4</sub>, and decreasing precipitation as the climate warms in response to solar forcing. The model-mean feedback response is negative per unit temperature change for all scenarios except 3xCH<sub>4</sub>, but the magnitude varies.

Increased CO<sub>2</sub> causes a large reduction in precipitation over the ECA region. The model-mean response to doubling CO<sub>2</sub> is dominated by the adjustment component ( $-91.1 \pm 90.6$  mm yr<sup>-1</sup>), with temperature-driven feedbacks making only a small contribution ( $-19.9 \pm 104.4$  mm yr<sup>-1</sup>). Despite the large model spread, the negative adjustment is very consistent, with 90% of models producing a negative adjustment to CO<sub>2</sub>. Although the adjustment term dominates in the model-mean, the temperature driven feedback often contributes significantly to the precipitation response on an individual model basis. In 50% of the models the temperature driven feedbacks are of the same magnitude or larger than the adjustment, but there is little agreement on the sign of the feedback response between models.

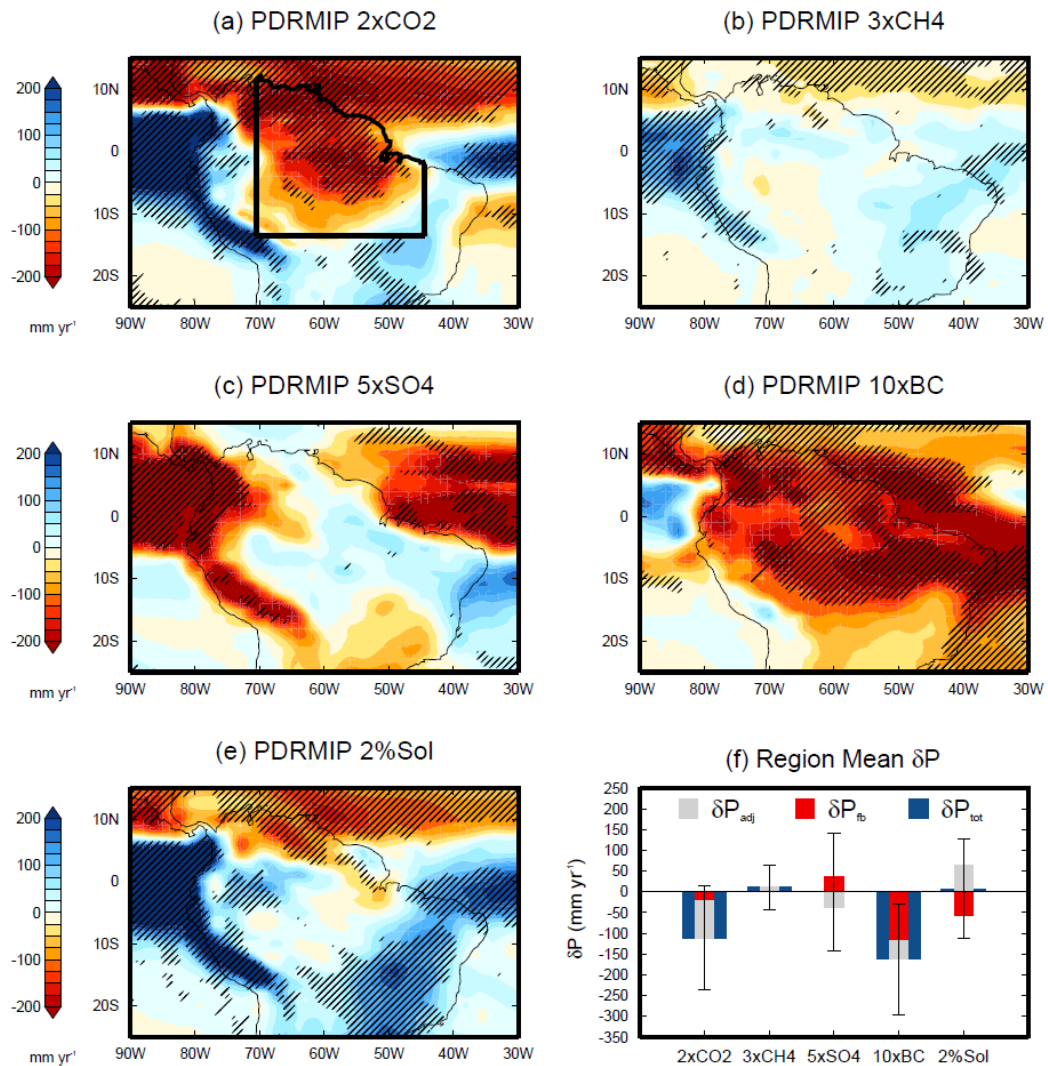


**Figure 1:** PDRMIP multi-model mean precipitation response to idealized abrupt forcing scenarios (a) 2xCO<sub>2</sub>, (b) 3xCH<sub>4</sub>, (c) 5xSO<sub>4</sub>, (d) 10xBC and (e) 2%SOL. Hatching denotes where 80% of the models agree on the sign of change. Panel (f) shows the PDRMIP multi-model region mean precipitation response for the ECA region outlined in panel (a). The total response is shown in blue, the adjustment in grey, and feedback in red. It should be noted that the responses to the different forcing scenarios are not normalized. Error bars denote the model spread standard deviation.

Increased black carbon also causes a large reduction in precipitation over the ECA region. In contrast to CO<sub>2</sub>, the model-mean response to 10xBC is dominated by the temperature driven feedbacks ( $-118.3 \pm 122.3 \text{ mm yr}^{-1}$ ), rather than the adjustment ( $-44.0 \pm 45.3 \text{ mm yr}^{-1}$ ). There is considerable model spread in the magnitude of the precipitation response, but the sign of the change is very robust, with all models agreeing on reduced precipitation over the region.

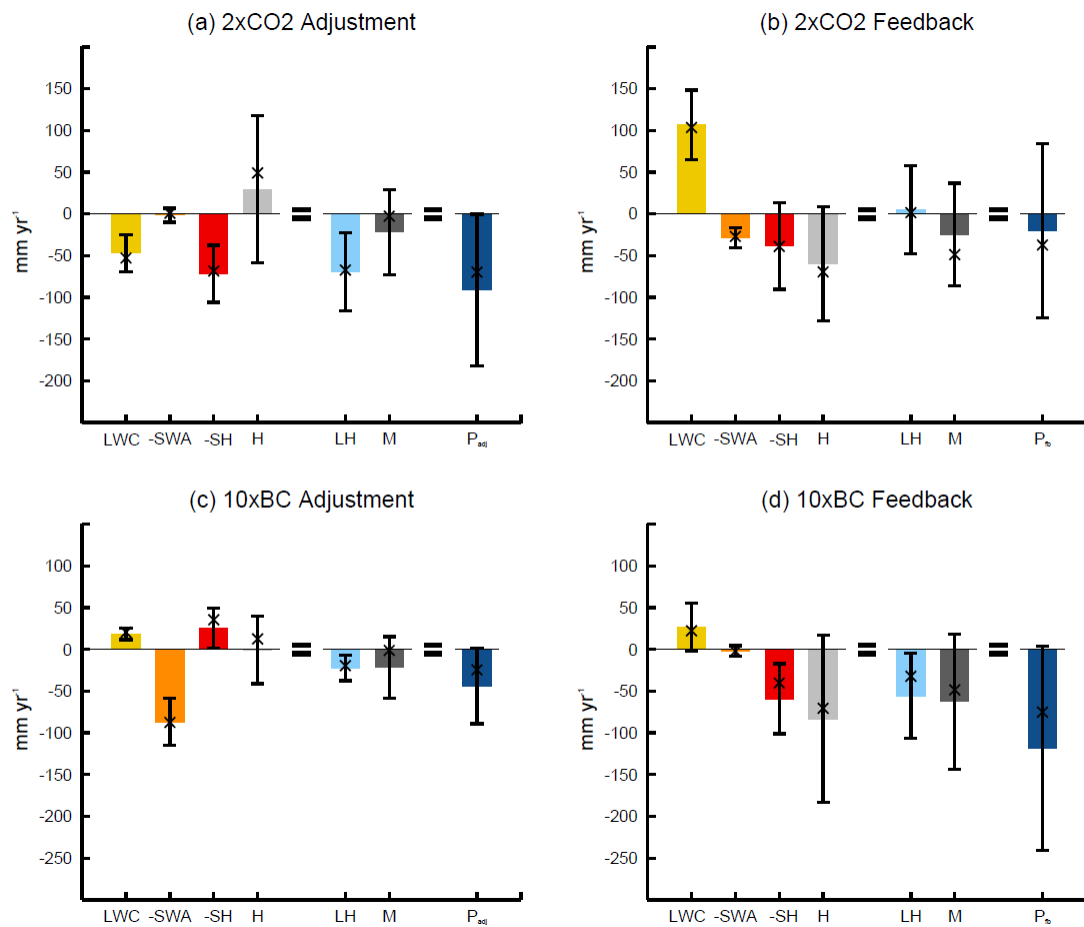


**Figure 2:** PDRMIP multi-model region mean precipitation, energy budget and moisture budget (see Equation 1) responses to (a, b) 2xCO<sub>2</sub> and (c, d) 10xBC, split into (a, c) adjustment and (b, d) feedback terms, for the ECA region highlighted in Figure 1a. The sign for each term is given according to Equation 1. All values are converted in to precipitation units ( $\text{mm yr}^{-1}$ ). Crosses indicate the median value and error bars denote the model spread standard deviation.

#### 5.4.2 Energy and moisture budget changes

To understand the mechanisms driving the precipitation response to CO<sub>2</sub> and black carbon over the Amazon region we analyse the energy and moisture budget (Eq. 1) changes (Fig. 2). The negative adjustment in response to CO<sub>2</sub> arises mainly due to a change in the partitioning of sensible and latent heat fluxes, as well as a reduction in LW cooling (Fig. 2a). The reduced LW cooling is due to enhanced CO<sub>2</sub> concentrations absorbing more LW radiation. CO<sub>2</sub> strongly affects the surface heat fluxes, reducing

LH flux and increasing SH flux. The large changes in surface heat fluxes are caused by the physiological forcing of CO<sub>2</sub>, as discussed in Section 3.3, and shown in Figure 3. The changes in horizontal heat and moisture transport, associated with circulation changes, are very uncertain. The LH flux response also exhibits considerable model spread, and is highly correlated with the precipitation adjustment inter-model spread ( $r = 0.92$ ).

The negative precipitation adjustment in response to black carbon is driven by a large increase in the atmospheric shortwave absorption (Fig. 2c). This is partially counteracted by an increase in LW cooling and a decrease in SH flux. The uncertainty largely arises from the circulation response, with the change in moisture convergence contributing most strongly to the inter-model spread in the precipitation adjustment ( $r = 0.95$ ).

The temperature-driven feedback response to 2xCO<sub>2</sub> is small due to counteracting energy budget feedbacks (Fig. 2b). LW cooling increases with warming, but this is countered by increased SW absorption, increased SH flux, and reduced divergence of dry static energy flux, resulting in a small negative precipitation feedback. The LW cooling, SW absorption and SH flux feedback responses per unit Kelvin of temperature change are very consistent between forcing scenarios, except for black carbon (see Fig. S3). The different precipitation feedbacks between forcing scenarios largely arises from the uncertain circulation responses.

For 2xCO<sub>2</sub>, the change in horizontal dry static energy and moisture fluxes are very uncertain (Fig. 2b), and contribute strongly to the inter-model spread in the precipitation feedback ( $r = 0.96$  and  $r = 0.92$ , respectively). Therefore, although the model-mean temperature-driven feedback is small, in individual models circulation feedbacks can drive large changes in precipitation. However, the feedback response shows little agreement in sign or magnitude for the region. Circulation changes are known to be important for tropical precipitation patterns (Chou et al., 2009; Seager et al., 2010; Chadwick et al., 2013). Future circulation changes are very uncertain and may be strongly influenced by chaotic natural variability and model errors (Shepherd, 2014).

Despite causing only a weak global temperature response, 10xBC produces a large negative precipitation feedback over the Amazon region. This is mainly driven by

circulation changes, indicated by reduced divergence of dry static energy flux and moisture convergence (Fig. 2d). There is also a shift in the partitioning of latent and sensible heat fluxes. Black carbon has been shown to drive northward shifts in the inter-tropical convergence zone (ITCZ) in global climate models (Chung and Seinfeld, 2005; Jones et al., 2007; Kovilakam and Mahajan, 2015), due to the asymmetric nature of the forcing. These circulation changes drive the robust, but highly variable in magnitude, negative precipitation feedback. However, it should be noted that the 10xBC perturbation is very large. If the total precipitation response is linearly scaled based on the TOA forcing to present-day levels (1981-2000), the PDRMIP results indicate a drying of  $-25.9 \pm 8.3$  mm yr<sup>-1</sup>.

### 5.4.3 CO<sub>2</sub> physiological effect

In Figure 3 we show the role of physiological effects on plants in driving the CO<sub>2</sub> precipitation adjustment for CMIP5 models. Figure 3 shows the precipitation response to quadrupling CO<sub>2</sub> in amip simulations (Fig. 3a), which do not include physiological effects, and in sstClim simulations (Fig. 3b), which do include physiological effects. In the amip simulations multi-model mean precipitation increases over most of tropical South America, except close to the eastern coast. In contrast, in the sstClim simulations drying extends much further inland from the east. The difference between the two scenarios is shown in Figure 3c. Over much of the Amazon region, particularly in the east, CO<sub>2</sub> physiological effects drive considerable drying in the multi-model mean. CO<sub>2</sub> physiological effects also appear to drive enhanced precipitation along the west coast. The multi-model mean response is generally in agreement with previous single-model studies (Andrews et al., 2010a; Pu and Dickinson, 2014; Abe et al., 2015).

The physiological effects on the energy and moisture budgets for the ECA region (outlined in Figure 1a) are shown in Figure 3d. It can be seen that the reduced precipitation due to CO<sub>2</sub> physiological forcing is almost entirely due to the change in partitioning of surface sensible and latent heat fluxes. The increased atmospheric CO<sub>2</sub> concentrations drive reduced stomatal conductance (Field et al., 1995), which therefore reduces evaporation. In the Amazon region, where water recycling is very important for the hydrological cycle, the reduction in evaporation drives considerable drying. The surface energy balance is maintained through an increase in sensible heat

flux. There is very little change in the horizontal heat and moisture fluxes, indicating the importance of the local changes.

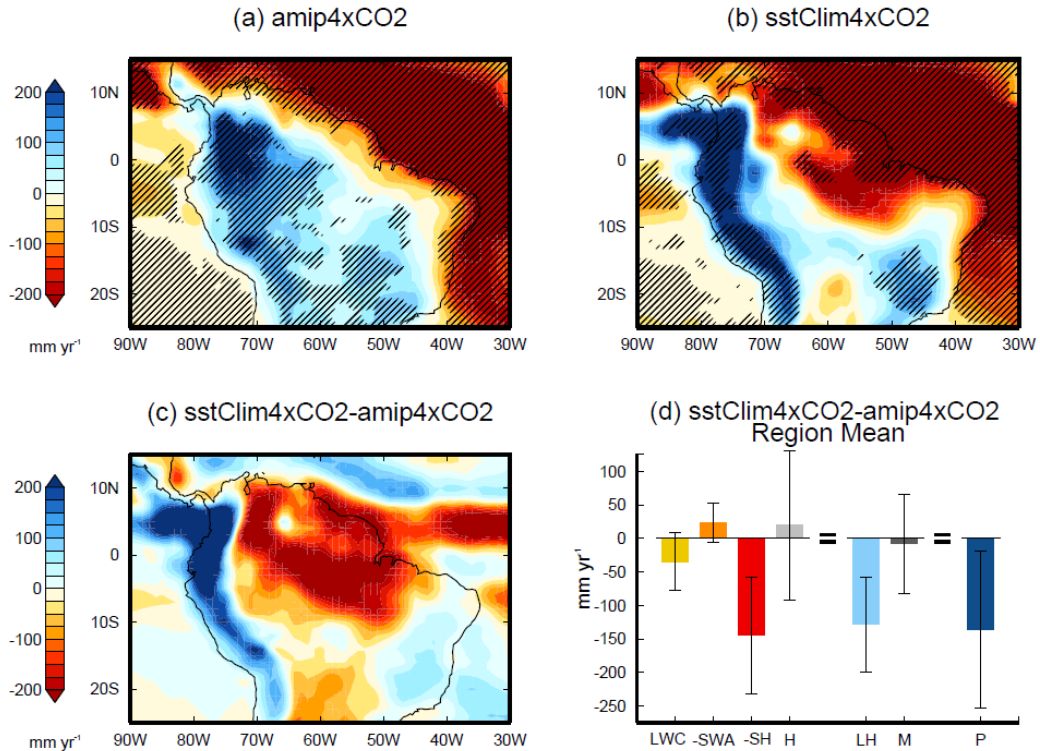


**Figure 3:** CMIP5 multi-model mean precipitation response to quadrupling CO<sub>2</sub> in (a) amip and (b) sstClim simulations and (c) the difference between the two (sstClim4xCO<sub>2</sub>-amip4xCO<sub>2</sub>). Hatching shows where 80% of the models agree on the sign of the change (not applied in panel (c) as not all of the same models performed each simulation). Panel (d) shows the difference between sstClim4xCO<sub>2</sub> and amip4xCO<sub>2</sub> energy and moisture budget response for the ECA region. All values are converted in to precipitation units (mm yr<sup>-1</sup>). Error bars denote the model spread standard deviation.

The physiological response to CO<sub>2</sub> also drives a large fraction of the precipitation adjustment uncertainty. The precipitation adjustment inter-model standard deviation in the sstClim simulations (109 mm yr<sup>-1</sup>) is over double that for the amip simulations (42 mm yr<sup>-1</sup>). Including CO<sub>2</sub> physiological effects considerably increases the uncertainty in the latent and sensible heat flux responses (see Fig. S4), which contribute strongly to the large model spread in the precipitation adjustment. In addition, the uncertain response of surface heat fluxes leads to a much larger

uncertainty in the change in horizontal transport of energy and moisture. Therefore, the uncertain circulation response to differing changes in latent heating, drives further uncertainty in the precipitation adjustment in response to CO<sub>2</sub>. DeAngelis et al. (2016b) showed that the physiological effects also contribute strongly to the spread in the global mean CO<sub>2</sub> precipitation adjustment.

#### **5.4.4 Projections of precipitation change**

We have shown that the reduction in precipitation over central and eastern Amazonia in response to CO<sub>2</sub> is dominated by the adjustment component, which is driven by the physiological effects on evapotranspiration. Therefore, given that CO<sub>2</sub> forcing increasingly dominates in future emission scenarios (van Vuuren et al., 2011), the CO<sub>2</sub> physiological effect could play a key role in future precipitation change over the Amazon. To quantify the potential contribution of CO<sub>2</sub> to precipitation change over the Amazon by the end of the 21<sup>st</sup> century we construct a simple model based on the PDRMIP results. Precipitation change over the Amazon is estimated by scaling the adjustment component based on TOA forcing for the end of the century, and scaling the feedback component based on global surface temperature change for the end of the century, as shown in Equation 2. The simple model estimates are compared with CMIP5 multi-model mean projections, including only models which include physiological effects (Collins et al., 2013), in Figure 4.

The CMIP5 projections indicate drying over large areas of the Amazon region particularly in the east, south and north. In contrast, along the west coast of South America and western regions of the Amazon, projections indicate an increase in precipitation. The changes are much larger for RCP8.5 which follows a business as usual emissions scenario, but the spatial pattern is very similar. Despite the large predicted changes, there is considerable variation between models. Over tropical South America there are very few regions in which more than 80% of the models agree on the sign of the change (hatching denotes 80% of models agree on sign). Although agreement on the spatial pattern is low, models consistently project large magnitude changes in this region (Chadwick et al., 2015).

The simple model predicts a very similar drying ( $-151.1 \pm 82 \text{ mm yr}^{-1}$ ) over the ECA region as the CMIP5 multi-model mean projections ( $-160.9 \pm 241 \text{ mm yr}^{-1}$ ) for the end

of the 21<sup>st</sup> century following RCP8.5, driven almost entirely by the CO<sub>2</sub> adjustment. For RCP4.5 the simple model predicts more drying ( $-87.1 \pm 47 \text{ mm yr}^{-1}$ ) than the CMIP5 projections ( $-34.5 \pm 120 \text{ mm yr}^{-1}$ ). The comparison suggests that projected drying in the ECA region is predominantly driven by CO<sub>2</sub> physiological forcing. The projected drying is independent of global warming trends, as demonstrated by the lack of correlation between global mean warming and precipitation change between CMIP5 models ( $r = 0.16$  and  $-0.09$  for RCP4.5 and RCP8.5 respectively).

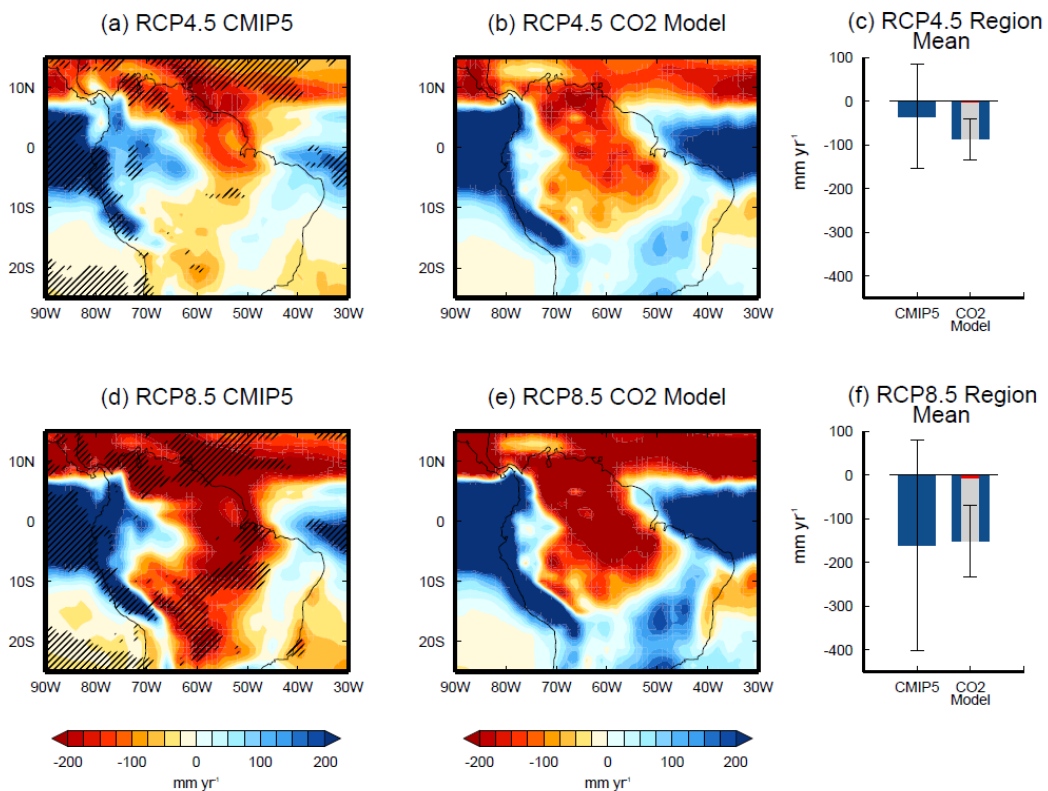


**Figure 4:** Projected precipitation change for the period 2081-2100 compared to pre-industrial, following (a, b, c) RCP4.5 and (d, e, f) RCP8.5, calculated using the (a, d) CMIP5 multi-model mean (including only models which include CO<sub>2</sub> physiological effects) and (b, e) a simple model based on the PDRMIP response to CO<sub>2</sub>, given by Equation 1. Hatching denotes where 80% of the models agree on the sign of the change. Panels (c) and (f) show the mean change for the ECA region. The total change is shown in blue, the adjustment in grey and the feedback in red. Error bars denote the standard deviation of the CMIP5 model spread, and the standard error of the simple model.



Spatially there are very similar features between the simple model and the CMIP5 projections for both RCP4.5 and RCP8.5. These include the significant drying over the eastern, southern and northern Amazon, and the increase in precipitation in the west, all of which are predominantly driven by the CO<sub>2</sub> adjustment. There are some notable differences between the CMIP5 projections and the simple model, such as in the northwest of the Amazon basin, where enhanced precipitation extends further east in the CMIP5 projections. The simple model indicates that CO<sub>2</sub> physiological forcing could dominate multi-model mean future projections of precipitation change over large areas of the Amazon region. However, as discussed above, individual models show that temperature driven circulation feedbacks can often be large, but are highly uncertain and show little agreement.

## 5.5 Conclusions

CMIP5 projections indicate drying over large areas of the Amazon for the end of the 21<sup>st</sup> century, particularly in the east, but the changes are highly uncertain. Amazonian drying could have significant implications on both the local and global climate system, and it is therefore important to reduce uncertainty and improve understanding of the key drivers of change. We have presented the precipitation response over the Amazon region to individual atmospheric forcings (CO<sub>2</sub>, CH<sub>4</sub>, SO<sub>4</sub>, black carbon and solar insolation) in idealized simulations using the PDRMIP global climate model ensemble. The responses were split into a forcing-dependent adjustment and temperature-driven feedback to help understand the driving mechanisms. The precipitation changes exhibit a large amount of inter-model spread, but there are some robust signals.

Increased black carbon produces a robust drying over much of the Amazon region, however the magnitude of the change varies considerably between models. The reduction in precipitation is largely due to temperature-driven circulation feedbacks, associated with a northward shift in the ITCZ. The precipitation adjustment in response to black carbon also contributes to drying due to enhanced SW absorption over the Amazon region.

Increased CO<sub>2</sub> concentrations drive reduced precipitation over the Amazon region, particularly in the east. The model-mean drying is dominated by the adjustment component, for which 90% of the models agree on a mean reduction in precipitation over the ECA region (outlined in Figure 1a). However, the magnitude of the reduction is highly variable between models. Through analysis of amip and sstClim simulations, using an ensemble of CMIP5 models, we isolate the contribution of CO<sub>2</sub> physiological forcing to the precipitation adjustment. We find that physiological effects dominate the CO<sub>2</sub> adjustment over the Amazon region, through a change in the partitioning of sensible and latent heat fluxes. Evapotranspiration decreases due to higher CO<sub>2</sub> concentrations reducing stomatal opening, which limits moisture availability and precipitation over much of the Amazon, particularly in the east. The physiological effects of CO<sub>2</sub> also drive increased precipitation along the west coast. The physiological effects contribute strongly to the uncertainty in precipitation changes over the Amazon, over doubling the inter-model spread for the ECA region.

Using a simple model based on TOA forcing and global surface temperature change we quantify the potential contribution of CO<sub>2</sub> to precipitation changes over the Amazon region by the end of the century (2081-2100) from pre-industrial. The simple model suggests that CMIP5 multi-model mean projected drying over the ECA region is predominantly driven by the CO<sub>2</sub> physiological effect. This implies projected Amazonian precipitation change is independent of rising temperatures, being predominantly driven by atmospheric CO<sub>2</sub> concentration. However, it should be noted that analysis of individual models shows that temperature-driven circulation feedbacks can be large, but due to little agreement between models, they largely cancel out in the multi-model mean. Our findings illustrate the importance of reducing uncertainties associated with vegetation schemes and establishing whether the uncertainties in the temperature-driven circulation feedbacks can be constrained. In addition, given the importance of short-timescale adjustment processes on precipitation in this region, the use of high resolution convection-permitting models could be of real benefit in reducing uncertainty and improving prediction of long-term change.

## **Acknowledgements**

T.B.R. was supported by a NERC CASE award in collaboration with the Met Office NE/K007483/1. P.M.F. was supported by a Royal Society Wolfson Merit Award and NERC grant NE/K006038/1. T.A. was supported by the Newton Fund through the Met Office Climate Science for Service Partnership Brazil (CSSP Brazil). B.H.S., G.M., and Ø.H. were funded by the Research Council of Norway, through the grant NAPEX (229778). D.S. and G. F. thank NASA GISS for funding and acknowledge the NASA High-End Computing Program through the NASA Center for Climate Simulation at Goddard Space Flight Center for computational resources. O.B. acknowledges HPC resources from TGCC under the gencmip6 allocation provided by GENCI (Grand Equipement National de Calcul Intensif). T.T. is supported by the NEC SX-ACE supercomputer system of the National Institute for Environmental Studies, Japan, the Environmental Research and Technology Development Fund (S-12-3) of the Ministry of Environment, Japan and JSPS KAKENHI Grant Numbers JP15H01728 and JP15K12190. M.K., D.S. and A.V. were supported by the Natural Environment Research Council under grant NE/K500872/1, and from the Grantham Institute at Imperial College. Simulations with HadGEM2 and HadGEM3-GA4 were performed using the MONSooN system, a collaborative facility supplied under the Joint Weather and Climate Research Programme, which is a strategic partnership between the Met Office and the Natural Environment Research Council.

---

**References**

- Abe, M., Shiogama, H., Yokohata, T., Emori, S., Nozawa, T., 2015. Asymmetric impact of the physiological effect of carbon dioxide on hydrological responses to instantaneous negative and positive CO<sub>2</sub> forcing. *Clim. Dyn.* 45, 2181–2192. doi:10.1007/s00382-014-2465-1
- Alves, L.M., Marengo, J.A., Fu, R., Bombardi, R.J., 2017. Sensitivity of Amazon Regional Climate to Deforestation. *Am. J. Clim. Chang.* 6, 75–98. doi:10.4236/ajcc.2017.61005
- Andrews, T., Doutriaux-Boucher, M., Boucher, O., Forster, P.M., 2010a. A regional and global analysis of carbon dioxide physiological forcing and its impact on climate. *Clim. Dyn.* 36, 783–792. doi:10.1007/s00382-010-0742-1
- Andrews, T., Forster, P.M., Boucher, O., Bellouin, N., Jones, A., 2010b. Precipitation, radiative forcing and global temperature change. *Geophys. Res. Lett.* 37. doi:10.1029/2010GL043991
- Aragão, L.E.O.C., Poulter, B., Barlow, J.B., Anderson, L.O., Malhi, Y., Saatchi, S., Phillips, O.L., Gloor, E., 2014. Environmental change and the carbon balance of Amazonian forests. *Biol. Rev.* 89, 913–931. doi:10.1111/brv.12088
- Betts, A. R., Cox, P. M., Lee, S.E., 1997. Contrasting Physiological and Structural Vegetation Feedbacks in Climate Change Simulations. *Nature* 387, 796–799. doi:10.1038/42924
- Boisier, J.P., Ciais, P., Ducharne, A., Guimberteau, M., 2015. Projected strengthening of Amazonian dry season by constrained climate model simulations. *Nat. Clim. Chang.* 5, 656–660. doi:10.1038/nclimate2658
- Bony, S., Bellon, G., Klocke, D., Sherwood, S., Fermepin, S., Denvil, S., 2013. Robust direct effect of carbon dioxide on tropical circulation and regional precipitation. *Nat. Geosci.* 6, 447–451. doi:10.1038/ngeo1799
- Booth, B.B.B., Chris, D.J., Mat, C., Ian, J.T., Peter, M.C., Stephen, S., Chris, H., Richard, A.B., Glen, R.H., Jon, L., 2012. High sensitivity of future global warming to land carbon cycle processes. *Environ. Res. Lett.* 7, 24002. doi:10.1088/1748-9326/7/2/024002
- Brienen, R.J.W., Phillips, O.L., Feldpausch, T.R., Gloor, E., Baker, T.R., Lloyd, J., Lopez-Gonzalez, G., Monteagudo-Mendoza, A., Malhi, Y., Lewis, S.L., Vásquez Martínez, R., Alexiades, M., Álvarez Dávila, E., Alvarez-Loayza, P., Andrade, A., Aragão, L.E.O.C., Araujo-Murakami, A., Arets, E.J.M.M., Arroyo, L., Aymard C, G.A., Bánki, O.S., Baraloto, C., Barroso, J., Bonal, D., Boot, R.G.A., Camargo, J.L.C., Castilho, C. V, Chama, V., Chao, K.J., Chave, J., Comiskey, J.A., Cornejo Valverde, F., da Costa, L., de Oliveira, E.A., Di Fiore, A., Erwin, T.L., Fauset, S., Forsthofer, M., Galbraith, D.R., Grahame, E.S., Groot, N., Hérault, B., Higuchi, N., Honorio Coronado, E.N., Keeling, H., Killeen, T.J., Laurance, W.F., Laurance, S., Licona, J., Magnussen, W.E., Marimon, B.S., Marimon-Junior, B.H., Mendoza, C., Neill, D.A., Nogueira, E.M., Núñez, P., Pallqui Camacho, N.C., Parada, A., Pardo-Molina, G., Peacock, J., Peña-Claros, M., Pickavance, G.C., Pitman, N.C.A., Poorter, L., Prieto, A., Quesada, C.A., Ramírez, F., Ramírez-Angulo, H., Restrepo, Z.,

- Roopsind, A., Rudas, A., Salomão, R.P., Schwarz, M., Silva, N., Silva-Espejo, J.E., Silveira, M., Stropp, J., Talbot, J., ter Steege, H., Teran-Aguilar, J., Terborgh, J., Thomas-Caesar, R., Toledo, M., Torello-Raventos, M., Umetsu, R.K., van der Heijden, G.M.F., van der Hout, P., Guimarães Vieira, I.C., Vieira, S.A., Vilanova, E., Vos, V.A., Zagt, R.J., 2015. Long-term decline of the Amazon carbon sink. *Nature* 519, 344–8. doi:10.1038/nature14283
- Cao, L., Bala, G., Caldeira, K., Nemani, R., Ban-Weiss, G., 2009. Climate response to physiological forcing of carbon dioxide simulated by the coupled Community Atmosphere Model (CAM3.1) and Community Land Model (CLM3.0). *Geophys. Res. Lett.* 36, 1–5. doi:10.1029/2009GL037724
- Chadwick, R., Boutle, I., Martin, G., 2013. Spatial Patterns of Precipitation Change in CMIP5: Why the Rich Do Not Get Richer in the Tropics. *J. Clim.* 26, 3803–3822. doi:10.1175/JCLI-D-12-00543.1
- Chadwick, R., Douville, H., Skinner, C.B., 2017. Timeslice experiments for understanding regional climate projections: applications to the tropical hydrological cycle and European winter circulation. *Clim. Dyn.* 0, 1–19. doi:10.1007/s00382-016-3488-6
- Chadwick, R., Good, P., Andrews, T., Martin, G., 2014. Surface warming patterns drive tropical rainfall pattern responses to CO<sub>2</sub> forcing on all timescales. *Geophys. Res. Lett.* 41, 610–615. doi:10.1002/2013GL058504
- Chadwick, R., Good, P., Martin, G., Rowell, D.P., 2015. Large rainfall changes consistently projected over substantial areas of tropical land. *Nat. Clim. Chang.* 1–6. doi:10.1038/nclimate2805
- Chou, C., Neelin, J.D., Chen, C.-A., Tu, J.-Y., 2009. Evaluating the “Rich-Get-Richer” Mechanism in Tropical Precipitation Change under Global Warming. *J. Clim.* 22, 1982–2005. doi:10.1175/2008JCLI2471.1
- Chung, S., Seinfeld, J., 2005. Climate response of direct radiative forcing of anthropogenic black carbon. *J. Geophys. Res.* 110, D11102. doi:10.1029/2004JD005441
- Collins, M., Knutti, R., Arblaster, J., Dufresne, J.-L., Fichet, T., Friedlingstein, P., Gao, X., Gutowski, W.J., Johns, T., Krinner, G., Shongwe, M., Tebaldi, C., Weaver, A.J., Wehner, M., 2013. Long-term Climate Change: Projections, Commitments and Irreversibility Pages 1029 to 1076, in: Intergovernmental Panel on Climate Change (Ed.), *Climate Change 2013 - The Physical Science Basis*. Cambridge University Press, Cambridge, pp. 1029–1136. doi:10.1017/CBO9781107415324.024
- DeAngelis, A.M., Qu, X., Hall, A., 2016a. Importance of vegetation processes for model spread in the fast precipitation response to CO<sub>2</sub> forcing. *Geophys. Res. Lett.* 550–559. doi:10.1002/2016GL071392
- DeAngelis, A.M., Qu, X., Hall, A., 2016b. Importance of vegetation processes for model spread in the fast precipitation response to CO<sub>2</sub> forcing. *Geophys. Res. Lett.* 1–10. doi:10.1002/2016GL071392
- Duffy, P.B., Brando, P., Asner, G.P., Field, C.B., 2015. Projections of future meteorological drought and wet periods in the Amazon. *Proc. Natl. Acad. Sci.*

112, 13172–13177. doi:10.1073/pnas.1421010112

Field, C.B., Jackson, R.B., Mooney, H.A., 1995. Stomatal responses to increased CO<sub>2</sub>: implications from the plant to the global scale. *Plant, Cell Environ.* 18, 1214–1225. doi:10.1111/j.1365-3040.1995.tb00630.x

Fu, R., Yin, L., Li, W., Arias, P.A., Dickinson, R.E., Huang, L., Chakraborty, S., Fernandes, K., Liebmann, B., Fisher, R., Myneni, R.B., 2013. Increased dry-season length over southern Amazonia in recent decades and its implication for future climate projection. *Proc. Natl. Acad. Sci.* 110, 18110–18115. doi:10.1073/pnas.1302584110

Fung, I.Y., Doney, S.C., Lindsay, K., John, J., 2005. Evolution of carbon sinks in a changing climate. *Proc. Natl. Acad. Sci. U. S. A.* 102, 11201–11206. doi:10.1073/pnas.0504949102

Gatti, L. V, Gloor, M., Miller, J.B., Doughty, C.E., Malhi, Y., Domingues, L.G., Basso, L.S., Martinevski, A., Correia, C.S.C., Borges, V.F., Freitas, S., Braz, R., Anderson, L.O., Rocha, H., Grace, J., Phillips, O.L., Lloyd, J., 2014. Drought sensitivity of Amazonian carbon balance revealed by atmospheric measurements. *Nature* 506, 76–80. doi:10.1038/nature12957

Gloor, M., Brienen, R.J.W., Galbraith, D., Feldpausch, T.R., Schöngart, J., Guyot, J.L., Espinoza, J.C., Lloyd, J., Phillips, O.L., 2013. Intensification of the Amazon hydrological cycle over the last two decades. *Geophys. Res. Lett.* 40, 1729–1733. doi:10.1002/grl.50377

Hilker, T., Lyapustin, A.I., Tucker, C.J., Hall, F.G., Myneni, R.B., Wang, Y., Bi, J., Mendes de Moura, Y., Sellers, P.J., 2014. Vegetation dynamics and rainfall sensitivity of the Amazon. *Proc. Natl. Acad. Sci.* 111, 16041–16046. doi:10.1073/pnas.1404870111

Joetzer, E., Douville, H., Delire, C., Ciais, P., 2013. Present-day and future Amazonian precipitation in global climate models: CMIP5 versus CMIP3. *Clim. Dyn.* 41, 2921–2936. doi:10.1007/s00382-012-1644-1

Jones, A., Haywood, J.M., Boucher, O., 2007. Aerosol forcing, climate response and climate sensitivity in the Hadley Centre climate model. *J. Geophys. Res.* 112, D20211. doi:10.1029/2007JD008688

Kovilakam, M., Mahajan, S., 2015. Black carbon aerosol-induced Northern Hemisphere tropical expansion. *Geophys. Res. Lett.* 42, 4964–4972. doi:10.1002/2015GL064559

Lambert, F.H., Faull, N.E., 2007. Tropospheric adjustment: The response of two general circulation models to a change in insolation. *Geophys. Res. Lett.* 34, L03701. doi:10.1029/2006GL028124

Li, W., Fu, R., Juárez, R.I.N., Fernandes, K., 2008. Observed change of the standardized precipitation index, its potential cause and implications to future climate change in the Amazon region. *Philos. Trans. R. Soc. Lond. B. Biol. Sci.* 363, 1767–72. doi:10.1098/rstb.2007.0022

Malhi, Y., Wood, D., Baker, T.R., Wright, J., Phillips, O.L., Cochrane, T., Meir, P., Chave, J., Almeida, S., Arroyo, L., Higuchi, N., Killeen, T.J., Laurance, S.G.,

- Laurance, W.F., Lewis, S.L., Monteagudo, A., Neill, D.A., Vargas, P.N., Pitman, N.C.A., Quesada, C.A., Salomão, R., Silva, J.N.M., Lezama, A.T., Terborgh, J., Martínez, R.V., Vinceti, B., 2006. The regional variation of aboveground live biomass in old-growth Amazonian forests. *Glob. Chang. Biol.* 12, 1107–1138. doi:10.1111/j.1365-2486.2006.01120.x
- Meinshausen, M., Smith, S.J., Calvin, K., Daniel, J.S., Kainuma, M.L.T., Lamarque, J., Matsumoto, K., Montzka, S.A., Raper, S.C.B., Riahi, K., Thomson, A., Velders, G.J.M., van Vuuren, D.P.P., 2011. The RCP greenhouse gas concentrations and their extensions from 1765 to 2300. *Clim. Change* 109, 213–241. doi:10.1007/s10584-011-0156-z
- Mitchell, J., Wilson, C., Cunnington, W., 1987. On CO<sub>2</sub> climate sensitivity and model dependence of results. *Q. J. R. Meteorol. Soc.* 113, 293–322. doi:10.1256/smsqj.47516
- Myhre, G., Forster, P.M., Samset, B.H., Hodnebrog, Ø., Sillmann, J., Aalbergstjø, S.G., Andrews, T., Boucher, O., Faluvegi, G., Fläschner, D., Iversen, T., Kasoar, M., Kharin, V., Kirkevåg, A., Lamarque, J.-F., Olivié, D., Richardson, T.B., Shindell, D., Shine, K.P., Stjern, C.W., Takemura, T., Voulgarakis, A., Zwiers, F., 2016. PDRMIP: A Precipitation Driver and Response Model Intercomparison Project, Protocol and preliminary results. *Bull. Am. Meteorol. Soc. BAMS-D-16-0019.1*. doi:10.1175/BAMS-D-16-0019.1
- Orlowsky, B., Seneviratne, S.I., 2013. Elusive drought: Uncertainty in observed trends and short-and long-term CMIP5 projections. *Hydrol. Earth Syst. Sci.* 17, 1765–1781. doi:10.5194/hess-17-1765-2013
- Phillips, O.L., Aragao, L.E.O.C., Lewis, S.L., Fisher, J.B., Lloyd, J., Lopez-Gonzalez, G., Malhi, Y., Monteagudo, A., Peacock, J., Quesada, C. a, van der Heijden, G., Almeida, S., Amaral, I., Arroyo, L., Aymard, G., Baker, T.R., Banki, O., Blanc, L., Bonal, D., Brando, P., Chave, J., de Oliveira, A.C.A., Cardozo, N.D., Czimczik, C.I., Feldpausch, T.R., Freitas, M.A., Gloor, E., Higuchi, N., Jimenez, E., Lloyd, G., Meir, P., Mendoza, C., Morel, A., Neill, D. a, Nepstad, D., Patino, S., Penuela, M.C., Prieto, A., Ramirez, F., Schwarz, M., Silva, J., Silveira, M., Thomas, A.S., Steege, H. Ter, Stropp, J., Vasquez, R., Zelazowski, P., Davila, E.A., Andelman, S., Andrade, A., Chao, K.-J., Erwin, T., Di Fiore, A., C., E.H., Keeling, H., Killeen, T.J., Laurance, W.F., Cruz, A.P., Pitman, N.C. a, Vargas, P.N., Ramirez-Angulo, H., Rudas, A., Salamao, R., Silva, N., Terborgh, J., Torres-Lezama, A., 2009. Drought Sensitivity of the Amazon Rainforest. *Science* (80-. ). 323, 1344–1347. doi:10.1126/science.1164033
- Pu, B., Dickinson, R.E., 2014. Hydrological changes in the climate system from leaf responses to increasing CO<sub>2</sub>. *Clim. Dyn.* 42, 1905–1923. doi:10.1007/s00382-013-1781-1
- Richardson, T.B., Forster, P., Andrews, T., Boucher, O., Faluvegi, G., Fläschner, D., Hodnebrog, Ø., Kasoar, M., Kharin, V., Kirkevåg, A., Lamarque, J.-F., Myhre, G., Olivié, D., Samset, B., Shawki, D., Shindell, D., Takemura, T., Voulgarakis, A., n.d. Drivers of precipitation change: An energetic understanding.
- Richardson, T.B., Forster, P.M., Andrews, T., Parker, D.J., 2016a. Understanding the

- Rapid Precipitation Response to CO<sub>2</sub> and Aerosol Forcing on a Regional Scale. *J. Clim.* 29, 583–594. doi:10.1175/JCLI-D-15-0174.1
- Richardson, T.B., Samset, B.H., Andrews, T., Myhre, G., Forster, P.M., 2016b. An assessment of precipitation adjustment and feedback computation methods. *J. Geophys. Res. Atmos.* 121, 11,608–11,619. doi:10.1002/2016JD025625
- Samset, B.H., Myhre, G., Forster, P.M., Hodnebrog, Ø., Andrews, T., Faluvegi, G., Fläschner, D., Kasoar, M., Kharin, V., Kirkevåg, A., Lamarque, J.-F., Olivié, D., Richardson, T.B., Shindell, D., Shine, K.P., Takemura, T., Voulgarakis, A., 2016. Fast and slow precipitation responses to individual climate forcings: A PDRMIP multi-model study. *Geophys. Res. Lett.* doi:10.1002/2016GL068064
- Seager, R., Naik, N., Vecchi, G. a., 2010. Thermodynamic and Dynamic Mechanisms for Large-Scale Changes in the Hydrological Cycle in Response to Global Warming. *J. Clim.* 23, 4651–4668. doi:10.1175/2010JCLI3655.1
- Shepherd, T.G., 2014. Atmospheric circulation as a source of uncertainty in climate change projections. *Nat. Geosci.* 7, 703–708. doi:10.1038/ngeo2253
- Spracklen, D. V., Garcia-Carreras, L., 2015. The impact of Amazonian deforestation on Amazon basin rainfall. *Geophys. Res. Lett.* 42, 9546–9552. doi:10.1002/2015GL066063
- Taylor, K.E., Stouffer, R.J., Meehl, G. A, 2011. A Summary of the CMIP5 Experiment Design 4, 1–33.
- van Vuuren, D.P., Edmonds, J., Kainuma, M., Riahi, K., Thomson, A., Hibbard, K., Hurtt, G.C., Kram, T., Krey, V., Lamarque, J.F., Masui, T., Meinshausen, M., Nakicenovic, N., Smith, S.J., Rose, S.K., 2011. The representative concentration pathways: An overview. *Clim. Change* 109, 5–31. doi:10.1007/s10584-011-0148-z
- Zhang, K., de Almeida Castanho, A.D., Galbraith, D.R., Moghim, S., Levine, N.M., Bras, R.L., Coe, M.T., Costa, M.H., Malhi, Y., Longo, M., Knox, R.G., Mcknight, S., Wang, J., Moorcroft, P.R., 2015. The fate of Amazonian ecosystems over the coming century arising from changes in climate, atmospheric CO<sub>2</sub>, and land use. *Glob. Chang. Biol.* 21, 2569–2587. doi:10.1111/gcb.12903



## **Chapter 6: Conclusions and Recommendations**

### **6.1 Summary and Conclusions**

Global mean precipitation change is well understood in terms of the atmospheric energy budget, whereby the latent heat released is balanced by atmospheric radiative cooling and sensible heat flux from the surface (O’Gorman et al., 2011). As a result, forcing agents drive precipitation change through forcing-dependent adjustments and temperature-driven feedbacks. The adjustment and feedback framework has proved fundamental in understanding global mean precipitation change (Andrews et al., 2010b; Samset et al., 2016). However, the most significant impacts of climate change are felt on regional scales. Regional projections are more uncertain and the physical processes are less understood. Some large-scale mechanisms over the ocean have been established through analysis of the atmospheric moisture and moist static energy budgets. These include the ‘wet-get-wetter’ and ‘warmer-get-wetter’ mechanisms (Held and Soden, 2006; Xie et al., 2010). However, understanding of regional precipitation changes over land has remained low (Boucher et al., 2013).

The global energetic understanding of precipitation change can be extended to regional scales through incorporating horizontal transport of dry static energy into the atmospheric energy budget (Muller and O’Gorman, 2011). Very few studies have utilized the energetic approach on regional scales, or separated local precipitation adjustment and feedback responses. The principal aim of this thesis was to improve understanding of how forcing agents affect regional precipitation patterns through both rapid adjustments, and temperature-driven feedbacks, using analysis of the local atmospheric energy budget.

Chapter 2 assessed different computation methods for separating precipitation adjustment and feedback components in response to forcing. There is no definitive method for making the decomposition, with different studies using a range of techniques. These include fixing sea surface temperatures (fSST) (e.g. Bala et al., 2009; Andrews et al., 2010b; Samset et al., 2016), using linear regression of precipitation change against surface temperature change (Lambert and Faull, 2007;

Andrews et al., 2009), or separating based on timescale (Cao et al., 2012; Bony et al., 2013). Results showed that important physical and quantitative differences in the precipitation adjustment and feedback values arise due to the computation method.

Separating based on timescale is problematic due to the significant surface temperature change which occurs in the first year after abrupt forcings. Reducing the timescale considerably increases the uncertainty. Globally, fSST and regression methods are generally in good agreement, but the fSST hydrological sensitivity is systematically larger and more consistent across forcings. Regionally, there are significant differences between methods. Using regression, the adjustment and feedback results are highly dependent on the regression length due to shifting patterns of change. This makes the physical interpretation of the two components difficult. The fSST method provides a more clearly defined separation. The adjustment term includes the direct impact of a forcing agent on the atmospheric energy budget, as well as any adjustments of the troposphere and land surface. The feedback term includes any effects mediated by SST change. The fSST method is less affected by methodological choices, and exhibits less variability. Therefore, the fSST method outlined in Chapter 2 was used for the analysis undertaken in Chapters 3-5.

Chapter 3 investigated the processes driving the spatial pattern of precipitation adjustments in response to CO<sub>2</sub> and aerosol forcing across an ensemble of CMIP5 models. Results showed that the precipitation adjustments in response to CO<sub>2</sub> and anthropogenic aerosols exhibit opposing spatial patterns, despite both scenarios reducing global mean precipitation. This is a result of the opposing surface forcing in the two scenarios. The rapid land surface response was found to be the primary driver of the spatial pattern in the tropics, in agreement with Chadwick et al. (2014). Increased CO<sub>2</sub> levels enhance LW surface radiative heating, which destabilizes the troposphere over tropical land regions, enhancing convection and precipitation. The opposite occurs in response to anthropogenic aerosols due to reduced downwelling SW radiation at the surface, caused by increased sulphate levels. The aerosol spatial distribution and direct influence on precipitation efficiency may also contribute to the precipitation pattern response to aerosol.

The tropical precipitation changes due to CO<sub>2</sub> forcing are much larger in magnitude over the ocean than over land. This is due to significantly reduced diabatic cooling of

the atmosphere over tropical land regions, which partially counteracts the enhanced convection. Over many mid-latitude land regions, precipitation change is dominated by the change in diabatic cooling. This produces widespread drying in response to CO<sub>2</sub>. The spatial pattern of the CO<sub>2</sub> induced precipitation adjustment shows good agreement between models, indicating uncertainty in long-term changes are mainly associated with SST-driven feedbacks (Ma and Xie, 2013).

Chapter 3 showed that in contrast to most tropical land regions, precipitation decreased over the eastern Amazon in response to CO<sub>2</sub>. This was due to significant drying of the lower troposphere. The Amazon has been highlighted as a region where the physiological effects of CO<sub>2</sub> on plants could be important (Andrews et al., 2010a). The Amazonian precipitation response to atmospheric forcings, including CO<sub>2</sub>, was examined using the PDRMIP model ensemble in Chapter 5.

Eastern Amazonian precipitation was found to be most sensitive to CO<sub>2</sub> and black carbon, with both causing drying. The black carbon response was mainly due to temperature-driven circulation feedbacks, and exhibited considerable model spread. The CO<sub>2</sub> response was mainly due to a robustly negative, but highly variable in magnitude, precipitation adjustment. Using a number of CMIP5 models, it was shown that the physiological effect of CO<sub>2</sub> is the dominant driver of the adjustment. This is due to the reduced evapotranspiration caused by higher CO<sub>2</sub> concentrations.

Future multi-model mean projections indicate substantial drying over the eastern Amazon by the end of the 21<sup>st</sup> century (Joetzjer et al., 2013; Boisier et al., 2015). Using a simple model it was shown that the projected drying is predominantly driven by the CO<sub>2</sub> physiological effect. This suggests that precipitation changes over the eastern Amazon are independent of global temperature change. However, analysis of individual models showed that temperature-driven circulation feedbacks can be large, but due to little agreement between models, they largely cancel out in the multi-model mean.

Chapter 4 investigated how precipitation adjustment and feedback responses to forcing are partitioned between land and sea. Chapter 3 identified a considerable contrast between precipitation adjustments over land and sea. This was explored further in Chapter 4 by analysing the precipitation and energy budget responses to five individual forcing agents (CO<sub>2</sub>, CH<sub>4</sub>, SO<sub>4</sub>, black carbon and solar), across the

PDRMIP model ensemble. Results showed that the non-absorbing drivers (SO<sub>4</sub> and solar) produce the strongest precipitation adjustments over land. This is due to the rapid land surface response affecting atmospheric stability, as outlined in Chapter 3. For drivers which strongly affect atmospheric absorption (CH<sub>4</sub>, CO<sub>2</sub>, black carbon), the circulation changes are largely balanced by the changes in atmospheric diabatic cooling over land. The land mean precipitation adjustment in response to CO<sub>2</sub> exhibited considerable inter-model spread. This can be traced to uncertain changes in land-atmosphere heat fluxes, likely due to physiological effects (DeAngelis et al., 2016a).

Across forcing agents the hydrological sensitivity was found to be significantly smaller over land than over sea, despite similar radiative cooling feedbacks. The difference is driven by enhanced horizontal energy transport from sea to land. This arises due to a larger increase in latent heat flux (evaporation) over the oceans, which fuels enhanced divergence. Therefore, forcing-dependent adjustments and natural variability have a large influence on land mean precipitation trends.

Based on the adjustment and feedback framework, a simple model was constructed to estimate land and sea mean precipitation change using a linear combination of forcing-dependent adjustments, and a temperature-driven feedback. The model, based on PDRMIP results, matches well with CMIP5 ensemble mean historical and future precipitation changes for RCP4.5 and RCP8.5. The simple model was used to disentangle the roles of the different forcing-driven adjustments. This indicated that throughout the 20<sup>th</sup> century the influence of rising global temperatures on land precipitation has been counteracted mainly by adjustments in response to anthropogenic sulphate and volcanic forcing. This helps explain why very little intensification of the hydrological cycle has been observed over land during the 20<sup>th</sup> century (Hartmann et al., 2013; Wu et al., 2013). However, as sulphate forcing declines and global temperatures continue to rise in the 21<sup>st</sup> century, a sustained positive trend in land precipitation is expected.

The findings in this thesis highlight the importance of short-timescale adjustments in driving land precipitation changes. The processes driving forcing-dependent adjustments, as outlined in Chapter 3, are vital for understanding historical changes in the hydrological cycle over land, as shown in Chapter 4. In addition, adjustments could

dominate future precipitation changes in regions such as the Amazon, as shown in Chapter 5. This work illustrates the usefulness of analysing the atmospheric energy budget to understand precipitation change at both global and regional scales.

## **6.2 Limitations and Recommendations for future research**

- Chapters 3-5 highlighted the importance of short-timescale adjustments in driving precipitation changes over land. Given the rapid nature of these processes, the use of short simulations with high-resolution convection-permitting models could improve understanding and confidence in regional precipitation projections. The findings in this thesis are based on analysis of global climate models which parameterize convection. One of the main limitations of global climate models is inadequate representation of the coupling between atmospheric water and circulation (Stevens and Bony, 2013). Uncertain tropical precipitation changes may arise due to the high dependence on poorly represented unresolved processes, such as moist convection and cloud formation (Oueslati and Bellon, 2013). Chapter 3 showed the importance of circulation changes in driving the spatial pattern of precipitation adjustments. Therefore, using models which explicitly resolve convective processes to simulate the rapid climate response to abrupt forcing scenarios could significantly improve our ability to predict regional precipitation changes.

Convection-permitting models could be of particular benefit for regions in which short-timescale adjustment processes dominate long-term precipitation change. Chapter 5 showed that the adjustment in response to CO<sub>2</sub> dominates projected precipitation changes over the eastern Amazon. Uncertain circulation changes contribute strongly to the inter-model spread in the adjustment. Convection-permitting models could reduce this uncertainty and improve confidence in projections. Other land regions over which adjustment processes may dominate include Africa and Australia (Samset et al., 2016).

In addition convection-permitting models could be used to investigate whether important meteorological systems are affected by the radiative effects of

forcing agents and associated tropospheric adjustments. For example, tropical cyclones have a significant impact on society due to their powerful and damaging effects. Do adjustment processes affect the frequency of formation, or characteristics of tropical cyclones?

- Chapters 4 and 5 highlighted the strong influence of vegetation on the precipitation response to CO<sub>2</sub> over land. Chapter 5 showed that the physiological forcing of CO<sub>2</sub> dominates projected precipitation change over the eastern Amazon and contributes strongly to the inter-model spread. Physiological effects may also be important in other tropical forested regions (Chadwick et al., 2017), and have been shown to contribute strongly to uncertainty in the global mean precipitation adjustment in response to CO<sub>2</sub> (DeAngelis et al., 2016b). Therefore future work should focus on evaluating the vegetation physiological response, including parameterizations of stomatal conductance. This could lead to significantly reduced uncertainty in the precipitation adjustment in response to CO<sub>2</sub>, both globally and regionally.
- The analysis in this thesis has focused on annual mean changes in precipitation. It would be useful to investigate how adjustment processes affect precipitation extremes, as well as seasonal and diurnal characteristics. Extreme flooding or drought events can have devastating effects on society. Therefore improving understanding of how forcing agents may affect extreme precipitation is of great importance.
- It would be useful for future work to gain observational evidence of adjustment processes. This is a complex task because in reality adjustment and feedback processes cannot be easily separated. Observational studies could focus on regions in which climate models indicate adjustment processes dominate precipitation changes, such as South America, Africa and Australia (Samset et al., 2016).

## References

- Andrews, T., Doutriaux-Boucher, M., Boucher, O., Forster, P.M., 2010a. A regional and global analysis of carbon dioxide physiological forcing and its impact on climate. *Clim. Dyn.* 36, 783–792. doi:10.1007/s00382-010-0742-1
- Andrews, T., Forster, P.M., Boucher, O., Bellouin, N., Jones, A., 2010b. Precipitation, radiative forcing and global temperature change. *Geophys. Res. Lett.* 37, doi:10.1029/2010GL043991
- Andrews, T., Forster, P.M., Gregory, J.M., 2009. A Surface Energy Perspective on Climate Change. *J. Clim.* 22, 2557–2570. doi:10.1175/2008JCLI2759.1
- Bala, G., Caldeira, K., Nemani, R., 2009. Fast versus slow response in climate change: implications for the global hydrological cycle. *Clim. Dyn.* 35, 423–434. doi:10.1007/s00382-009-0583-y
- Boisier, J.P., Ciais, P., Ducharne, A., Guimberteau, M., 2015. Projected strengthening of Amazonian dry season by constrained climate model simulations. *Nat. Clim. Chang.* 5, 656–660. doi:10.1038/nclimate2658
- Bony, S., Bellon, G., Klocke, D., Sherwood, S., Fermepin, S., Denvil, S., 2013. Robust direct effect of carbon dioxide on tropical circulation and regional precipitation. *Nat. Geosci.* 6, 447–451. doi:10.1038/ngeo1799
- Boucher, O., Randall, D., Artaxo, P., Bretherton, C., Feingold, G., Forster, P., Kerminen, V.-M.V.-M., Kondo, Y., Liao, H., Lohmann, U., Rasch, P., Satheesh, S.K., Sherwood, S., Stevens, B., Zhang, X.Y., Zhan, X.Y., 2013. Clouds and Aerosols. *Clim. Chang.* 2013 Phys. Sci. Basis. Contrib. Work. Gr. I to Fifth Assess. Rep. Intergov. Panel Clim. Chang. doi:10.1017/CBO9781107415324.016
- Cao, L., Bala, G., Caldeira, K., 2012. Climate response to changes in atmospheric carbon dioxide and solar irradiance on the time scale of days to weeks. *Environ. Res. Lett.* 7, 34015. doi:10.1088/1748-9326/7/3/034015
- Chadwick, R., Douville, H., Skinner, C.B., 2017. Timeslice experiments for understanding regional climate projections: applications to the tropical hydrological cycle and European winter circulation. *Clim. Dyn.* 0, 1–19. doi:10.1007/s00382-016-3488-6
- Chadwick, R., Good, P., Andrews, T., Martin, G., 2014. Surface warming patterns drive tropical rainfall pattern responses to CO<sub>2</sub> forcing on all timescales. *Geophys. Res. Lett.* 41, 610–615. doi:10.1002/2013GL058504
- DeAngelis, A.M., Qu, X., Hall, A., 2016a. Importance of vegetation processes for model spread in the fast precipitation response to CO<sub>2</sub> forcing. *Geophys. Res. Lett.* 550–559. doi:10.1002/2016GL071392
- DeAngelis, A.M., Qu, X., Hall, A., 2016b. Importance of vegetation processes for model spread in the fast precipitation response to CO<sub>2</sub> forcing. *Geophys. Res. Lett.* 1–10. doi:10.1002/2016GL071392
- Hartmann, D.J., Klein Tank, A.M.G., Rusticucci, M., Alexander, L. V, Brönnimann, S., Charabi, Y.A.-R., Dentener, F.J., Dlugokencky, E.J., Easterling, D.R.,

- Kaplan, A., Soden, B.J., Thorne, P.W., Wild, M., Zhai, P., 2013. Observations: Atmosphere and Surface. *Clim. Chang. 2013 Phys. Sci. Basis. Contrib. Work. Gr. I to Fifth Assess. Rep. Intergov. Panel Clim. Chang.* 159–254. doi:10.1017/CBO9781107415324.008
- Held, I., Soden, B., 2006. Robust responses of the hydrological cycle to global warming. *J. Clim.* 5686–5699.
- Joetzier, E., Douville, H., Delire, C., Ciais, P., 2013. Present-day and future Amazonian precipitation in global climate models: CMIP5 versus CMIP3. *Clim. Dyn.* 41, 2921–2936. doi:10.1007/s00382-012-1644-1
- Lambert, F.H., Faull, N.E., 2007. Tropospheric adjustment: The response of two general circulation models to a change in insolation. *Geophys. Res. Lett.* 34, L03701. doi:10.1029/2006GL028124
- Ma, J., Xie, S.-P., 2013. Regional Patterns of Sea Surface Temperature Change: A Source of Uncertainty in Future Projections of Precipitation and Atmospheric Circulation. *J. Clim.* 26, 2482–2501. doi:10.1175/JCLI-D-12-00283.1
- Muller, C.J., O’Gorman, P. a., 2011. An energetic perspective on the regional response of precipitation to climate change. *Nat. Clim. Chang.* 1, 266–271. doi:10.1038/nclimate1169
- O’Gorman, P.A., Allan, R.P., Byrne, M.P., Previdi, M., 2011. Energetic Constraints on Precipitation Under Climate Change. *Surv. Geophys.* 33, 585–608. doi:10.1007/s10712-011-9159-6
- Oueslati, B., Bellon, G., 2013. Convective Entrainment and Large-Scale Organization of Tropical Precipitation: Sensitivity of the CNRM-CM5 Hierarchy of Models. *J. Clim.* 26, 2931–2946. doi:10.1175/JCLI-D-12-00314.1
- Samset, B.H., Myhre, G., Forster, P.M., Hodnebrog, Ø., Andrews, T., Faluvegi, G., Fläschner, D., Kasoar, M., Kharin, V., Kirkevåg, A., Lamarque, J.-F., Olivie, D., Richardson, T.B., Shindell, D., Shine, K.P., Takemura, T., Voulgarakis, A., 2016. Fast and slow precipitation responses to individual climate forcings: A PDRMIP multi-model study. *Geophys. Res. Lett.* doi:10.1002/2016GL068064
- Stevens, B., Bony, S., 2013. What are Climate Models Missing? *Science (80-. )*. 340, 1053–1054.
- Wu, P., Christidis, N., Stott, P., 2013. Anthropogenic impact on Earth’s hydrological cycle. *Nat. Clim. Chang.* 3, 807–810. doi:10.1038/nclimate1932
- Xie, S.-P., Deser, C., Vecchi, G. a., Ma, J., Teng, H., Wittenberg, A.T., 2010. Global Warming Pattern Formation: Sea Surface Temperature and Rainfall. *J. Clim.* 23, 966–986. doi:10.1175/2009JCLI3329.1



## **Appendices - Supporting Information for Chapters 2-5**

## **Appendix 1 - Supporting Information for Chapter 2**

## **An assessment of precipitation adjustment and feedback computation methods**

Richardson T. B.<sup>1</sup>, Samset B. H.<sup>2</sup>, Andrews T.<sup>3</sup>, Myhre G.<sup>2</sup>, Forster P. M.<sup>1</sup>

1. School of Earth and Environment, University of Leeds, Leeds, UK, 2. Centre for International Climate and Environmental Research, Oslo, Norway, 3. Met Office Hadley Centre, Exeter, UK

### **Contents of this file**

Figures S1- S8  
Table S1

### **Introduction**

This supporting information includes supplementary plots showing additional spatial and zonal plots of precipitation adjustment and hydrological sensitivity in response to 2xCO<sub>2</sub> and 5xSul calculated using the fSST, regression and YR1 methods for both HadGEM2 and CESM-CAM4 (Figures S1-S6). Figure S7 shows the PDRMIP multi-model mean atmospheric energy budget feedback response to 10xBC calculated using the fSST and regression methods. Figure S8 shows the energy budget response to quadrupling CO<sub>2</sub> for HadGEM2 with different SST climatologies. Table S1 shows precipitation adjustment results calculated using the first month of ocean coupled abrupt forcing simulations for HadGEM2 and CESM1-CAM4.

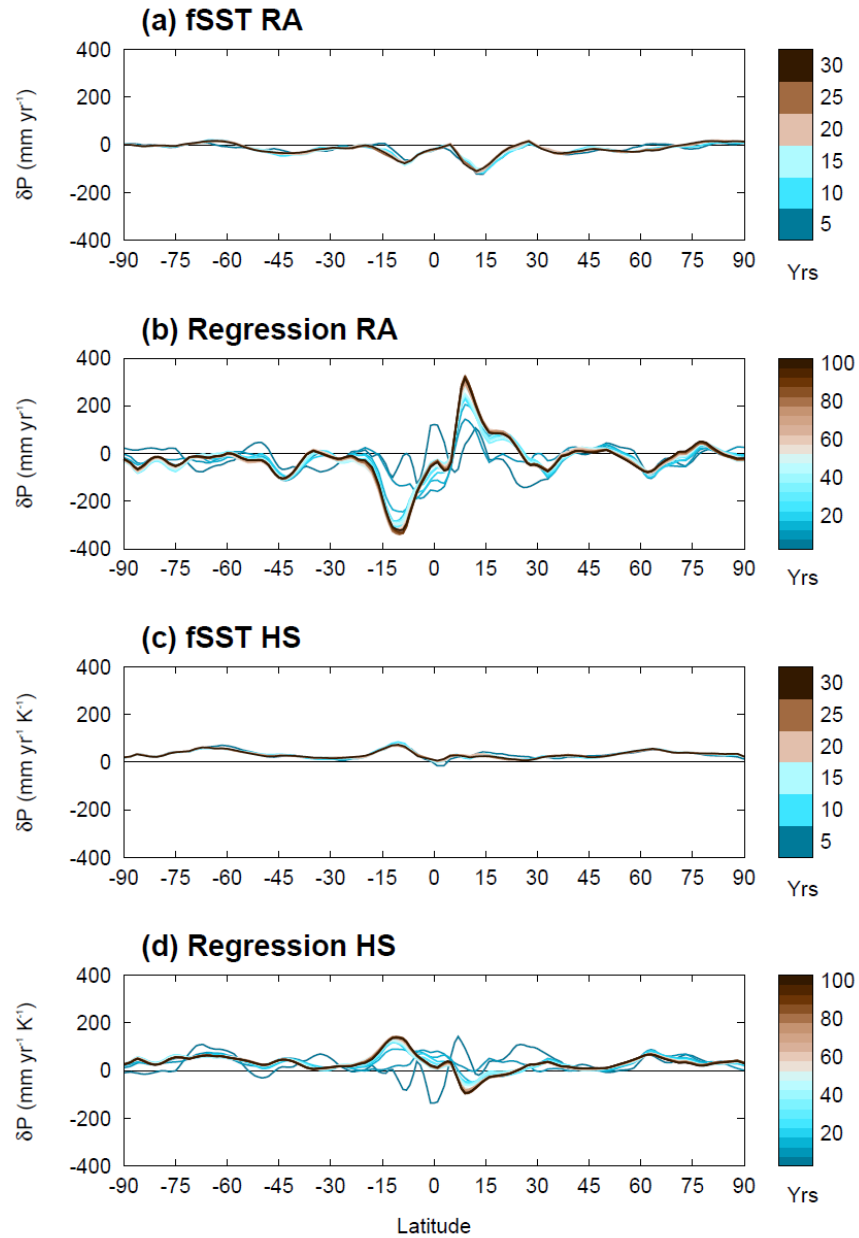


**Figure S1:** CESM1-CAM4 zonally averaged precipitation adjustment (RA) and hydrological sensitivity (HS) in response to 2xCO<sub>2</sub> calculated using (a, c) fSST and (b, d) regression methods. Each shaded line shows the response calculated using an integration/regression length increasing incrementally by 5 years.

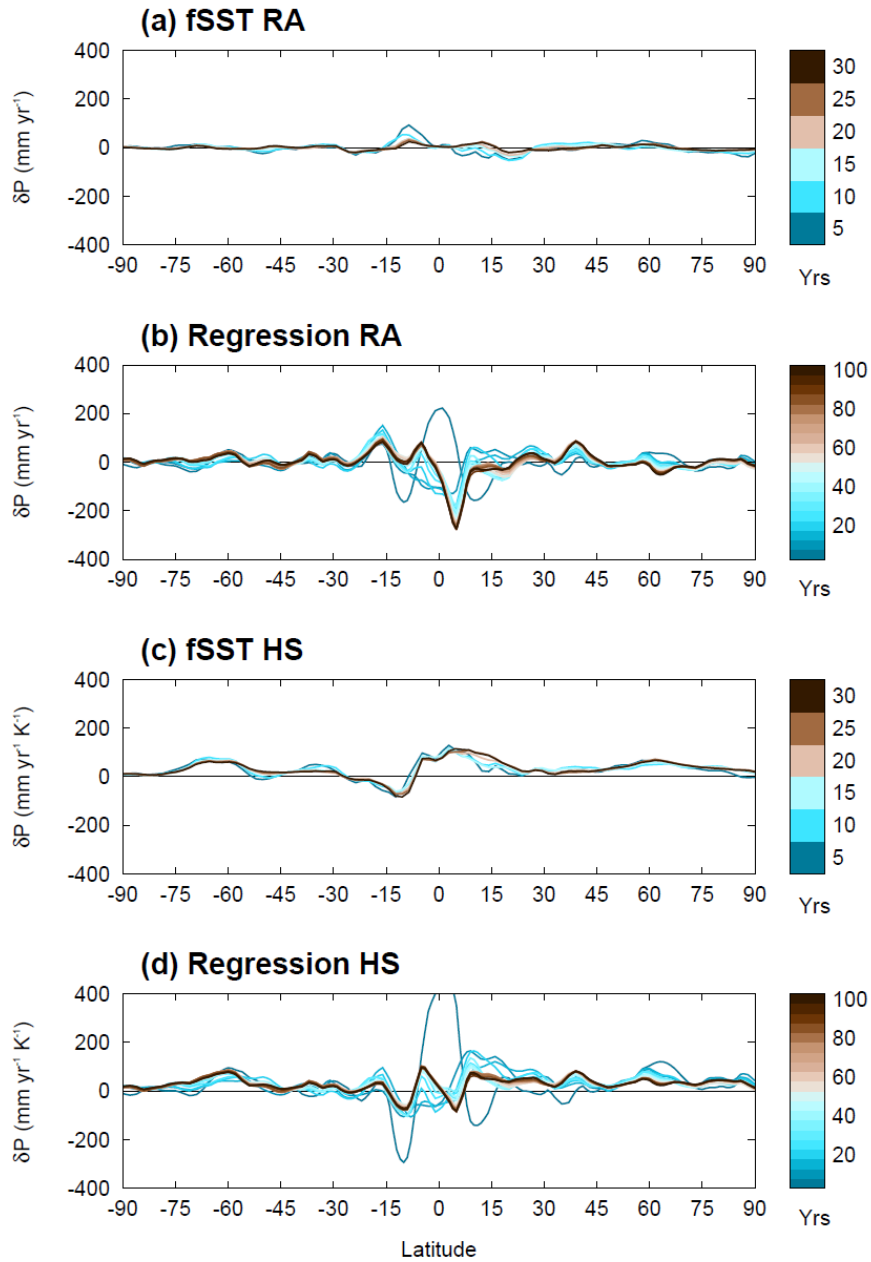


**Figure S2:** CESM1-CAM4 zonally averaged precipitation adjustment (RA) and hydrological sensitivity (HS) in response to 5xSul calculated using (a, c) fSST and (b, d) regression methods. Each shaded line shows the response calculated using an integration/regression length increasing incrementally by 5 years.

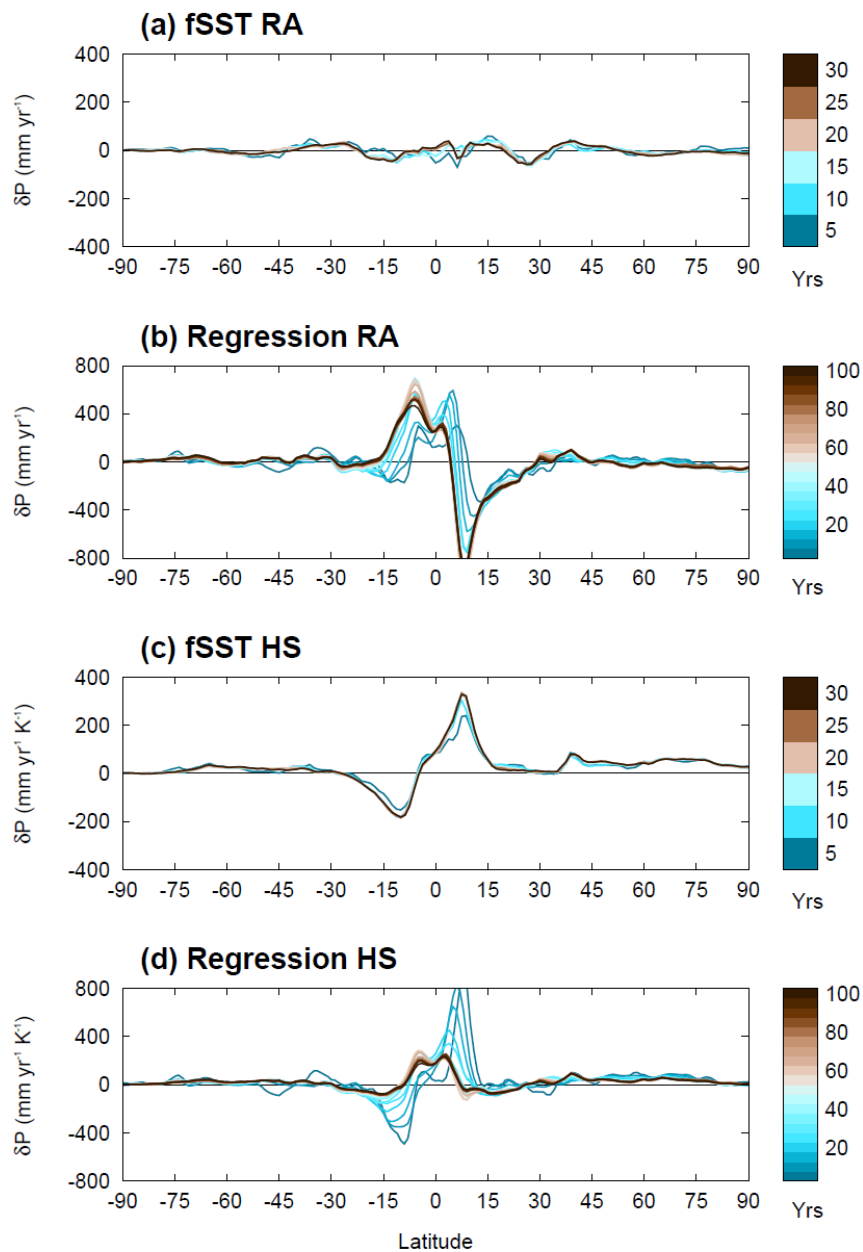


**Figure S3:** HadGEM2 zonally averaged precipitation adjustment (RA) and hydrological sensitivity (HS) in response to 5xSul calculated using (a, c) fSST and (b, d) regression methods. Each shaded line shows the response calculated using an integration/regression length increasing incrementally by 5 years.

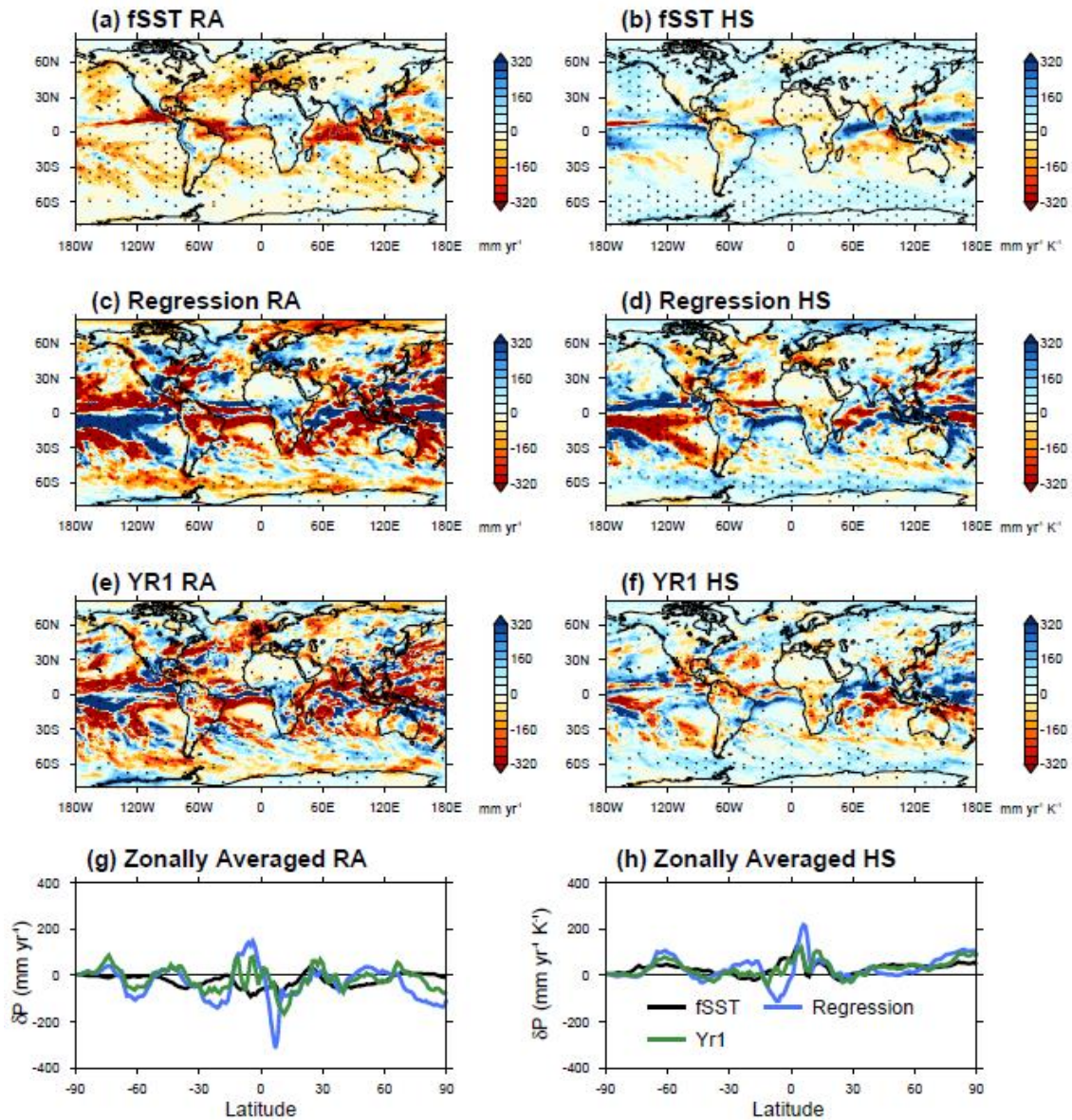


**Figure S4:** HadGEM2 regional precipitation adjustment (left) and hydrological sensitivity (right) response to doubling  $\text{CO}_2$  calculated using (a, b) fsST, (c, d) regression, and (e, f) YR1 methods. The lower two plots (g, h) show the zonally averaged response for all three methods. Stippling shows where the signal is greater than the standard error. An integration/regression length of 20 years is used to compute the responses.

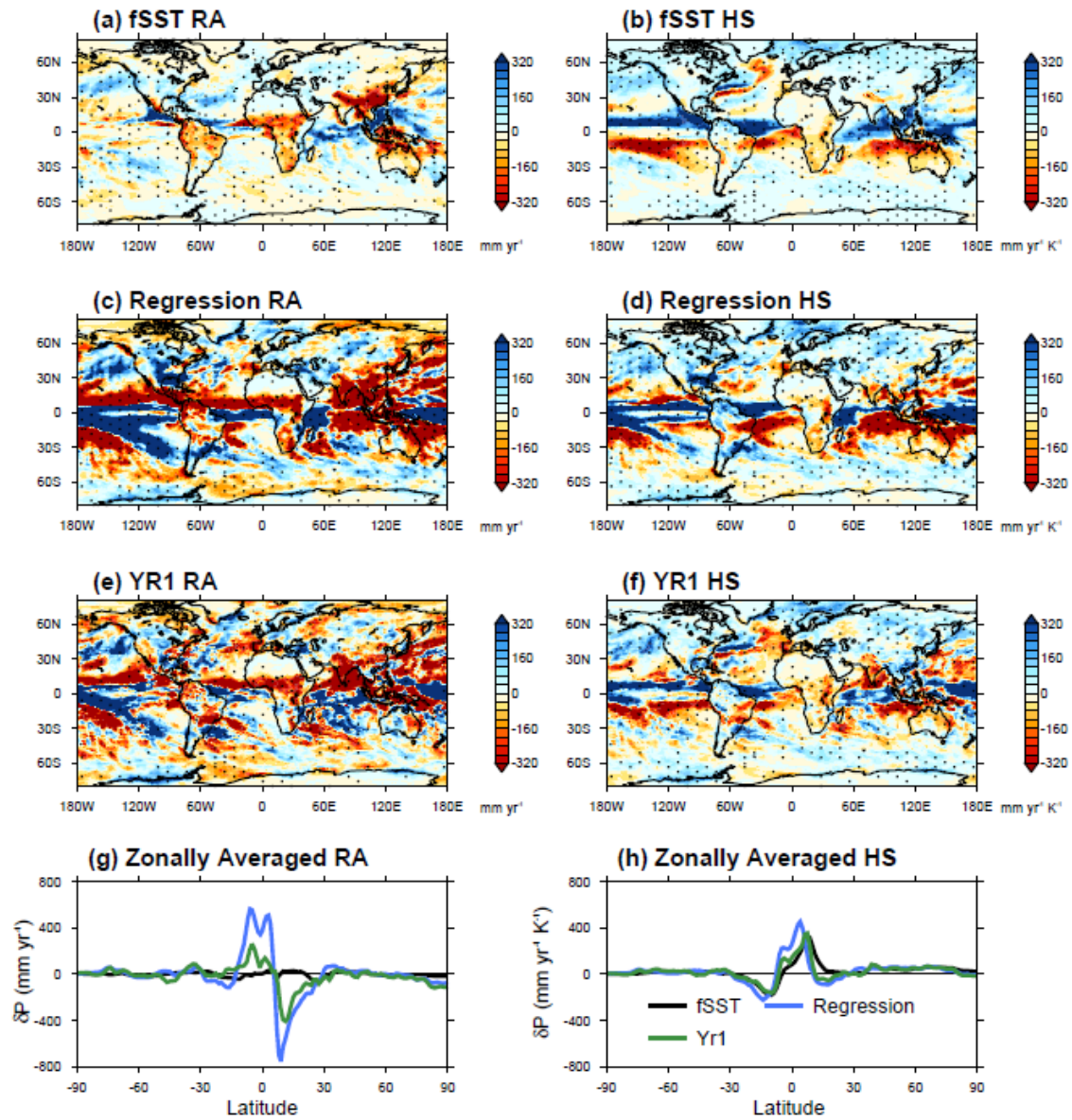


**Figure S5:** HadGEM2 regional precipitation adjustment (left) and hydrological sensitivity (right) response to 5xSul calculated using (a, b) fSST, (c, d) regression, and (e, f) YR1 methods. The lower two plots (g, h) show the zonally averaged response for all three methods. Stippling shows where the signal is greater than the standard error. An integration/regression length of 20 years is used to compute the responses.



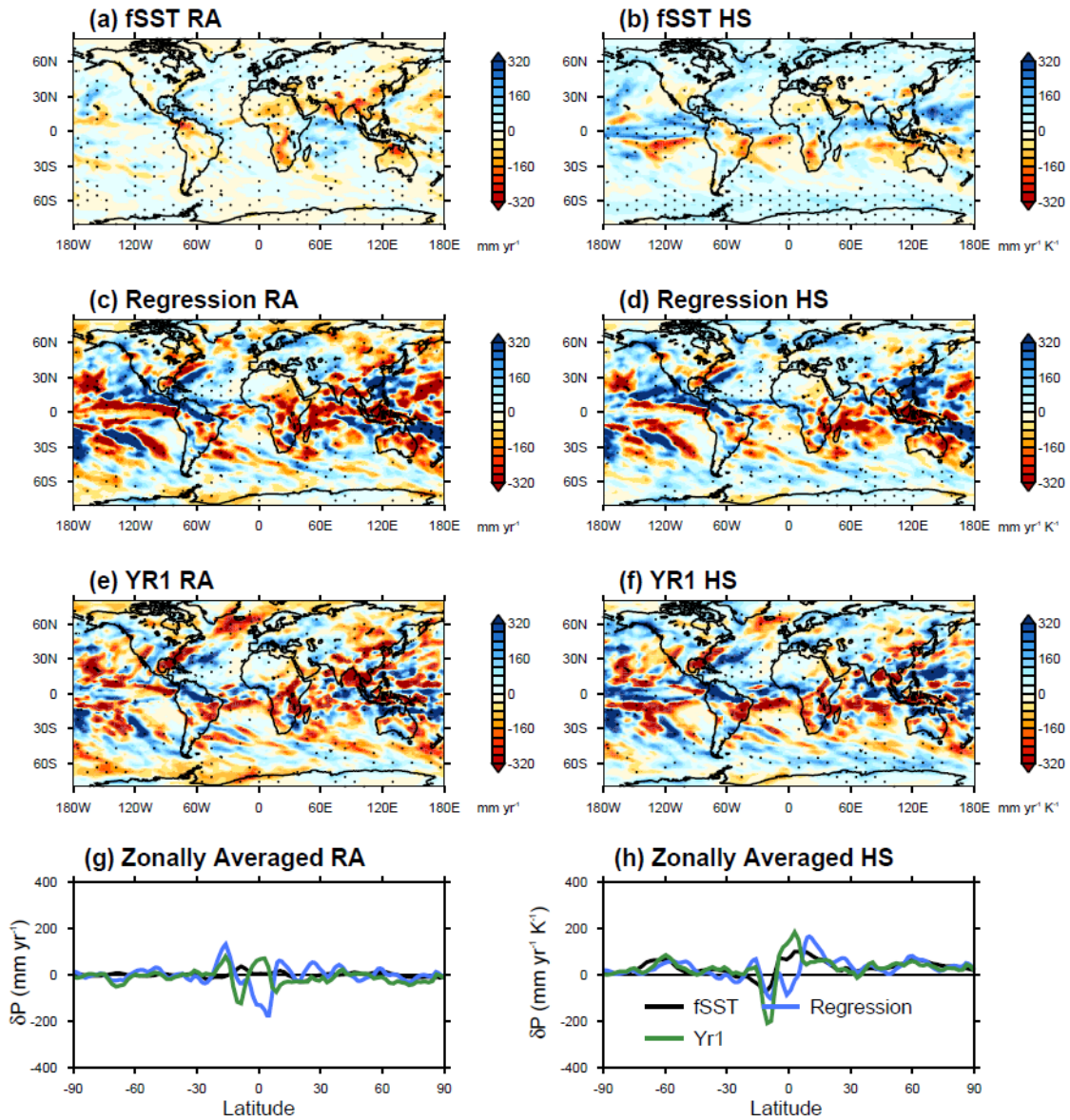


**Figure S6:** CESM1-CAM4 regional precipitation adjustment (left) and hydrological sensitivity (right) response to 5xSul calculated using (a, b) fSST, (c, d) regression, and (e, f) YR1 methods. The lower two plots (g, h) show the zonally averaged response for all three methods. Stippling shows where the signal is greater than the standard error. An integration/regression length of 20 years is used to compute the responses.

## 10xBC Atmospheric Energy Budget Feedback

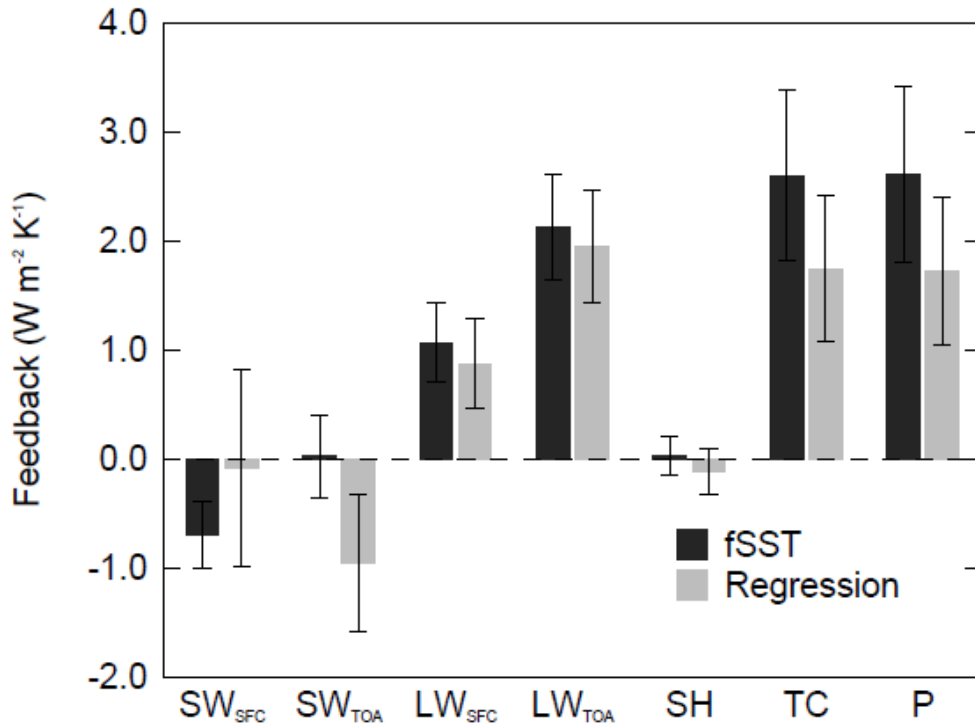


**Figure S7:** PDRMIP multi-model global mean atmospheric energy budget and precipitation feedback response to 10xBC calculated using the fSST and regression methods. Terms shown are the shortwave (SW) and longwave (LW) flux at the surface (SFC) and top of the atmosphere (TOA), surface sensible heat flux (SH), net tropospheric cooling (TC), and precipitation (P). The sign for all terms is such that a positive change contributes positively to precipitation. All values are shown in W m<sup>-2</sup> K<sup>-1</sup>.

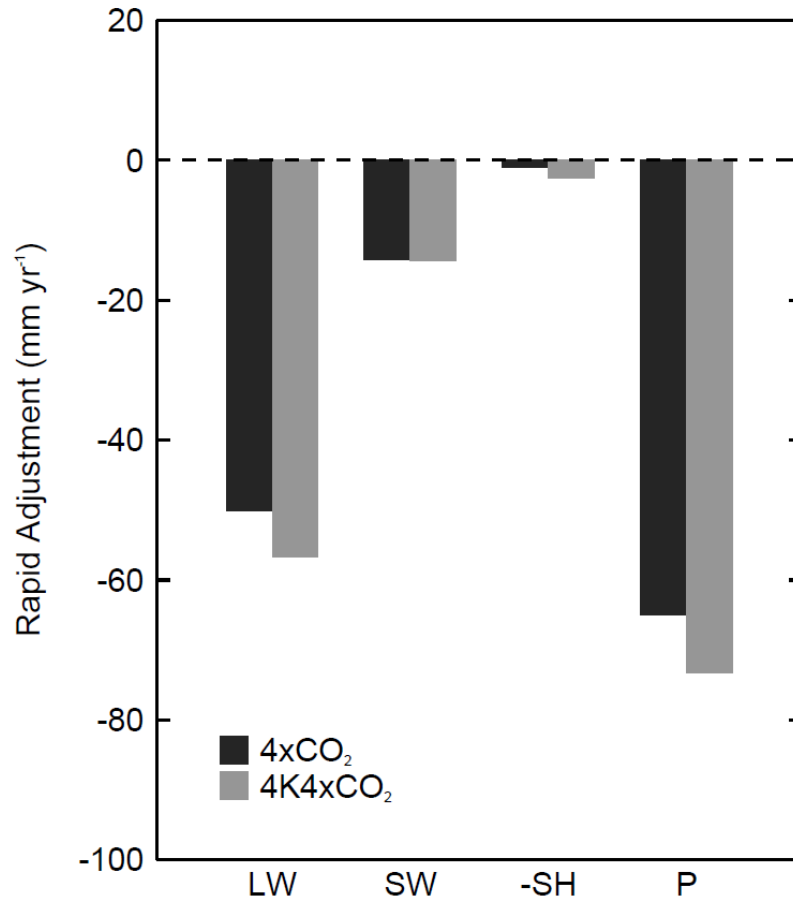


**Figure S8:** Atmospheric energy budget response to quadrupling CO<sub>2</sub> calculated using fSST simulations with pre-industrial SST climatology (4xCO<sub>2</sub>) and pre-industrial plus 4K climatology (4K4xCO<sub>2</sub>). Energy budget terms shown are the change in net atmospheric longwave cooling (LW), shortwave cooling (SW), sensible heat flux from the surface (SH) and precipitation (P). All values are converted to precipitation units (mm yr<sup>-1</sup>).

**Table S1:** Rapid precipitation adjustment results calculated using the first month of coupled abrupt forcing simulations for HadGEM2 and CESM1-CAM4. Uncertainties are the monthly standard deviation due to natural variability. All values are given in  $\text{mm yr}^{-1}$ .

<b>Forcing Scenario</b>	<b>HadGEM2</b>	<b>CESM1-CAM4</b>
2xCO2	-21.7±30.5	-47.1±33.8
3xCH4	-1.13±30.5	-24.7±33.8
5xSul	-1.96±30.5	-25.8±33.8
10xBC	-11.7±30.5	-43.8±33.8
SOL	2.32±30.5	-28.9±33.8

## **Appendix 2 - Supporting Information for Chapter 3**

# **Supplemental Material: Understanding the Rapid Precipitation Response to CO<sub>2</sub> and Aerosol Forcing on a Regional Scale**

Thomas B. Richardson, Piers M. Forster Timothy Andrews, Doug J. Parker

## **1. Supplementary Information**

### **1.1 Fixed SST Surface Energy Budget**

Figure S.4 shows the surface energy budget anomaly for the sstClim4xCO<sub>2</sub> simulation over land and sea. The surface energy budget response to forcing is very different over land and sea partly due to the imposed SST. Over land, increased CO<sub>2</sub> significantly increases downwelling LW radiation. The land surface responds with increasing temperature, therefore increasing upwelling LW radiation and SH. Over the sea, the temperature is fixed so the upwelling LW radiation and SH do not increase. The increased downwelling LW radiation, combined with a reduction in LH flux from the surface, produce a large net energy flux into the ocean. Therefore the fixed SST experiment emulates the initial response of fully coupled models, where the land surface adjusts, but the ocean continues to absorb energy and the surface temperature adjusts on much longer timescales.

### **1.2 Aerosol Indirect Effects**

Aerosols can affect precipitation through their direct effect, and indirect effects due to their role as cloud condensation and ice nuclei. The direct effect alters the tropospheric energy budget, and hence precipitation, through scattering and absorbing radiation. The first indirect effect also affects precipitation through altering the tropospheric energy budget as a result of changes in cloud albedo. The second indirect effect takes into account the influence of aerosols on precipitation efficiency. The models used in this study differ on which aerosol effects they represent as shown in table S.1. Figures S.5 and S.6 show the precipitation and temperature response for models categorized by which aerosol effects they include for the sstClimSulphate and sstClimAerosol simulations respectively.

In figure S.5 it can be seen that the precipitation and temperature responses to increased sulphate are very similar between the different model categories. This indicates that the radiative effects of aerosols alone drive a similar spatial pattern of response to that when all aerosol effects are included. This is consistent with the radiatively driven mechanisms explained in the main text. In figure S.6 it can be seen that the precipitation response to increased all aerosol exhibits a very similar spatial pattern for models that include the first indirect effect, and models which include both the first and second indirect effects. However, the precipitation and temperature response to all aerosols are noticeably different when only the aerosol direct effect is included (top row, Figure S6). This implies that the cloud albedo effect has a significant impact on the tropospheric energy budget, land surface temperature and precipitation pattern.

Aerosol effects on precipitation efficiency may further reduce precipitation over tropical land regions, but do not significantly alter the spatial pattern of change except for over South America.

## 2. Supplementary Tables

**Table S1:** Models categorized based on their representation of aerosol indirect effects.

<b>Direct Effect</b>	<b>Direct + 1st Indirect</b>	<b>Direct + 1st and 2nd Indirect Effects</b>
BCC-CSM1-1	CanESM2	CSIRO-Mk3.6.0
FGOALS-s2	IPSL-CM5A-LR	GFDL-CM3
MPI-ESM-LR		HadGEM2-A
		MIROC5
		MRI-CGCM3
		NorESM1-M

## 3. Supplementary Figures

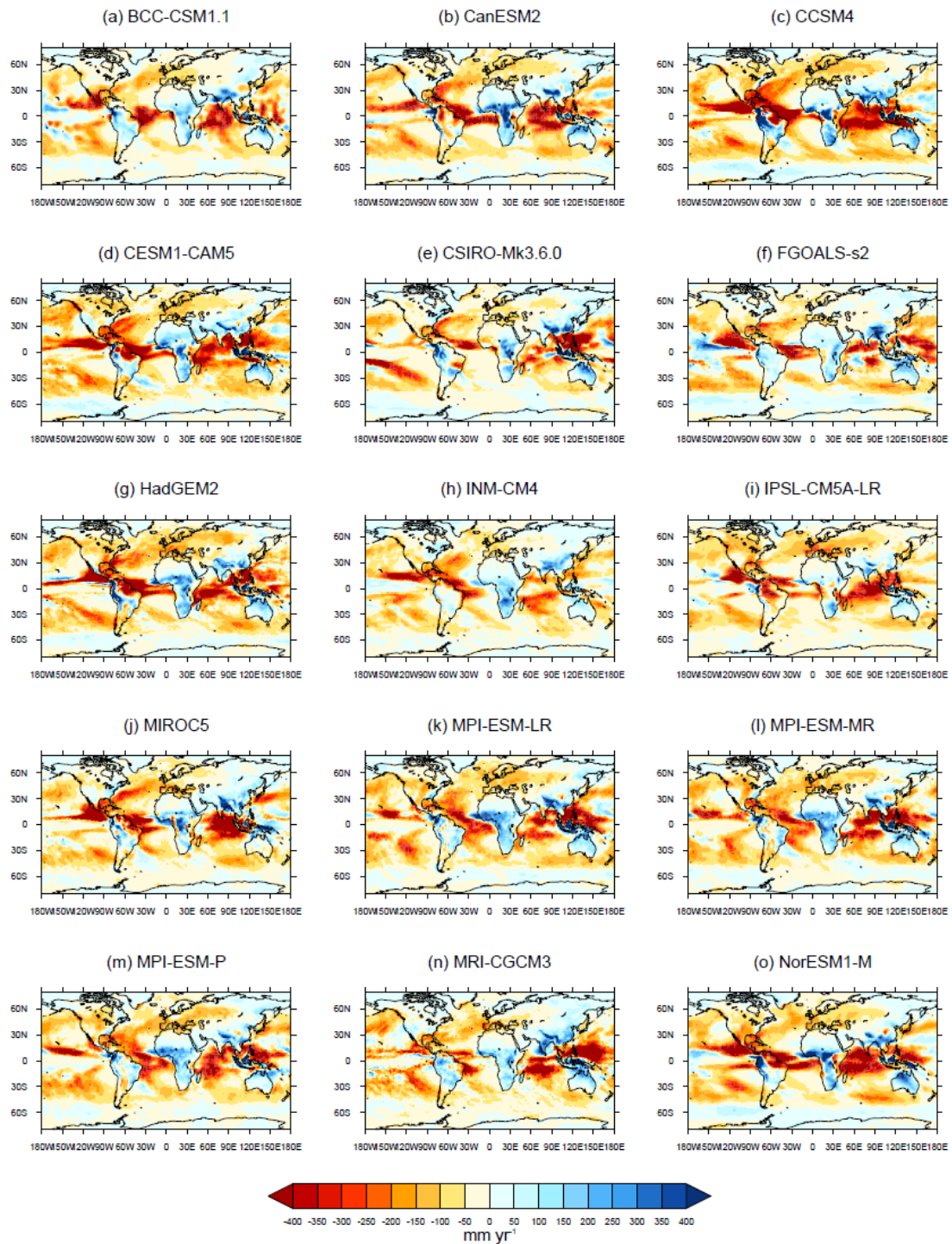


**Figure S.1:** CMIP5 models sstClim4xCO<sub>2</sub> precipitation (mm yr<sup>-1</sup>) anomalies. It can be seen that the spatial pattern of precipitation change is very consistent between all models.



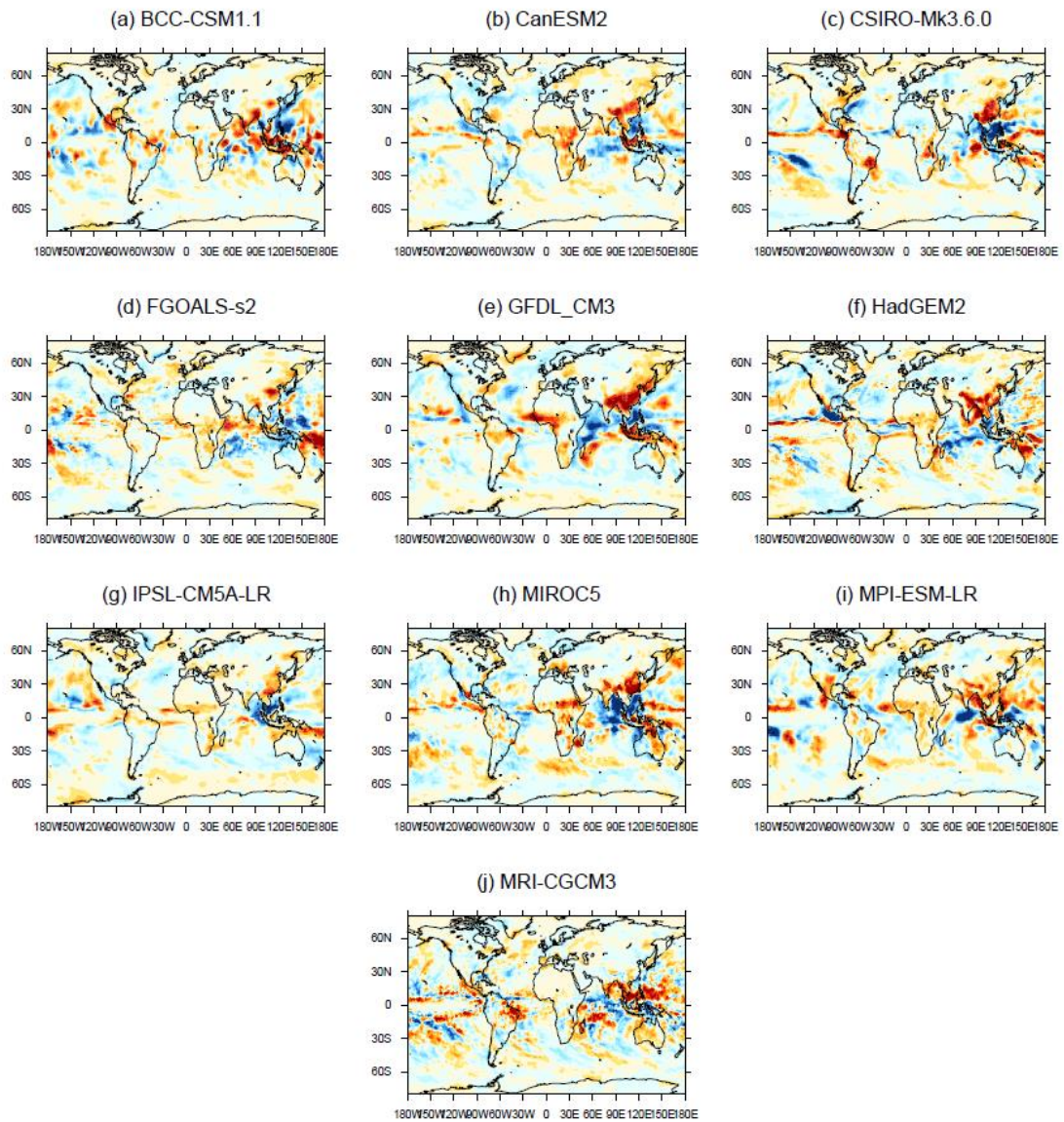


**Figure S.2:** CMIP5 models sstClimSulphate precipitation ( $\text{mm yr}^{-1}$ ) anomalies. Some features are evident in most models, such as drying over southeast Asia. However, there is considerably more spatial variation between different model responses than for the  $\text{CO}_2$  experiment.

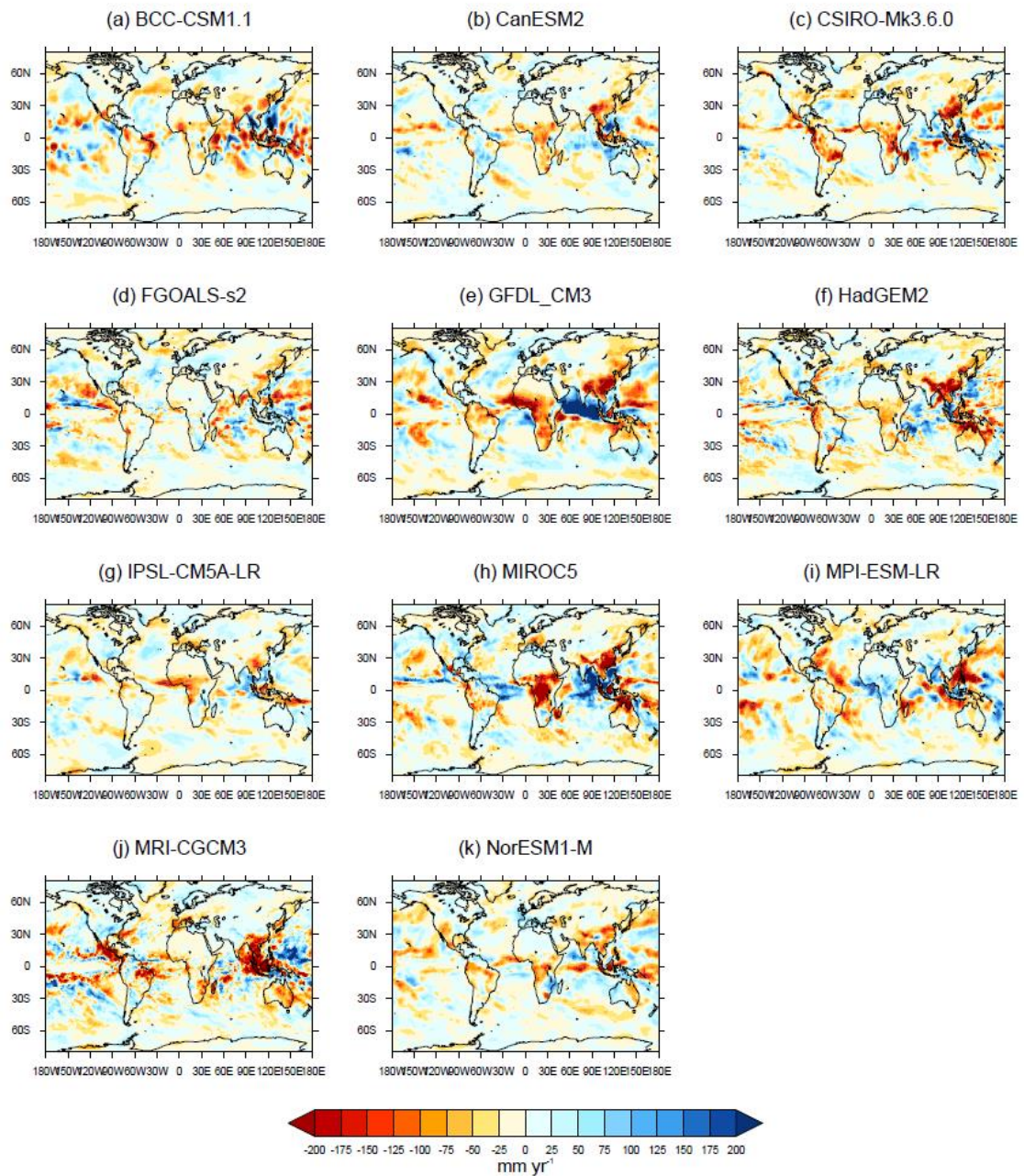


**Figure S.3:** CMIP5 models sstClimAerosol precipitation ( $\text{mm yr}^{-1}$ ) anomalies. Similar to the sulphate experiment some features are evident in many of the models, such as drying over southeast Asia. However, there is considerably more spatial variation between different model responses than for the  $\text{CO}_2$  experiment.

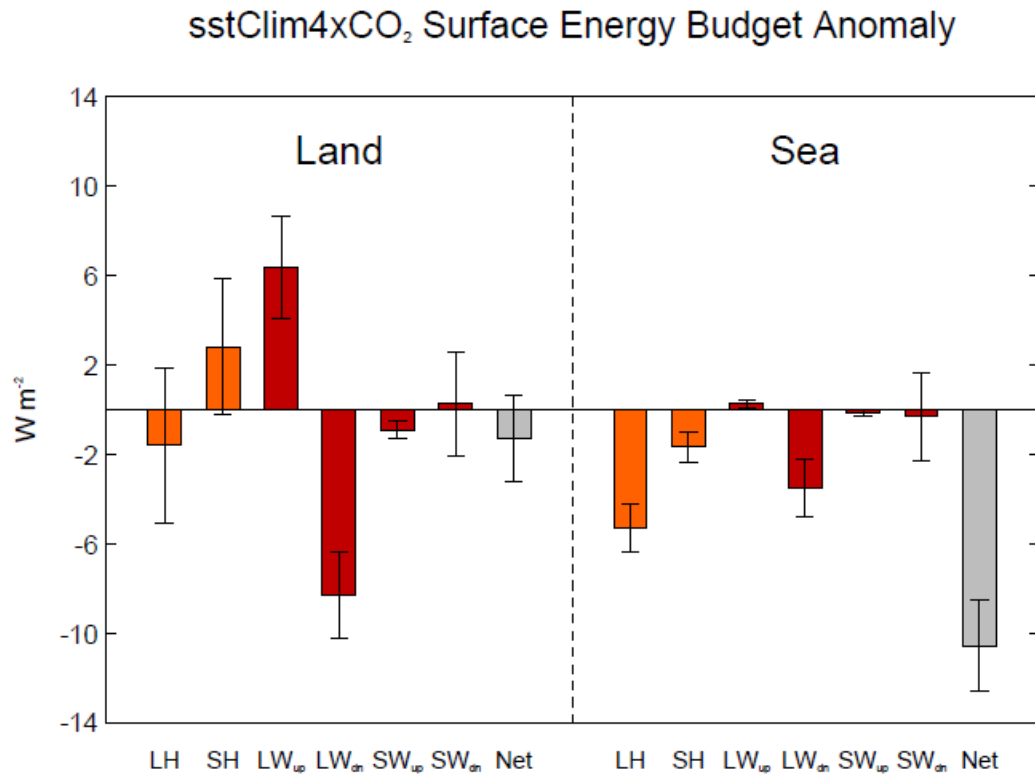


**Figure S.4:** Multi-model mean sstClim4xCO<sub>2</sub> surface energy budget anomaly over land and sea. Positive values represent an increase in energy flux from the surface to the atmosphere. Columns show the change in latent heat flux (LH), sensible heat flux (SH), longwave radiation (LW), shortwave radiation (SW), and net energy flux (Net). Subscripts ‘up’ and ‘dn’ denote that the change is in upwelling or downwelling radiation respectively. Error bars represent the 5-95% uncertainty assuming a normal distribution.

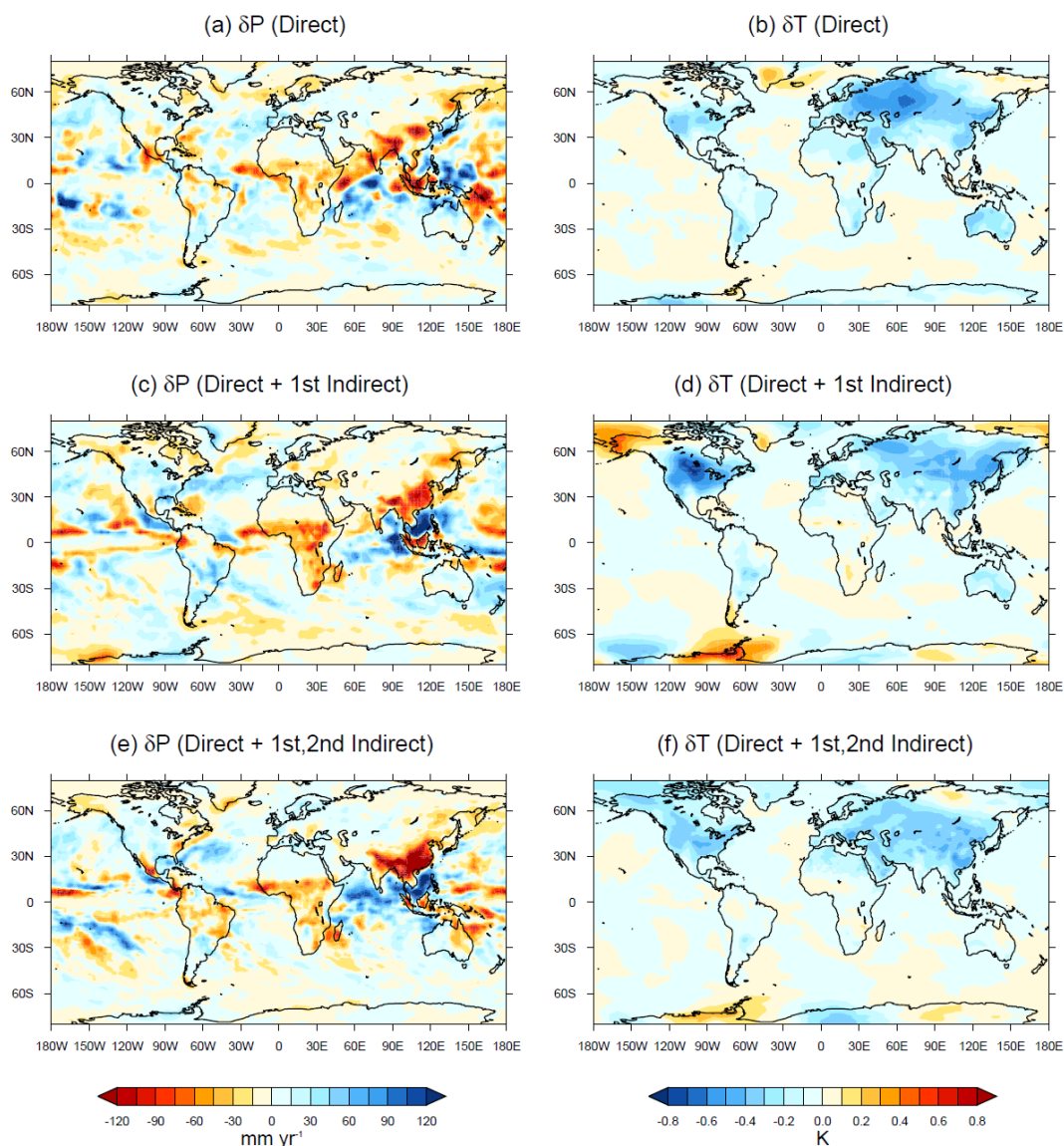


**Figure S.5:** Precipitation ( $\text{mm yr}^{-1}$ ) (left column) and near surface air temperature (K) (right column) anomaly for sstClimSulphate simulation. The models are split into those which include only the direct aerosol effect (a, b), those which include the direct and first indirect effect (c, d), and those which include the direct and first and second indirect effects as outlined in table S.1.

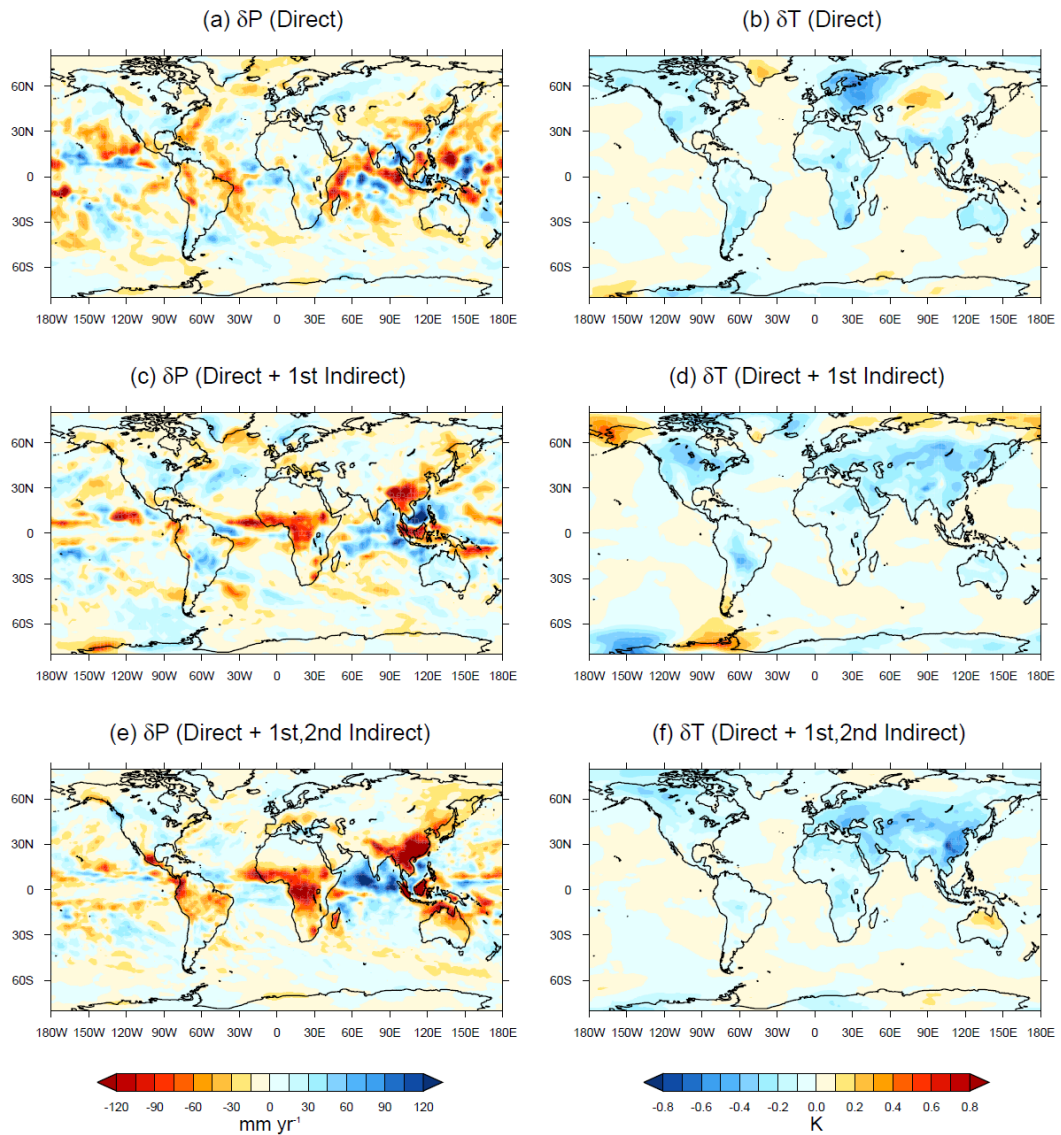


**Figure S.6:** Precipitation (left column) and near surface air temperature (right column) anomaly for sstClimAerosol simulation. The models are split into those which include only the direct aerosol effect (a, b), those which include the direct and first indirect effect (c, d), and those which include the direct and first and second indirect effects as outlined in table S.1.

## **Appendix 3 - Supporting Information for Chapter 4**

## Drivers of precipitation change: An energetic understanding: Supplementary Materials

**Table S1:** PDRMIP model details.

<b>Model</b>	<b>Version</b>	<b>Ocean Setup</b>	<b>Aerosol Setup</b>	<b>Baseline</b>
CanESM2	2010	Coupled Ocean	Emissions	Present-day
CESM1-CAM4	1.0.3	Slab Ocean	Fixed Concentrations	Present-day
CESM1-CAM5	1.1.2	Coupled Ocean	Emissions	Present-day
GISS-E2-R	E2-R	Coupled Ocean	Fixed Concentrations	Present-day
HadGEM2	6.6.3	Coupled Ocean	Emissions	Pre-industrial
HadGEM3	GA 4.0	Coupled Ocean	Fixed Concentrations	Present-day
IPSL-CM5A	CMIP5	Coupled Ocean	Fixed Concentrations	Present-day
MPI-ESM	1.1.00p2	Coupled Ocean	N/A	Present-day
NorESM1	M (intermediate resolution)	Coupled Ocean	Fixed Concentrations	Present-day
MIROC-SPRINTARS	5.9.0	Coupled Ocean	Emissions	Present-day

**Table S2:** CMIP5 models used for historical and future analysis. Crosses indicate model data was available and dashes indicate data was not available.

Model	Historical	RCP4.5	RCP8.5
CNRM-CM5	X	X	X
CNRM-CM5.2	X	-	-
FGOALS-g2	X	X	X
GFDL-CM2.1	X	-	-
GFDL-CM3	X	X	X
GFDL-ESM2G	X	X	X
GFDL-ESM2M	X	X	X
GISS-E2-H	X	X	X
GISS-E2-H-CC	X	-	X
GISS-E2-R	X	X	X
GISS-E2-R-CC	X	X	X
HadCM3	X	-	-
HadGEM2-AO	X	X	X
HadGEM2-CC	X	X	X
HadGEM2-ES	X	X	X
INM-CM4	X	X	X
IPSL-CM5A-LR	X	X	X
IPSL-CM5A-MR	X	X	X
IPSL-CM5B-LR	X	X	X
MIROC5	X	X	X
MIROC-ESM	X	X	X
MIROC-ESM-CHEM	X	X	X
MPI-ESM-LR	X	X	X
MPI-ESM-MR	X	X	X
MPI-ESM-P	X	-	-
MRI-CGCM3	X	X	X
NorESM1-ME	X	X	X



**Table S3:** PDRMIP multi-model mean (median in brackets)  $R$  factors (precipitation adjustment per unit global mean TOA forcing) and hydrological sensitivities ( $HS$ ) in response to the five forcing scenarios. Values are given for the global, land and sea mean.

Forcing Scenario	$R$ Factor ( $P_{adj}/F_{TOA}$ ) ( $\text{mm yr}^{-1}/\text{W m}^{-2}$ )		
	Global	Land	Sea
<b>2xCO2</b>	-7.53 (-7.46) $\pm$ 1.5	0.17 (1.30) $\pm$ 4.4	-10.7 (-11.1) $\pm$ 1.2
<b>3xCH4</b>	-5.52 (-5.35) $\pm$ 2.9	4.46 (3.83) $\pm$ 3.4	-9.62 (-9.04) $\pm$ 3.8
<b>5xSul</b>	0.57 (0.11) $\pm$ 2.0	10.8 (11.0) $\pm$ 3.8	-3.62 (-4.08) $\pm$ 1.9
<b>10xBC</b>	-28.7 (-26.2) $\pm$ 6.8	-5.24 (-4.85) $\pm$ 10.3	-38.3 (-34.8) $\pm$ 7.7
<b>2%Sol</b>	-1.93 (-2.11) $\pm$ 0.5	8.17 (7.78) $\pm$ 1.3	-6.06 (-6.00) $\pm$ 0.6
	$HS$ ( $\text{mm yr}^{-1} \text{K}^{-1}$ )		
	Global	Land	Sea
<b>2xCO2</b>	31.2 (30.0) $\pm$ 4.3	14.3 (14.2) $\pm$ 5.4	38.1 (36.2) $\pm$ 5.9
<b>3xCH4</b>	34.9 (33.9) $\pm$ 7.1	15.1 (18.2) $\pm$ 10.5	43.1 (38.7) $\pm$ 10.2
<b>5xSul</b>	32.0 (31.2) $\pm$ 4.9	12.1 (11.6) $\pm$ 6.3	40.1 (37.9) $\pm$ 7.3
<b>10xBC</b>	32.3 (29.9) $\pm$ 10.6	-11.6 (-20.6) $\pm$ 20.0	50.2 (44.3) $\pm$ 18.7
<b>2%Sol</b>	32.6 (32.4) $\pm$ 5.2	8.04 (8.76) $\pm$ 7.0	42.6 (39.7) $\pm$ 8.1

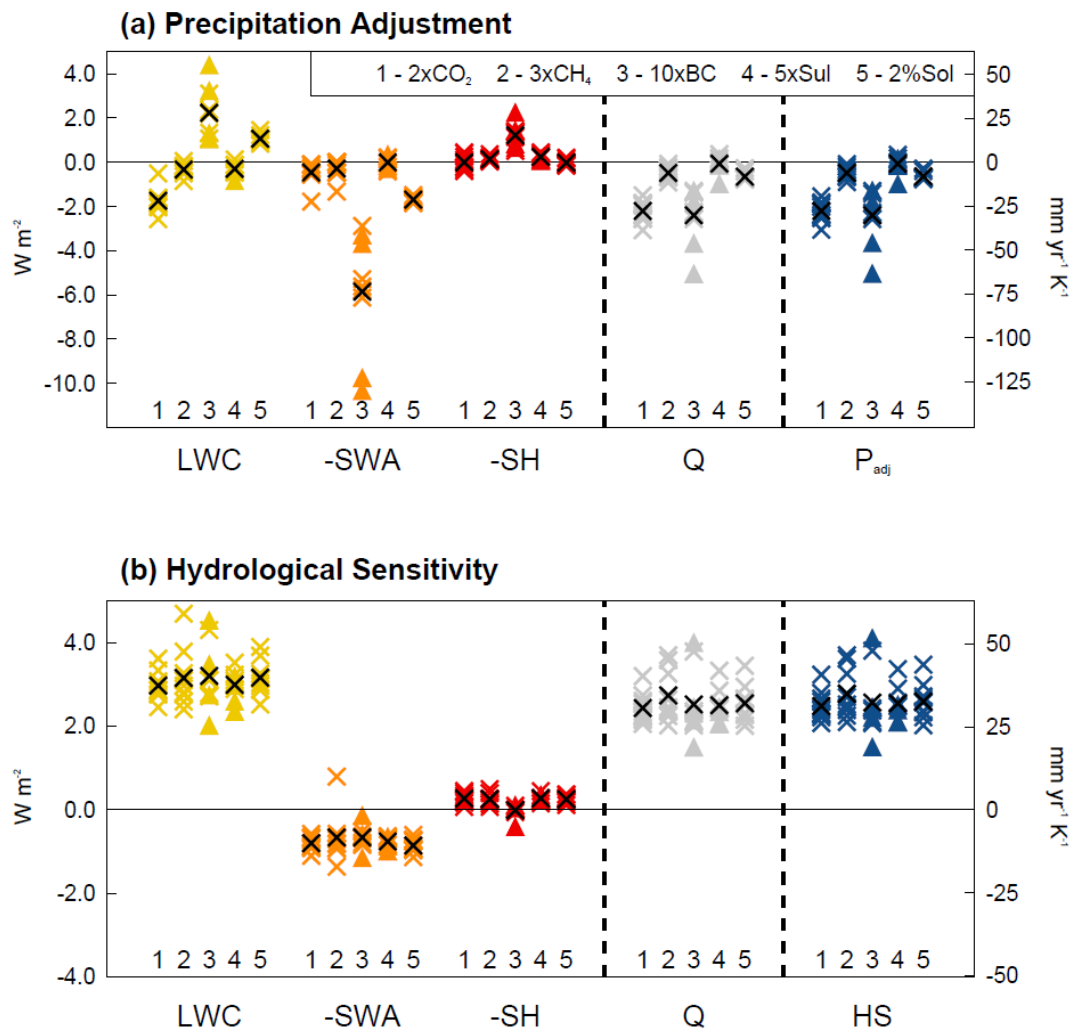


**Figure S1:** Global mean (a) precipitation adjustment ( $P_{ra}$ , blue) and (b) hydrological sensitivity ( $HS$ , blue) in response to the five PDRMIP forcing scenarios.  $P_{ra}$  and  $HS$  are decomposed in to the contributions from the atmospheric energy budget: net longwave cooling ( $LWC$ , yellow), net shortwave absorption ( $SWA$ , orange), sensible heat flux from the surface ( $SH$ , red) and the net atmospheric cooling ( $Q$ , light grey). Each cross denotes the response of one PDRMIP model. The multi-model mean is shown by the black cross. Triangles denote models which used emissions for the aerosol perturbations. The sign of change in each component is given such that a positive value contributes positively to precipitation change. Results are shown in both energetic units (left axis) [(a)  $W m^{-2}$ , (b)  $W m^{-2} K^{-1}$ ], and precipitation units (right axis) [(a)  $mm yr^{-1}$  and (b)  $mm yr^{-1} K^{-1}$ ].

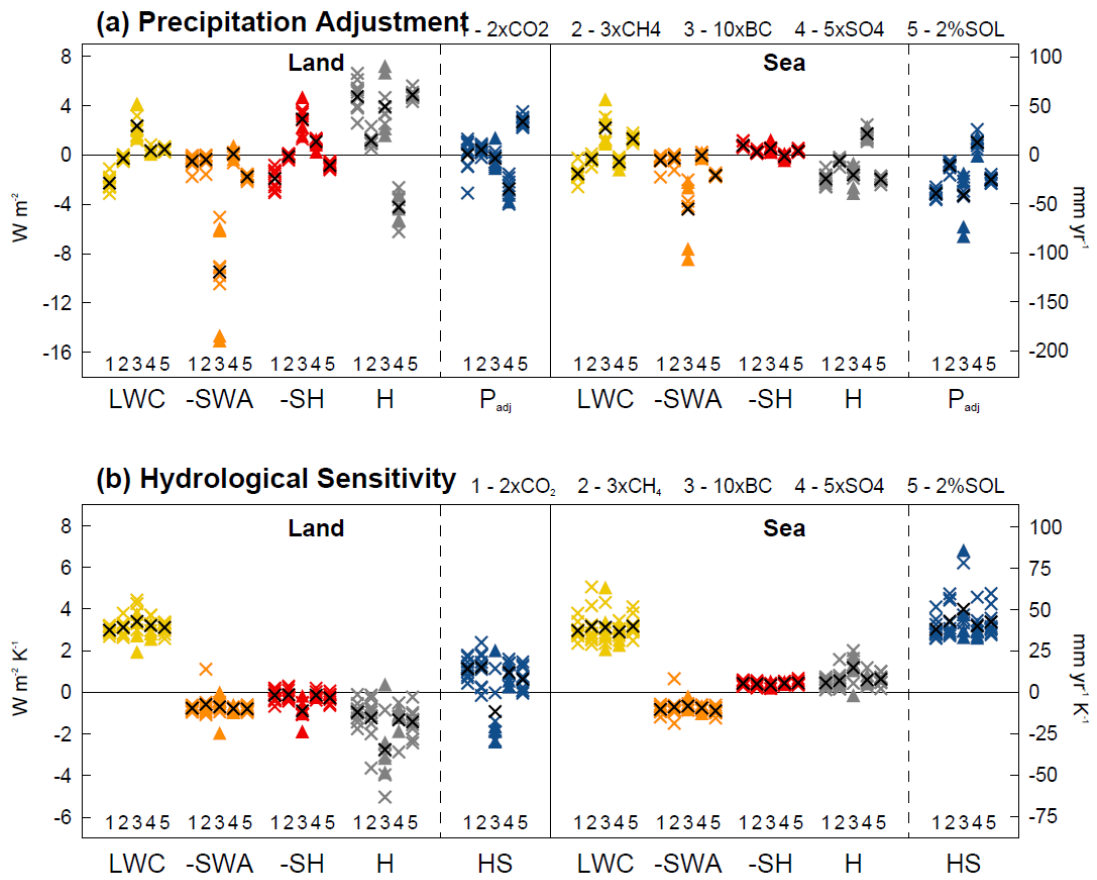


**Figure S2:** Land and sea mean (a) precipitation adjustment ( $P_{ra}$ , blue) and (b) hydrological sensitivity ( $HS$ , blue) in response to the PDRMIP forcing scenarios.  $P_{ra}$  and  $HS$  are decomposed in to the contributions from the local atmospheric energy budget: net longwave cooling ( $LWC$ , yellow), net shortwave absorption ( $SWA$ , orange), sensible heat flux from the surface ( $SH$ , red) and the dry static energy flux divergence ( $H$ , dark grey). Each cross denotes the response of one PDRMIP model. The multi-model mean is shown by the black cross. Triangles denote models which used emissions for the aerosol perturbations. The sign of change in each component is given such that a positive value contributes positively to precipitation change. Results are shown in both energetic units (left axis) [(a)  $Wm^{-2}$ , (b)  $Wm^{-2}K^{-1}$ ], and precipitation units (right axis) [(a)  $mm\ yr^{-1}$  and (b)  $mm\ yr^{-1}K^{-1}$ ].

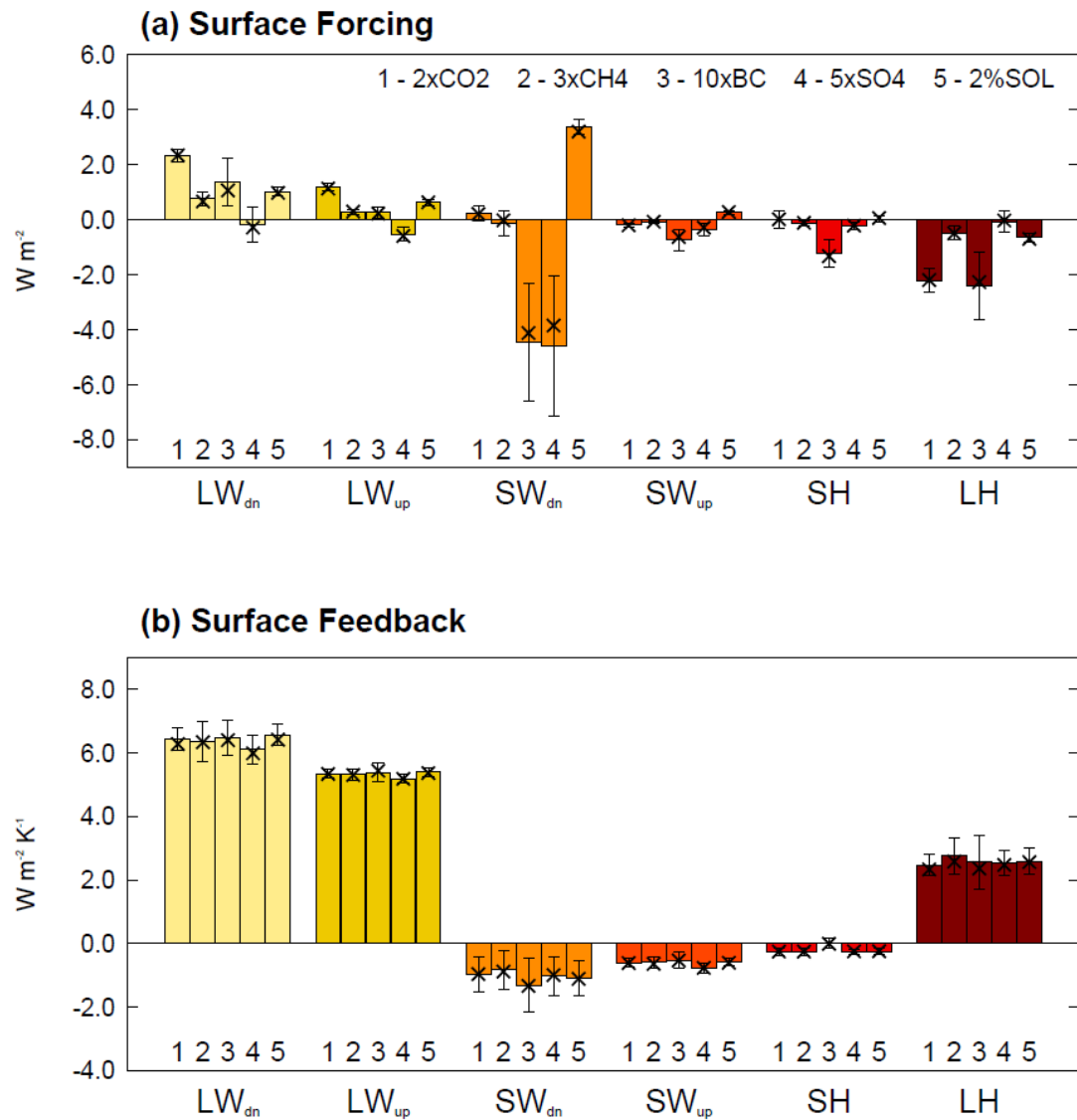


**Figure S3:** Multi-model global mean (a) forcing and (b) feedbacks for surface fluxes in response to the five PDRMIP forcing scenarios. Surface fluxes shown are downwelling longwave ( $LW_{dn}$ ), upwelling longwave ( $LW_{up}$ ), downwelling shortwave ( $SW_{dn}$ ), upwelling shortwave ( $SW_{up}$ ), sensible heat ( $SH$ ) and latent heat ( $LH$ ). Forcings are given in  $W m^{-2}$ , and feedbacks in  $W m^{-2} K^{-1}$ . Error bars denote the standard deviation of model spread, and crosses show the median value.

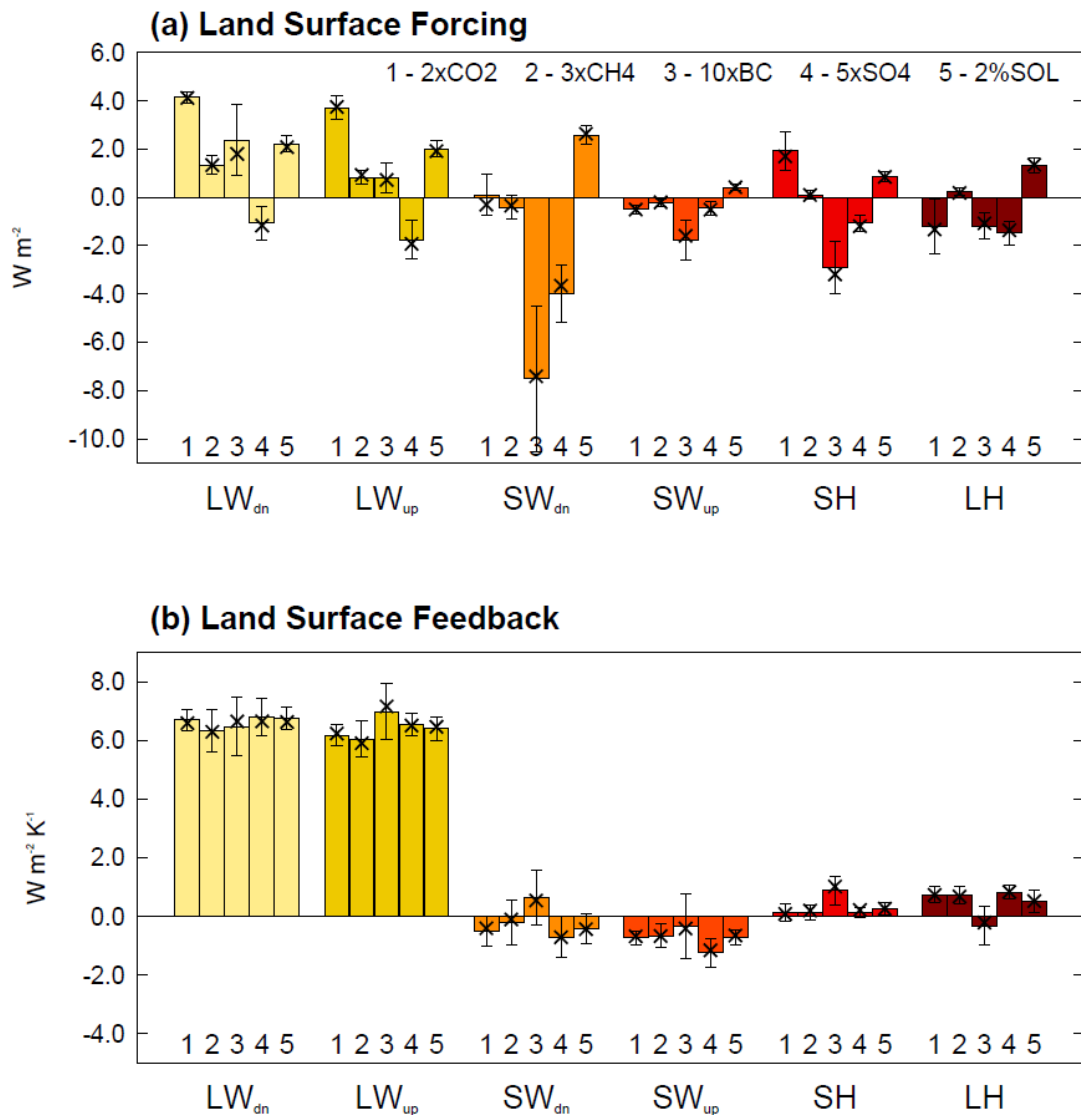


**Figure S4:** Multi-model land mean (a) forcing and (b) feedbacks for surface fluxes in response to the five PDRMIP forcing scenarios. Surface fluxes shown are downwelling longwave ( $LW_{dn}$ ), upwelling longwave ( $LW_{up}$ ), downwelling shortwave ( $SW_{dn}$ ), upwelling shortwave ( $SW_{up}$ ), sensible heat ( $SH$ ) and latent heat ( $LH$ ). Forcings are given in  $W m^{-2}$ , and feedbacks in  $W m^{-2} K^{-1}$ . Error bars denote the standard deviation of model spread, and crosses show the median value.

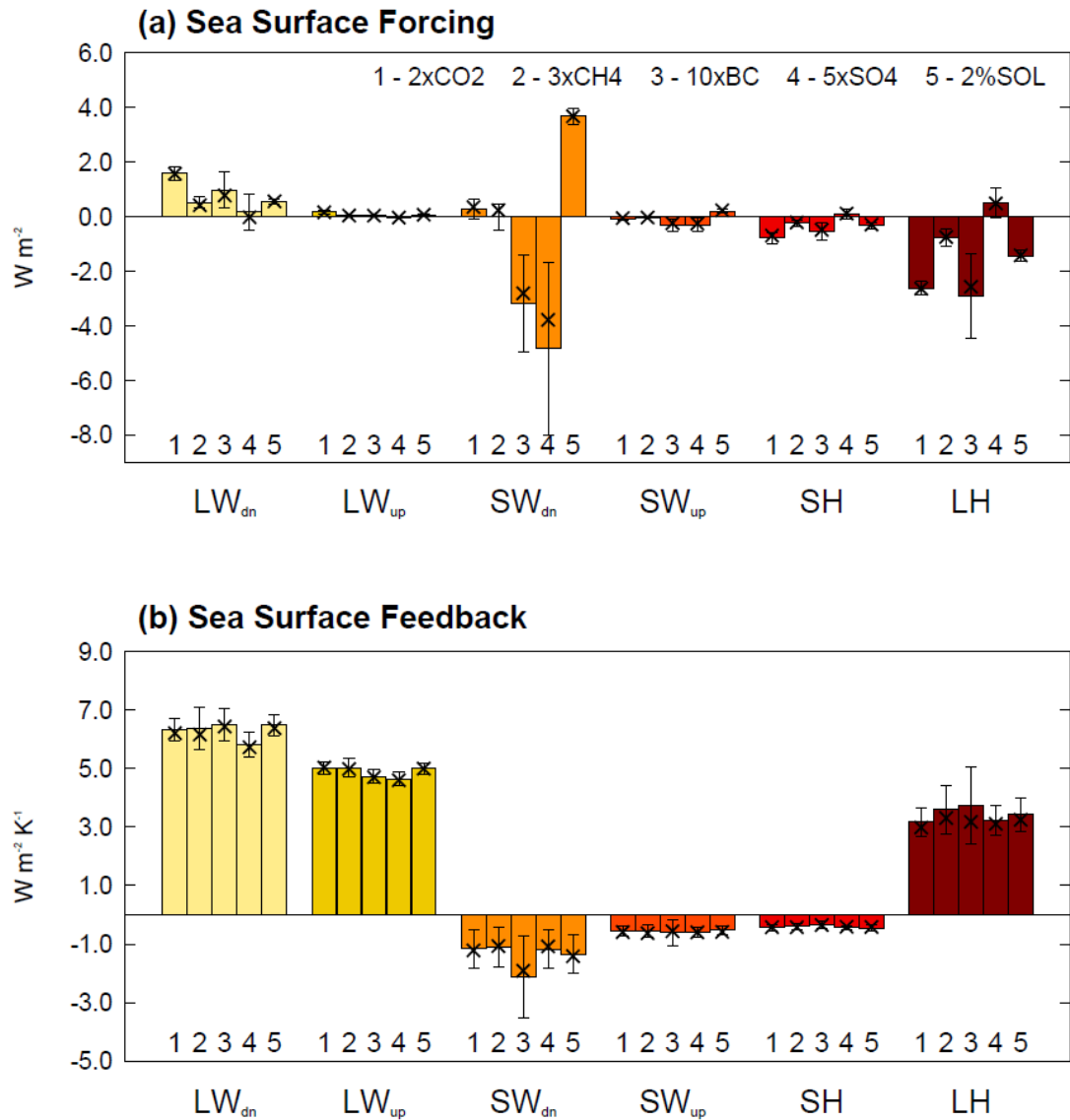


**Figure S5:** Multi-model sea mean (a) forcing and (b) feedbacks for surface fluxes in response to the five PDRMIP forcing scenarios. Surface fluxes shown are downwelling longwave ( $LW_{dn}$ ), upwelling longwave ( $LW_{up}$ ), downwelling shortwave ( $SW_{dn}$ ), upwelling shortwave ( $SW_{up}$ ), sensible heat ( $SH$ ) and latent heat ( $LH$ ). Forcings are given in  $W m^{-2}$  and feedbacks in  $W m^{-2} K^{-1}$ . Error bars denote the standard deviation of model spread, and crosses show the median value.

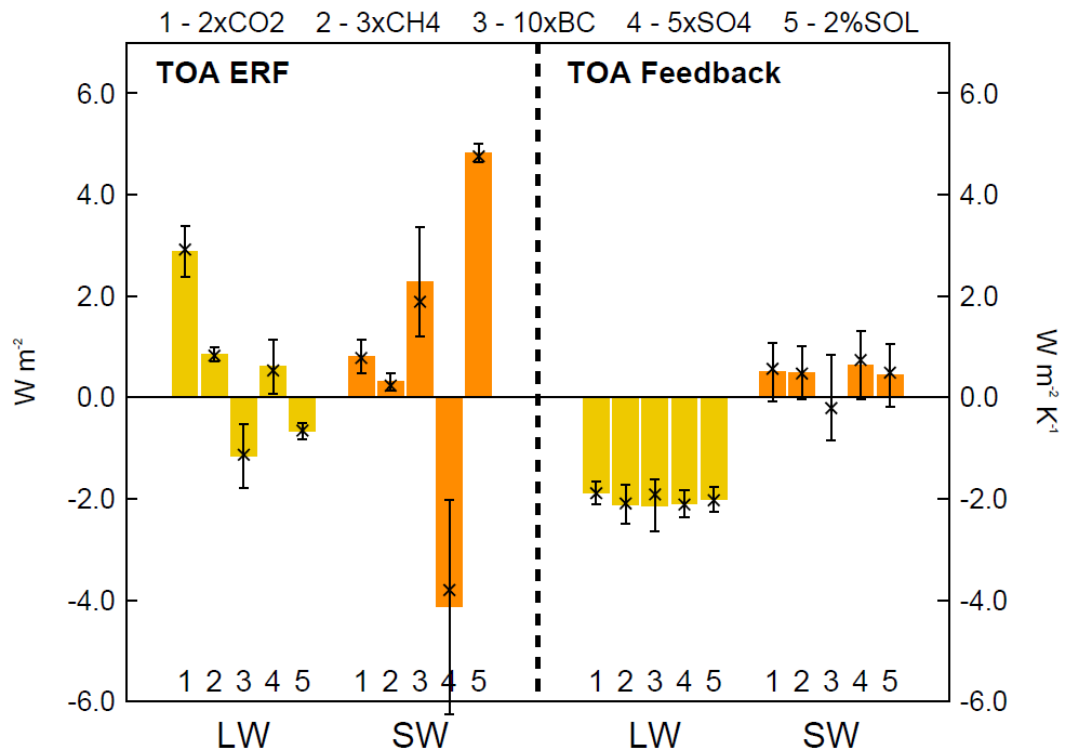


**Figure S6:** Multi-model global mean forcing (left) and feedbacks (right) for top of the atmosphere (*TOA*) longwave (*LW*) and shortwave (*SW*) fluxes in response to the five PDRMIP forcing scenarios. Values are positive downward. Forcings are given in  $W m^{-2}$ , and feedbacks in  $W m^{-2} K^{-1}$ . Error bars denote the standard deviation of model spread, and crosses show the median value.

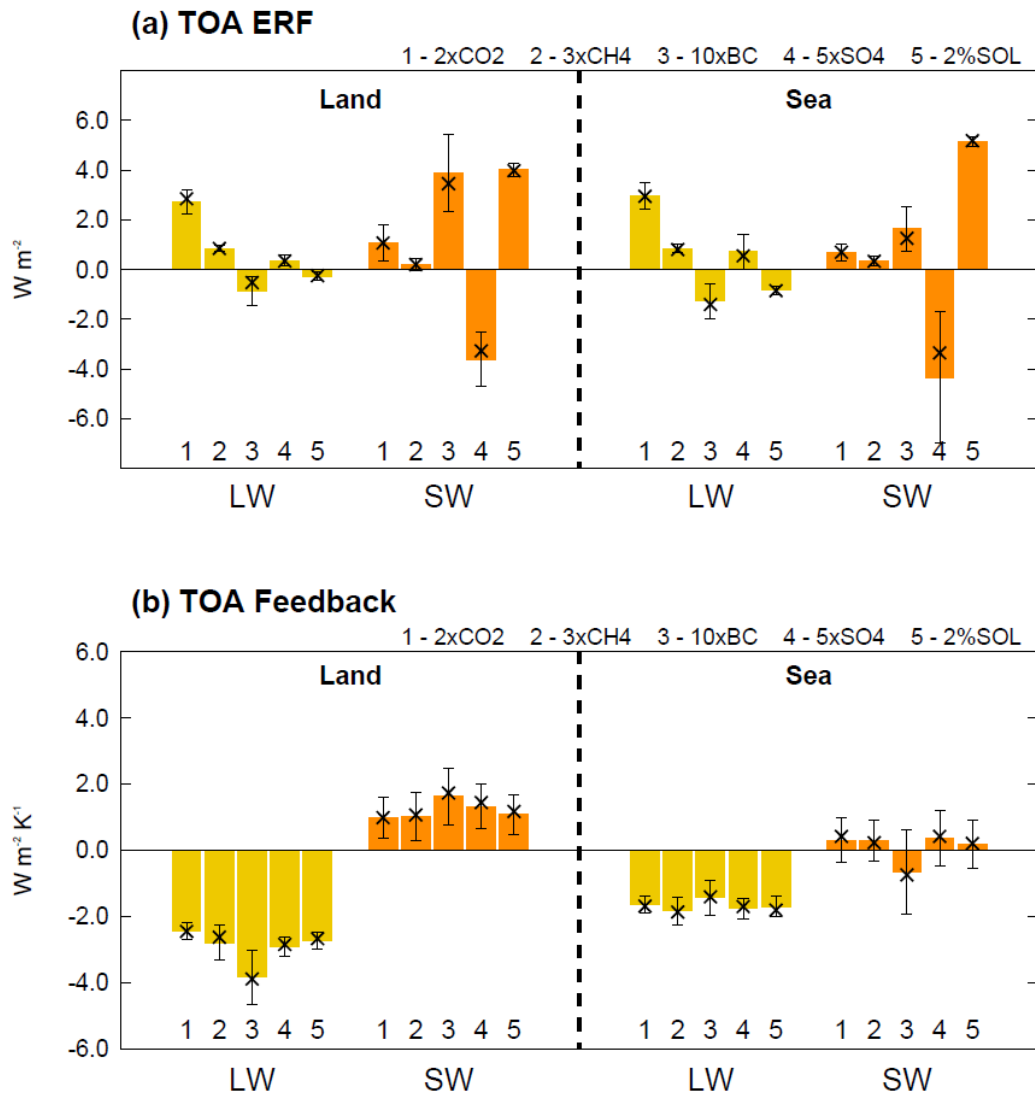


**Figure S7:** Multi-model mean (a) forcing and (b) feedbacks for top of the atmosphere (*TOA*) longwave (*LW*) and shortwave (*SW*) fluxes over land (left) and sea (right) in response to the five PDRMIP forcing scenarios. Values are positive downward. Forcings are given in  $W m^{-2}$ , and feedbacks in  $W m^{-2} K^{-1}$ . Error bars denote the standard deviation of model spread, and crosses show the median value.



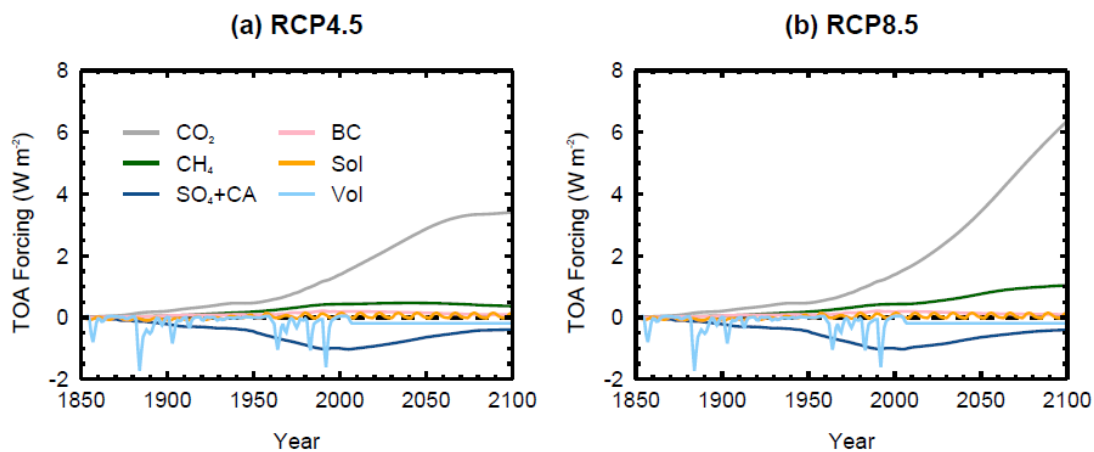


**Figure S8:** Global mean top of the atmosphere radiative forcing from 1850 to 2100 taken from Meinshausen et al. (2011) for each of the forcing agents included in the simple model.

## References

Meinshausen, M., Smith, S.J., Calvin, K., Daniel, J.S., Kainuma, M.L.T., Lamarque, J., Matsumoto, K., Montzka, S.A., Raper, S.C.B., Riahi, K., Thomson, A., Velders, G.J.M., van Vuuren, D.P.P., 2011. The RCP greenhouse gas concentrations and their extensions from 1765 to 2300. *Clim. Change* 109, 213–241. doi:10.1007/s10584-011-0156-z

## **Appendix 4 - Supporting Information for Chapter 5**

## Importance of carbon dioxide physiological forcing on projected Amazonian rainfall change – Supplementary Materials

**Table S1:** List of CMIP5 model output used for analysis. Crosses indicate which models were used for each experiment.

Model	RCP4.5	RCP8.5	amip4xCO2	sstClim4xCO2
CanESM2	-	-	-	X
CCSM4	-	-	-	X
CNRM-CM5	-	-	X	-
GFDL-CM3	X	X	-	-
GFDL-ESM2G	X	X	-	-
GFDL-ESM2M	X	X	-	-
HadGEM2-AO	X	X	X	X
HadGEM2-CC	X	X	-	-
HadGEM2-ES	X	X	-	-
IPSL-CM5A-LR	X	X	X	X
IPSL-CM5A-MR	X	X	-	-
IPSL-CM5B-LR	X	X	X	-
MIROC5	X	X	-	X
MIROC-ESM	X	X	-	-
MIROC-ESM-CHEM	X	X	-	-
MPI-ESM-LR	X	X	X	X
MPI-ESM-MR	X	X	X	X
MPI-ESM-P	-	-	-	X
MRI-CGCM3	-	-	X	-
NorESM1-M	-	-	X	X
NorESM1-ME	X	X	-	-

**Table S2:** List of vegetation scheme references for models which performed sstClim simulations.

<b>Model</b>	<b>Vegetation Scheme Reference</b>
CanESM2	(Arora, 2003) <a href="http://www.cccma.ec.gc.ca/ctem/">http://www.cccma.ec.gc.ca/ctem/</a>
CCSM4	(Oleson et al., 2010)
HadGEM2-ES	(Cox et al., 1999)
IPSL-CM5A-LR	(Krinner et al., 2005)
MIROC5	(Takata et al., 2003)
MPI-ESM-LR	<a href="http://www.mpimet.mpg.de/en/science/models/jsbach/">http://www.mpimet.mpg.de/en/science/models/jsbach/</a>
MPI-ESM-MR	
MPI-ESM-P	
NorESM1-M	(Oleson et al., 2010)

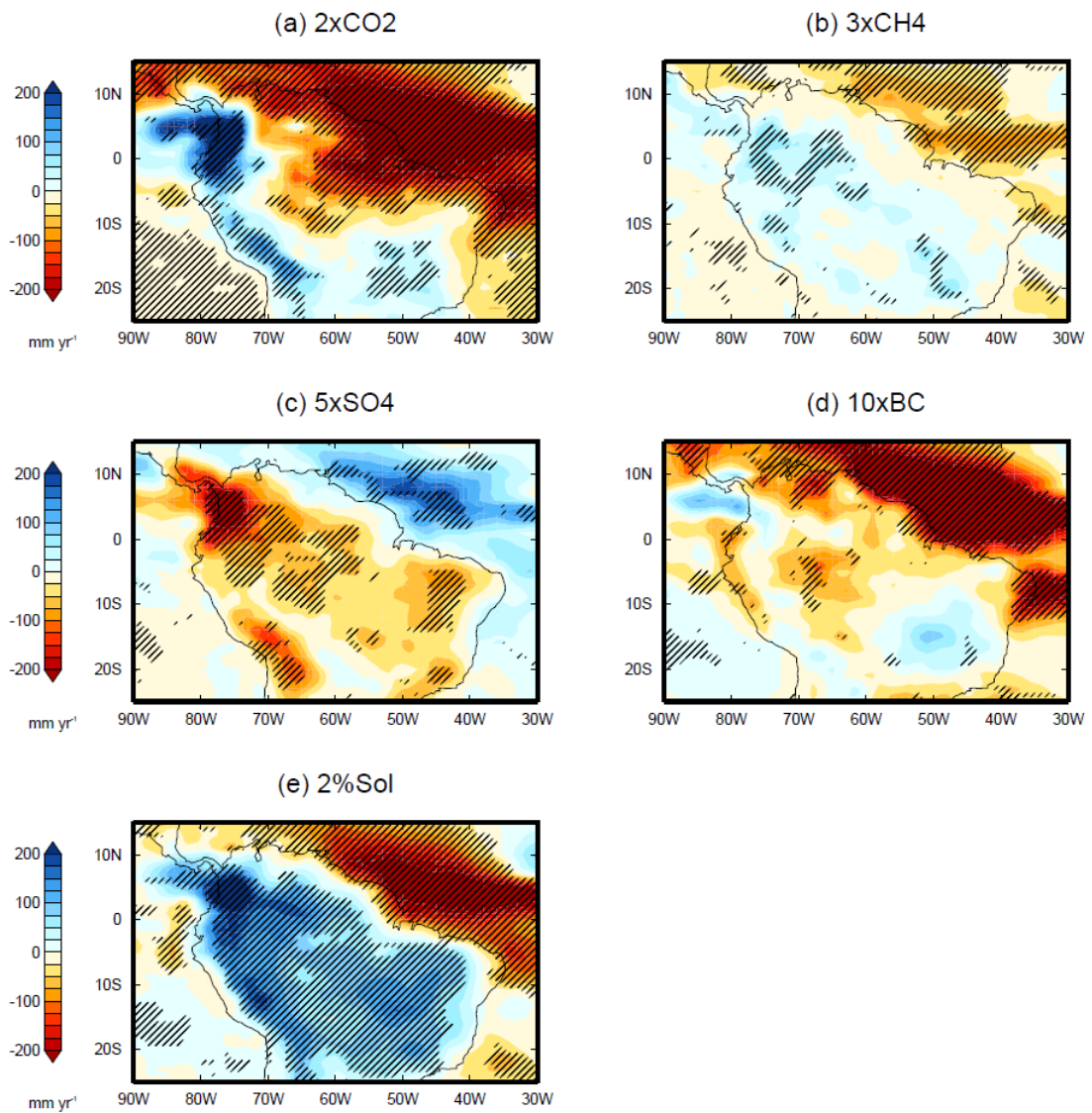


**Figure S1:** PDRMIP multi-model mean precipitation adjustment in response to (a) 2xCO<sub>2</sub>, (b) 3xCH<sub>4</sub>, (c) 5xSO<sub>4</sub>, (d) 10xBC and (e) 2%SOL. Hatching denotes where 80% of the models agree on the sign of the change.

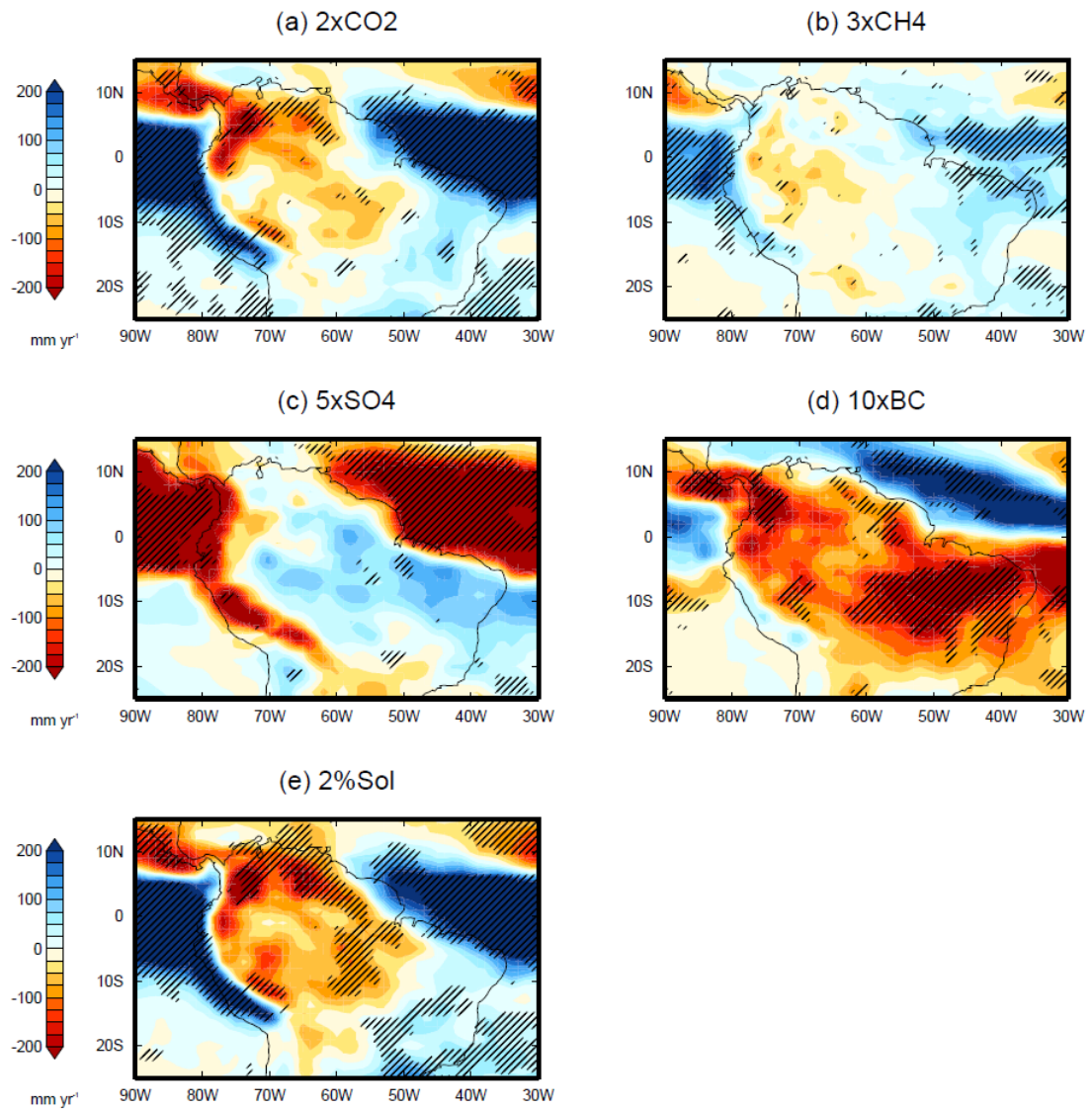


**Figure S2:** PDRMIP multi-model mean precipitation feedback response for (a) 2xCO<sub>2</sub>, (b) 3xCH<sub>4</sub>, (c) 5xSO<sub>4</sub>, (d) 10xBC and (e) 2%SOL. Hatching denotes where 80% of the models agree on the sign of the change.

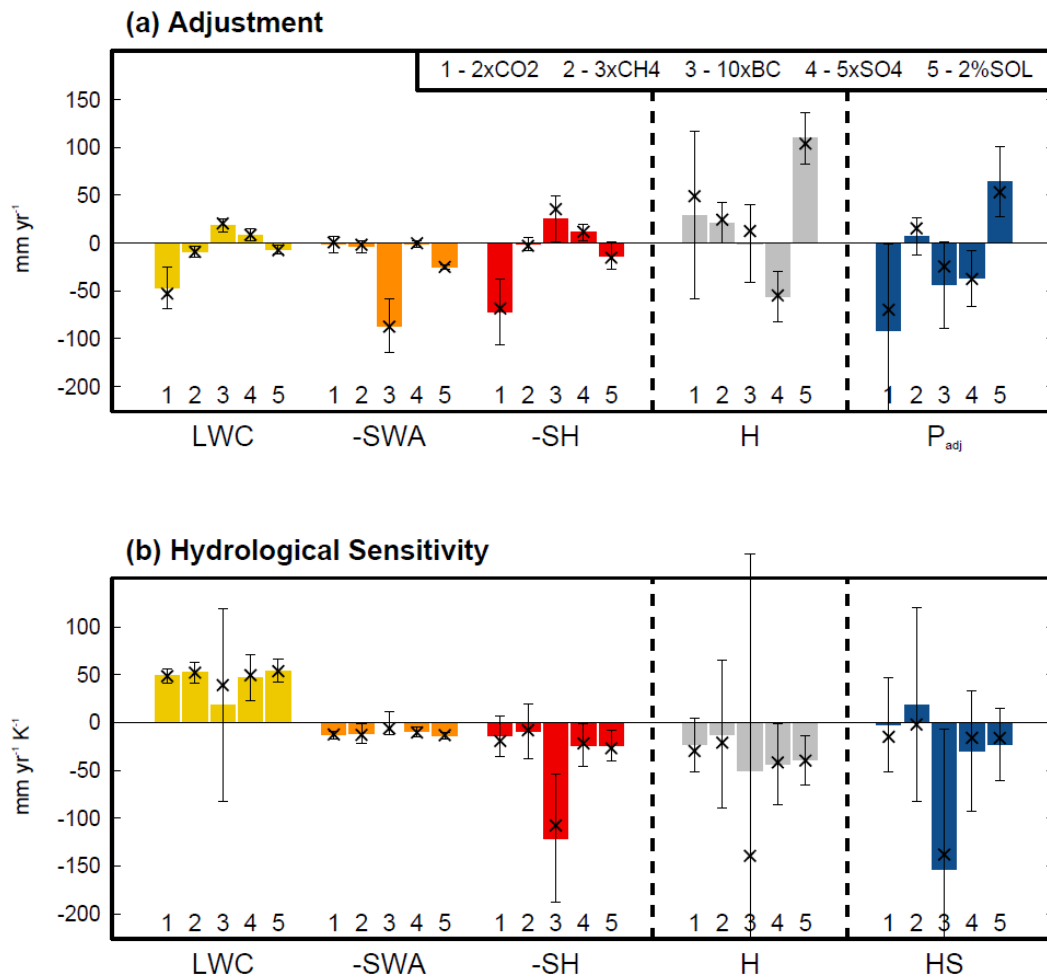


**Figure S3:** PDRMIP multi-model mean (a) precipitation adjustment and (b) hydrological sensitivity (feedback response per unit kelvin) in response to the five forcing scenarios for the ECA region. The adjustment and feedback are decomposed into the contributions from the atmospheric energy budget as described by Equation 1. The sign for each term is given according to Equation 1. Results are shown in precipitation units ((a) mm yr<sup>-1</sup> and (b) mm yr<sup>-1</sup> K<sup>-1</sup>). Error bars denote the standard deviation of model spread, and crosses show the median value.

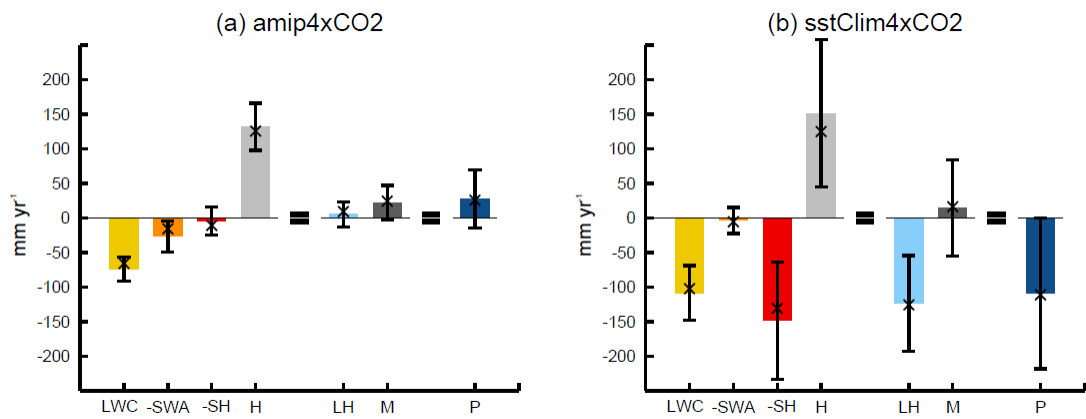


**Figure S4:** CMIP5 multi-model mean atmospheric energy budget and moisture budget (described in Equation 1) responses to quadrupling CO<sub>2</sub> in (a) amip and (b) sstClim simulations. The sign for each term is given according to Equation 1. Results are given in precipitation units (mm yr<sup>-1</sup>). Error bars denote the standard deviation of model spread, and crosses show the median value.



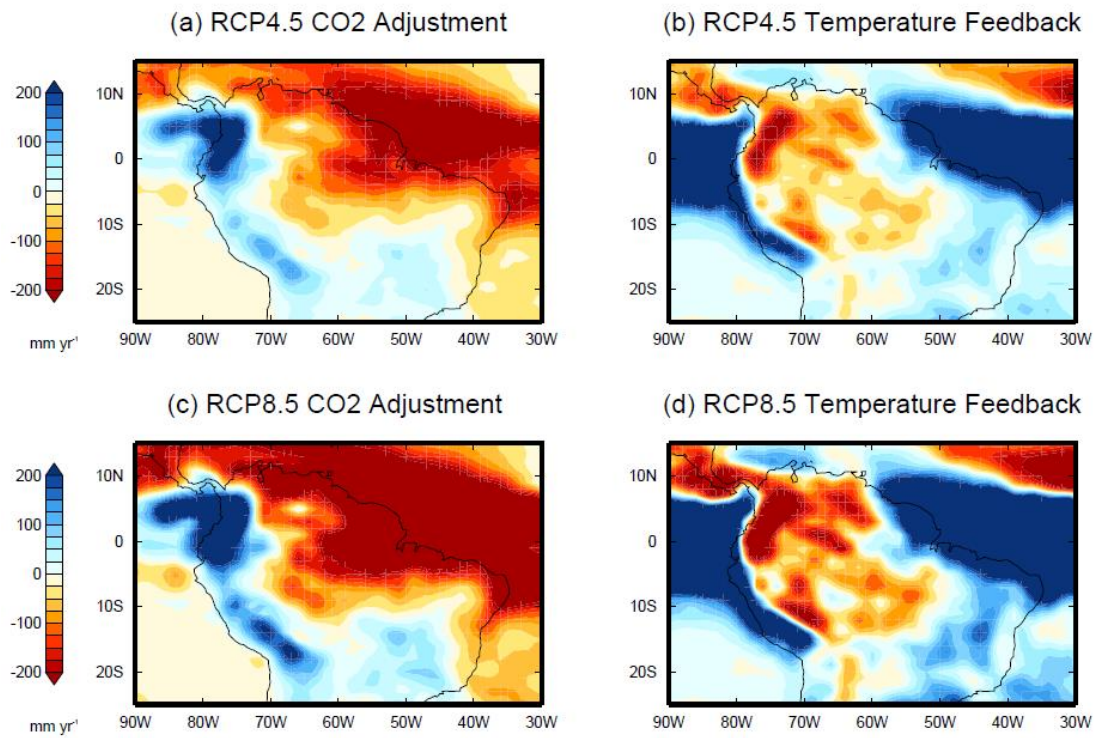


**Figure S5:** Contribution to predicted precipitation change from (a, c) CO<sub>2</sub> adjustment and (b, d) temperature-driven feedback, for the period 2081-2100 compared to pre-industrial, following (a, b) RCP4.5 and (c, d) RCP8.5, calculated using the simple model based on the PDRMIP response to CO<sub>2</sub>, described by Equation 2.

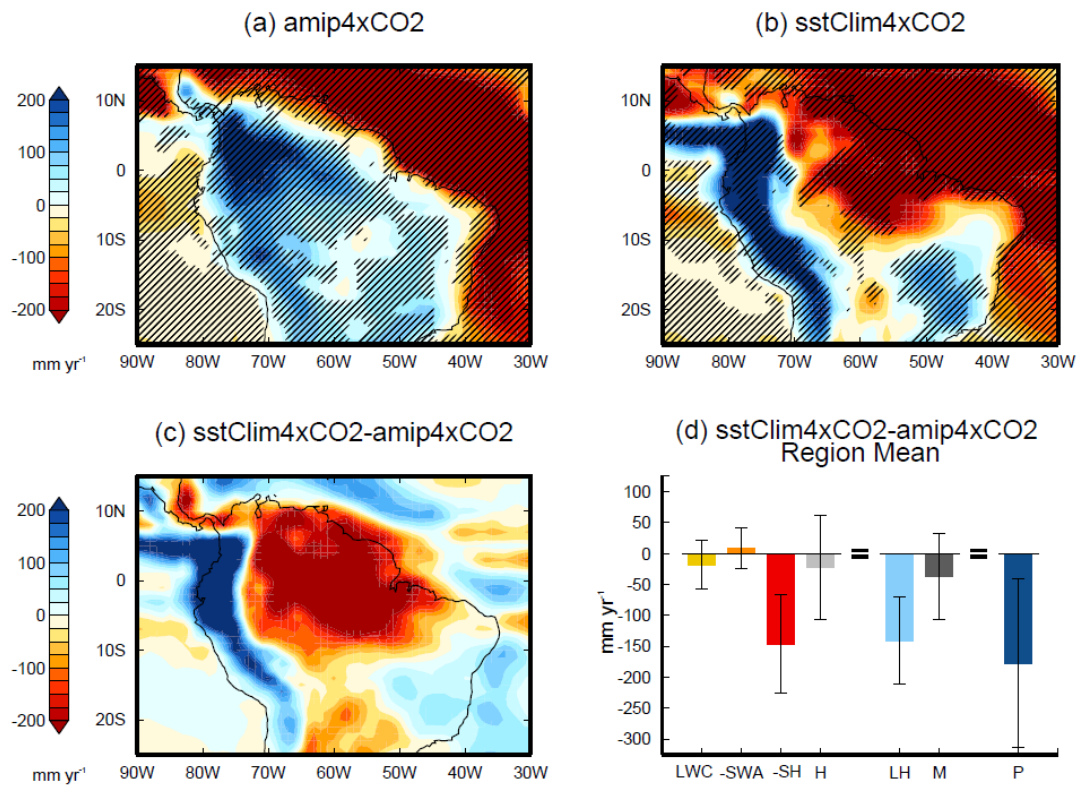


**Figure S6:** CMIP5 multi-model mean (including only 5 models which performed both sstClim and amip simulations) precipitation response to quadrupling CO<sub>2</sub> in (a) amip and (b) sstClim simulations and (c) the difference between the two (sstClim4xCO<sub>2</sub>-amip4xCO<sub>2</sub>). Hatching shows where all models agree on the sign of the change (not applied in panel (c) as not all of the same models performed each simulation). Panel (d) shows the difference between sstClim4xCO<sub>2</sub> and amip4xCO<sub>2</sub> energy and moisture budget response for the ECA region. All values are converted in to precipitation units (mm yr<sup>-1</sup>). Error bars denote the model spread standard deviation.

## References

- Arora, V.K., 2003. Simulating energy and carbon fluxes over winter wheat using coupled land surface and terrestrial ecosystem models. *Agric. For. Meteorol.* 118, 21–47. doi:10.1016/S0168-1923(03)00073-X
- Cox, P.M., Betts, R.A., Bunton, C.B., Essery, R.L.H., Rowntree, P.R., Smith, J., 1999. The impact of new land surface physics on the GCM simulation of climate and climate sensitivity. *Clim. Dyn.* 15, 183–203. doi:10.1007/s003820050276
- Krinner, G., Viovy, N., de Noblet-Ducoudré, N., Ogée, J., Polcher, J., Friedlingstein, P., Ciais, P., Sitch, S., Prentice, I.C., 2005. A dynamic global vegetation model for studies of the coupled atmosphere-biosphere system. *Global Biogeochem. Cycles* 19, 1–33. doi:10.1029/2003GB002199
- Oleson, K.W., Lawrence, D.M., Gordon, B., Flanner, M.G., Kluzek, E., Peter, J., Levis, S., Swenson, S.C., Thornton, E., Dai, A., Decker, M., Dickinson, R., Feddema, J., Heald, C.L., Lamarque, J., Niu, G., Qian, T., Running, S., Sakaguchi, K., Slater, A., Stöckli, R., Wang, A., Yang, L., Zeng, X., Zeng, X., 2010. Technical Description of version 4 . 0 of the Community Land Model ( CLM ). NCAR Tech. Note.
- Takata, K., Emori, S., Watanabe, T., 2003. Development of the minimal advanced treatments of surface interaction and runoff. *Glob. Planet. Change* 38, 209–222. doi:10.1016/S0921-8181(03)00030-4